NASA Contractor Report 191468

SPACE ENVIRONMENTAL EFFECTS ON THE INTEGRITY OF CHROMIC ACID ANODIZED COATINGS

W. L. Plagemann

BOEING DEFENSE & SPACE GROUP
Seattle, Washington

Contracts NAS1-18224 and NAS1-19247
May 1993

National Aeronautics and
Space Administration

Langley Research Center
Hampton, Virginia 23681-0001

FOREWORD

This report describes the results from the testing and analysis of chromic acid anodized aluminum hardware flown on the Long Duration Exposure Facility (LDEF). Boeing's activities were supported by the following NASA Langley Research Center Contracts (LaRC); "LDEF Materials Special Investigation Group Support" contracts NAS1-18224, Tasks 12 & 15 (October 1989 through January 1991) and NAS1-19247, Tasks 1, 2 & 8 (initiated May 1991). Sponsorship for these two programs was provided by the National Aeronautics and Space Administration, Langley Research Center, Hampton, Virginia and The Strategic Defense Initiative Organization, Key Technologies Office, Washington D.C.

Mr. Lou Teichman, NASA LaRC, was the NASA Task Technical Monitor. Mr. Teichman was replaced by Ms. Joan Funk, NASA LaRC, following his retirement. Mr. Bland Stein, NASA LaRC, was the Material Special Investigation Group Chairman, replaced by Ms Joan Funk and Dr. Ann Whitaker, NASA MSFC, following Mr. Stein's retirement. The Materials & Processes Technology organization of the Boeing Defense & Space Group was responsible for providing the support to both contracts. The following Boeing personnel provided critical support throughout the program.

Sylvester Hill	Program Manager
Dr. Gary Pippin	Technical Leader
Dr. Wally Plagemann	Testing and Data Analysis
Dr. Johnny Golden	Data Analysis

TABLE OF CONTENTS

List of Tables

List of Figures

SPACE ENVIRONMENTAL EFFECTS ON THE INTEGRITY OF CHROMIC ACID ANODIZED COATINGS

1.0 INTRODUCTION

The objective of this study was to characterize the performance of the anodized coating as a function of space environmental exposure. The analyses employed included specular and diffuse reflectance, scanning electron microscopy and metallography, surface analysis, and solar absorptance and emittance measurements.

The Long Duration Exposure Facility (LDEF) tray clamps used to hold the experiment trays in place on the LDEF have been analyzed to determine the effects of long term space exposure on the performance of the chromic acid anodize coating. Spectroscopic anomalies observed appeared to be random and related to application techniques as opposed to exposure or position on LDEF. Thickness measurements indicated that the coating was less than one micron and was probably not degraded by space exposure. Emittance values for the coating decreased uniformly by an average of 6.8% while solar absorbance values increased for trailing edge and decreased for leading edge specimens. The absorbance/emittance ratio for the coating also increased as a result of long term space exposure.

Anodize finishings of aluminum are being considered as a candidate thermal control coating for use on Space Station Freedom and other spacecraft planned for use at low earth orbit (LEO). LDEF was retrieved from orbit by the Space Shuttle Columbia on January 12, 1990 after spending 69 months in space. The performance of the chromic acid anodized coatings on LDEF is important in that it is a measure of how anodized coatings in general may perform during extended space exposure. LDEF offered the unique opportunity to evaluate the performance of chromic acid anodizing after prolonged space exposure. The constant orientation of LDEF relative to the ram direction throughout its entire mission has resulted in a unique distribution of exposure conditions. Since the tray clamps were positioned uniformly around the satellite, they represent each direct environmental exposure condition to both atomic oxygen and ultraviolet flux experienced by LDEF. The condition of the clamps provided a complete picture of the combined space effects on the performance and durability of the chromic acid anodized coating.

2.0 EQUIPMENT AND PROCEDURES

Specular and diffuse reflectance measurements in the UltraViolet (UV), Visible (Vis), and Near Infrared (NIR) regions of the spectrum were obtained on a Perkin Elmer Lambda IX UV-Vis/NIR Spectrophotometer with a barium sulfate coated integrating sphere attachment. Measurements in the mid-Infrared region were obtained on a Biorad FTS-60 Fourier Transform Infrared (FTIR) Spectrophotometer with a diffuse gold coated integrating sphere attachment.

SEM and metallography analysis were performed on an AMR 1400 Scanning Electron Microscope. Elemental analysis was also performed on the AMR 1400 using an Energy Dispersive X-Ray Analysis (EDX) attachment. Surface analysis was accomplished via Electron Spectroscopy for Chemical Analysis (ESCA) on a Surface Science M-Probe Surface Spectrometer.

The Solar Absorptance measurements were made on a Perkin Elmer Lambda IX UV-Vis/NIR spectrophotometer. All measurements were calculated from spectra obtained in the total reflectance mode over the spectral range of 0.25 - 2.5 microns. The calculations were made using a 29 point integration over the air mass zero solar spectrum. A National Bureau of Standards spectral tile served as a standard material of known absorptance to which all spectra were corrected. The tile absorptance.was measured each time a set of specimens were measured. All tests were conducted in accordance with ASTM E424, Method A.

The thermal emittance measurements were made in accordance with ASTM E408, Method A on a Gier-Dunkle DB 100 Infrared Reflectometer. The values reported are averages of five measurements per specimen. Boeing Metrology Laboratory reference materials were used to recalibrate the instrument prior to evaluating each material.

3.0 RESULTS

3.1 Specular and Diffuse Reflectance

Total, specular and diffuse reflectance spectra were obtained for each tray clamp analyzed. Data was obtained in the ultraviolet, visible, near infrared, and mid-infrared regions of the spectrum. The individual spectra were examined for anomalies and particular changes in the various spectral signatures of the coating with respect to the type of exposure the clamps had seen on LDEF.

3.1.1 UV-Vis/NIR Region

There were large variations in the reflectance data obtained from different specimens, especially in the UV-Vis/NIR region of the spectrum. Two representative UV-Vis/NIR diffuse reflectance spectra are shown in figure 1. The data indicates nearly a 20% difference in the diffuse reflectance component between the two spectra. The total reflectance values, however, exhibited little variation in any of the clamps tested. There was also no apparent correlation between the differences observed when the reflectance values of the exposed surfaces were compared to those on the reverse side of the clamps and the position on LDEF except for the leading and trailing edge specimens. There was a trend toward decreased diffuse and increased specular reflectance on leading edge specimens while the reverse was true for the trailing edge. The total reflectance, however, remained unchanged. It appears however, that the majority of the spectral changes observed were related more to variations in application techniques than to space effects. All of

the spectra obtained during this phase of the investigation are included in the appendix A. The differences observed are summarized in Table I.

3.1.2 Mid-Infrared Region

The IR spectra presented in the appendix were obtained using an integrated sphere attachment to the spectrophotometer. Several measurements were also made employing a spectra tech diffuse reflectance attachment. Figure 2 contains representative diffuse reflectance spectra obtained over the mid infrared region of the spectrum by this second method. A typical spectrum from the reverse side of the clamp, which was shielded from any space effects except vacuum and thermal cycling, is presented in Figure 2B. As seen in this figure there is distinct evidence of organic contamination in the protected surfaces of the tray clamps as evidenced by the CH_2-CH_3 absorptions around 2900 cm^{-1} and the carbonyl absorptions near 1640 cm^{-1}. The exposed surfaces show significant reductions in the magnitude of the peaks in both of these regions indicating that space exposure may actually have "cleaned" some of the initial contamination from the LDEF surfaces. An additional absorption peak was observed on many of the exposed surfaces. This peak can be seen around 1070 cm^{-1} in the spectrum shown in Figure 2A. The presence of this peak has tentatively been attributed to the formation of silicate compounds associated with the silicone contamination observed on many of the LDEF surfaces.

3.2 SEM and Metallography

3.2.1 Coating Thickness Measurements

SEM analysis was employed to measure the anodize coating thickness on the tray clamps. Small specimens cut from the clamps were fractured and photomicrographs were obtained of the fracture surfaces from both the front and back of the clamps. The coating thicknesses were then measured directly from the photomicrographs. The back side of each clamp acted as a control and the data was evaluated to determine if space exposure had any effect on the coating thickness. Typical photomicrographs showing the anodize coating are presented in Figure 3. All of the photomicrographs evaluated are included in appendix B.

The thickness data is summarized in Table II. The data represents five measurements on both the front and back of each clamp. The data indicate no effect of space exposure on the thickness of the anodize coating. The SEM analysis did indicate that the coating was extremely thin averaging only between 0.4 and 0.8 μm.

3.2.2 Evaluation of Tray Clamps with Copper Grounding Straps

Copper straps for grounding the silverized teflon blankets for experiment AO-178 were attached to specific tray clamps on LDEF. One such clamp is pictured in Figure 4. These samples were significant because they had both

exposed and protected areas on the same side of the clamp. Figure 5 contains photographs of a clamp which had part of the exposed surface protected by shims. The areas on the clamp which were protected by the shim and the ground strap, as indicated in Figure 5 by arrows A & B respectively, can be easily detected as lighter regions on the clamp surface. Contamination from external sources contributed much of the discoloration on the exposed surfaces shown as darker regions on the clamp surface.

Figure 6 contains photomicrographs of cross sections obtained from exposed areas of clamps and areas of clamps shielded by copper grounding straps. Clamps from both leading edge (Figure 6 A & B) and trailing edge (Figure 6 C & D) locations were examined. The most notable feature in these figures is what appears to be debris on the protected surfaces of the clamps. SEM photomicrographs (Figure 7) revealed that what appeared to be debris was actually a discrete layer on the surface of the clamp. EDX analysis of this layer (Figure 8) indicated that it was comprised solely of aluminum, most likely in the form of aluminum oxide. This indicates that an oxidation process may have occurred on the surface subsequent to the anodizing. The exact source of this layer is not known. However, the anodize coating on the clamps is extremely thin and porous. The configuration of copper in contact with the aluminum clamp allowed the potential for galvanic corrosion to occur. Exposure to humidity before or after the flight would have been sufficient to provide a conductive path, leading to galvanic action, producing the type of deposit observed. Figure 6 shows that the "extra" layer is absent from exposed areas on the surfaces of the clamps, further supporting the possibility that galvanic corrosion produced the surface layer observed under the copper straps.

3.2.3 Coating Porosity

Figure 9 contains SEM photomicrographs of both exposed (Figure 9A & C) and protected (Figure 9 B & D) areas from the surface of a trailing edge clamp. As seen in these figures, the surface of the clamp appears to be moderately pitted and there is no significant variation in the amount of pitting present on the exposed or protected surfaces. Figure 10 contains SEM photomicrographs of exposed (Figure 10 A & C) and protected (Figure 10 B & D) areas from a leading edge clamp. While pits are again present in both the exposed and protected areas of the coating, the number of pits on the exposed surface of this leading edge clamp is considerably greater than on the protected areas. However further investigation of other leading edge clamps did not show this effect. Other photomicrographs are included in appendix C.

3.3 Surface Analysis

ESCA spectra were obtained from selected earth and space end clamps. The results are presented in Figures 11-14. As seen in these figures, the silicon contamination which was observed over all of LDEF (Ref. 1) was detected. Fluorine was also observed in one of the spectra. The silicon contamination was also observed during surface analysis studies of the paint disks. Since no

real anomalies were observed during these initial investigations the surface analysis characteration of the tray clamps was discontinued and efforts were directed to other analyses.

3.4 Solar Absorptance and Emittance

The tray clamps were anodized prior to flight to achieve an α/ε ratio of 2.1+/- 0.2. The stability of this ratio is both a measurement of the durablility of the coating and an indication of its effectiveness in thermally protecting the spacecraft. Since the effects of long term space exposure on the survivablity of the anodize coating is an important parameter to be considered by designers of low earth orbit spacecraft, considerable effort was expended in analyzing the absorptance and emittance of as many clamps as possible. As of this report 228 clamps have been analyzed. The data obtained from these clamps is summarized in Table III.

There was considerable variability observed in the optical property values obtained between tray clamps. Solar absorptance values ranged from 0.30-0.40; emittance values range from 0.12-0.20; and the calculated α/ε ratio ranged from 1.60-2.80. Some of this variability was undoubtedly due to inconsistencies in the anodizing application techniques. In addition, there were only four ground control specimens available and any anomalies associated with the method of application of the coating would also be manifested in these specimens. Under normal circumstances this would have made any meaningful statistical analysis of the results impossible. Fortunately, the reverse side of each clamp did not see the effects of the total space exposure. This afforded a built in control for each clamp and allowed elimination much of the variability expected between individual clamps. The fact that the optical values for the exposed and protected sides of the clamps could be compared allowed us to conduct meaningful paired "t" analyses of the differences between the front and back of the clamps and determine the statistical significance of the results (Ref. 2).

The most obvious conclusions which can be drawn from the data presented in Table III are that emittance values apparently decreased by an average of 5.6% as a result of space exposure and the α/ε ratio increased by 5.6% While these values are small, they are statistically significant at the 99% confidence level. The data in Table III also indicates that the clamps subjected to earth end exposure were the only ones which exhibited no change as a result of space exposure. This infers that UV exposure may have had an adverse effect on the performance of the anodize layer.

A number of subtle differences were observed which are not apparent from the average values presented in Table III. These will be discussed in the subsequent sections.

3.4.1 Solar Absorptance

While the data in Table III indicates that the average solar absorptance values remained unchanged, closer scrutiny reveals some interesting trends. Figure 15 contains a graph of the average change in solar absorptance values between the front and back of the clamps as a function of position on LDEF. As seen in this figure, leading edge exposure has resulted in a slight decrease in solar absorptance values with respect to the unexposed side of the clamps, while trailing edge exposure has resulted in an increase. There also appears to be a transition zone in row 6 where there were little or no differences between exposed and protected values. Although these values are small, they are statistically significant at the 99% confidence level. Table IV contains the results of a Duncan's New Multiple Range Test on the data from Figure 15. Duncan's New Multiple Range test is employed to determine statistical differences between multiple means (Ref. 2). Means which are not statistically different from one another are underlined in Table IV.

In general the data indicates that the values from the leading edge clamps are significantly different from those obtained from trailing edge specimens. The data also indicates that the values obtained from row 6 specimens were different from both the leading and trailing edge. This is important because row 6 is an area where the AO model fluence predictions fall from 1E+21 to 5E+19 impacts per square cm. Adjacent trailing edge specimens have predicted AO fluences of approximately 1E+17 impacts per square cm (Ref. 3). This suggests that atomic oxygen may have played a role in the observed differences.

Figure 16 is a plot of the change in solar absorptance values as a function of atomic oxygen flux. The data indicates that solar absorptance values generally decrease with increasing levels of atomic oxygen exposure. The relationship between the change in solar absorptance values and equivalent sun hours is presented in Figure 17. At first glance the data in Figure 17 appears to be quite scattered. A closer look, however, reveals that there are actually two distinct relationships indicated here. The first is for trailing edge specimens and it indicates a slight increase in solar absorptance with increasing sun hours. Leading edge specimens, however, actually show a decrease with increasing sun hours.

3.4.2 Thermal Emittance

The relationship between the change in emittance values and the position on LDEF is presented in Figure 18. As seen in this figure, the emittance values decreased relatively uniformly. This decrease is significant at the 99% confidence level and is apparently independent of the position of the clamps on the satellite. This would seem to indicate that the observed changes in emittance may be related to the silicon contamination which was generally present over the entire spacecraft. There were no correlations observed when the change in emittance values were plotted against either the atomic oxygen flux or the equivalent sun hours as seen in Figures 19 & 20.

3.4.3 The Ratio of Absorptance to Emittance

Figure 21 contains the relationship between the change in α/ε and the position of the clamps on the satellite. The data indicates that space exposure increased the α/ε ratio for the tray clamps. This relationship was again significant at the 99% confidence level. In general, the observed change was more dramatic for trailing edge clamps than for those placed on the leading edge. There were no correlations when the changes in α/ε were plotted against the atomic oxygen flux or the equivalent sun hours (Figures 22 & 23).

While the observed changes in the optical properties of the anodized coating were relatively small, they were statistically significant. It is unknown what effect longer exposure will have on the coating. Assuming that the observed changes were induced by space exposure, they could have already reached their maximum levels and will now be constant with time or they could be following an Arrhenius relationship and may increase with further exposure.

4.0 CONCLUSIONS

- Spectroscopic anomalies were random and are likely related to application techniques as opposed to space exposure or position on LDEF.

- Anodize coating thicknesses were less than one micron and were not substantially degraded by space exposure.

- Thermal emittance values decreased uniformly by an average of 6.8%, most likely due to the silicon contamination.

- Solar absorptance values increased for trailing edge specimens and decreased for leading edge specimens. This combination of effects was likely due to darkening of contaminant layers under solar exposure on the trailing edge and removal of the contamination layer on leading edge clamps by atomic oxygen.

5.0 REFERENCES

1. Harvey, G. A. "Sources and Transport of Silicone NVR". NASA Conference Pub. 3162, Part 1. LDEF Materials Workshop. NASA LaRC, 1991.

2. Torrie, J. H. and R. G. D. Steel, Principles and Procedures of Statistics, 2nd Ed., 1980. McGraw-Hill Book Co. New York, New York.

3. Borrassa, R. J. and J. R. Gillis "Atomic Oxygen Exposure of LDEF Experiment Trays". NASA Contractor Report 189627, 1992.

TABLE I. Summary of Reflectance Changes for Anodized Coating as a Function of Position on LDEF

	REFLECTANCE CHANGES			
	IR		UV-VIS	
AREA	DIFFUSE	TOTAL	DIFFUSE	TOTAL
SPACE END				
H09-6	-	NC	-	NC
H09-3	-	NC	-	NC
H01-6	+	NC	+	NC
H01-4	NC	+	-	NC
H09-4	NC	NC	+	NC
H01-2	NC	-	-	NC
H09-5	-	+	-	+
EARTH END				
G04-11	+	NC	+	NC
G12-8	+	NC	+	NC
G06-8	-	NC	-	+
G08-8	-	+	-	NC
G12-2	+	NC	+	NC
G08-9	-	+	-	+
G12-3	NC	NC	-	+
G12-1	NC	NC	+	NC
LEADING EDGE				
C08-5	-	NC	-	+
A09-3	-	NC	-	NC
F09-8	NC	NC	-	NC
F09-6	+	NC	NC	NC
A10-3	NC	+	-	NC
TRAILING EDGE				
E02-6	NC	NC	NC	NC
E02-7	-	NC	+	NC
A03-5	+	NC	+	NC
F04-2	NC	NC	+	NC
C03-2	+	NC	+	NC
E03-8	NC	NC	+	NC

\- = decrease in reflectance between front and back surfaces
\+ = increase in reflectance between front and back surfaces
NC - No Change

TABLE II. Average Thickness of Chromic Acid Anodize Coating

	Average Thickness (μm)			
Clamp	Front	Standard Deviation	Back	Standard Deviation
G08-6	0.84	0.11	0.70	0.03
G02-9	0.70	0.11	0.69	0.02
H12-8	0.80	0.06	0.68	0.13
H01-3	0.63	0.08	0.61	0.05
H12-6	0.62	0.06	0.59	0.06
H09-6	0.81	0.09	0.63	0.09
F10-4	0.64	0.10	0.65	0.05
B08-1	0.68	0.07	0.78	0.10
E09-2	0.60	0.08	0.51	0.05
F03-2	0.47	0.05	0.77	0.05
B01-1	0.74	0.02	0.74	0.04
E03-1	0.66	0.04	0.59	0.09

TABLE III. Average of n Solar Absorptance and Emittance Measurements for Chromic Acid Anodize Coating on LDEF Tray Clamps where n is the number of clamps from that row analyzed.

		Front (Exposed)			Back (Protected)		
Row	n	α	ε	α/ε	α	ε	α/ε
1	16	.349	.153	2.28	.337	.164	2.06
2	21	.349	.152	2.30	.342	.157	2.18
3	15	.350	.149	2.35	.341	.156	2.19
4	9	.352	.151	2.33	.339	.161.	2.11
5	13	.347	.151	2.30	.342	.161	2.12
6	17	.348	.155	2.25	.347	.161	2.16
7	17	.331	.151	2.19	.335	.163	2.06
8	9	.334	.150	2.27	.342	.160	2.14
9	15	.339	.145	2.33	.343	.155	2.21
10	12	.334	.149	2.24	.346	.163	2.12
11	13	.335	.151	2.22	.345	.167	2.07
12	17	.334	.142	2.35	.338	.155	2.18
SPACE	28	.348	.158	2.20	.350	.170	2.06
EARTH	24	.348	.168	2.07	.347	.169	2.05
AVE.	**228**	**.343**	**.153**	**2.24**	**.343**	**.162**	**2.12**

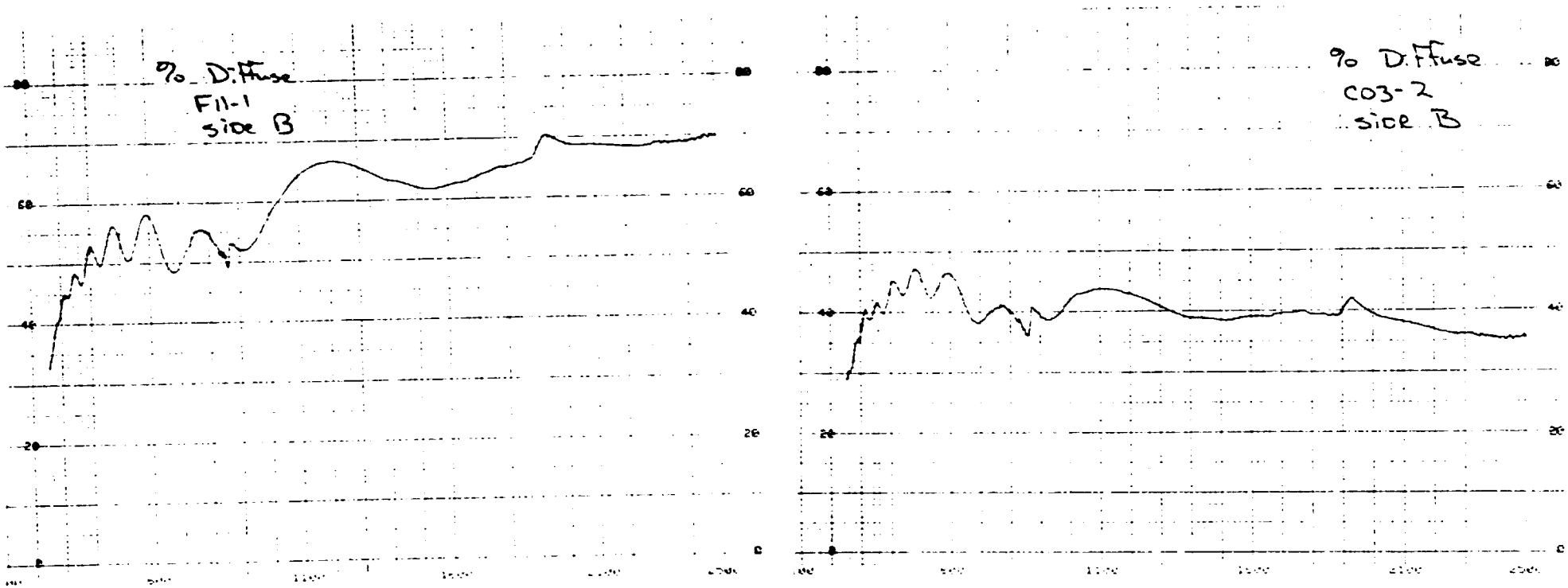

FIGURE 1. UV-Vis/NIR diffuse reflectance spectra from two tray clamps showing extremes in variations observed between samples.

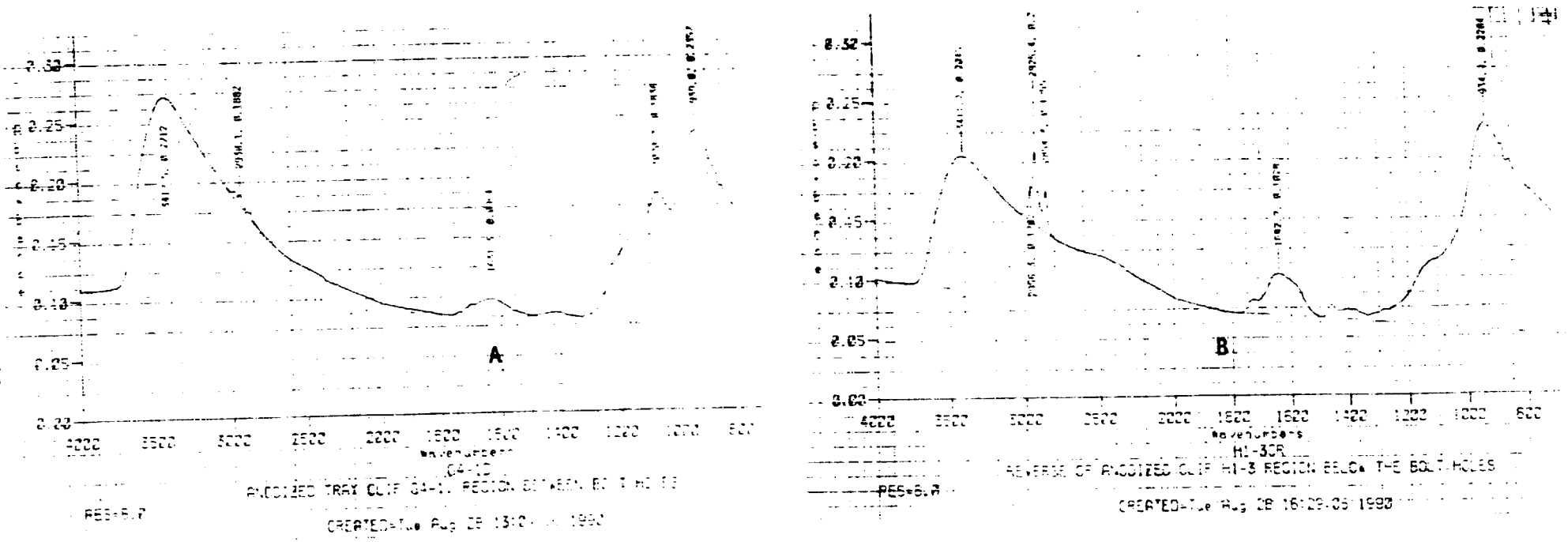

FIGURE 2. Infrared diffuse reflectance spectra of (A) exposed and (B) protected surfaces of LDEF tray clamps

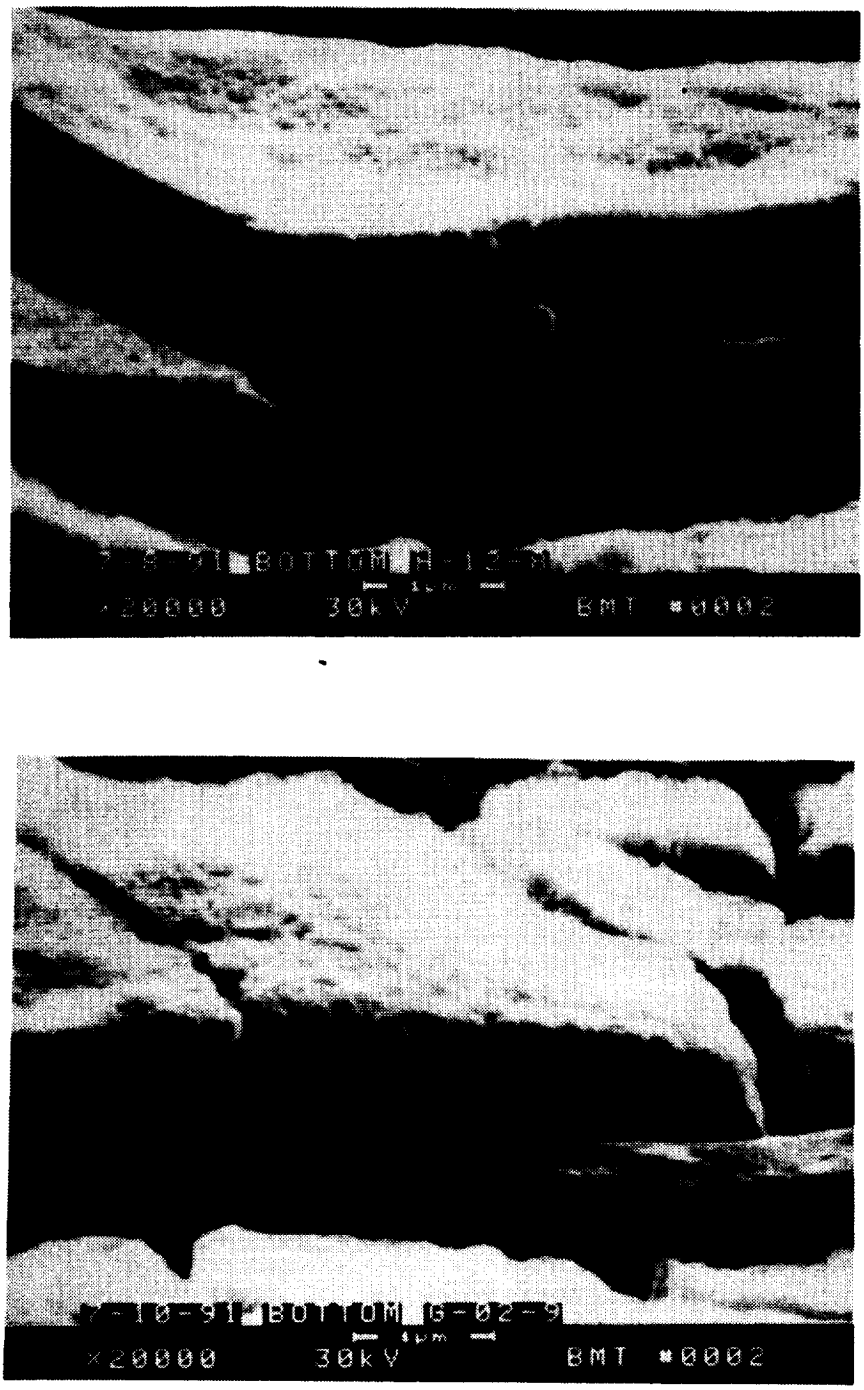

FIGURE 3. Typical SEM photomicrographs showing anodize coating thickness

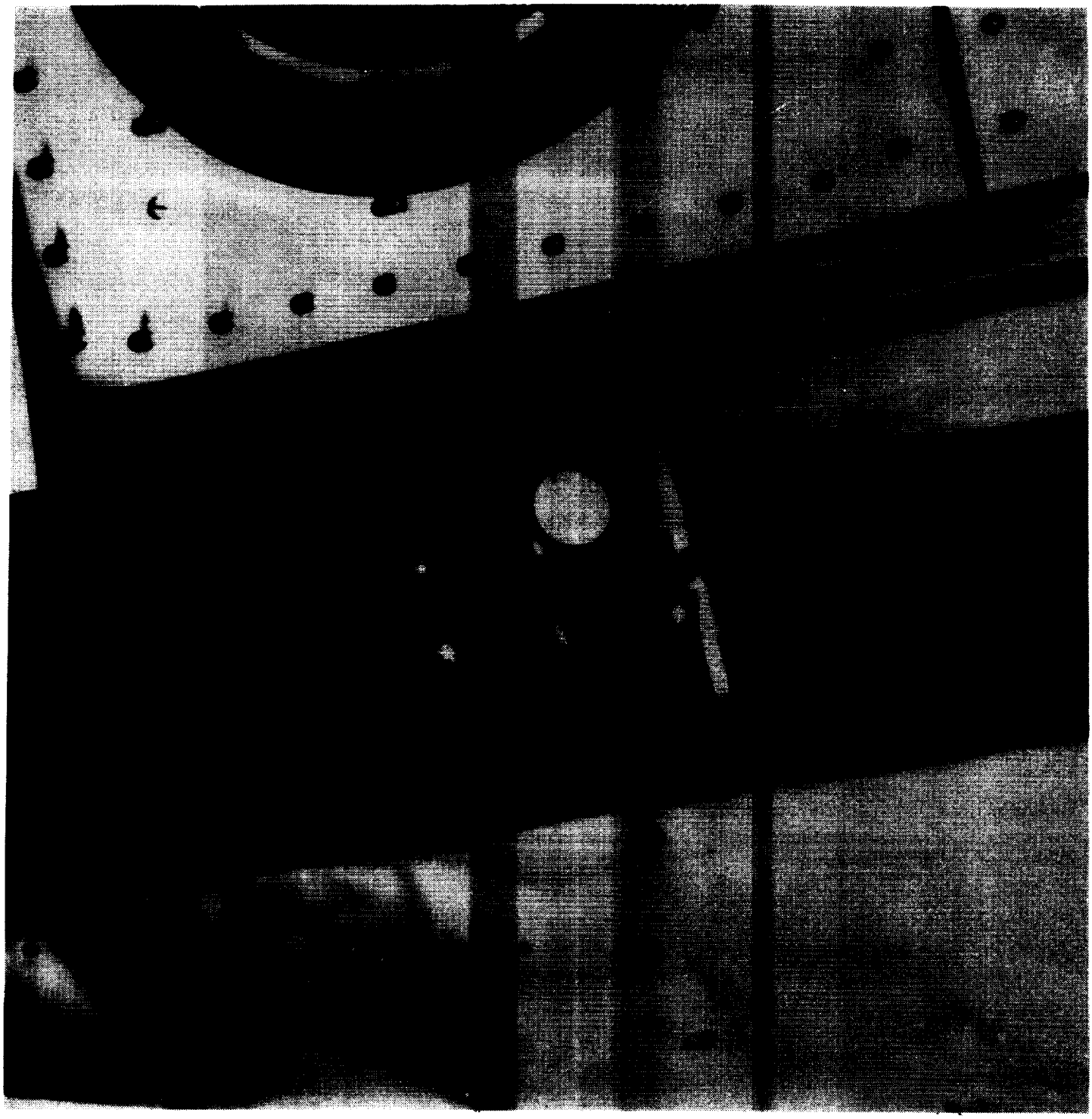

FIGURE 4. Photograph showing position of copper grounding strap on LDEF tray clamp.

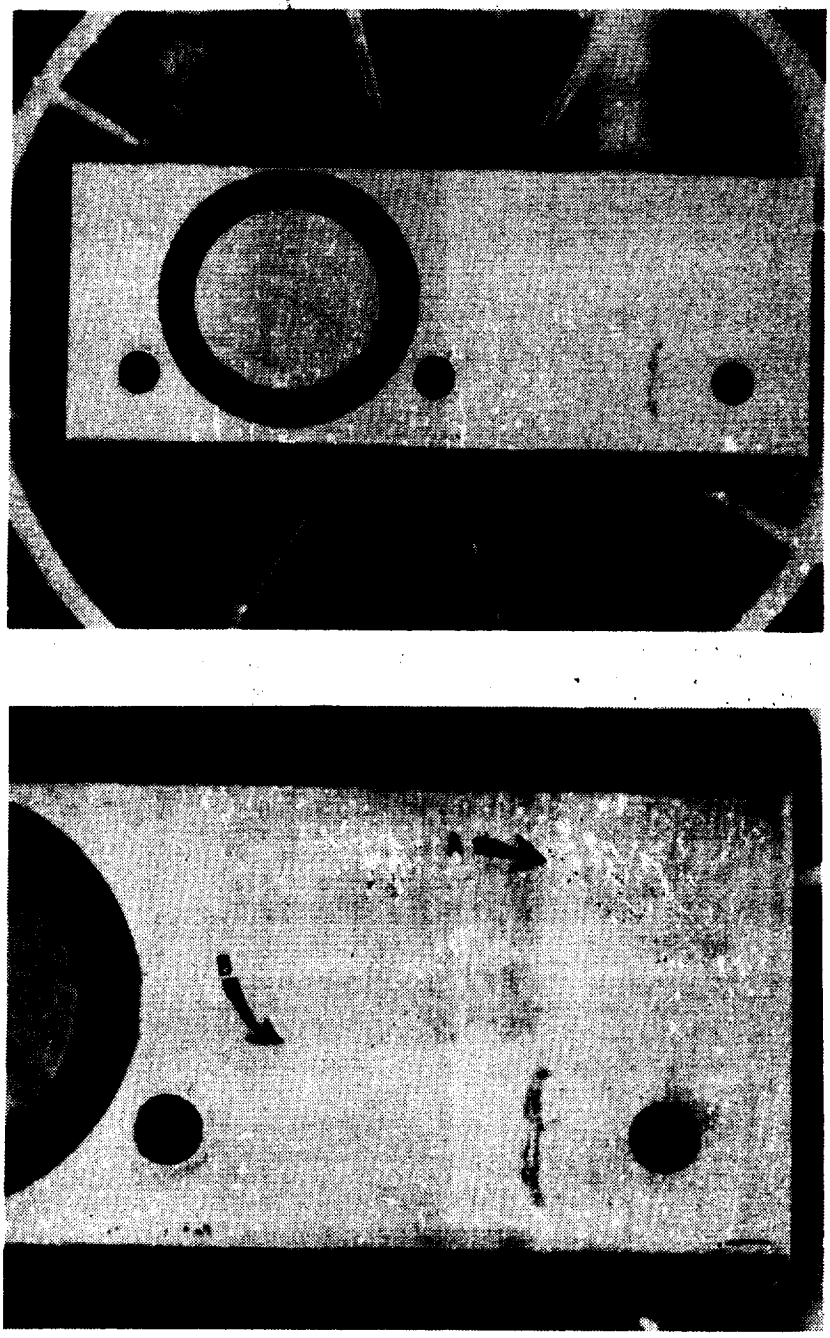

FIGURE 5. Photograph of tray clamp with arrows indicating boundaries between exposed regions and those protected by (A) the copper ground strap and (B) the aluminum shim.

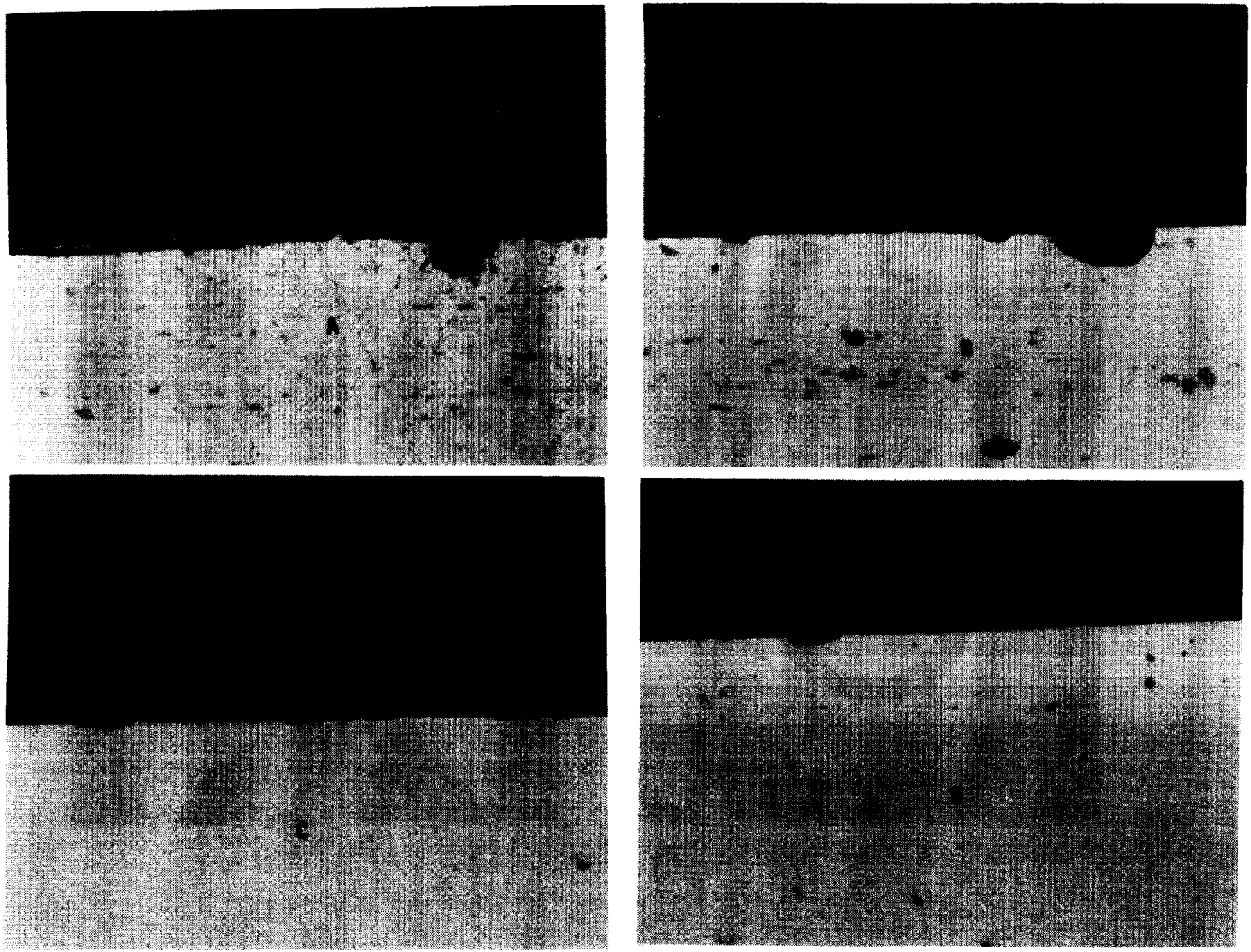

FIGURE 6. Optical photomicrographs at 1000X depicting (A) protected and (B) exposed regions from the surface of leading edge clamp E10-6 and from (C) protected and (D) exposed areas from trailing edge clamp E02-6.

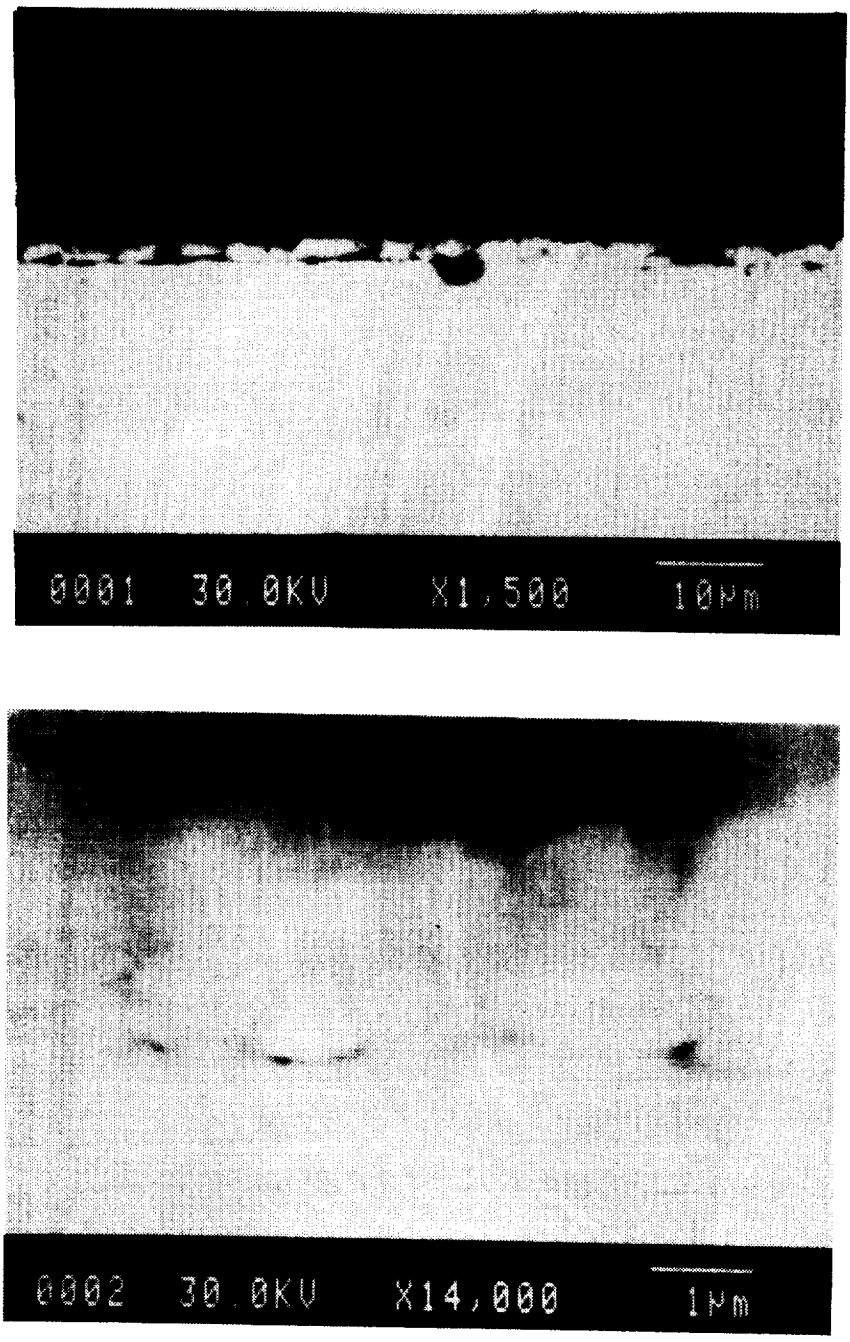

FIGURE 7 Higher magnification scanning electron photomicrographs depicting the observed surface layer on the protected surfaces of tray clamp E10-6.

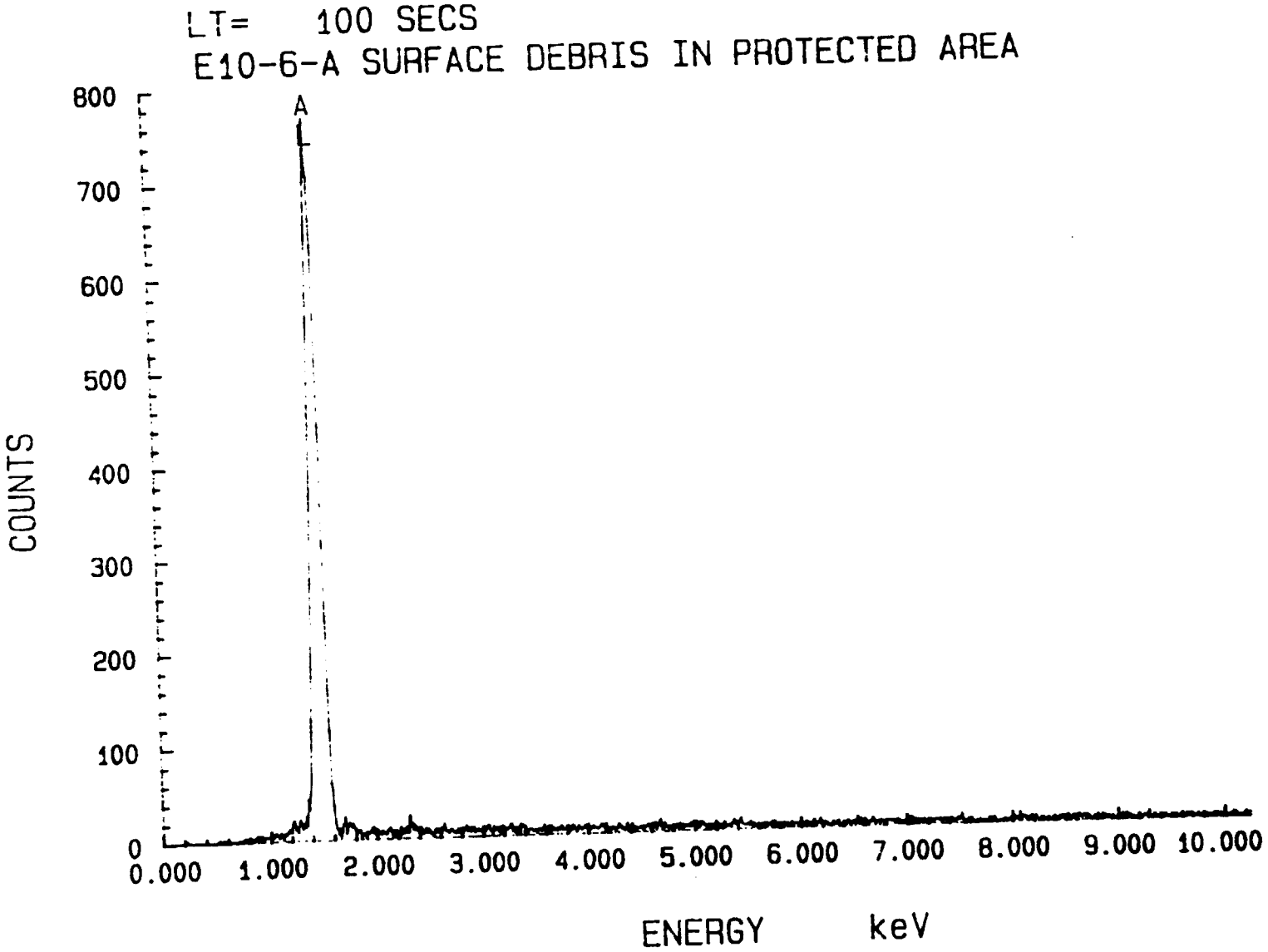

FIGURE 8. EDX elemental spectrum of surface layer observed on protected surface of tray clamp E10-6

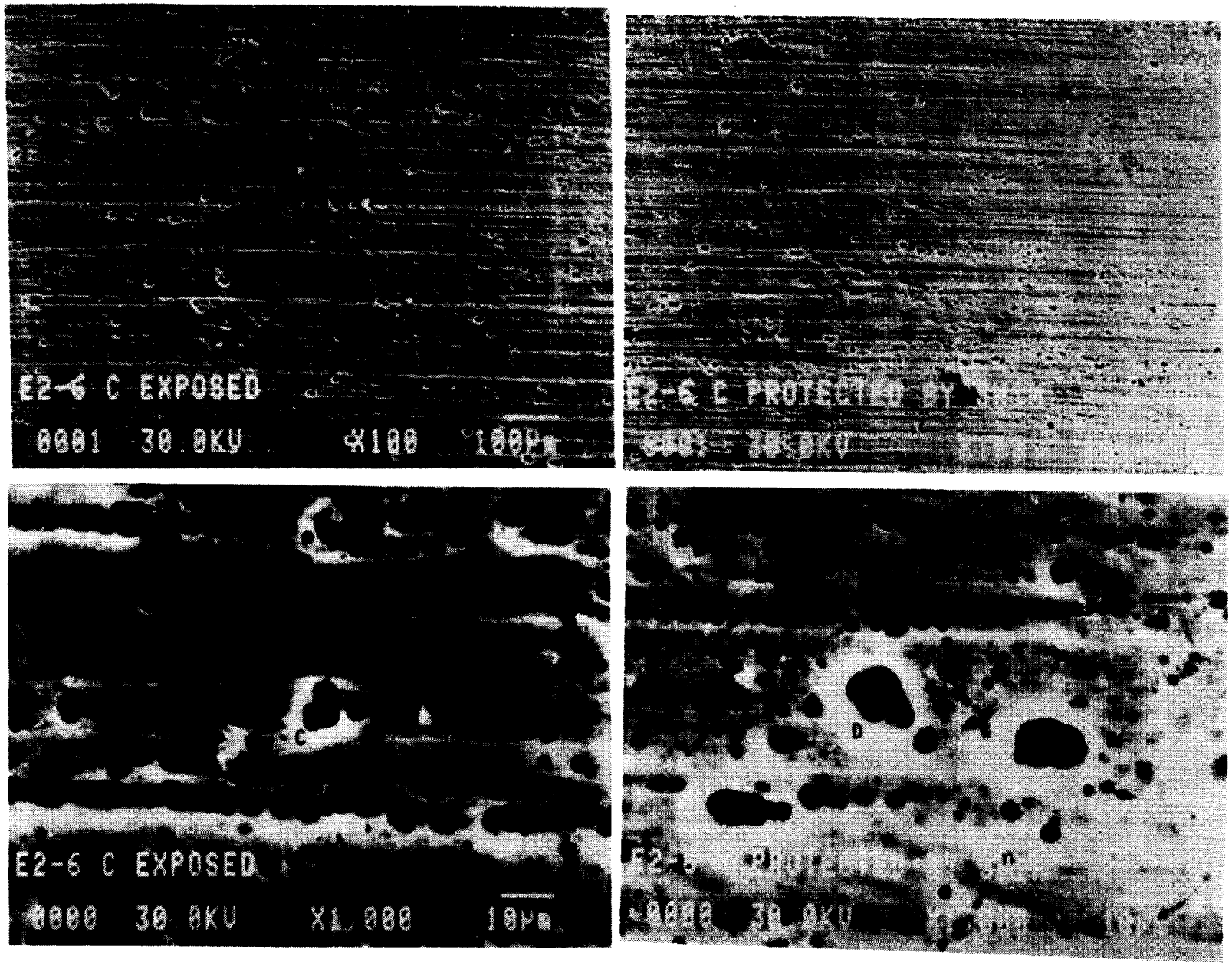

FIGURE 9. SEM photomicrographs depicting surface porosity on (A) exposed and (B) protected at 100X and (C) exposed and (D) protected at 1000X for trailing edge clamp E02-6.

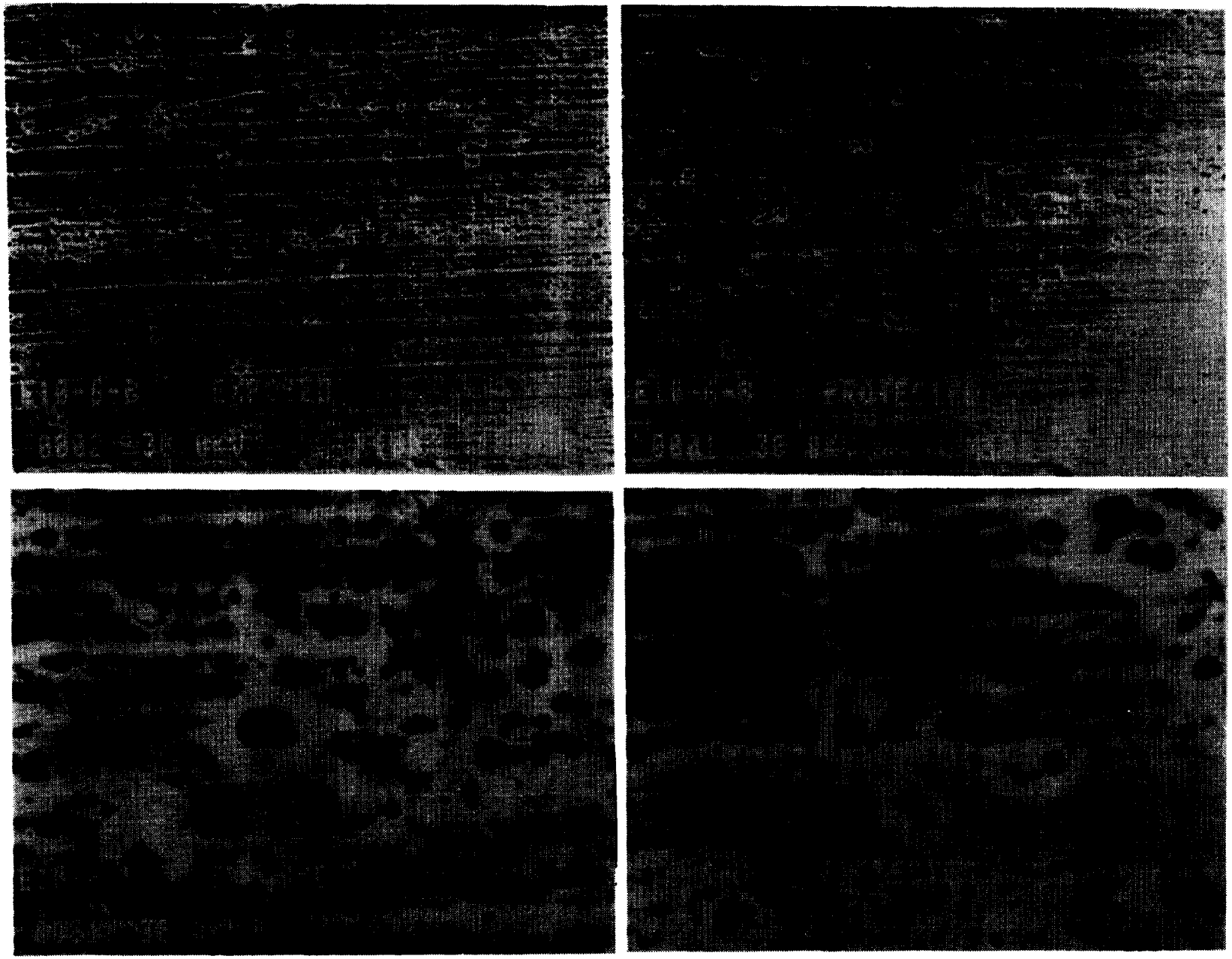

FIGURE 10. SEM photomicrographs depicting surface porosity on (A) exposed and (B) protected at 100X and (C) exposed and (D) protected at 1000X for leading edge clamp E10-6.

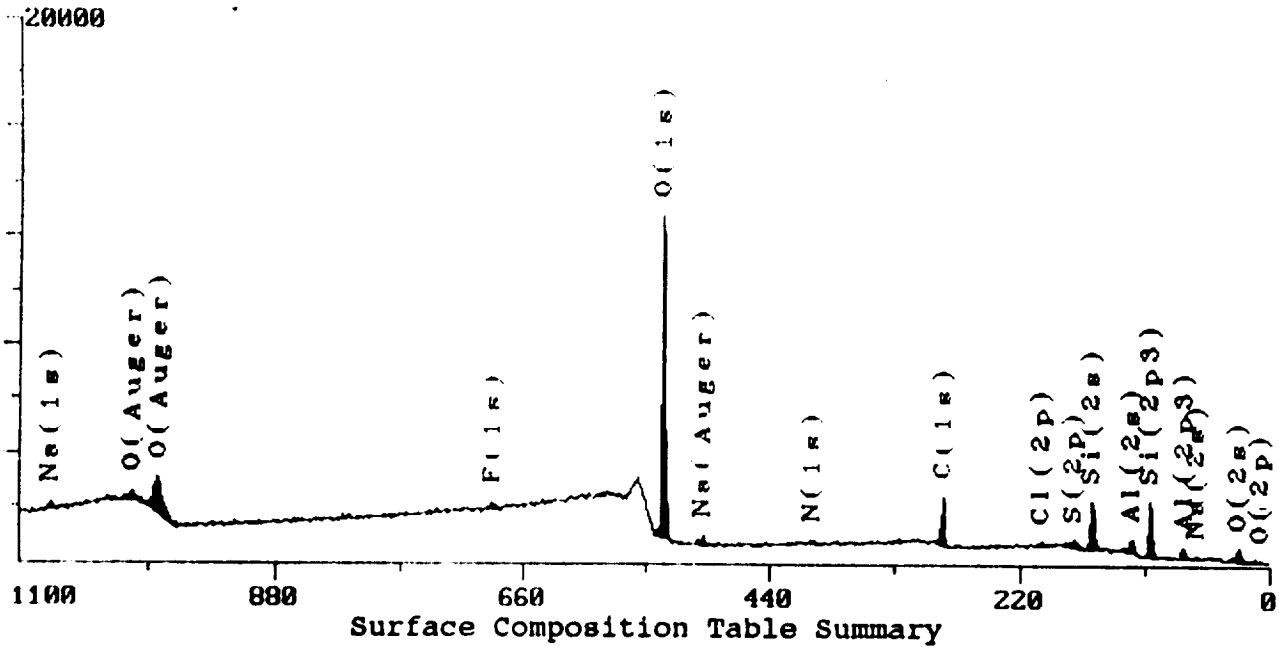

Surface Composition Table Summary

Element	Binding Energy	atom %
Na (1s)	1073.81	0.82 %
F (1s)	687.31	1.24 %
O (1s)	533.71	46.24 %
N (1s)	401.07	0.73 %
C (1s)	285.78	16.51 %
Cl (2p)	200.39	0.74 %
S (2p)	170.99	4.02 %
Si (2s)	155.11	20.60 %
Al (2s)	120.07	9.09 %
	Total Percent	100.00 %

FIGURE 11. ESCA spectrum of anodize coating from clamp with Earth end exposure

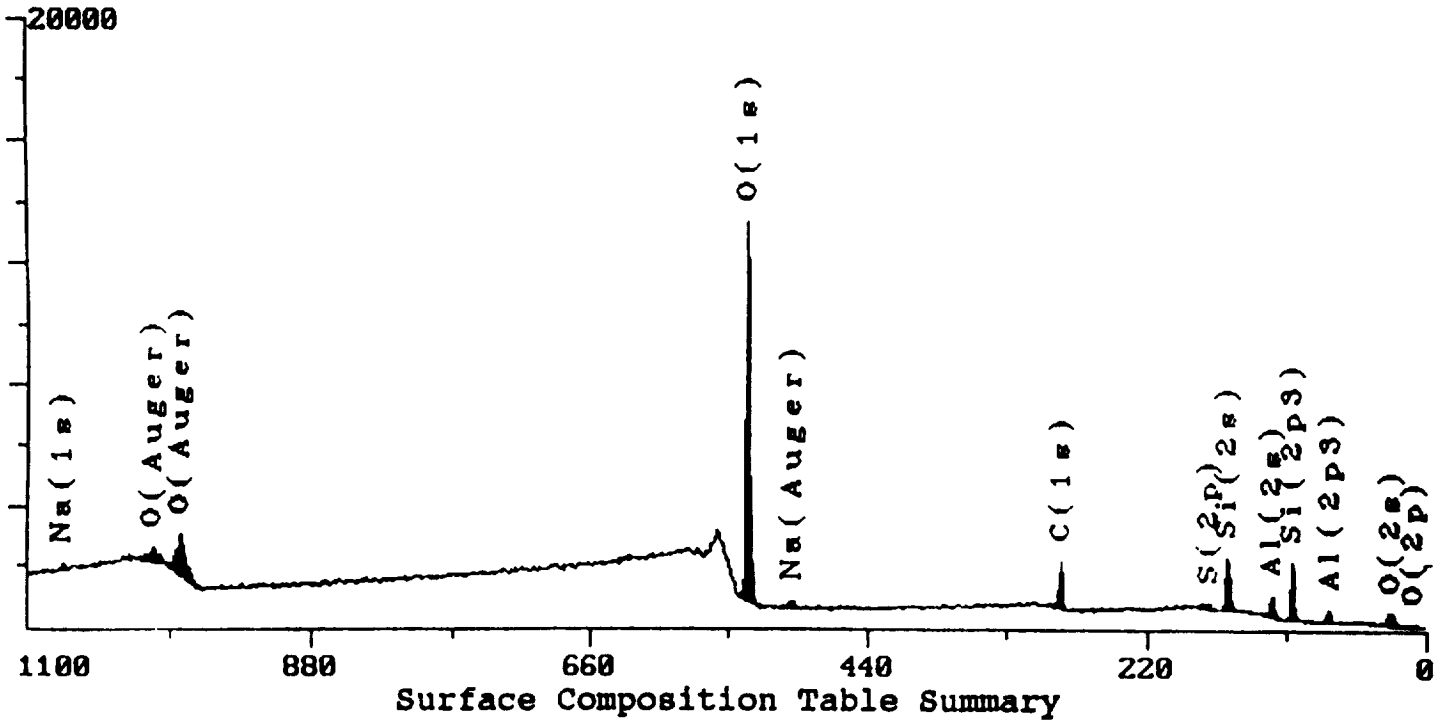

Element	Binding Energy	atom %
Na (1s)	1073.85	0.61 %
O (1s)	533.88	50.68 %
C (1s)	286.18	15.58 %
S (2p)	170.53	3.46 %
Si (2s)	155.28	20.22 %
Al (2s)	120.36	9.45 %
	Total Percent	100.00 %

FIGURE 12. ESCA spectrum of anodize coating from clamp with Earth end exposure

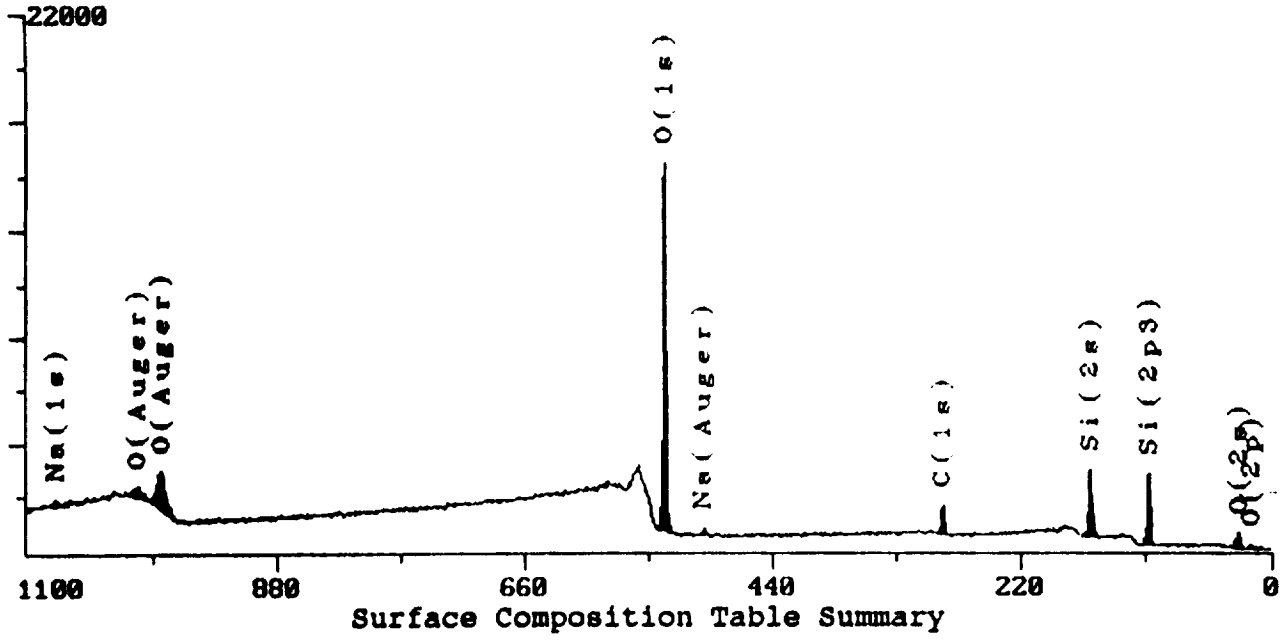

Element	Binding Energy	atom %
Na (1s)	1075.33	0.74 %
O (1s)	535.30	56.83 %
C (1s)	287.26	11.58 %
Si (2s)	156.59	30.84 %
	Total Percent	100.00 %

FIGURE 13. ESCA spectrum of anodize coating from clamp with space end exposure

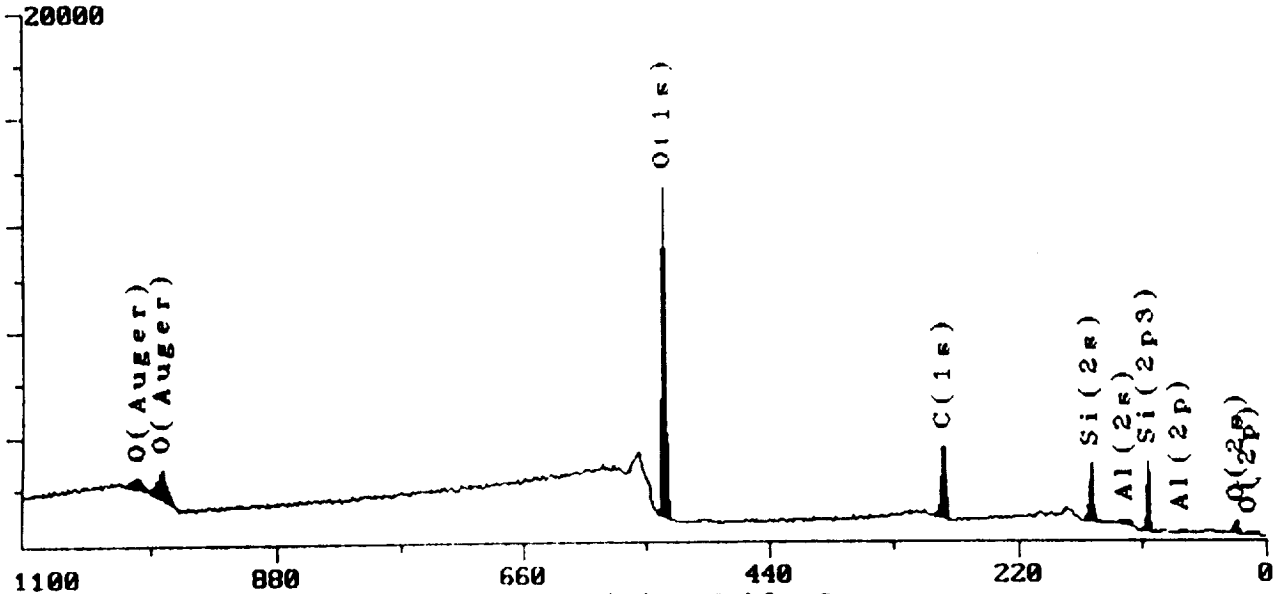

Surface Composition Table Summary

Element	Binding Energy	atom %
O (1s)	532.52	44.64 %
C (1s)	284.39	28.26 %
Si (2s)	153.79	25.25 %
Al (2p)	73.36	1.85 %
Total Percent		100.00 %

FIGURE 14. ESCA spectrum of anodize coating from clamp with space end exposure

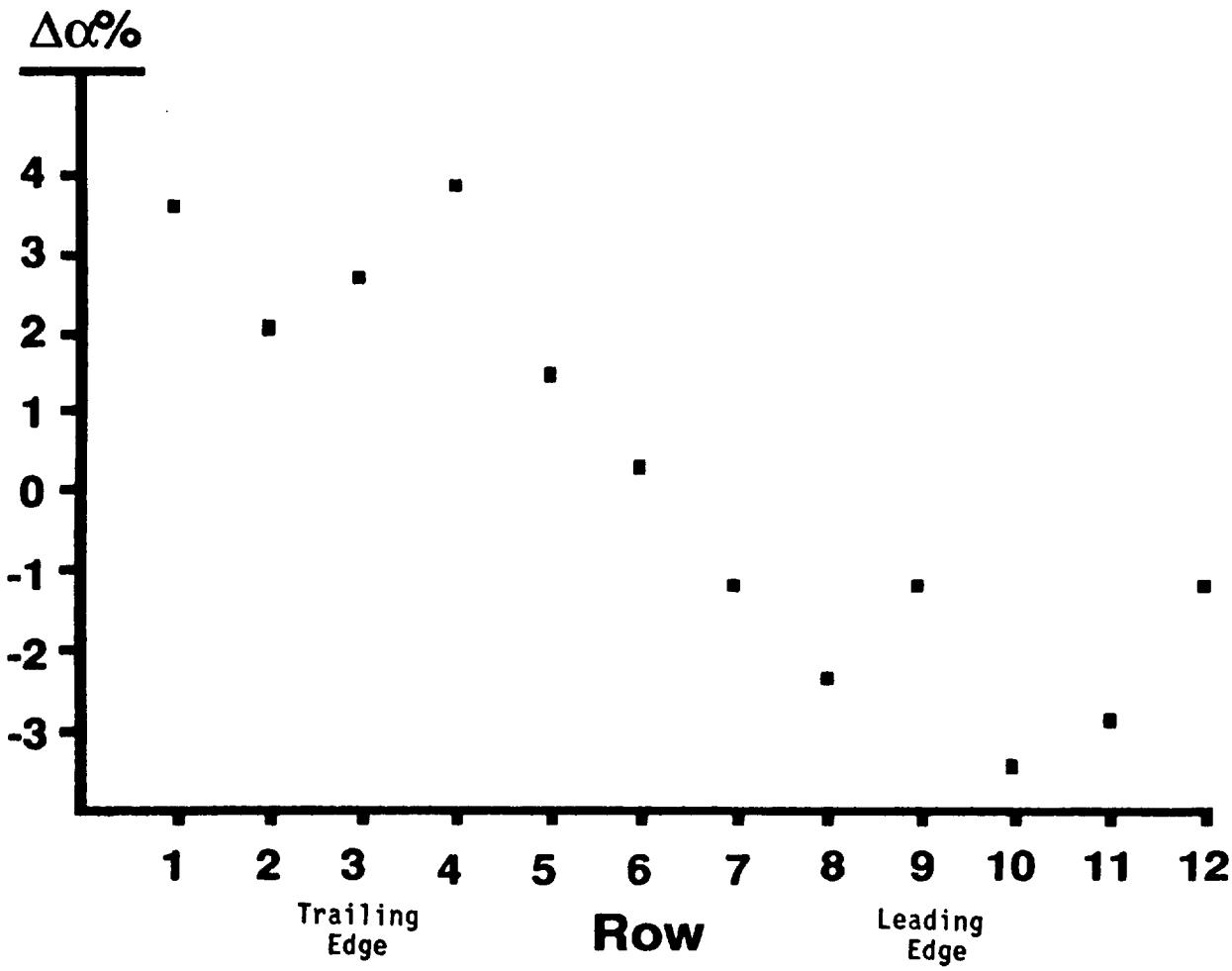

FIGURE 15. Percent change in solar absorptance as a function of position on LDEF

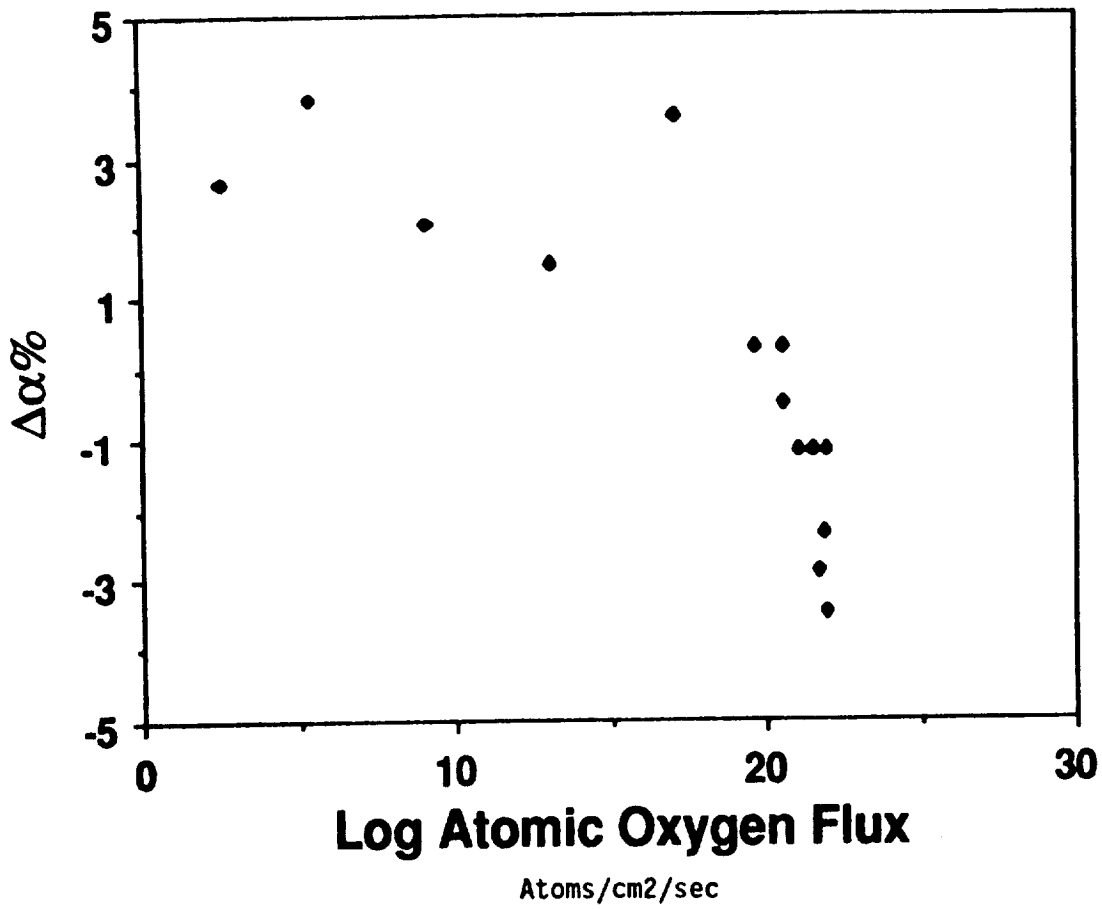

FIGURE 16. Percent change in solar absorptance as a function of atomic oxygen flux

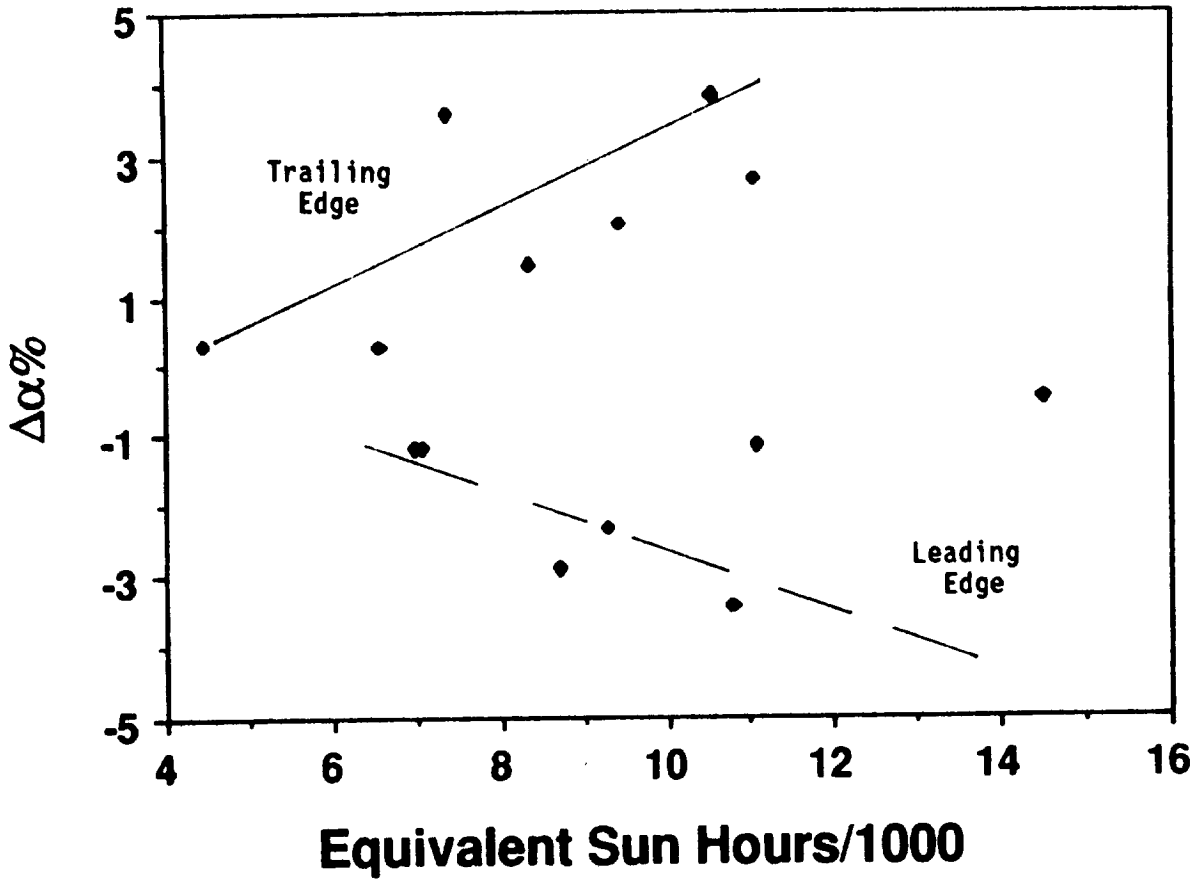

FIGURE 17. Percent change in solar absorptance as a function of equivalent sun hours

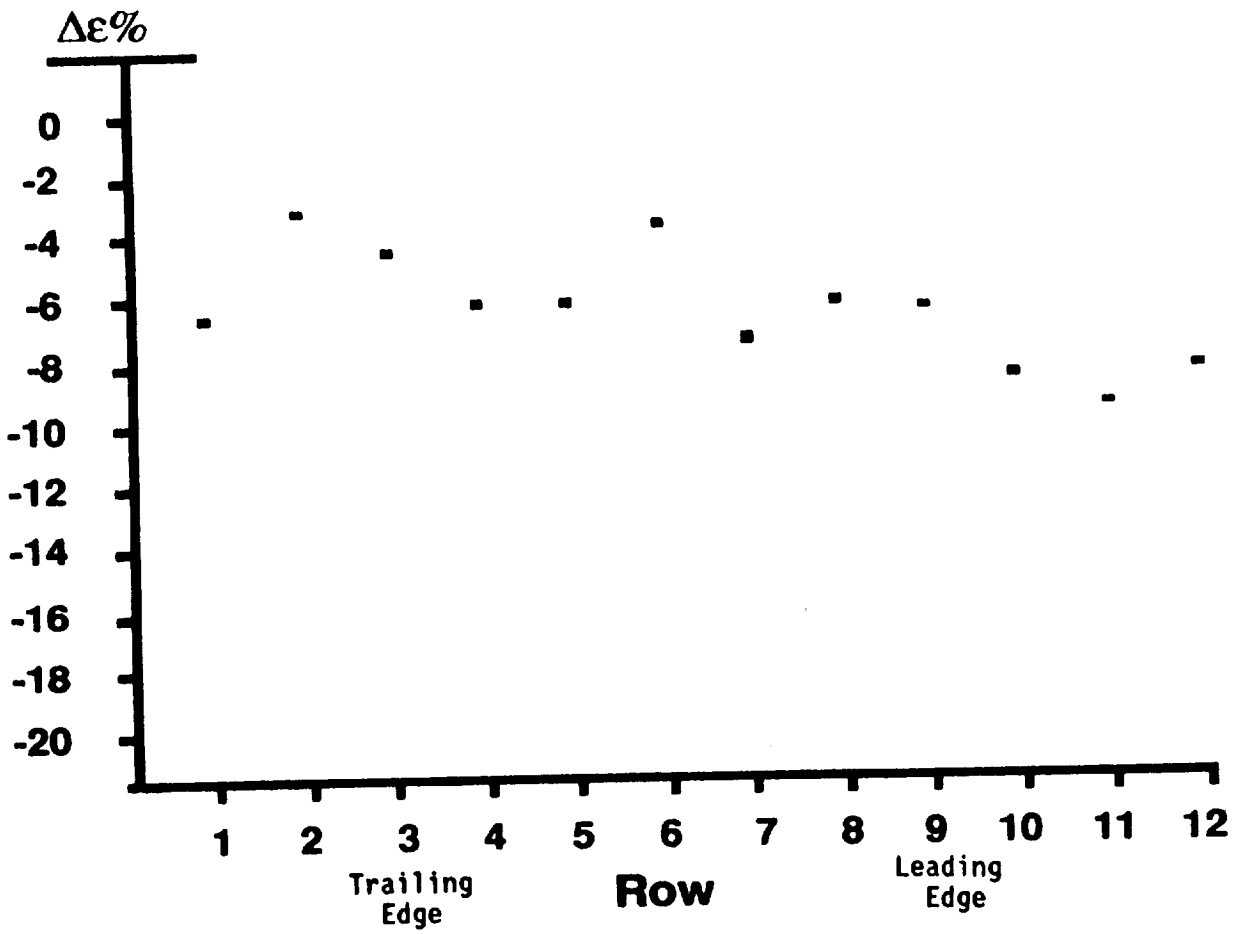

FIGURE 18. Percent change in thermal emittance as a function of position on LDEF

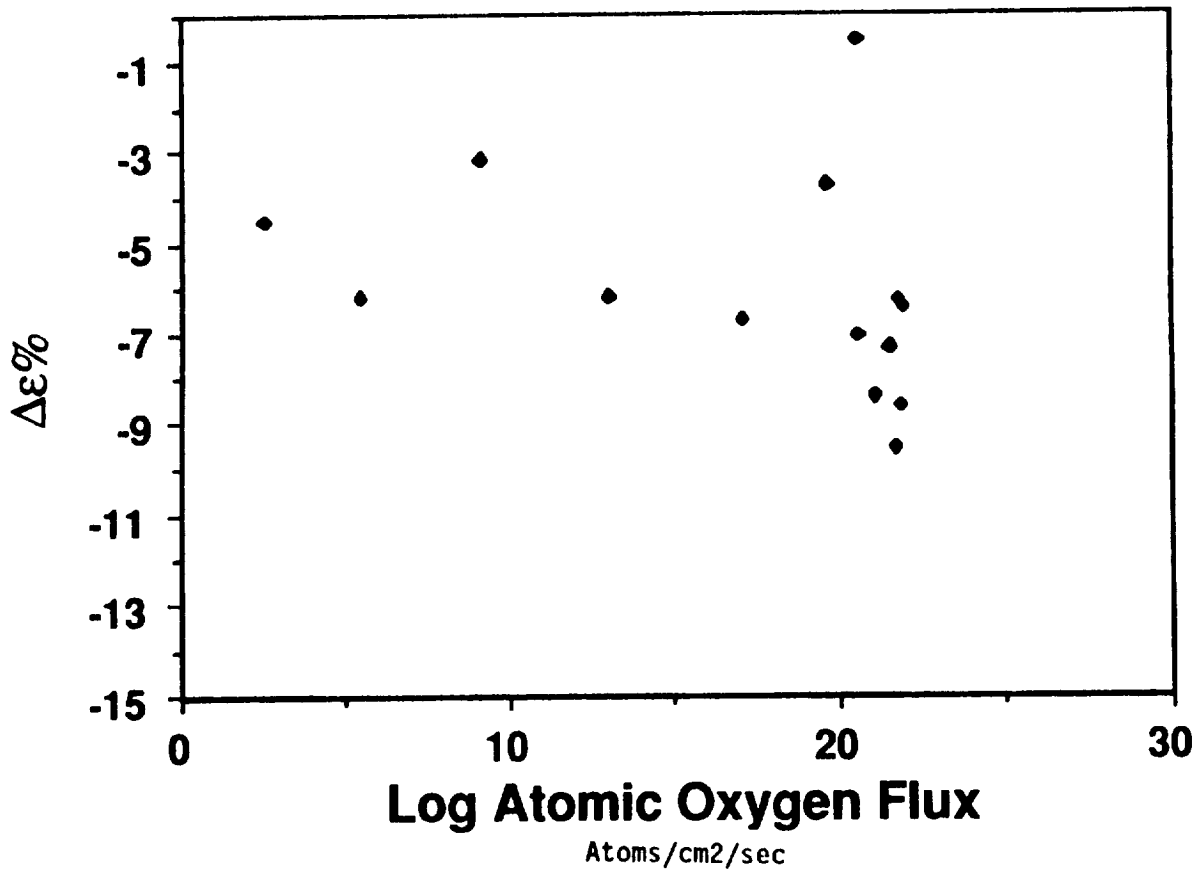

FIGURE 19. Percent chance in thermal emittance as a function of atomic oxygen flux

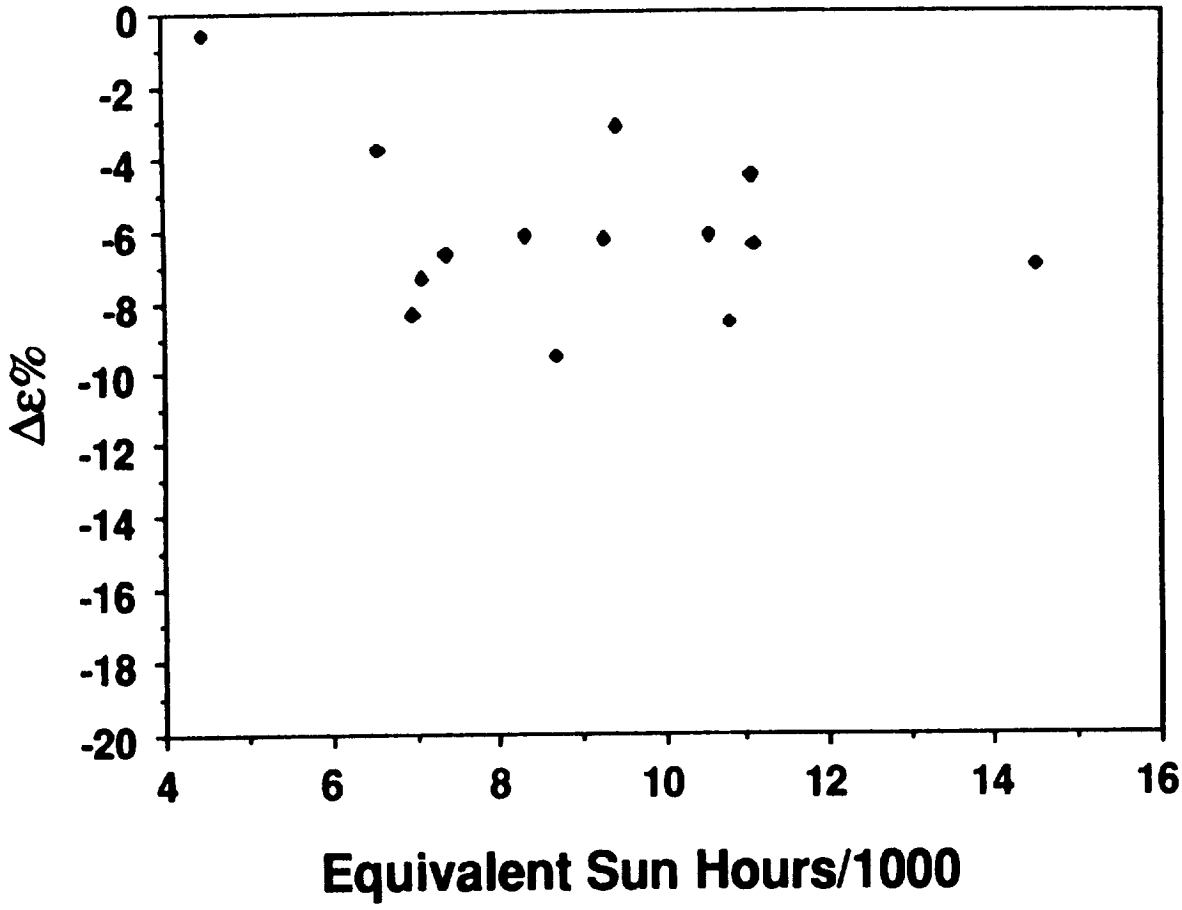

FIGURE 20. Percent change in thermal emittance as a function of equivalent sun hours

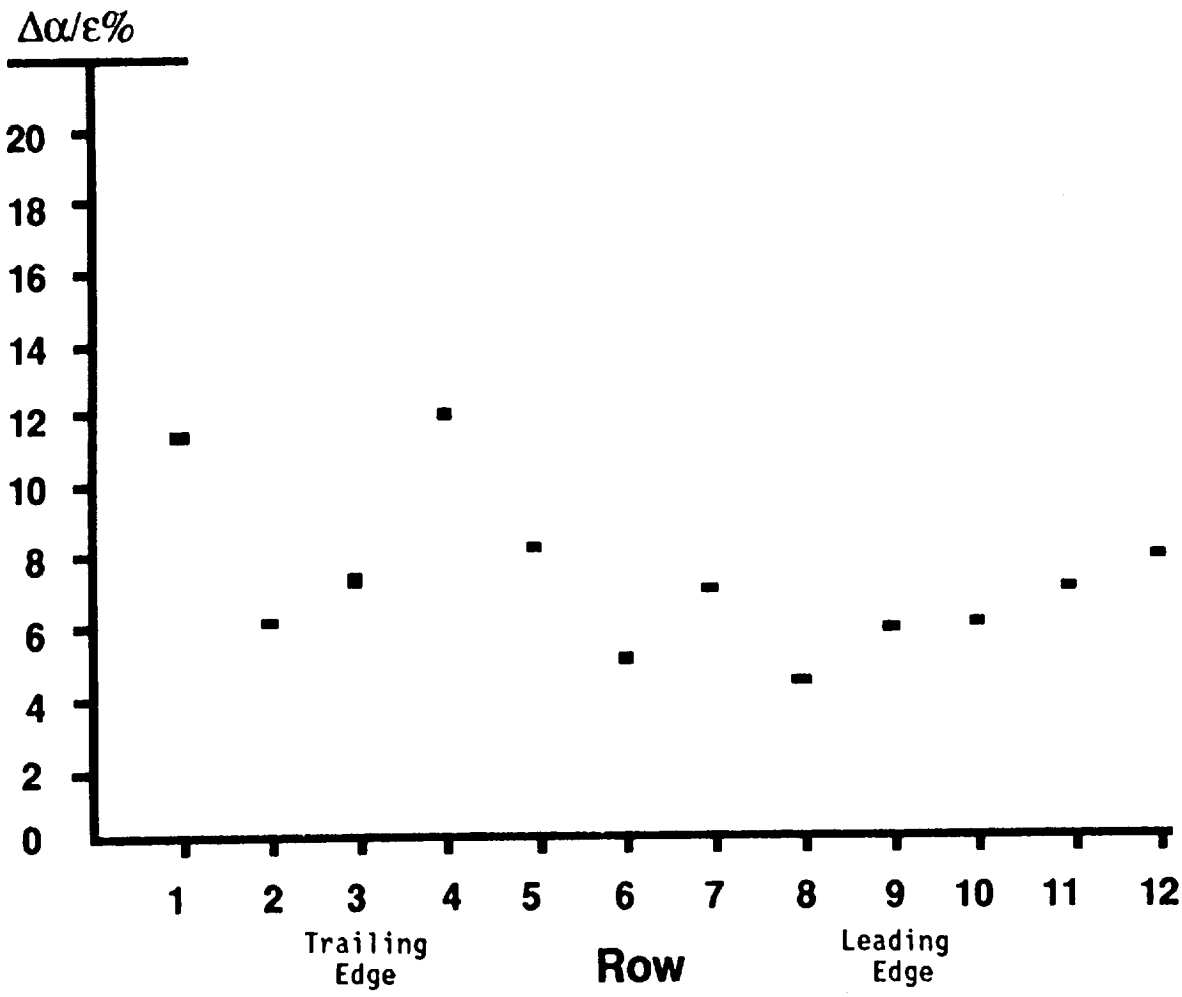

FIGURE 21. Percent change in α/ε ratio as a function of position on LDEF

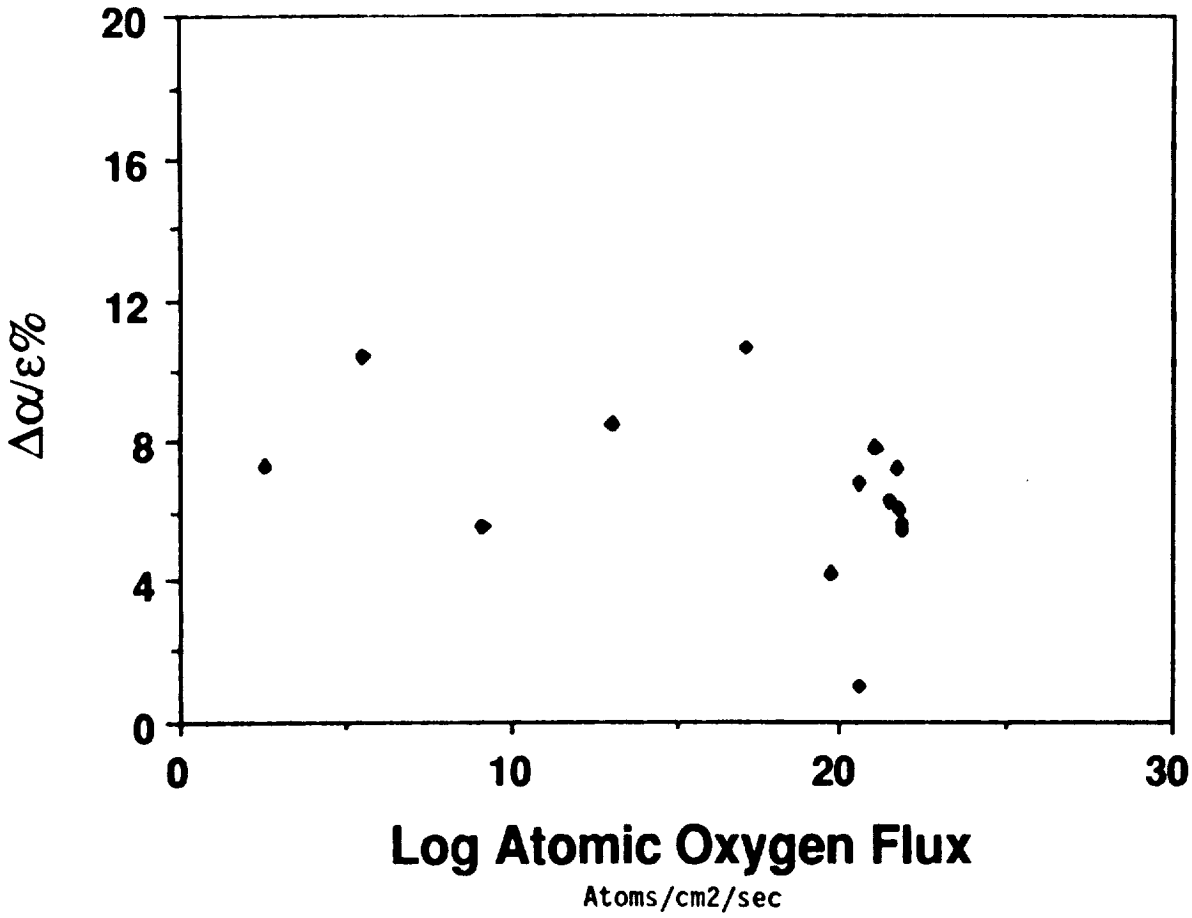

FIGURE 22. Percent change in α/ε ratio as a function of atomic oxygen flux

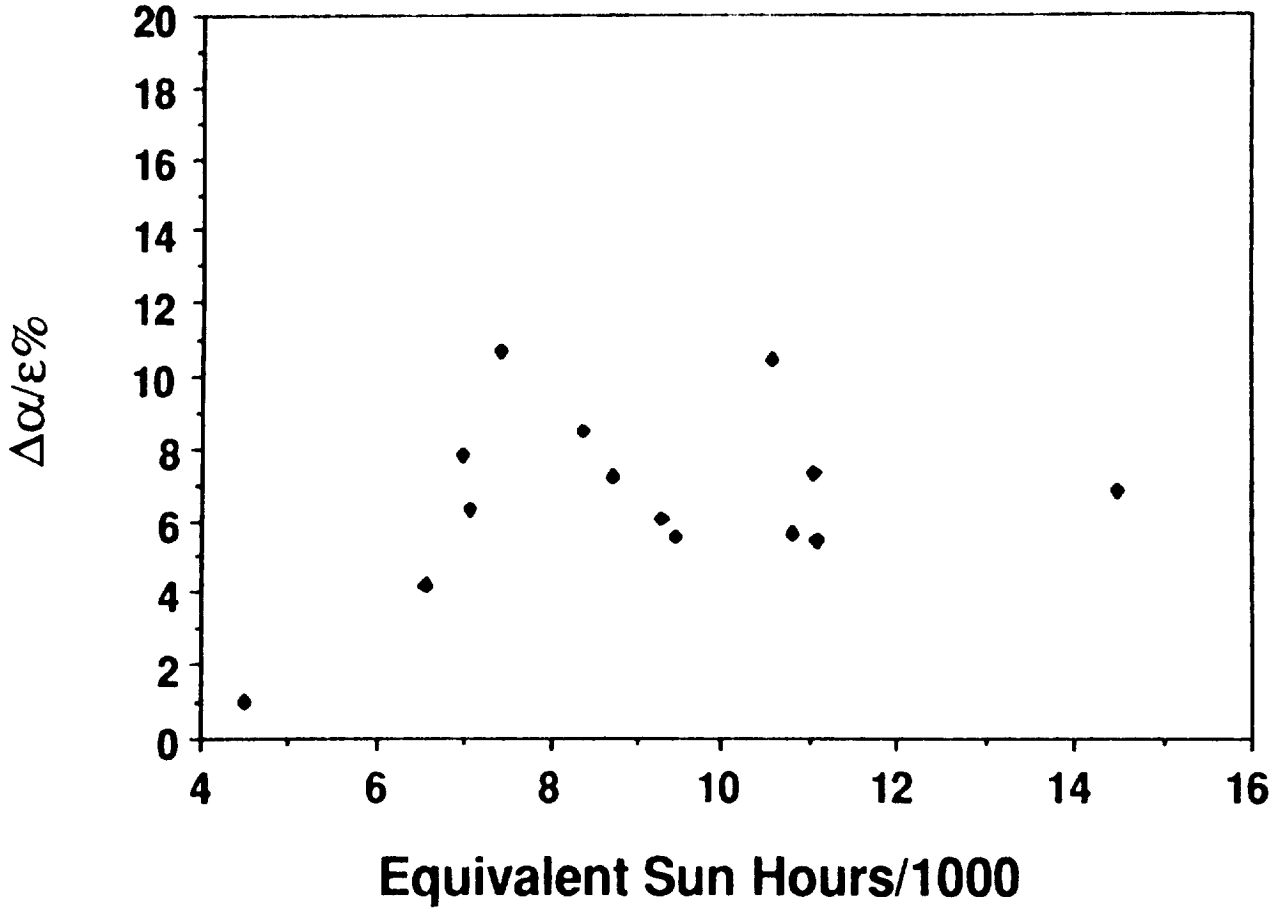

FIGURE 23. Percent change in α/ε ratio as a function of equivalent sun hours

APPENDIX A

Reflectance Spectra

EARTH END

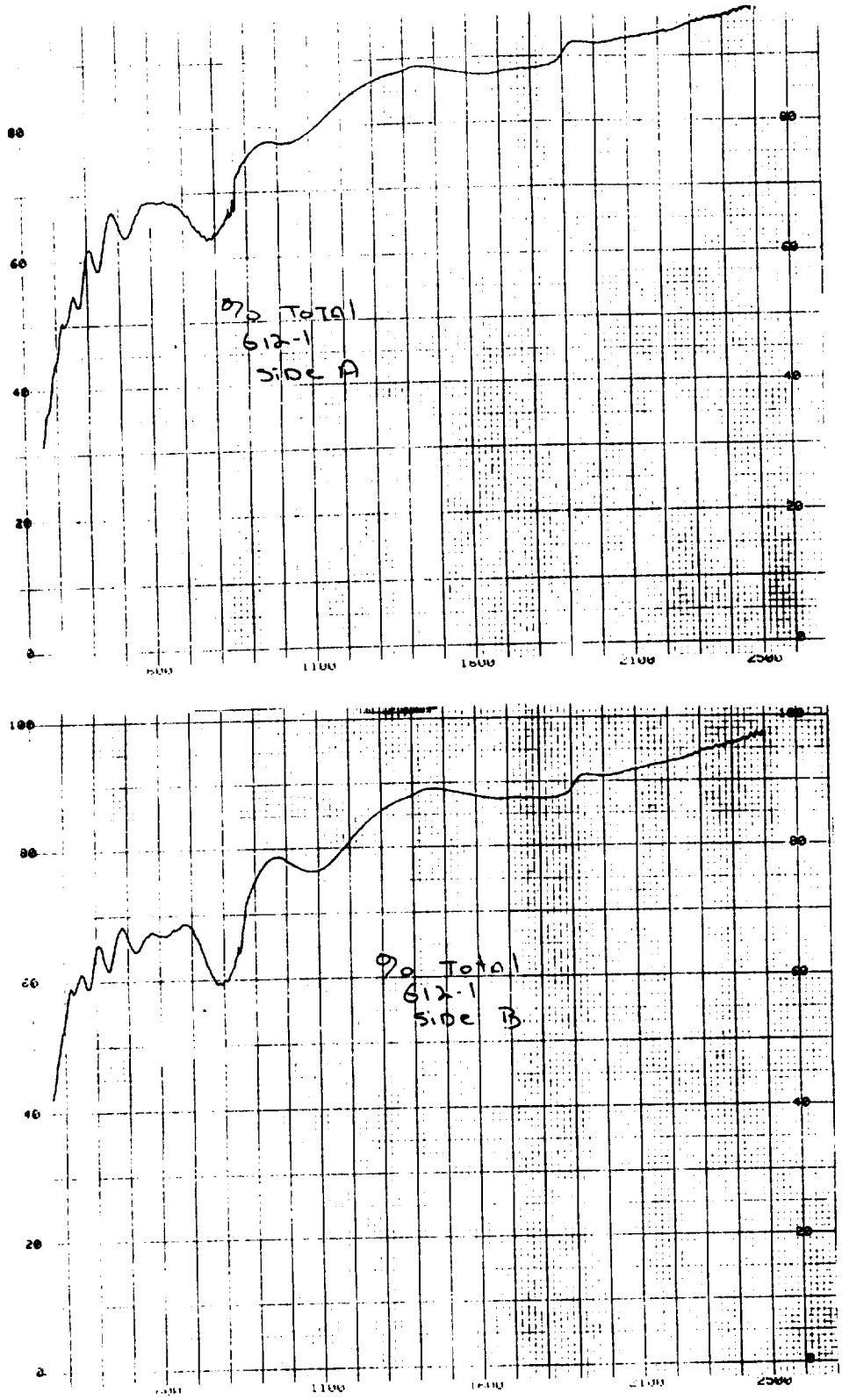

Figure A1: UV-Vis/NIR Total Reflectance of clamp G12-1, (A) Front (B) Back.

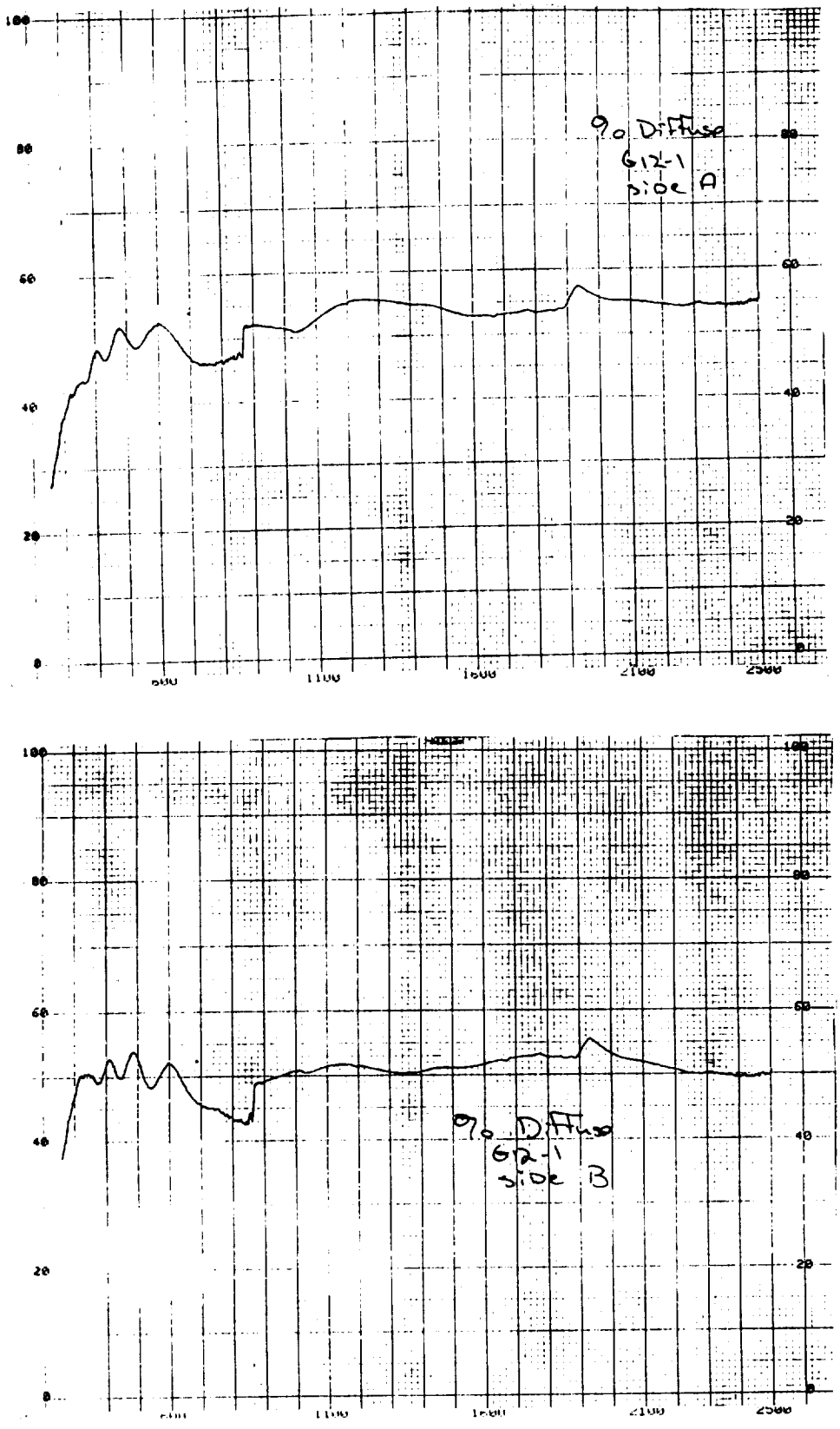

Figure A2: UV-Vis/NIR Diffuse Reflectance of Clamp G12-1, (A) Front (B) Back

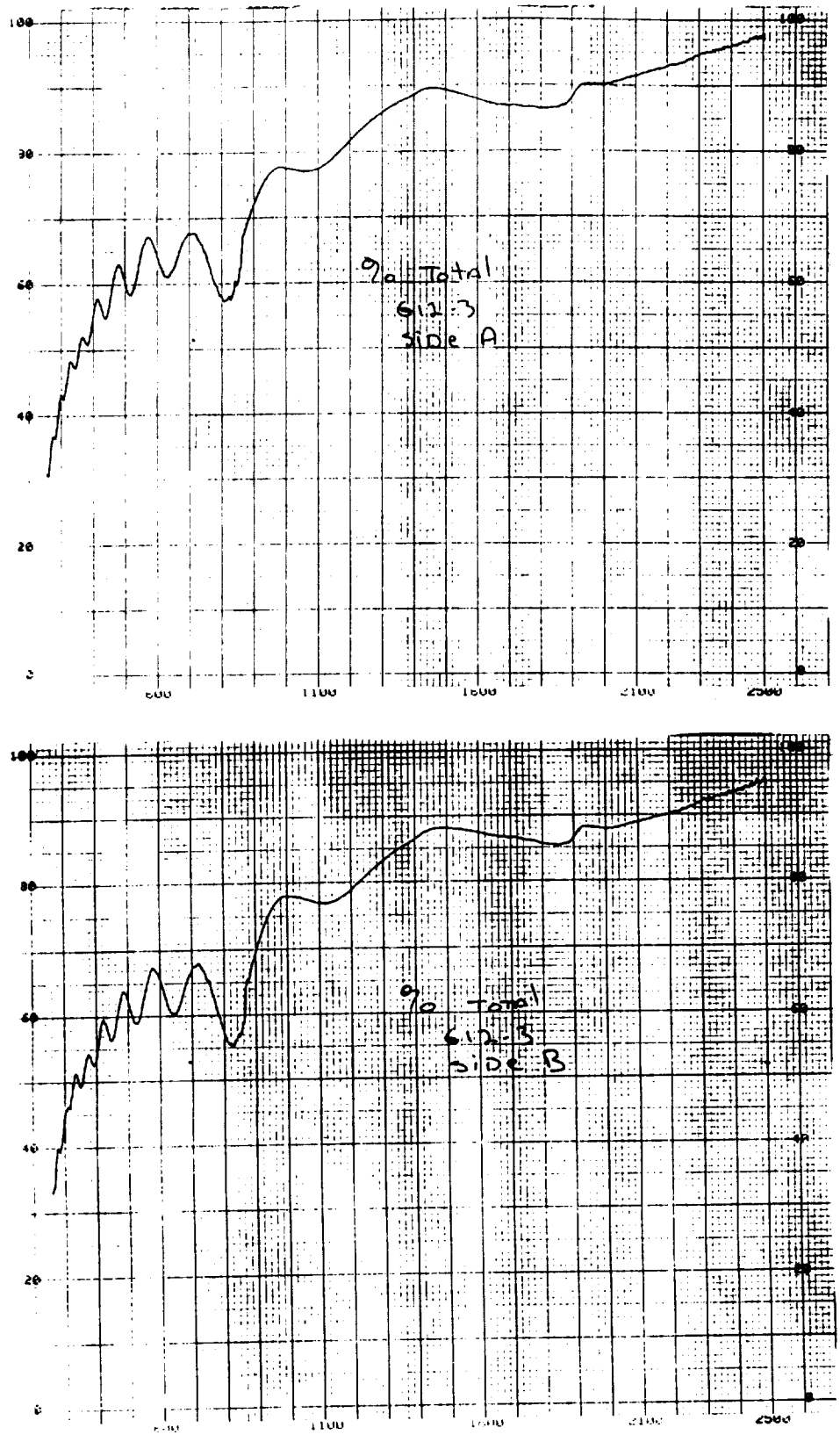

Figure A3: UV-Vis/NIR Total Reflectance of clamp G12-3, (A) Front (B) Back.

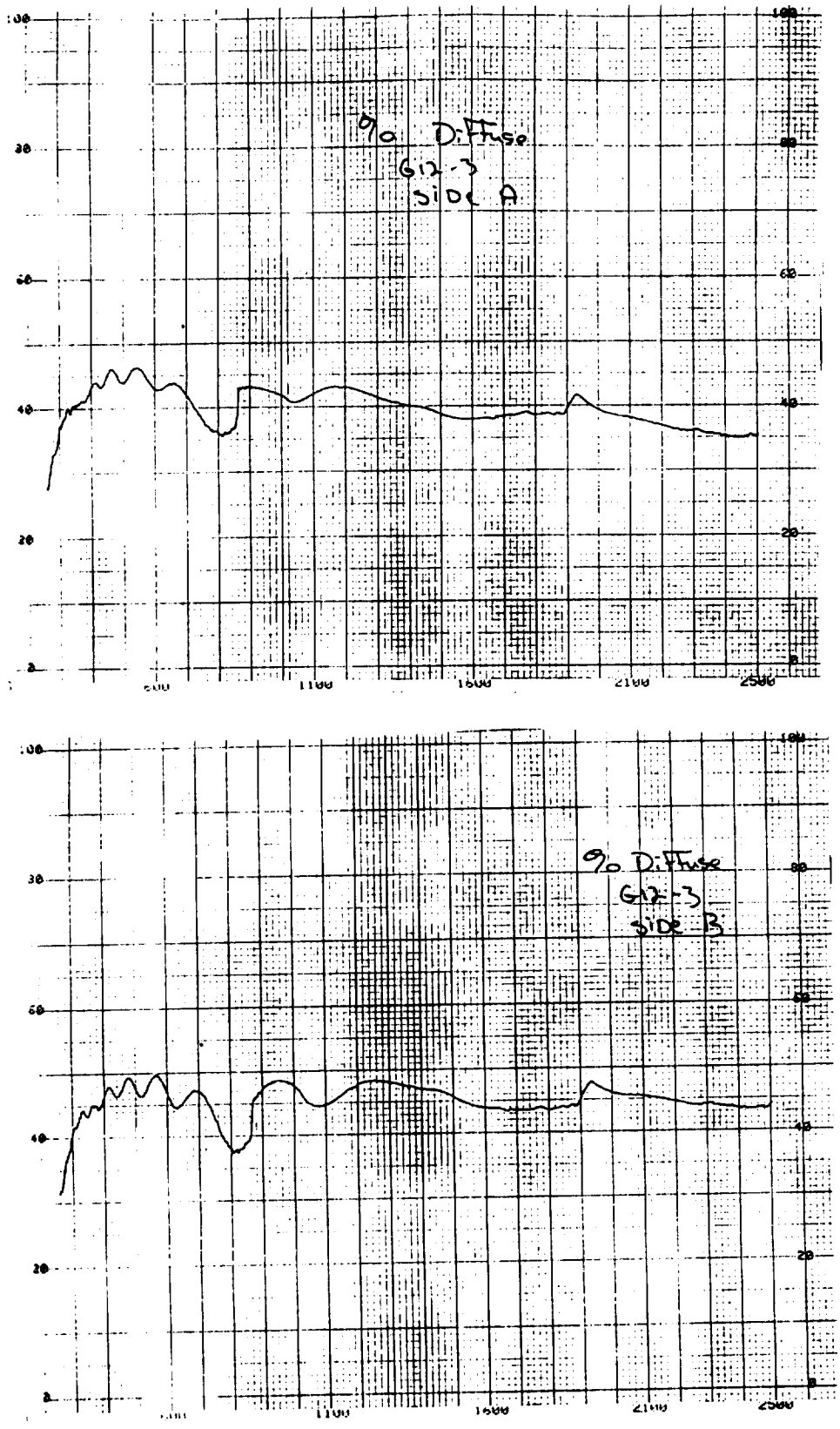

Figure A4: UV-Vis/NIR Diffuse Reflectance of clamp G12-3, (A) Front (B) Back.

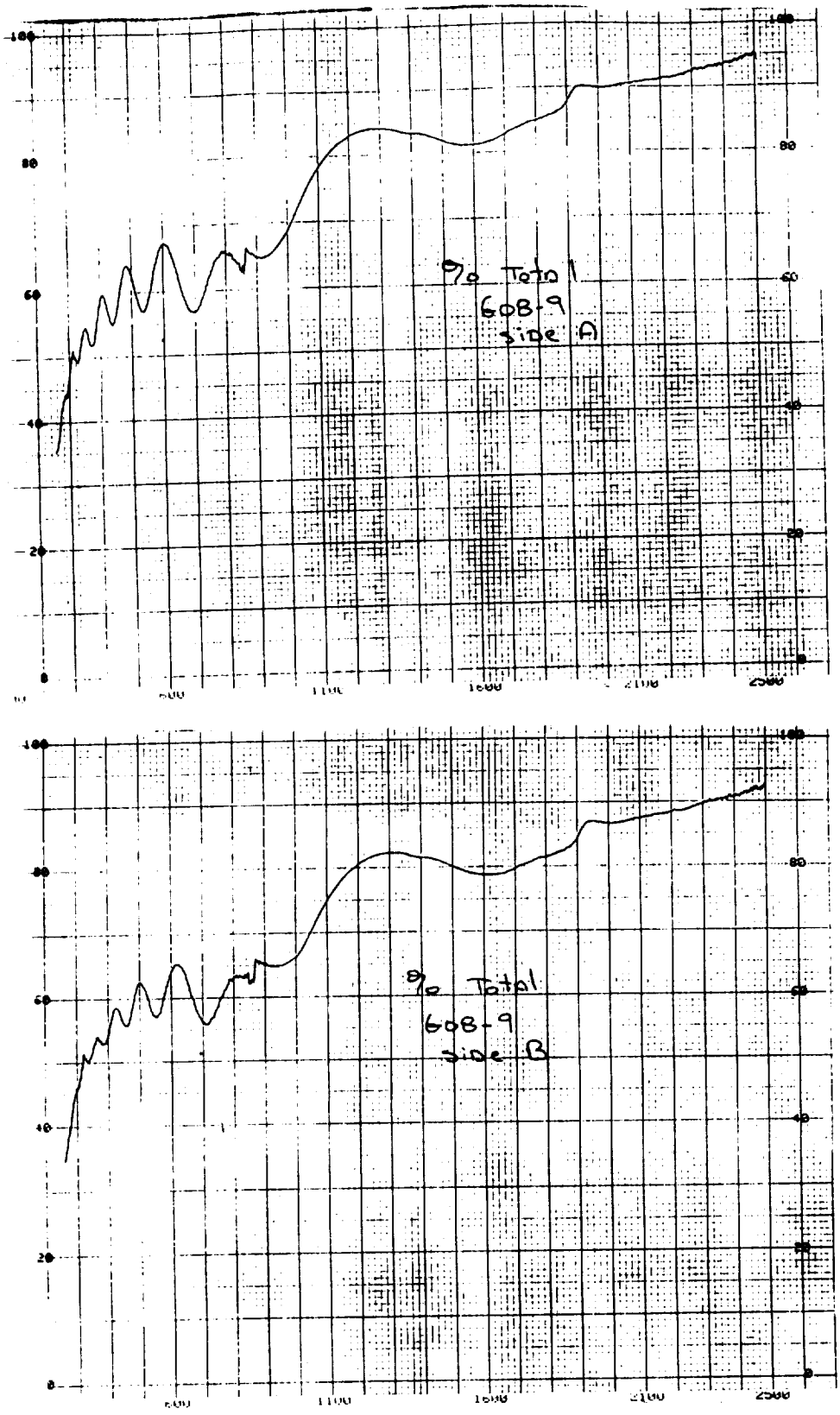

Figure A5: UV-Vis/NIR Total Reflectance of clamp G08-9, (A) Front (B) Back.

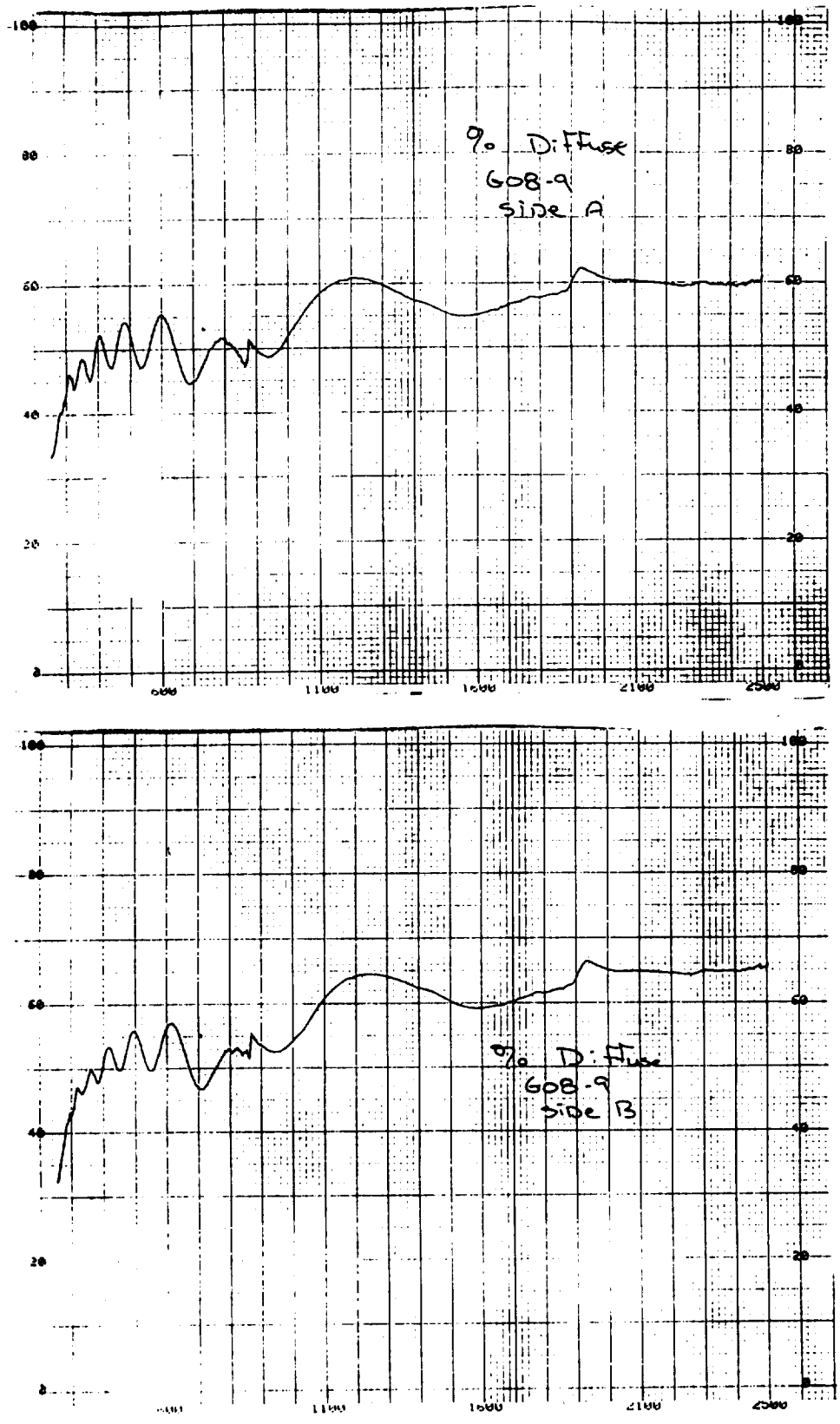

Figure A6: UV-Vis/NIR Diffuse of clamp G08-9, (A) Front (B)Back.

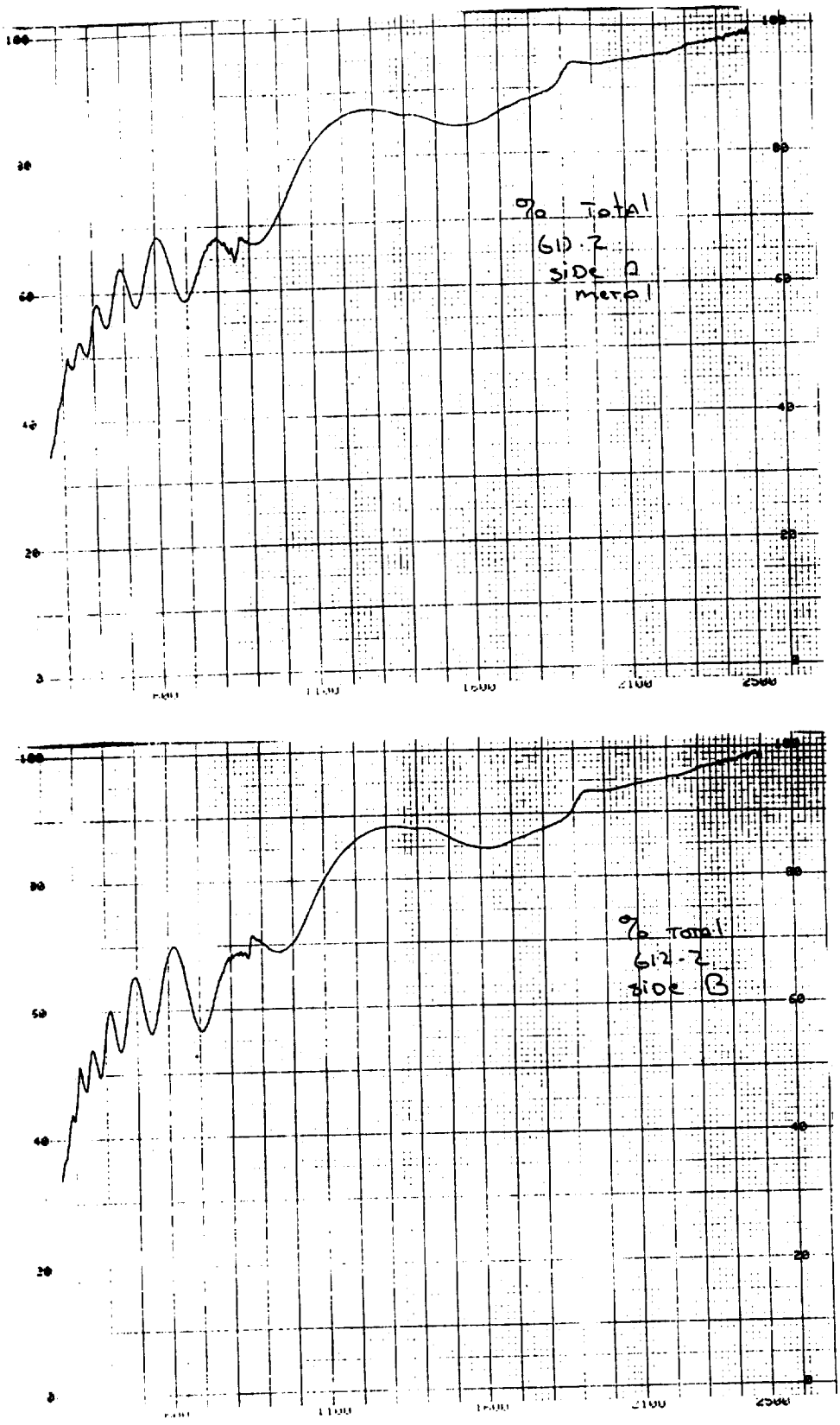

Figure A7: UV-Vis/NIR Total Reflectance of clamp G12-2, (A) Front (B)Back.

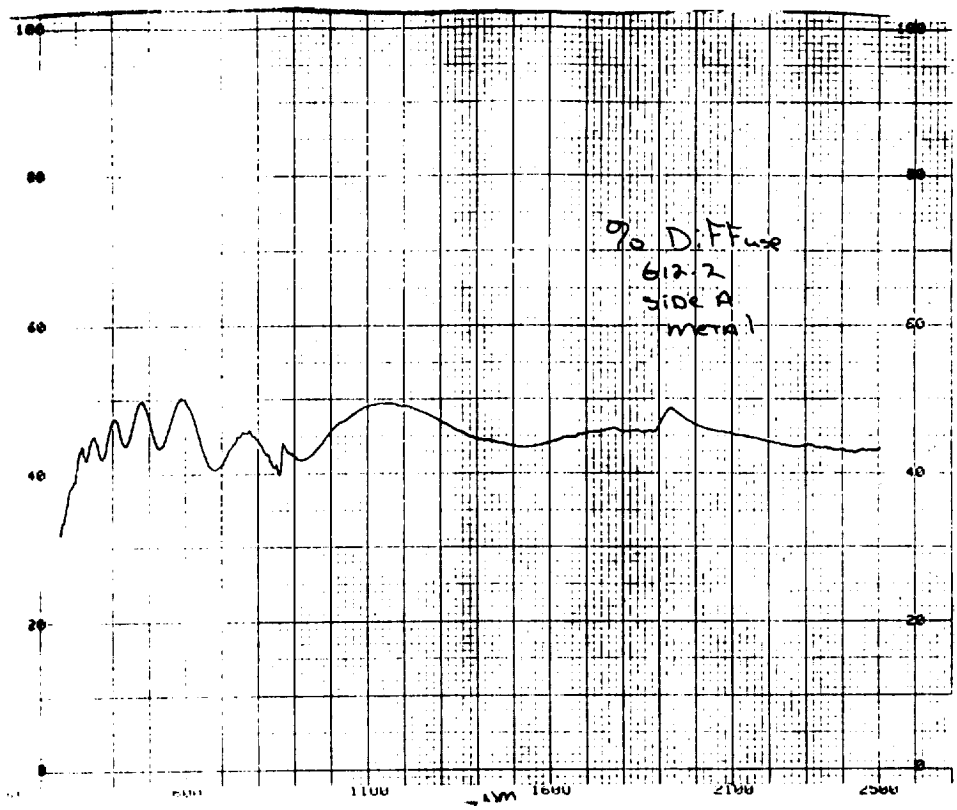

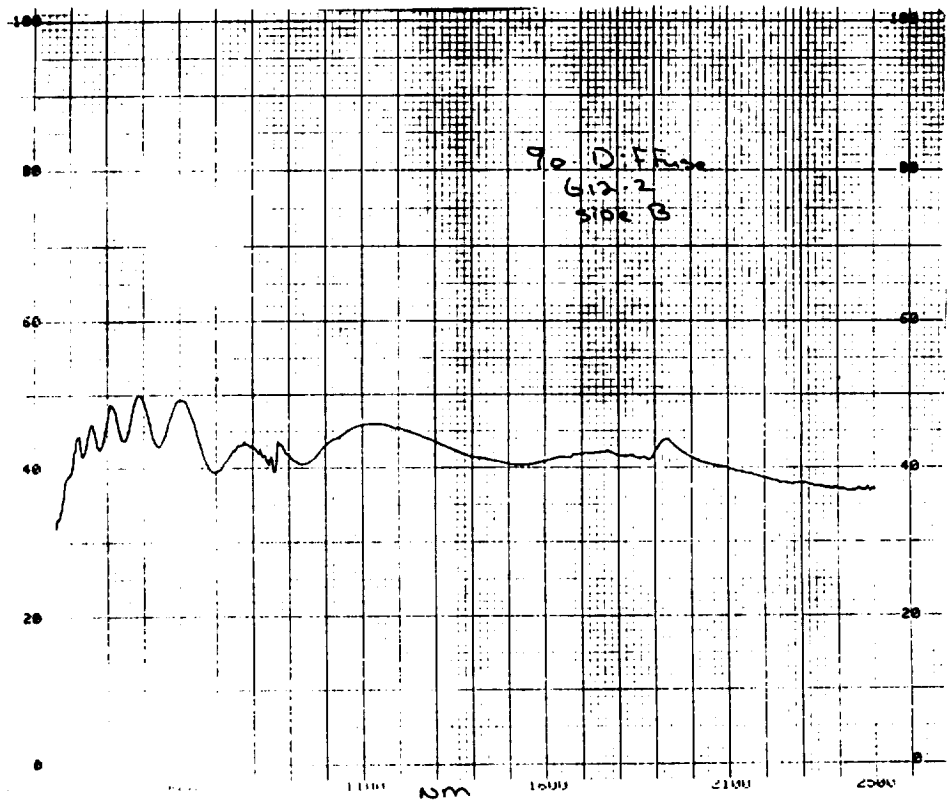

Figure A8: UV-Vis/NIR Diffuse Reflectance of clamp G12-2, (A) Front (B) Back.

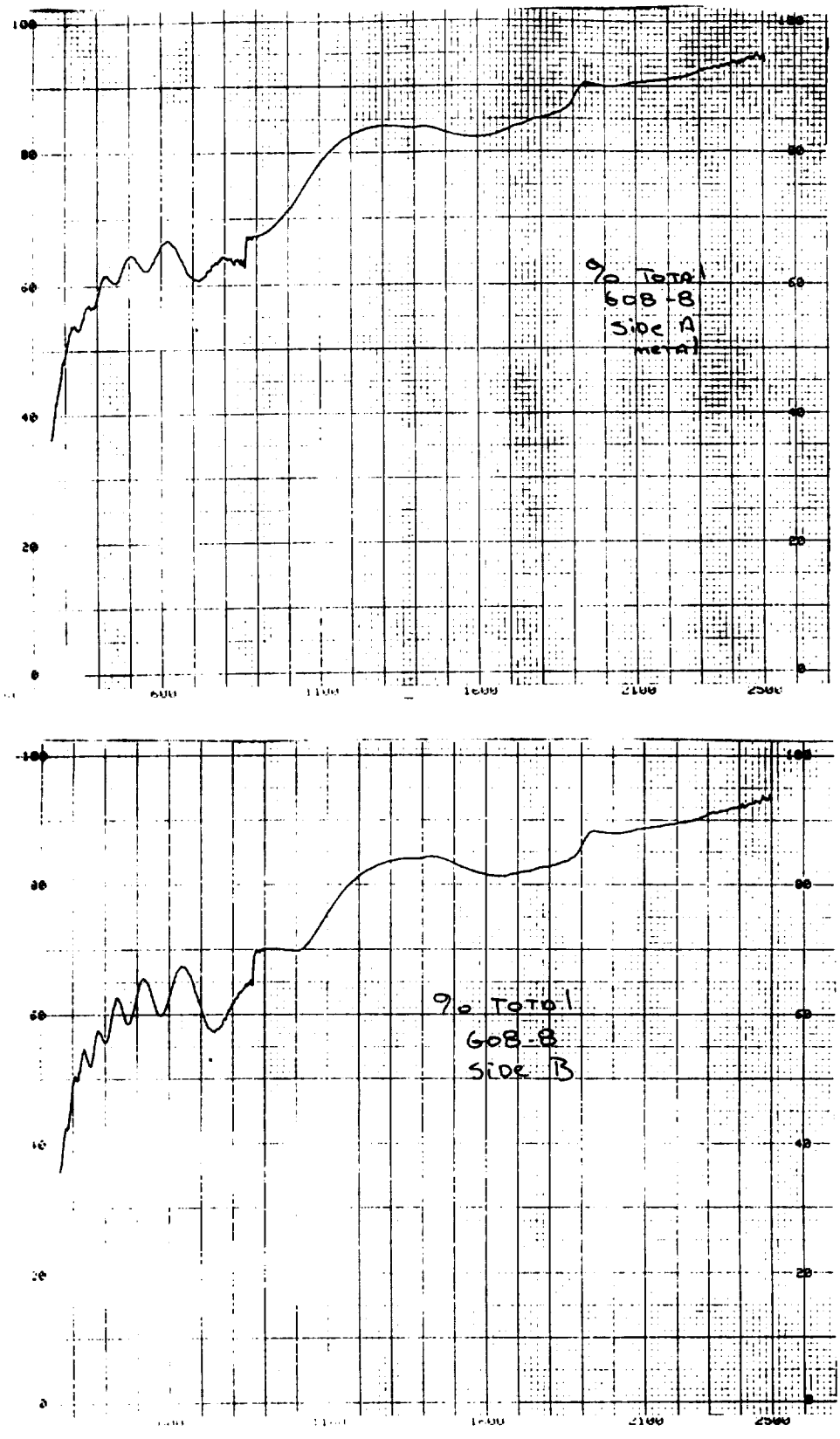

Figure A9: UV-Vis/NIR Total Reflectance of clamp G08-8, (A) Front (B) Back.

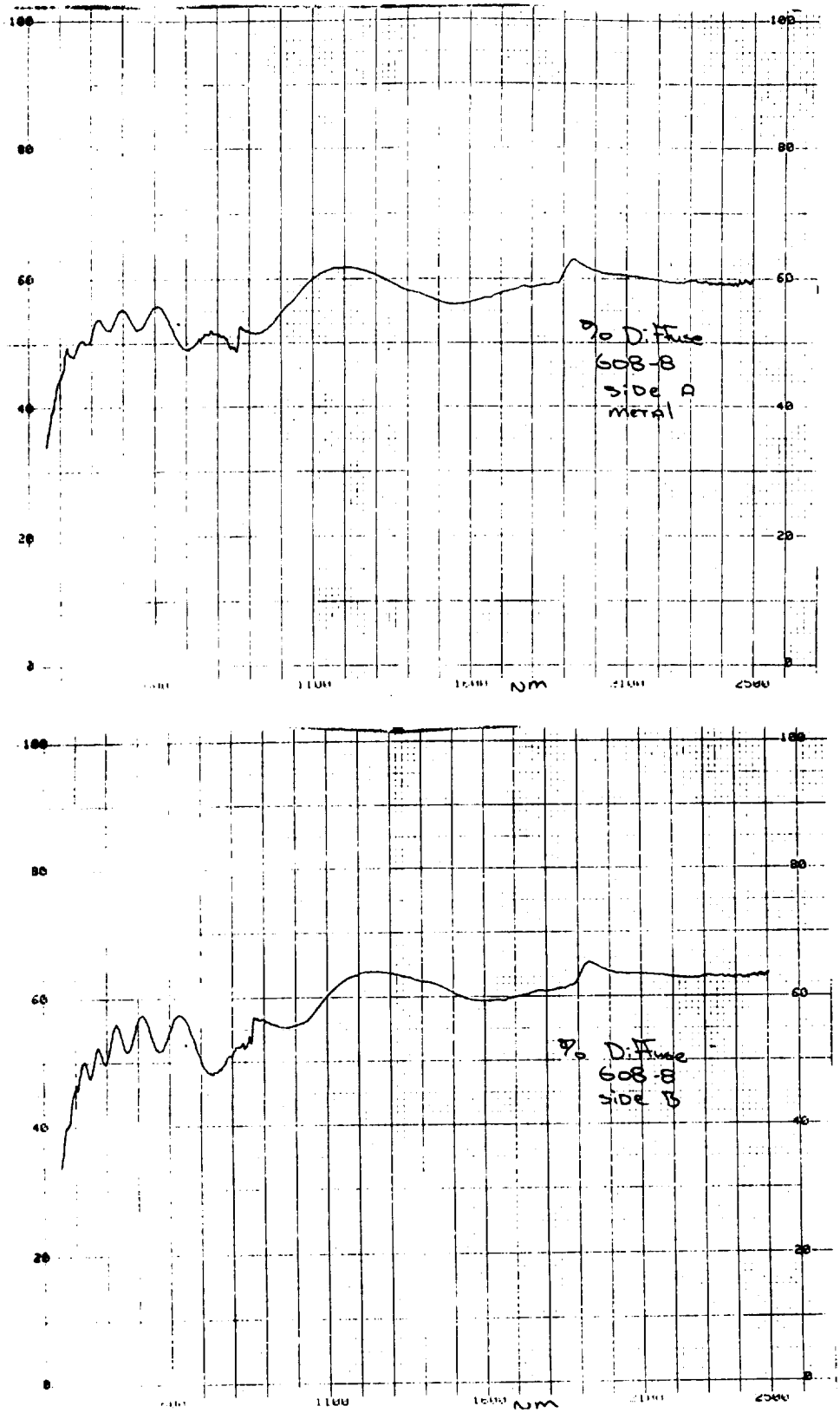

Figure A10: UV-Vis/NIR Diffuse Reflectance of clamp G08-8, (A) Front (B) Back.

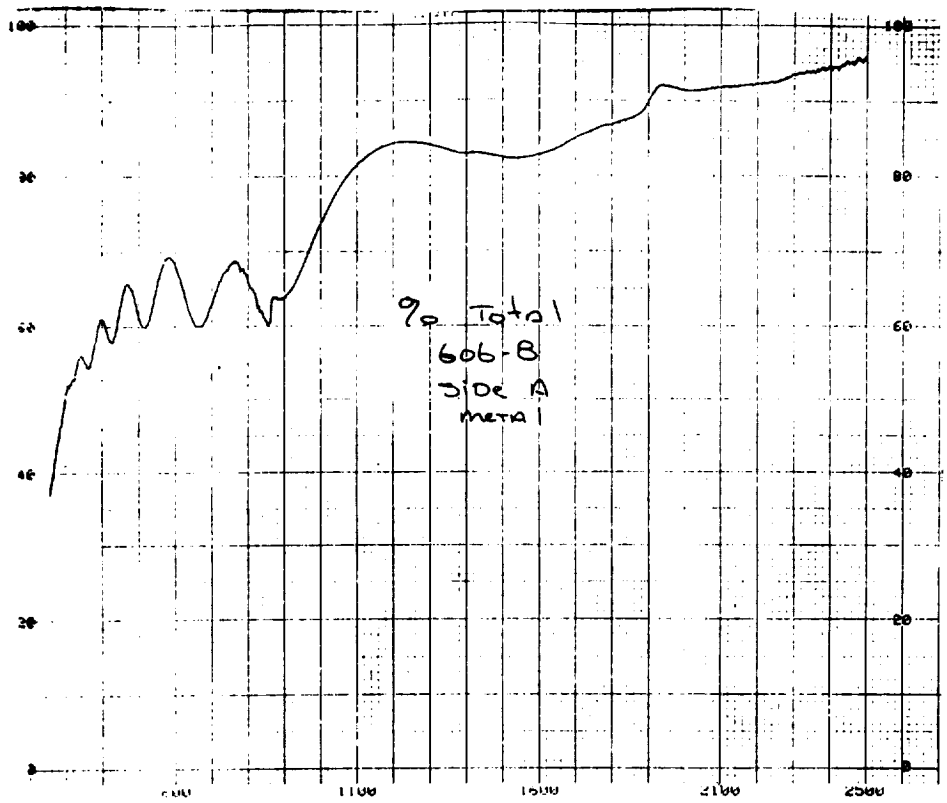

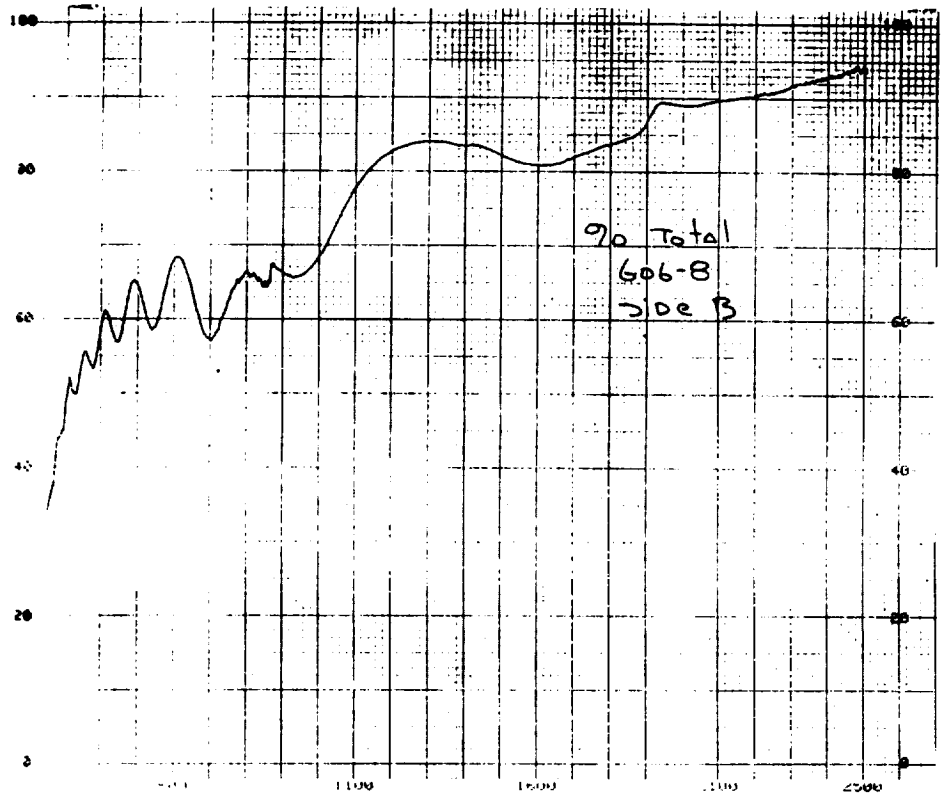

Figure A11: UV-Vis/NIR Total Reflectance of clamp G06-8, (A) Front (B) Back.

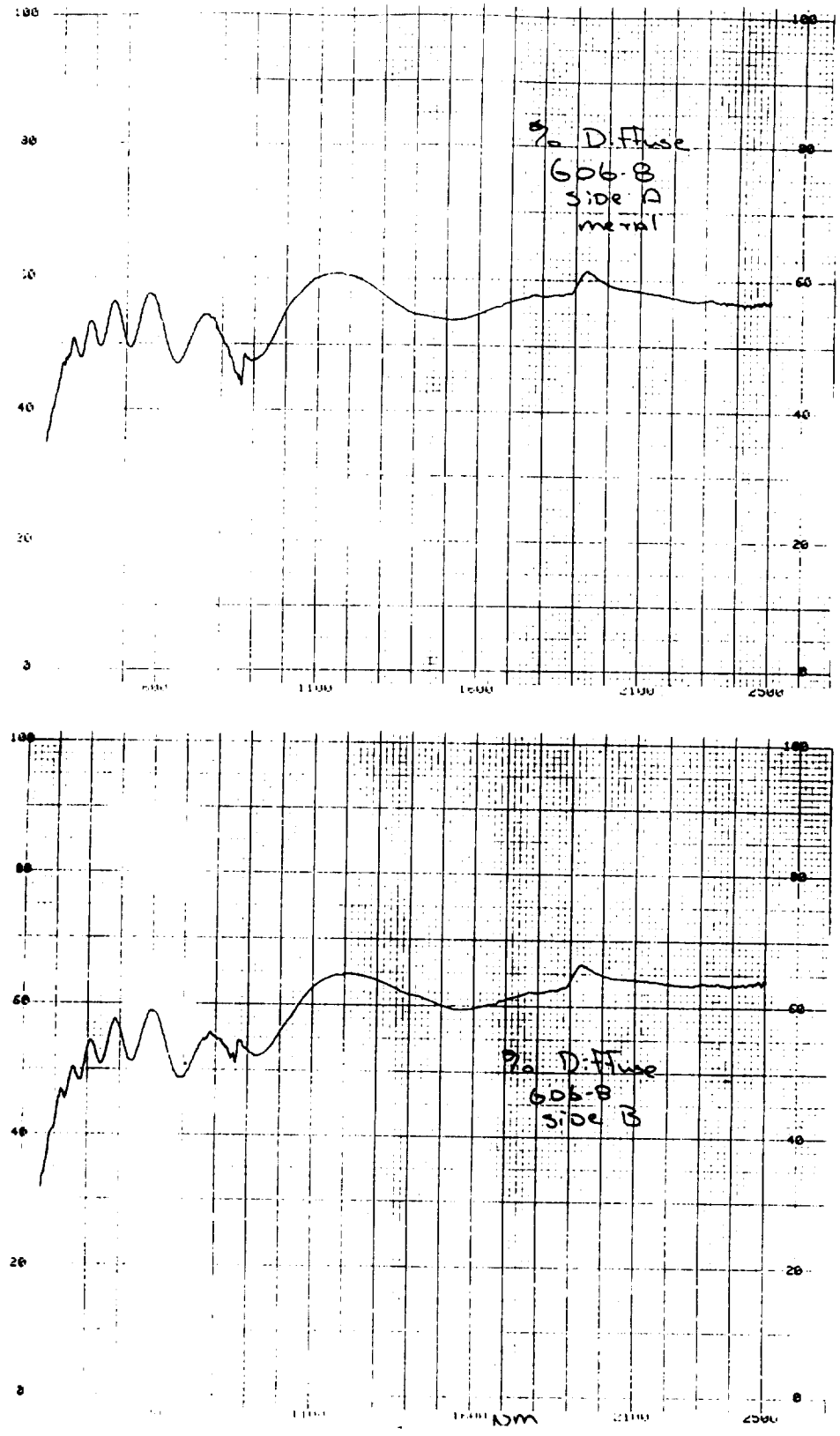

Figure A12: UV-Vis/NIR Diffuse Reflectance of clamp G06-8, (A) Front (B) Back.

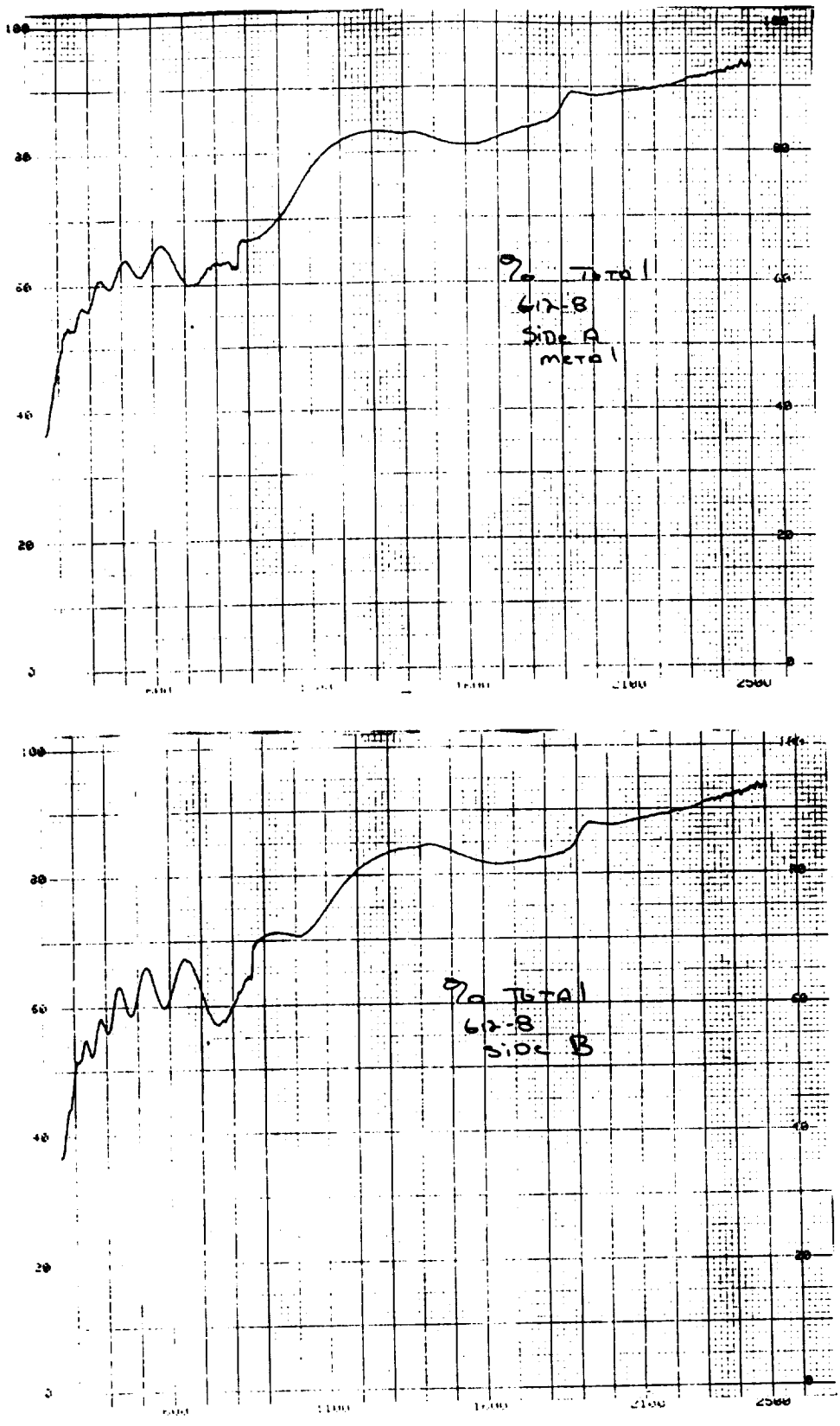

Figure A13: UV-Vis/NIR Total Reflectance of clamp G12-8, (A) Front (B) Back.

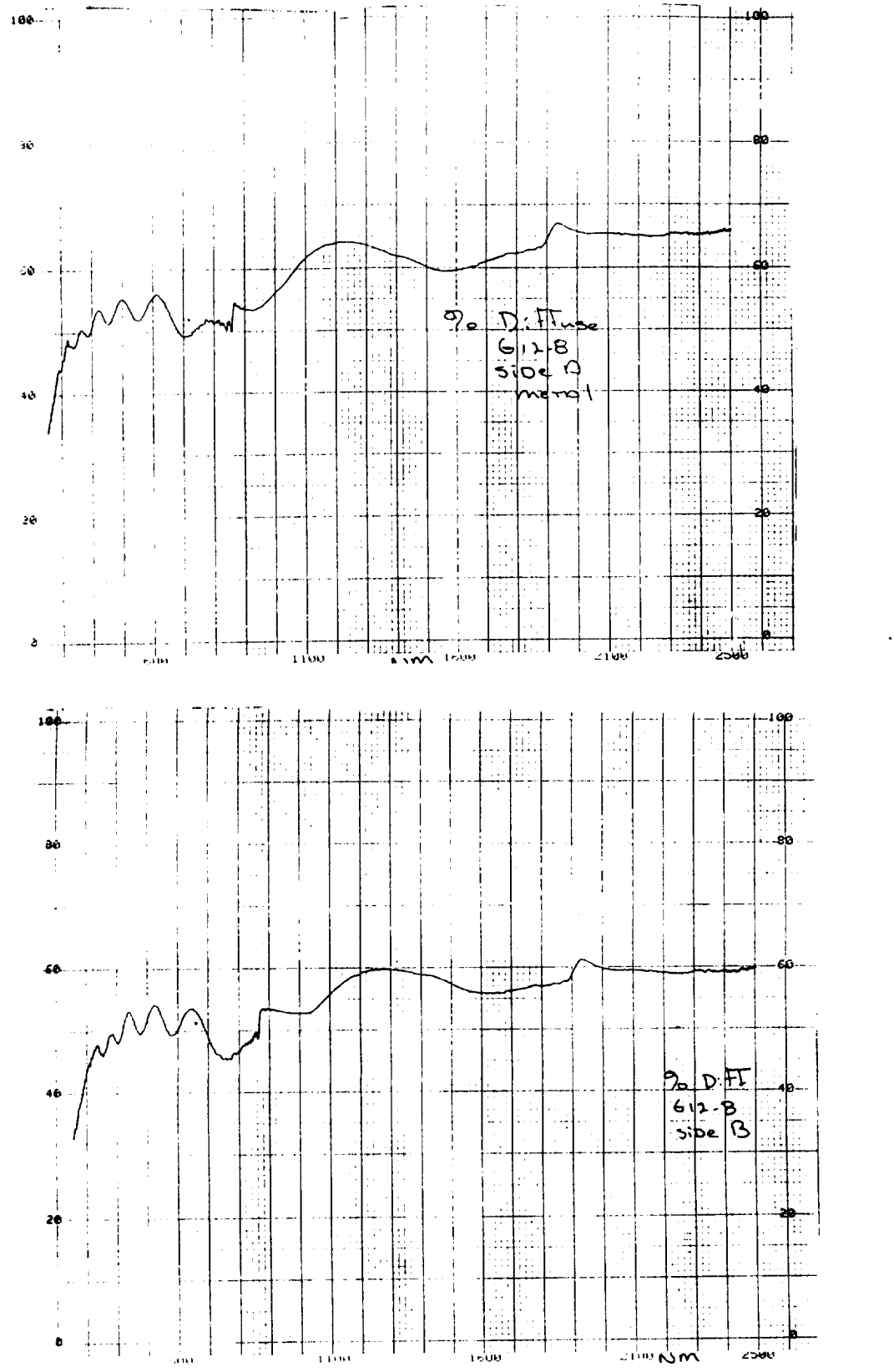

Figure A14: UV-Vis/NIR Diffuse Reflectance of clamp G12-8, (A) Front (B) Back.

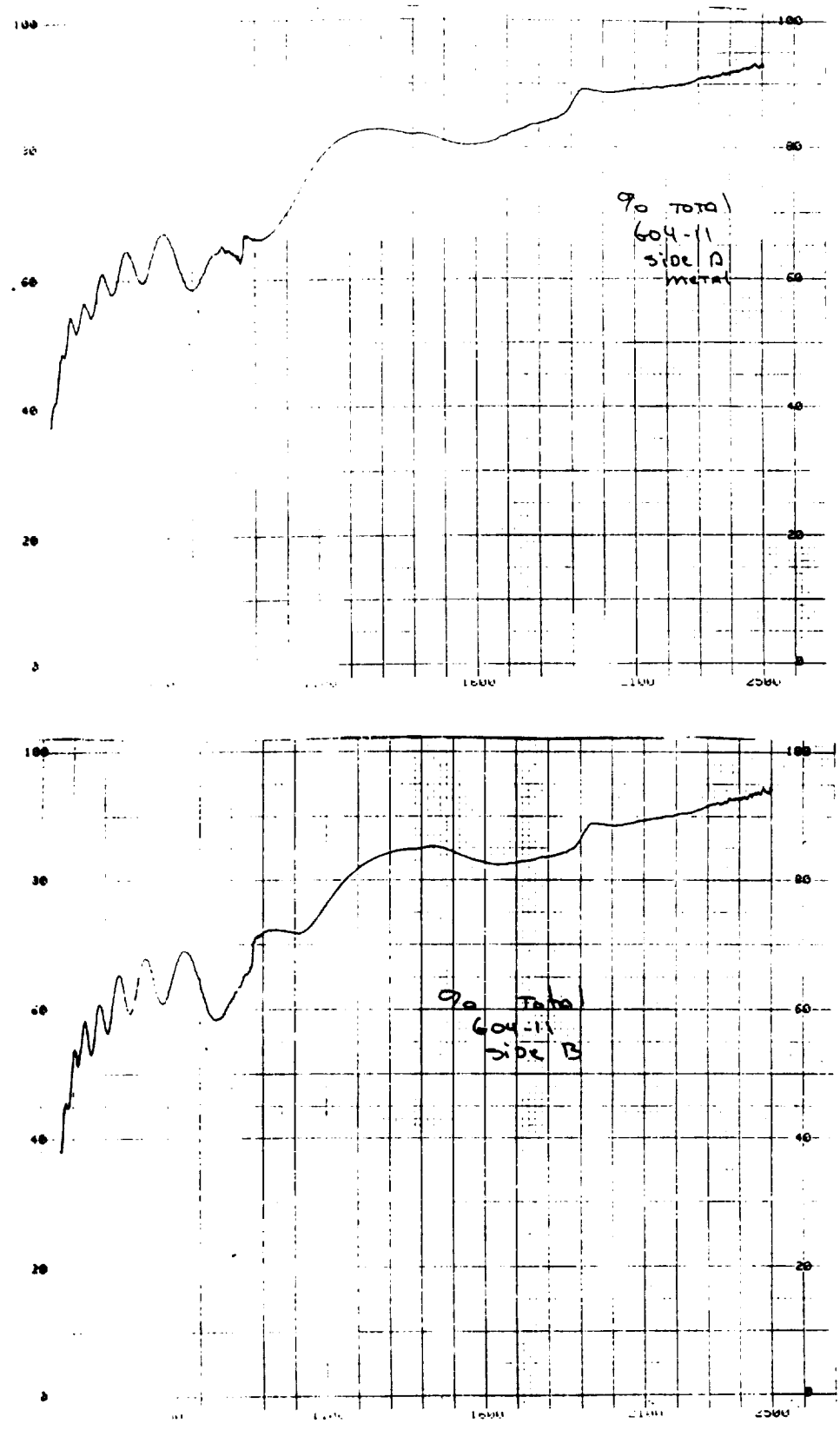

Figure A15: UV-Vis/NIR Total Reflectance of clamp G04-11, (A) Front (B) Back

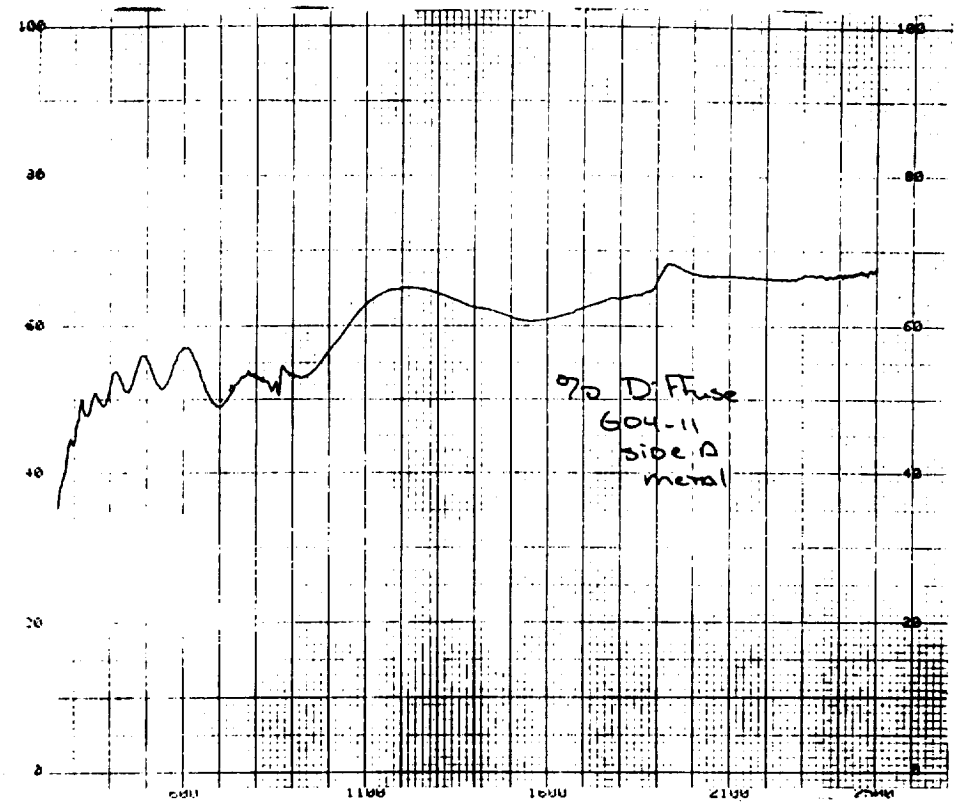

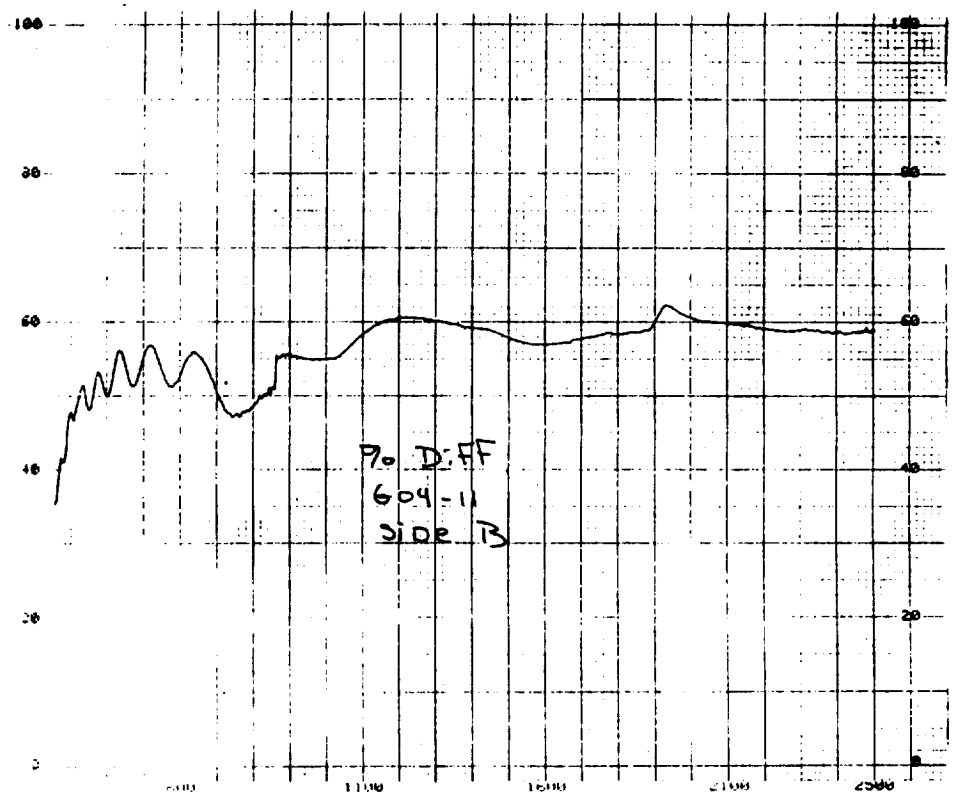

Figure A16: UV-Vis/NIR Diffuse Reflectance of clamp G04-11 (A) Front (B) Back

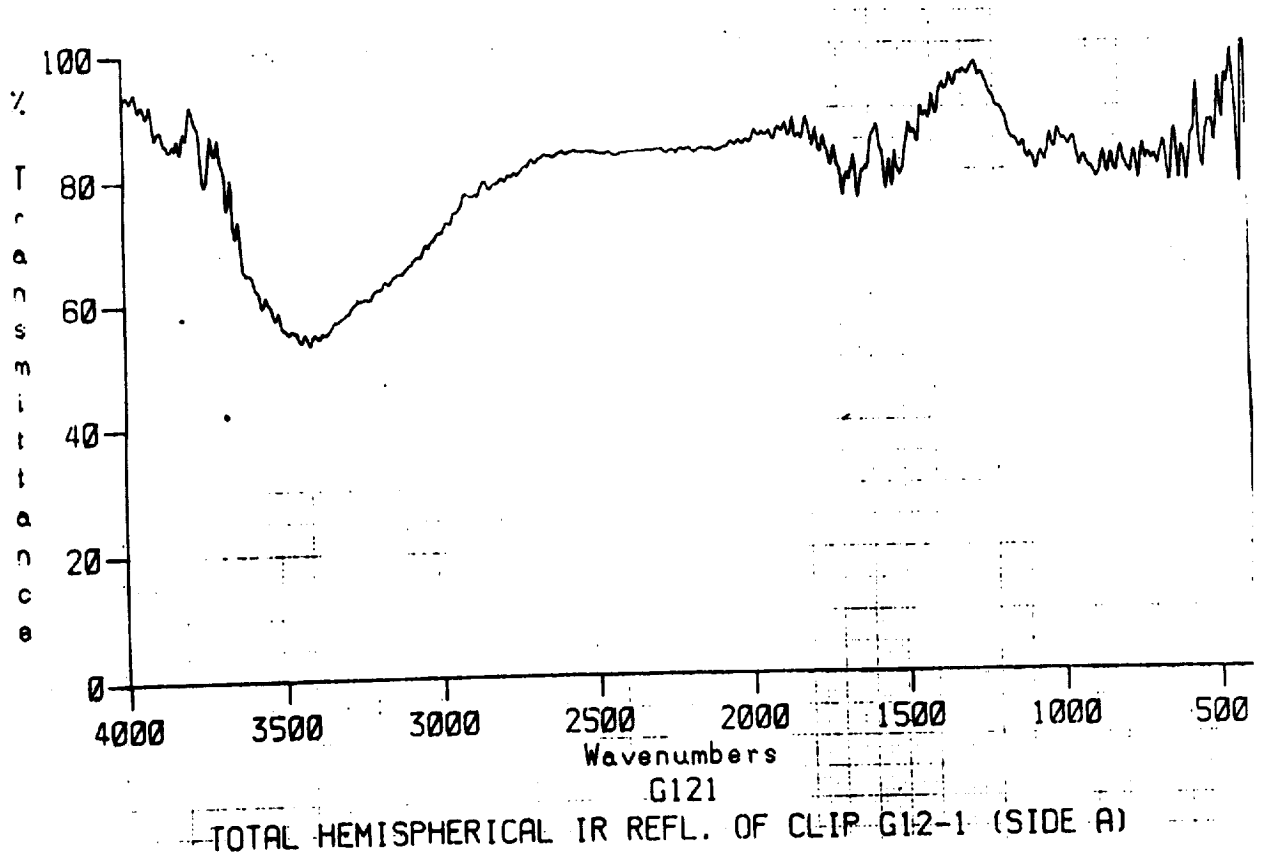

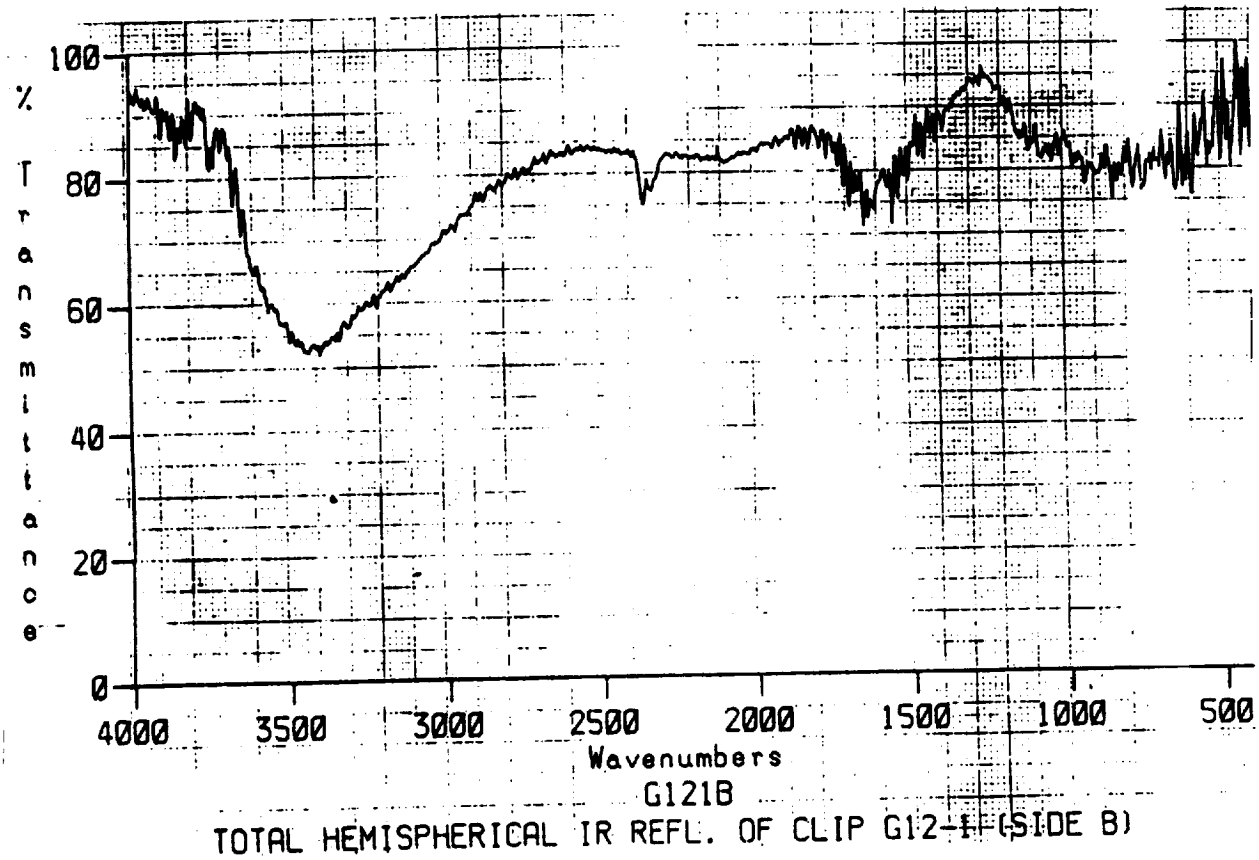

Figure A17: Total Hemispherical IR Reflectance of clamp G12-1 , (A) Front (B) Back

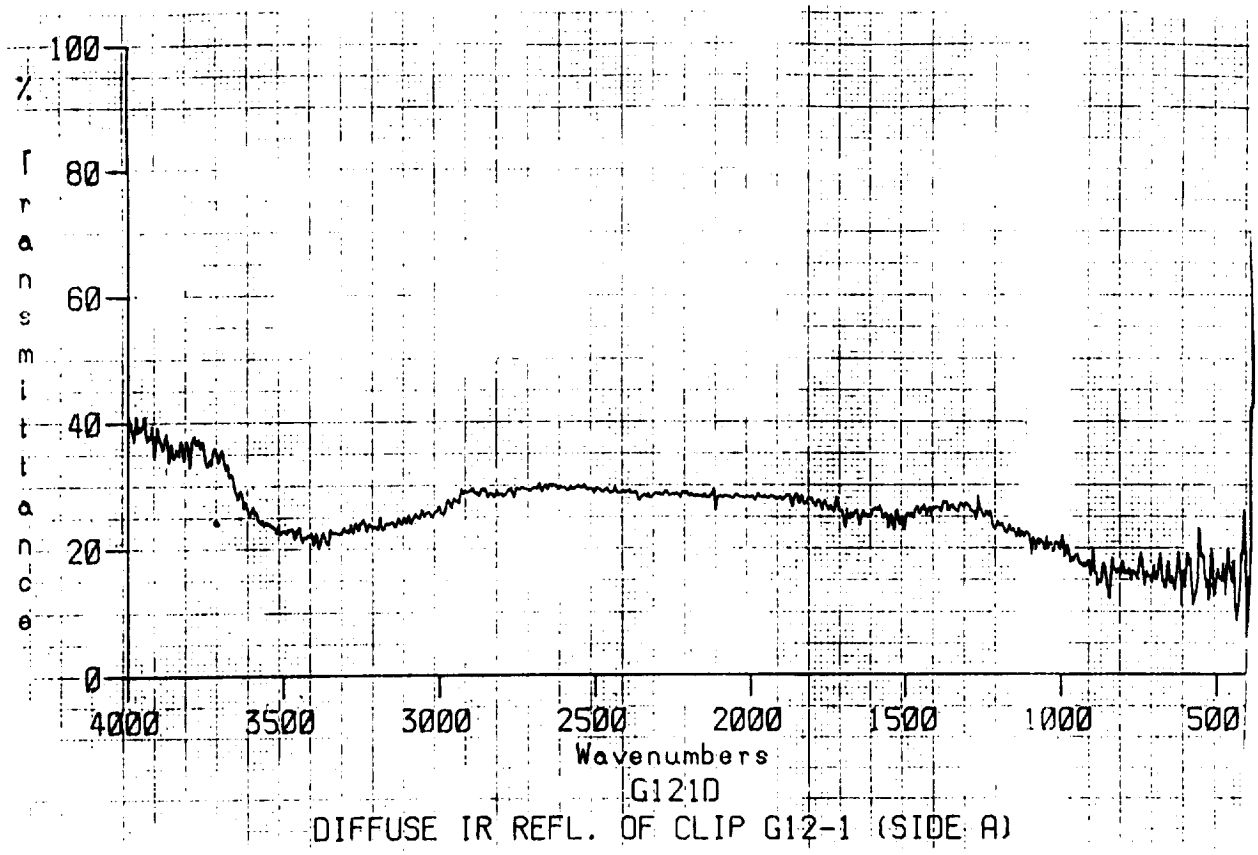

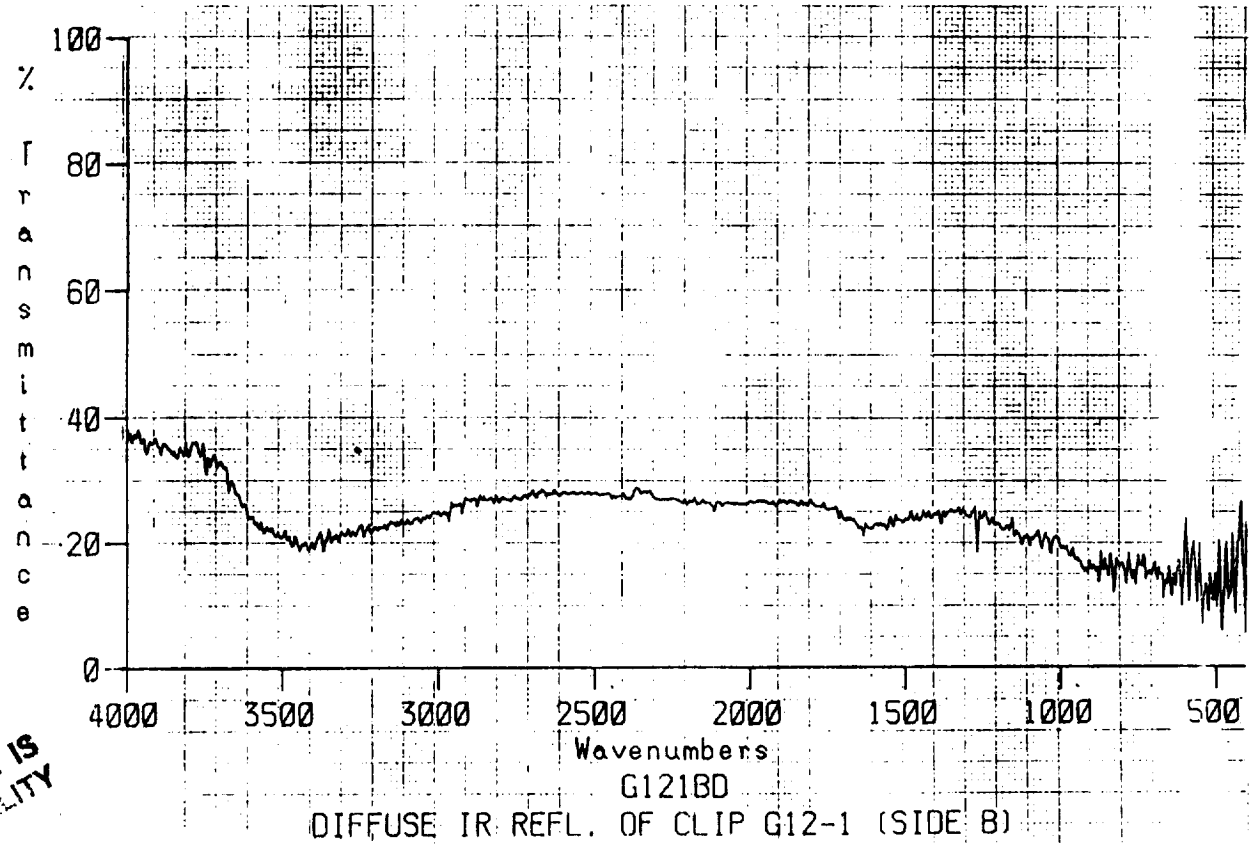

Figure A18: Diffuse IR Reflectance of clip G12-1, (A) Front (B) Back.

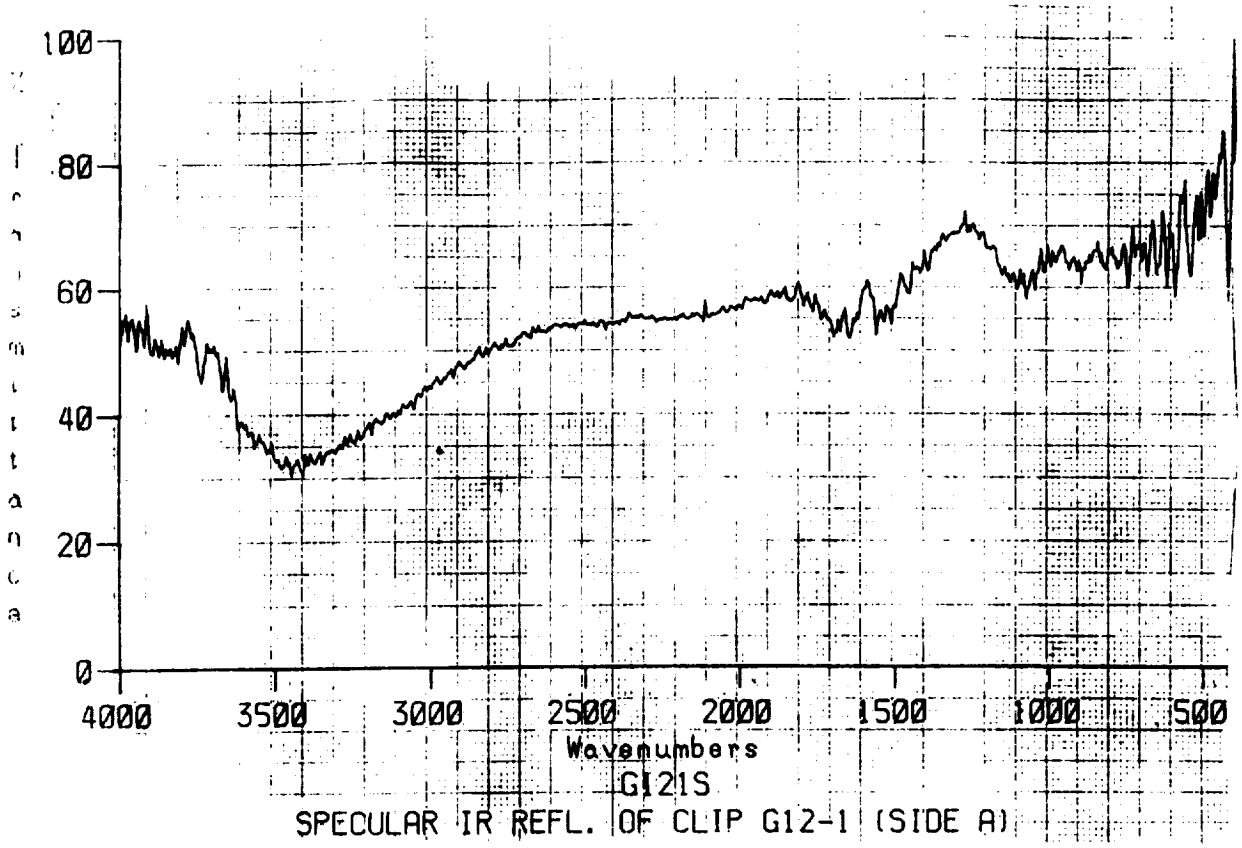

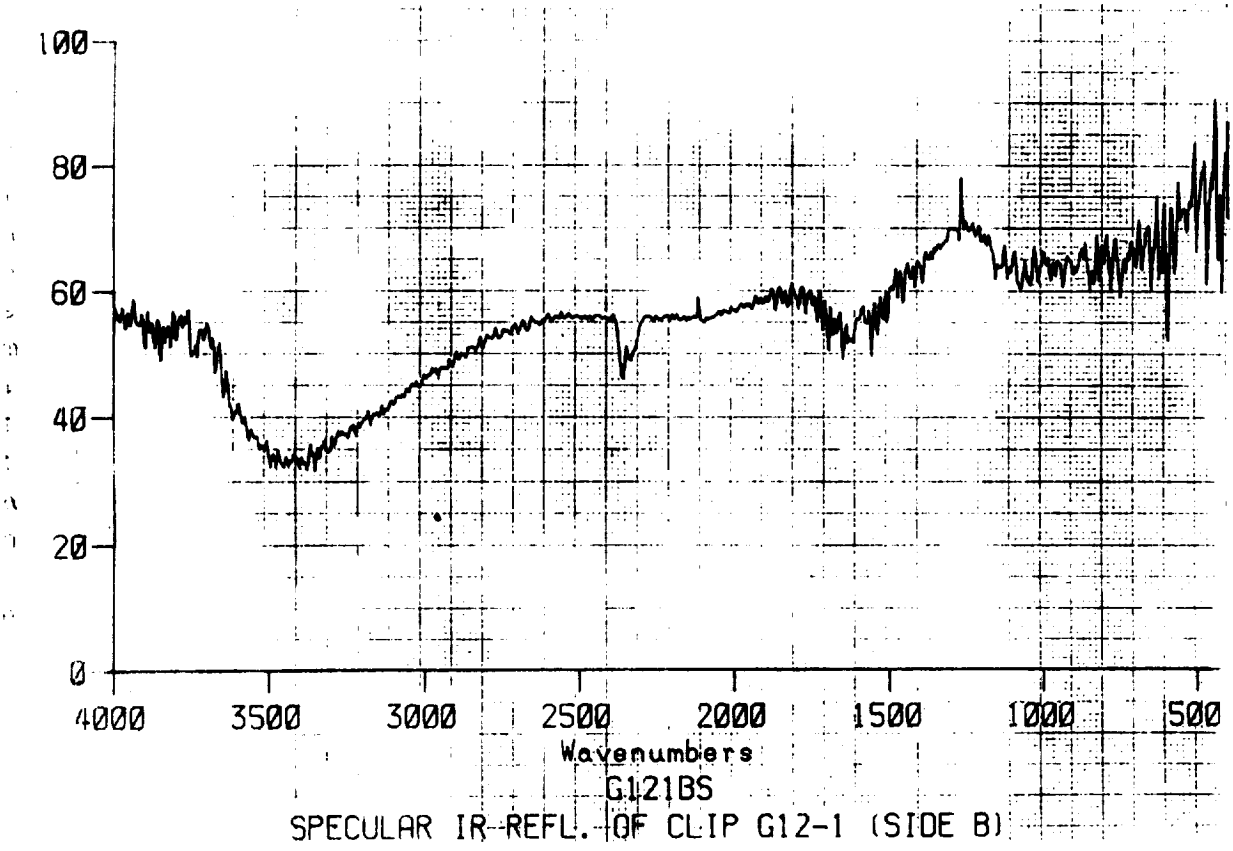

Figure A19: Specular IR Reflectance of clip G12-1, (A) Front (B) Back.

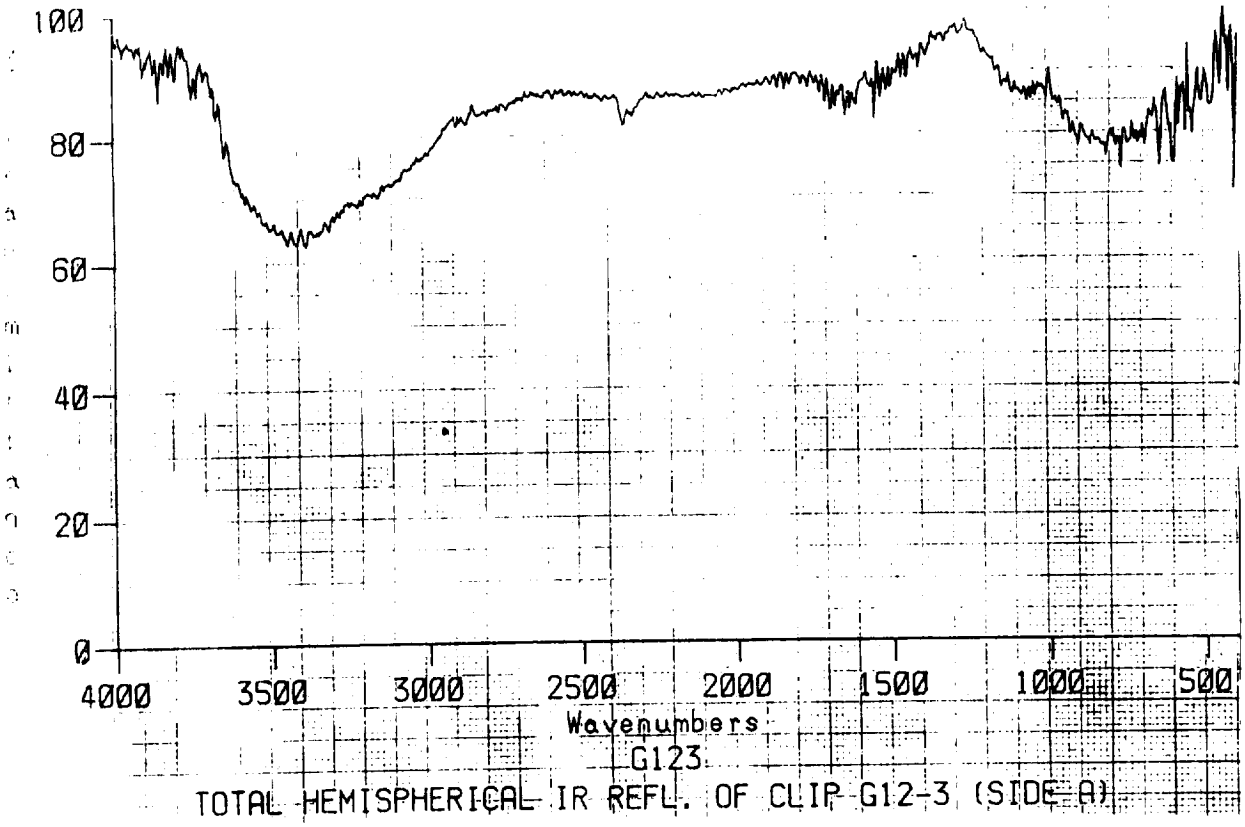

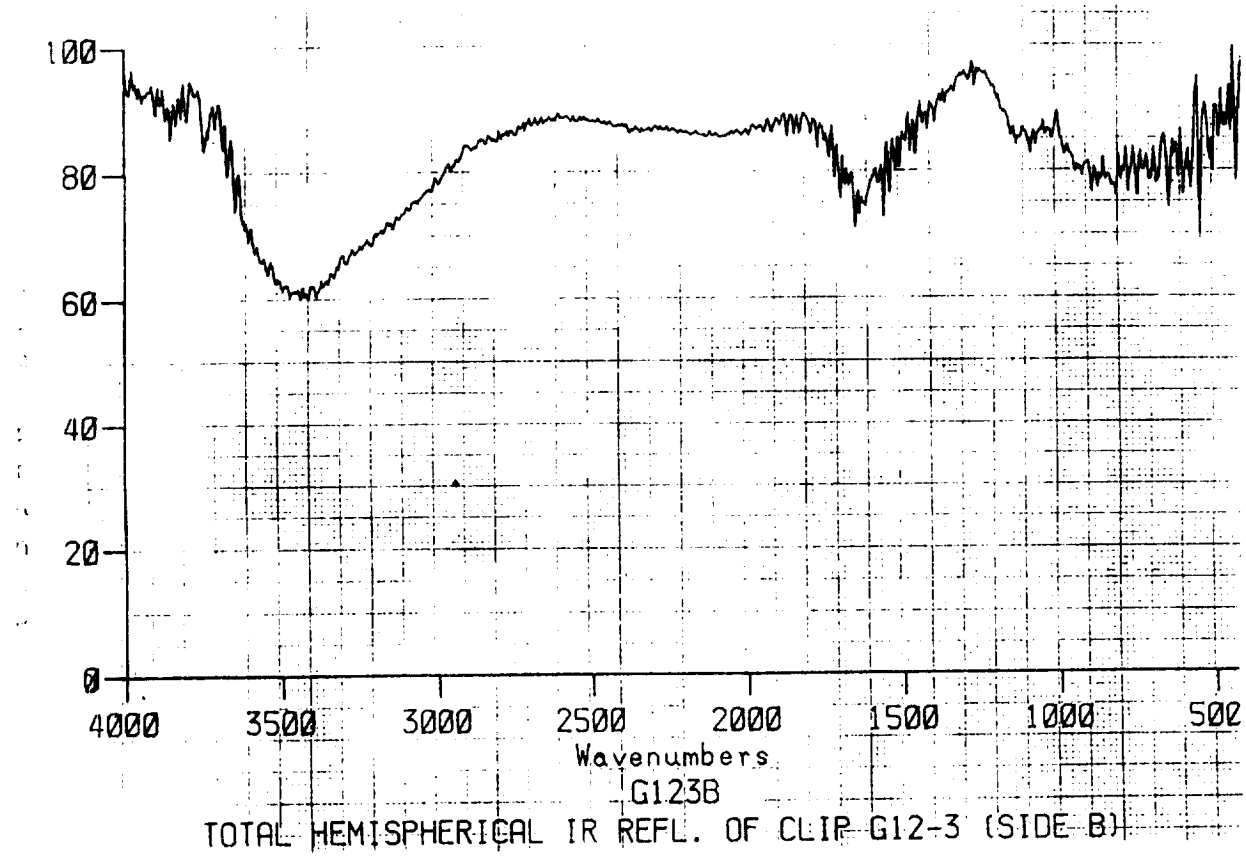

Figure A20: Total Hemispherical IR Reflectance of clip G12-3, (A) Front (B) Back.

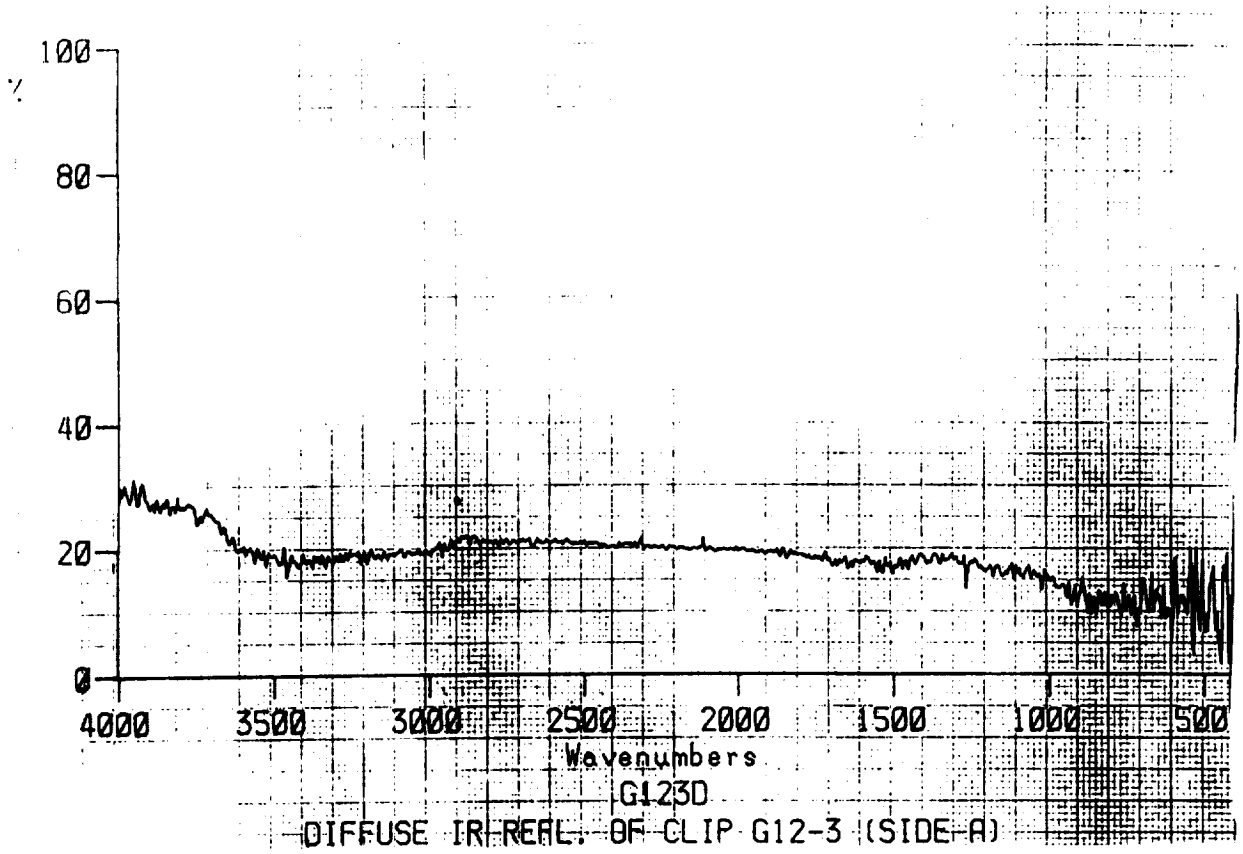

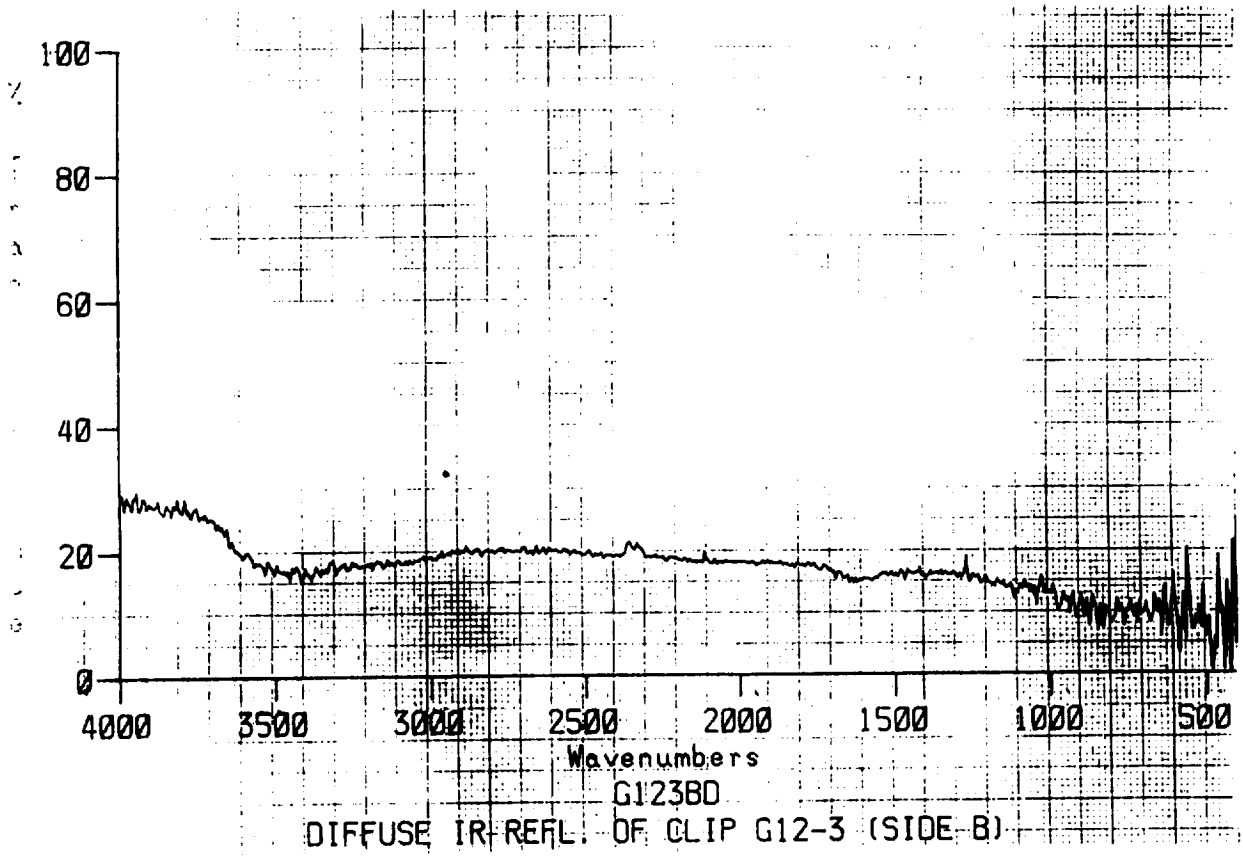

Figure A21: Diffuse IR Reflectance of clip G12-3, (A) Front (B) Back.

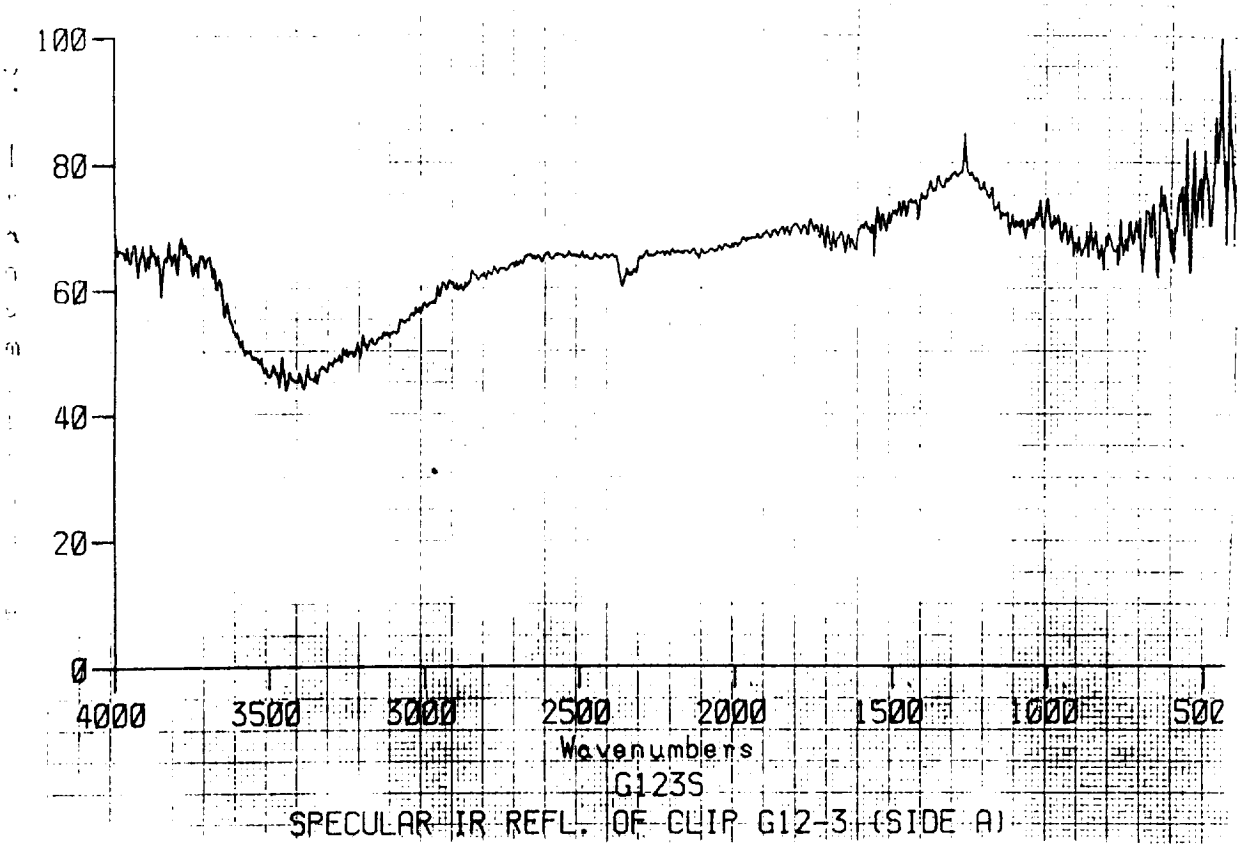

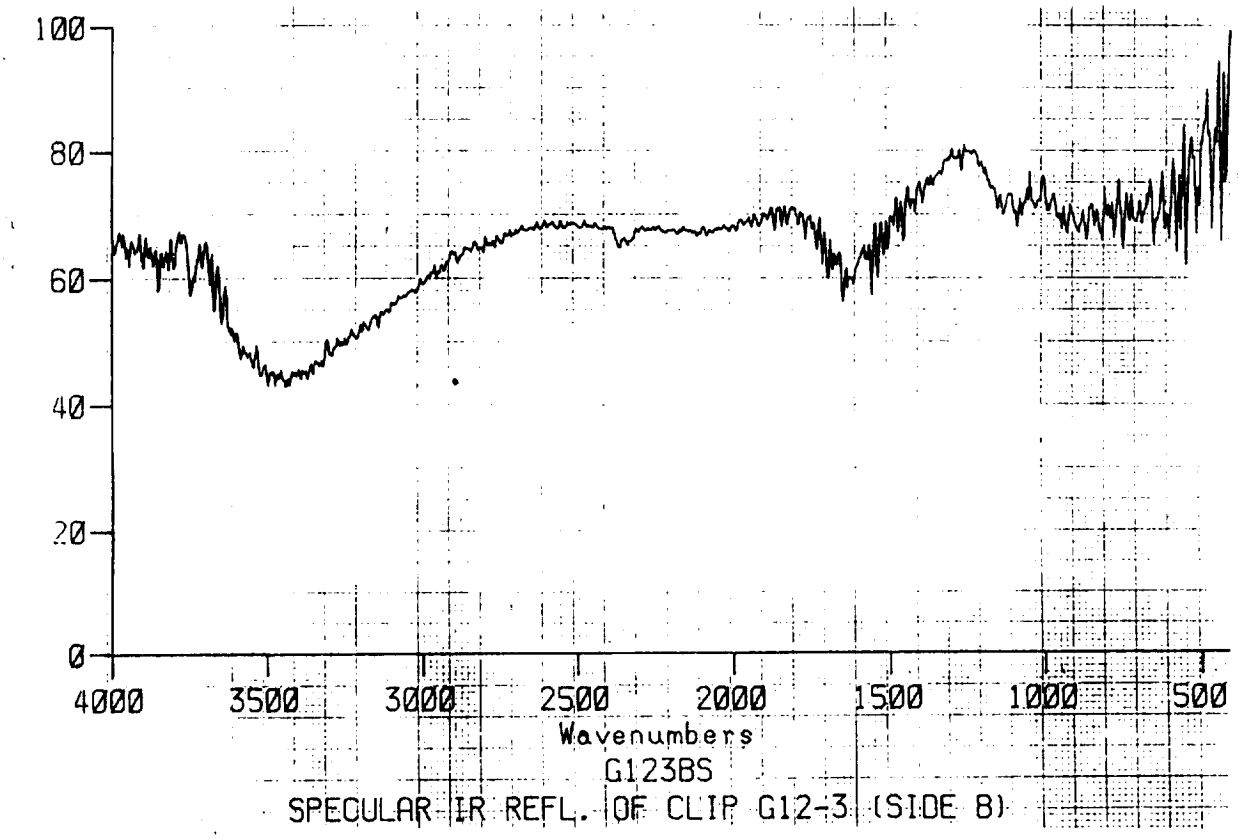

Figure A22: Specular IR Reflectance of clip G12-3, (A) Front (B) Back.

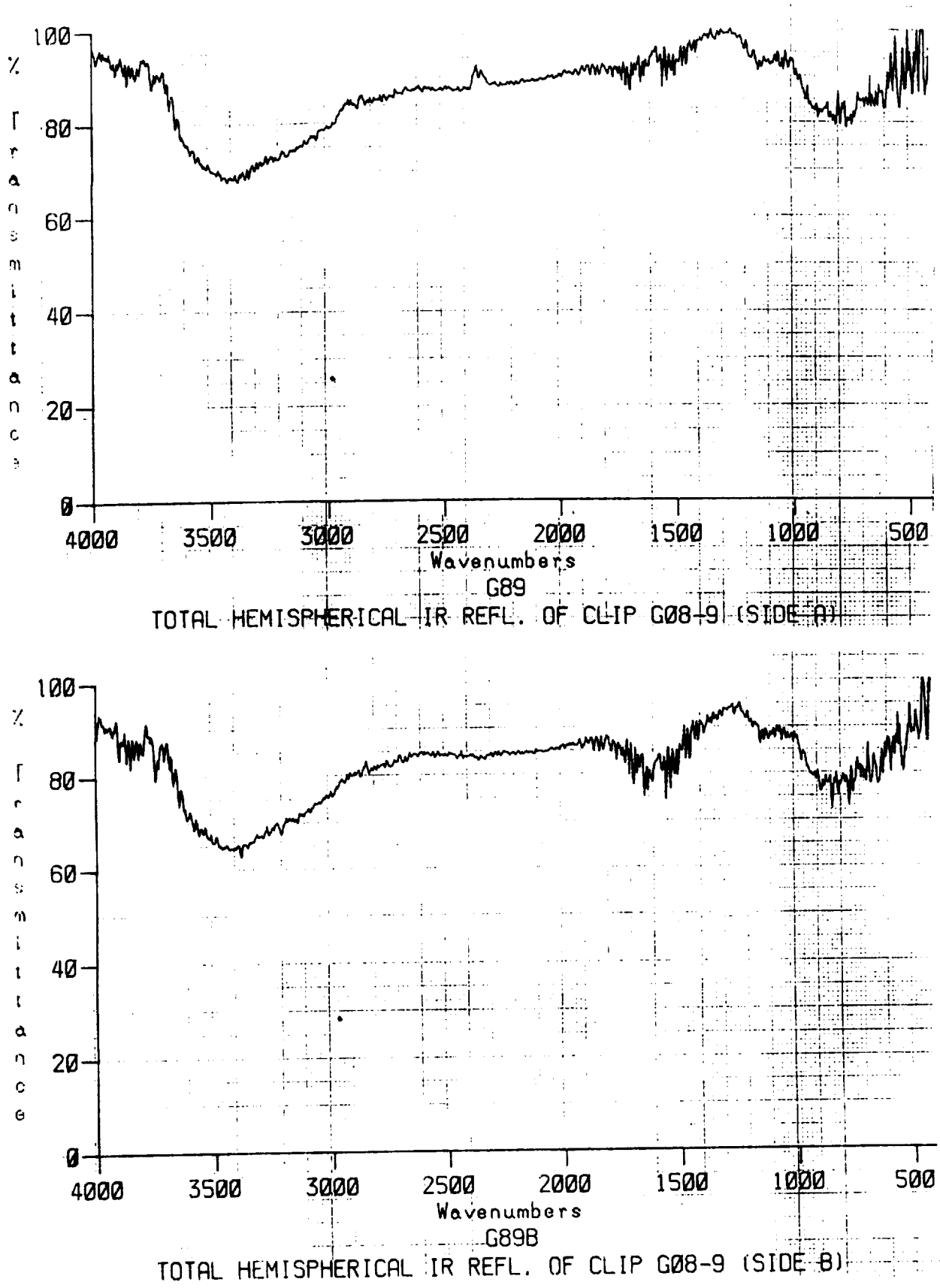

Figure A23: Total Hemispherical IR Reflectance of clip G08-9, (A) Front (B) Back.

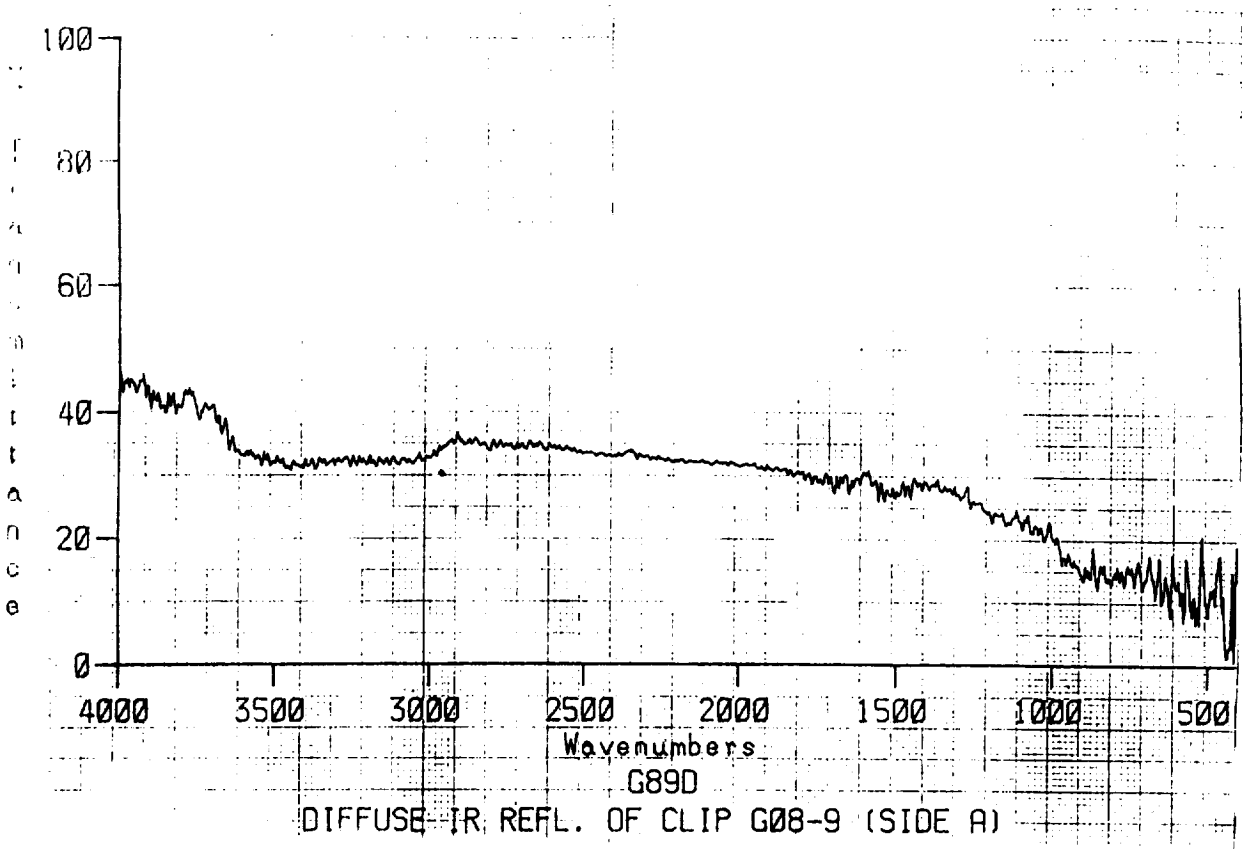

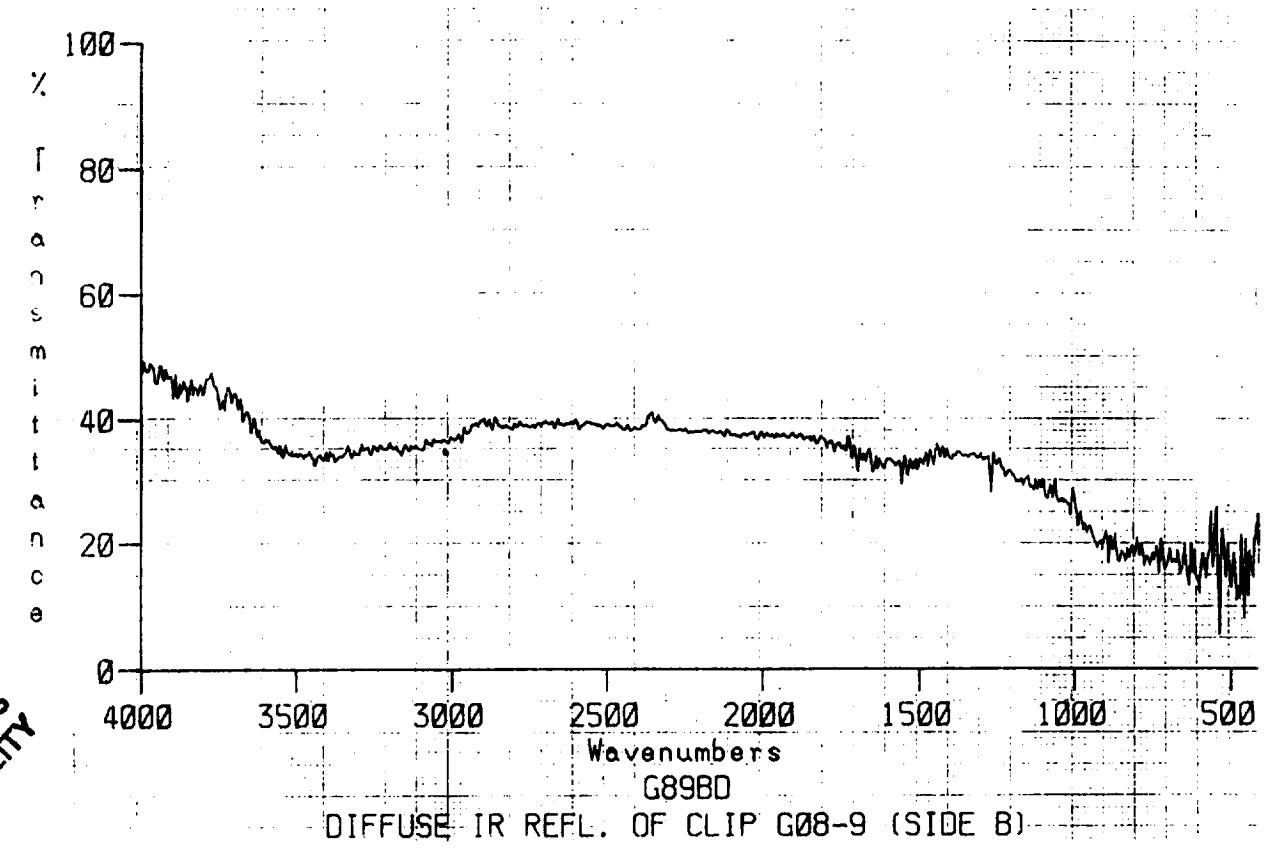

Figure A24: Diffuse IR Reflectance of clip G08-9, (A) Front (B) Back.

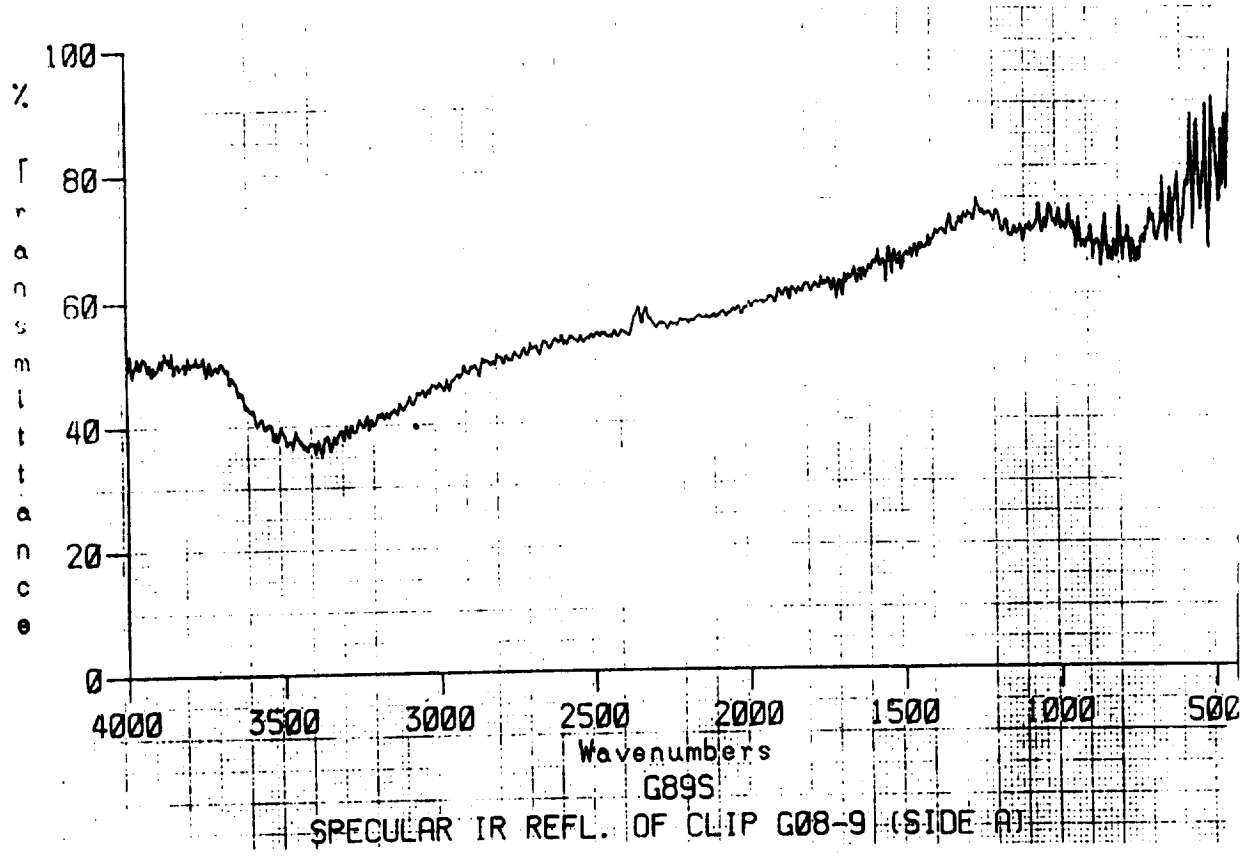

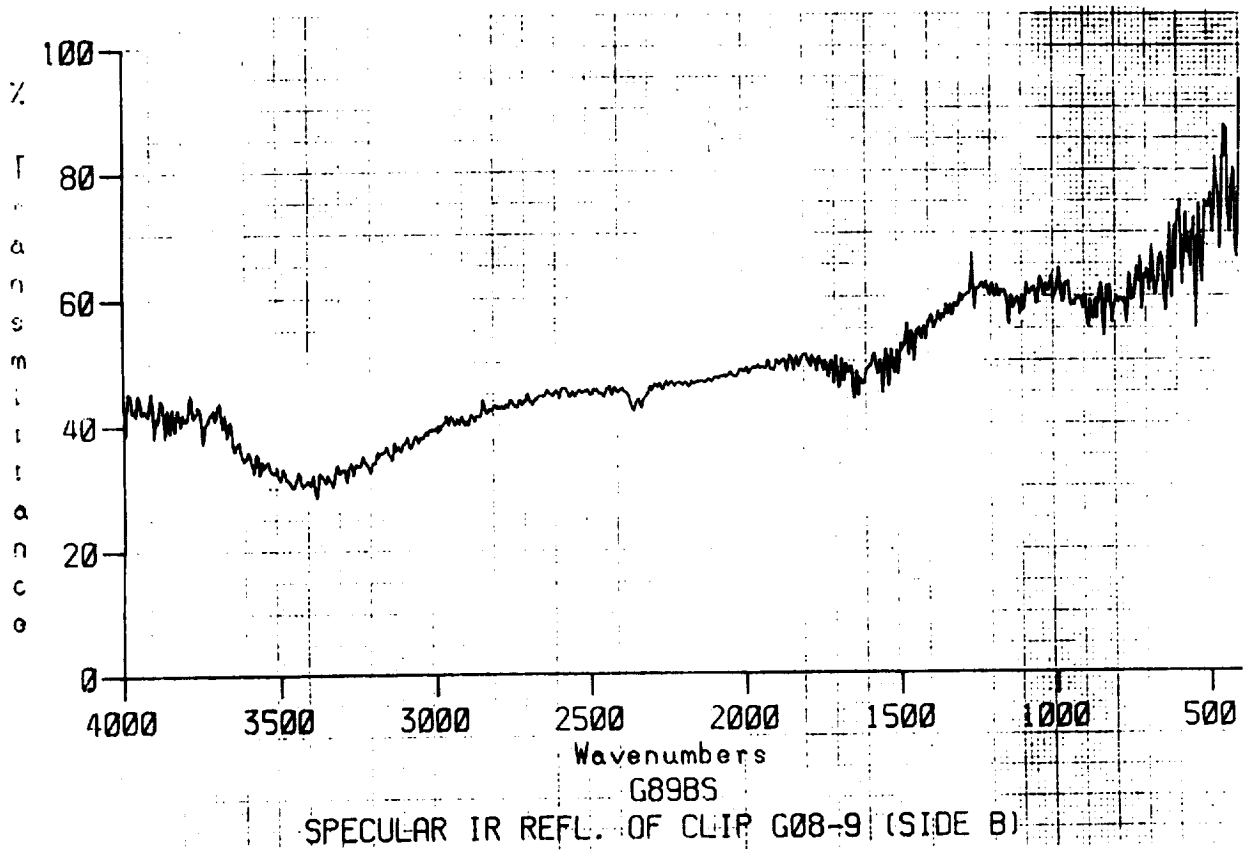

Figure A25: Specular IR Reflectance of clip G08-9 (A) Front (B) Back.

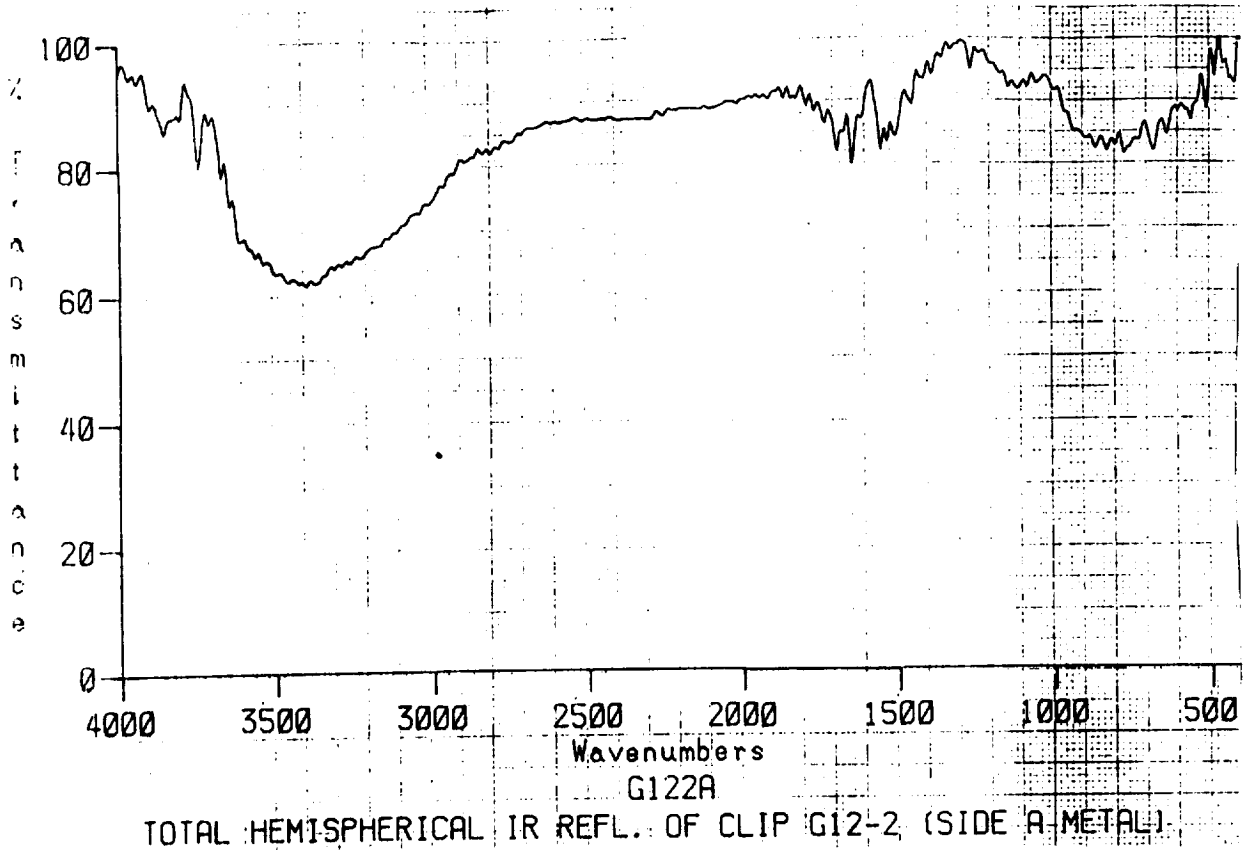

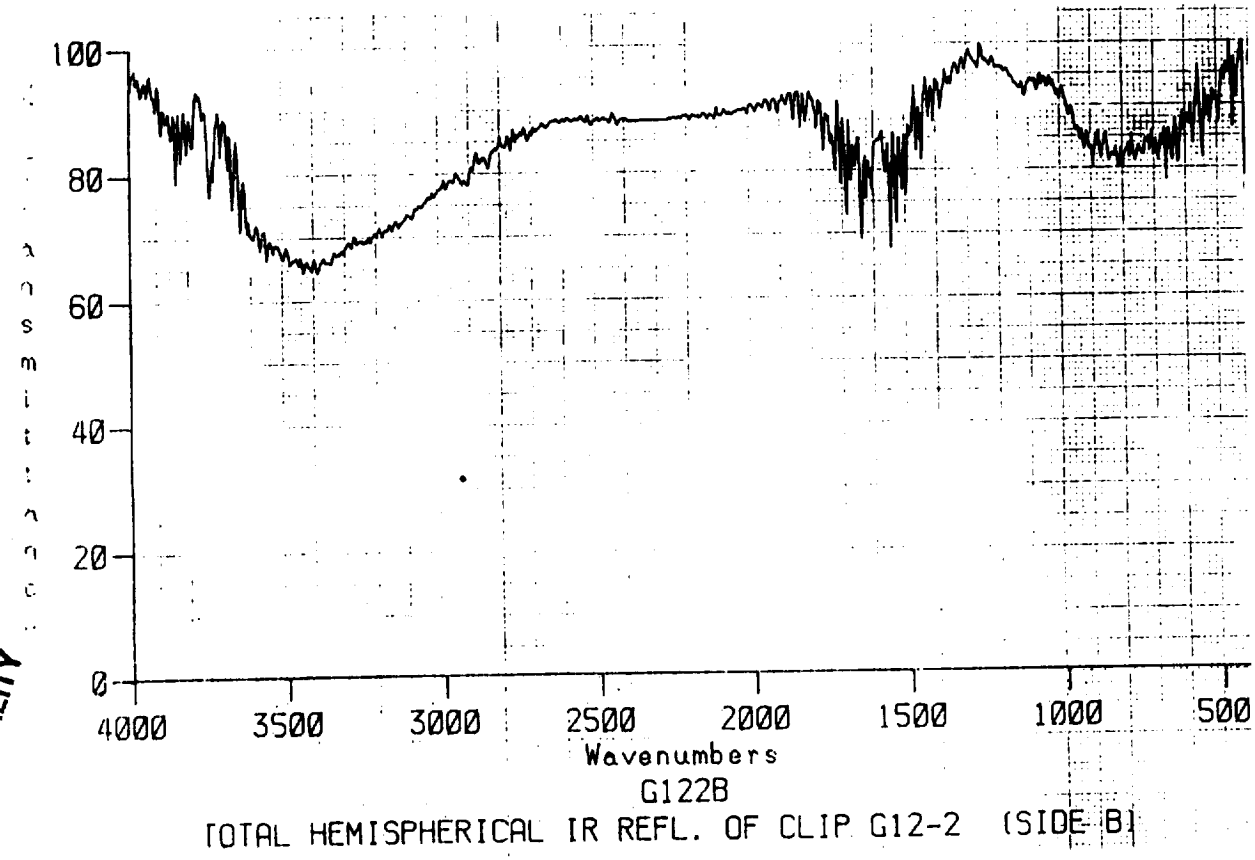

Figure A26: Total Hemispherical IR Reflectance of clip G12-2, (A) Front (B)Back.

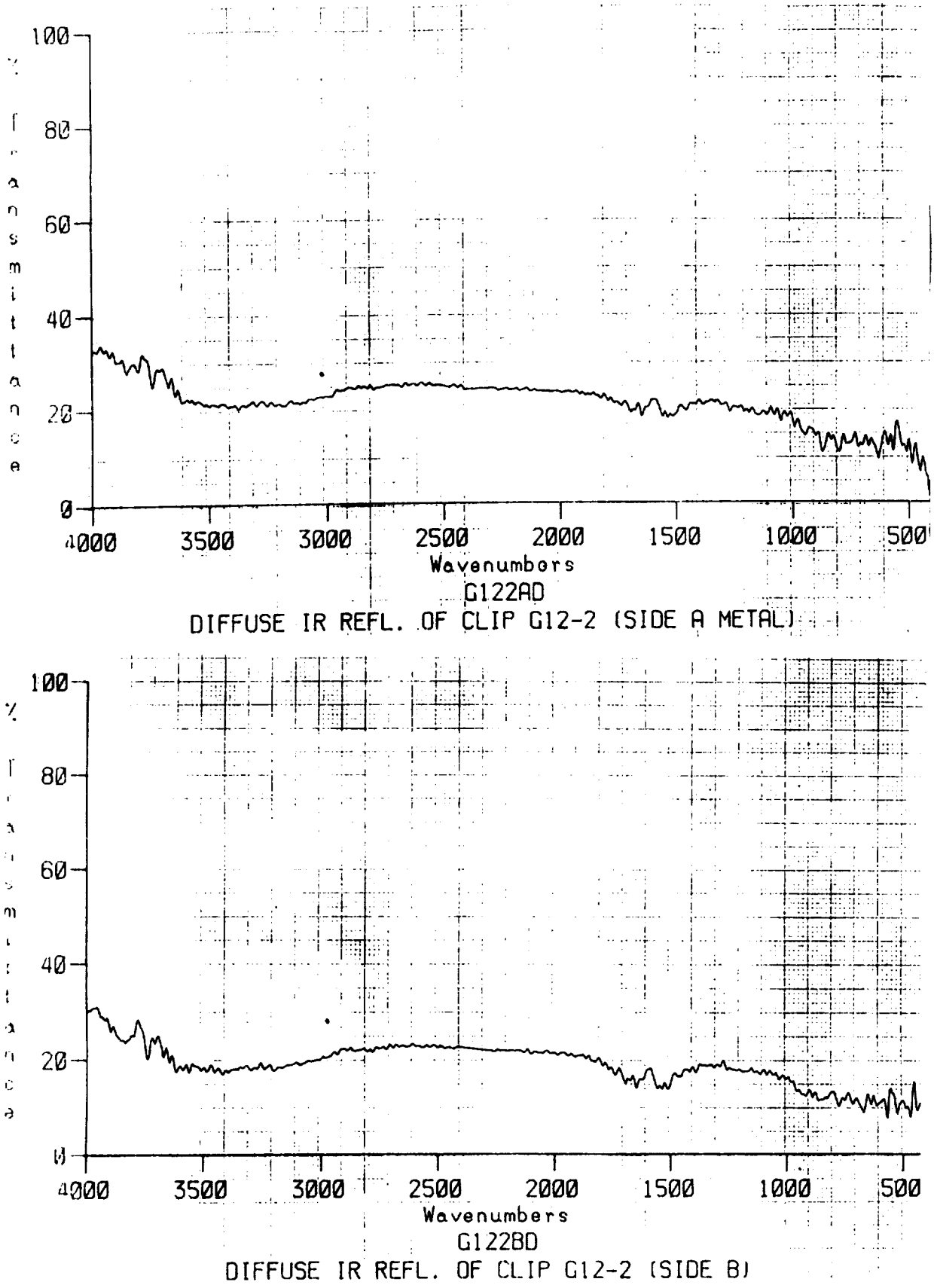

Figure A27: Diffuse IR Reflectance of clip G12-2, (A) Front (B) Back.

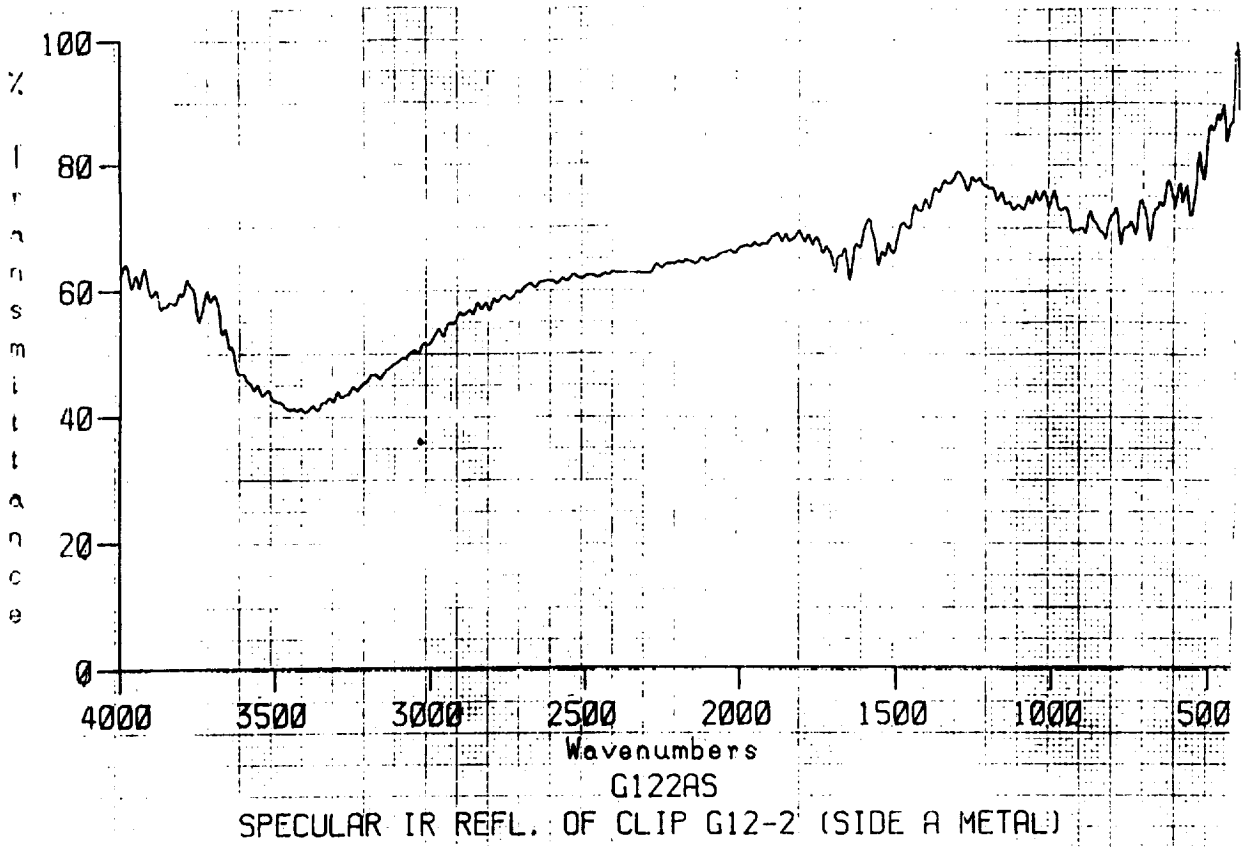

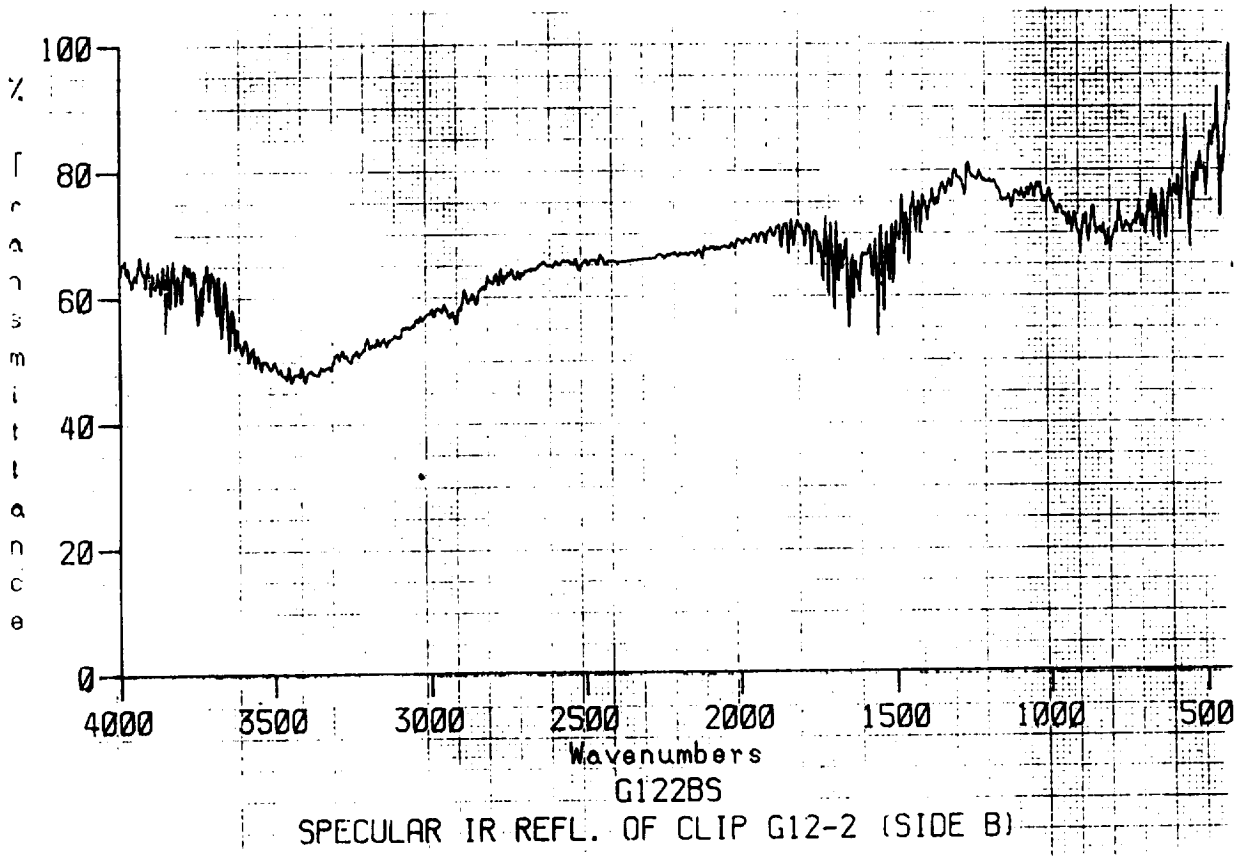

Figure A28: Specular IR Reflectance of clip G12-2, (A) Front (B) Back.

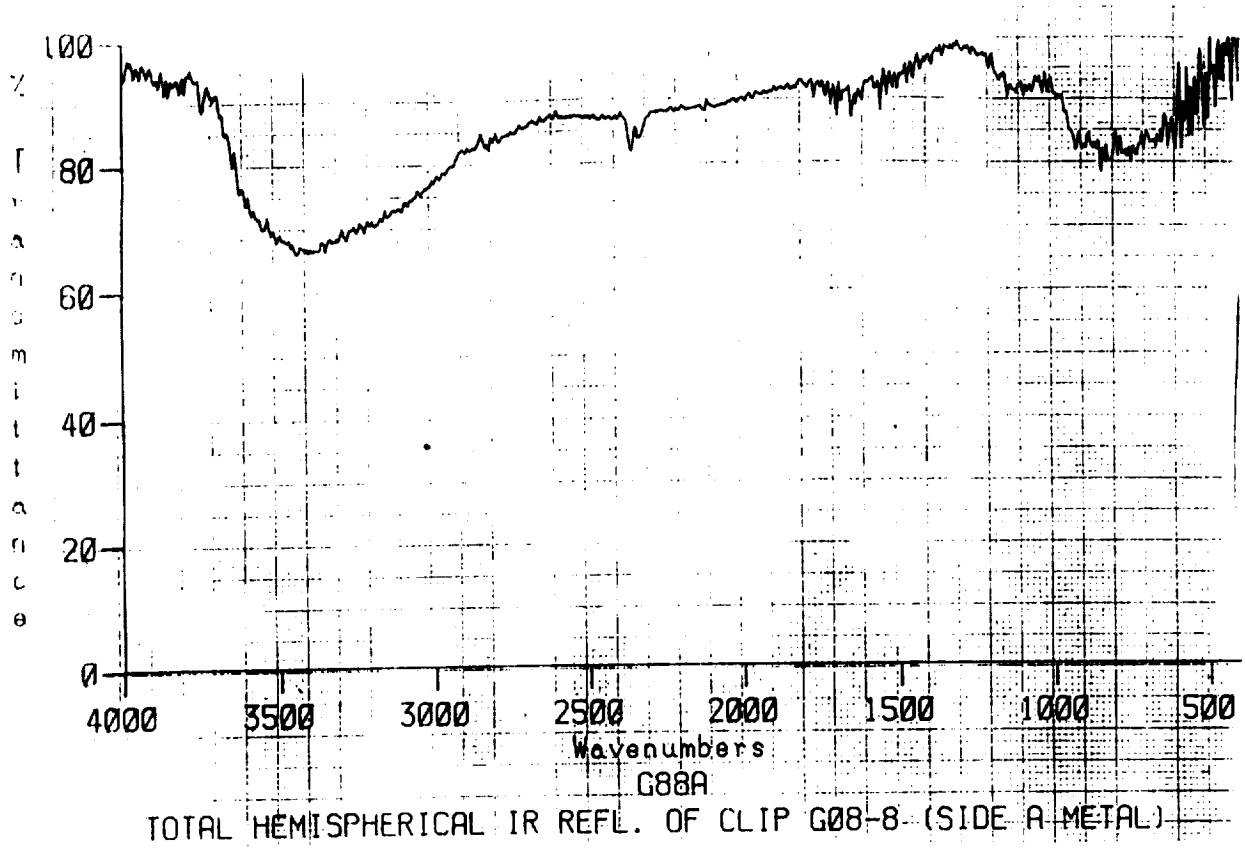

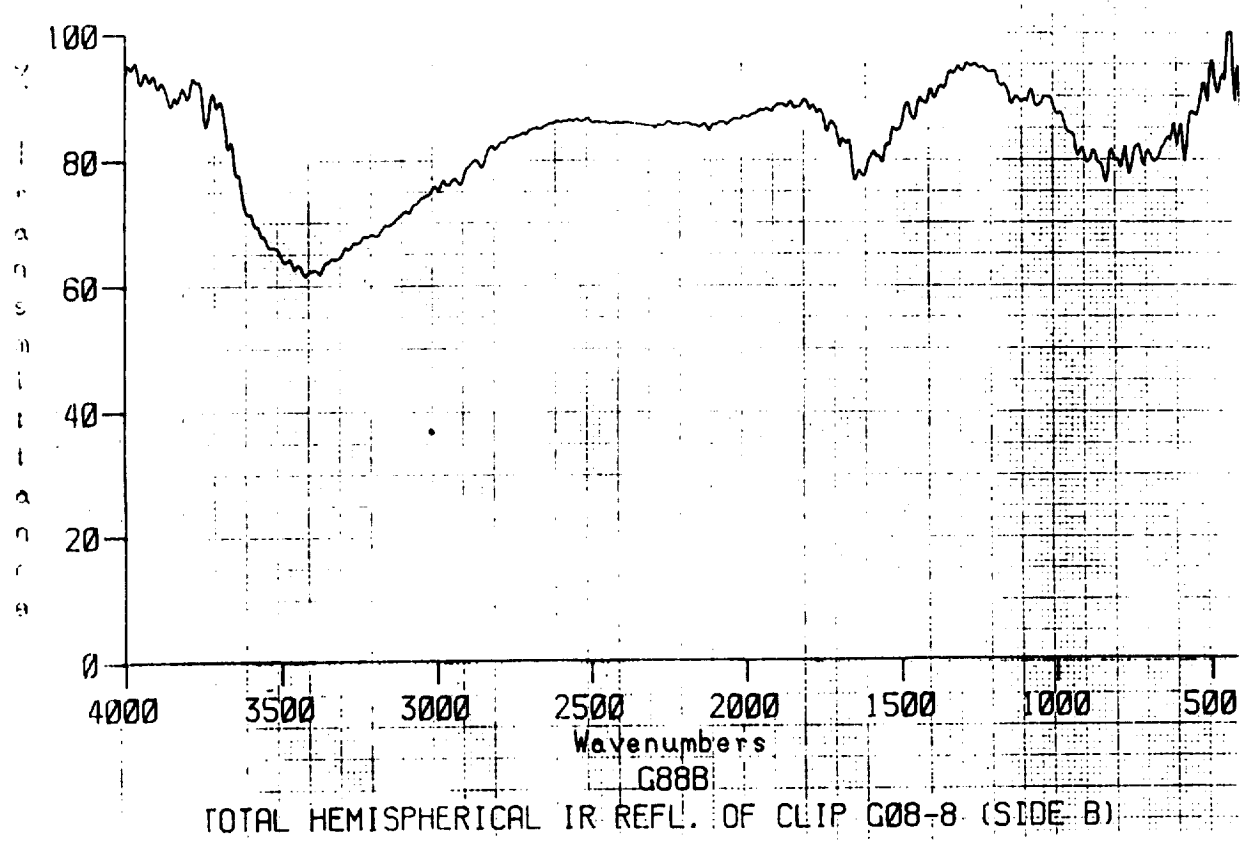

Figure A29: Total Hemispherical IR Reflectance of clip G08-8, (A)Front (B) Back.

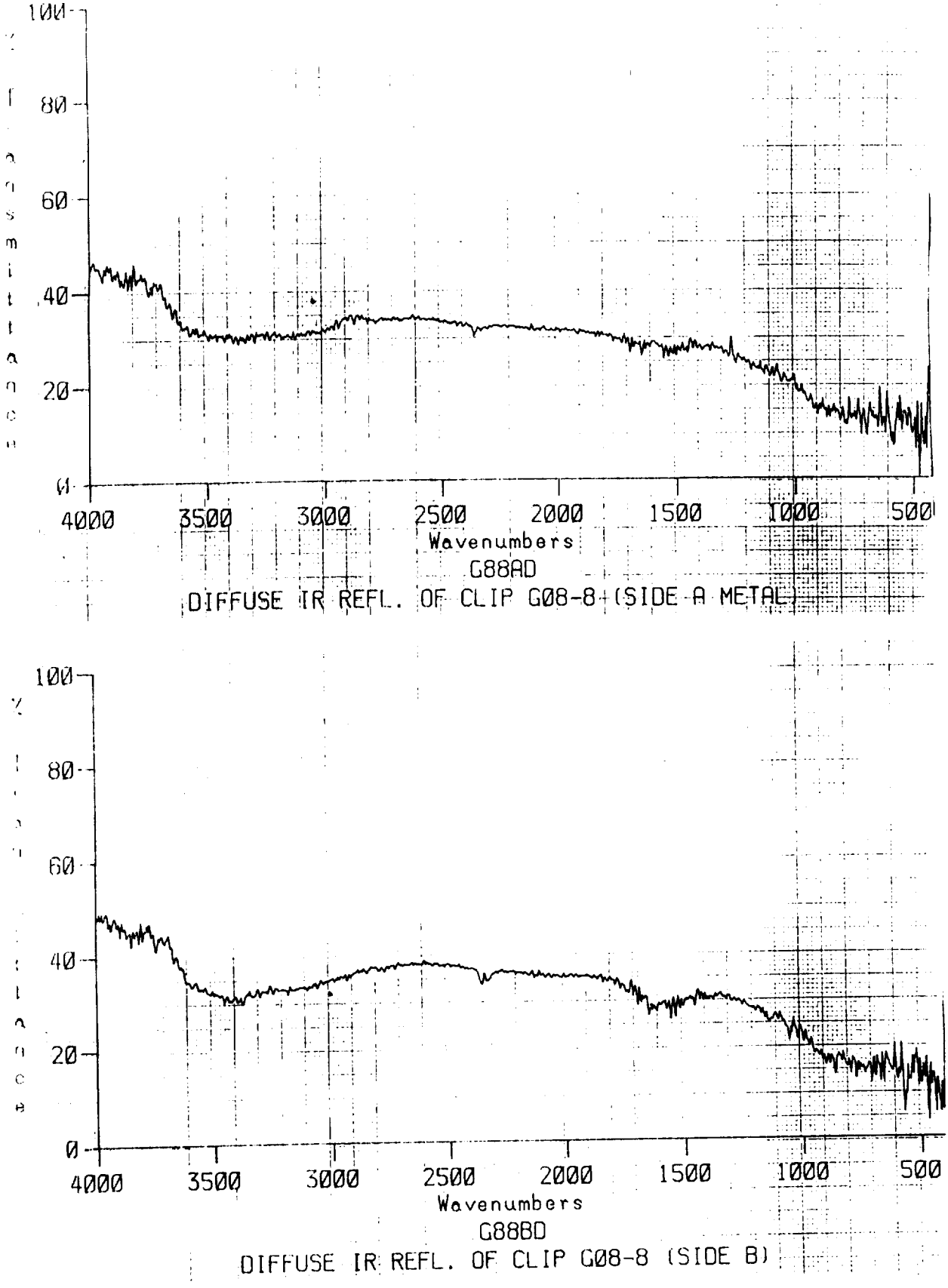

Figure A30: Diffuse IR Reflectance of clip G08-8, (A) Front (B) Back.

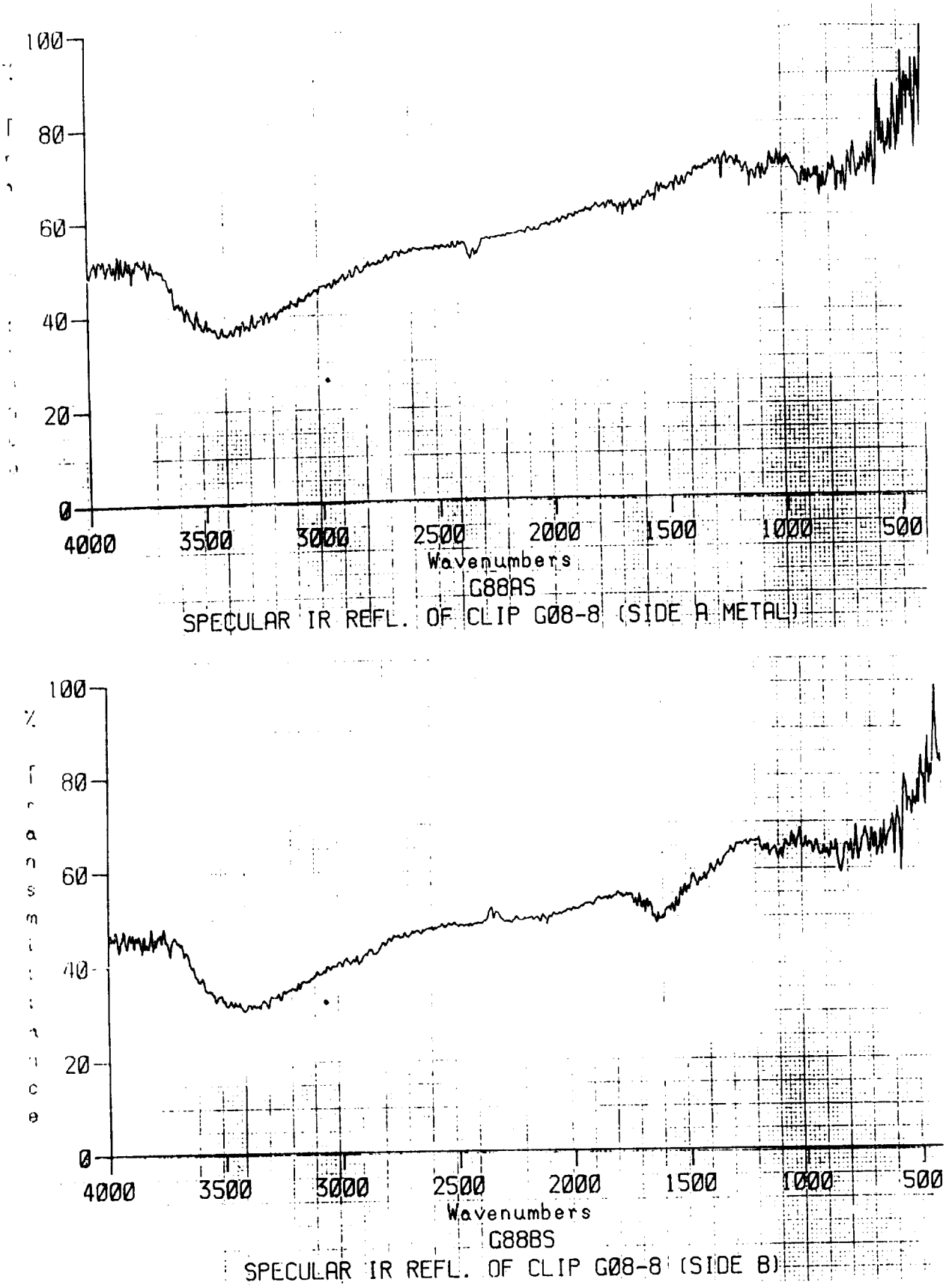

Figure A31: Specular IR Reflectance of clip G08-8, (A) Front (B) Back.

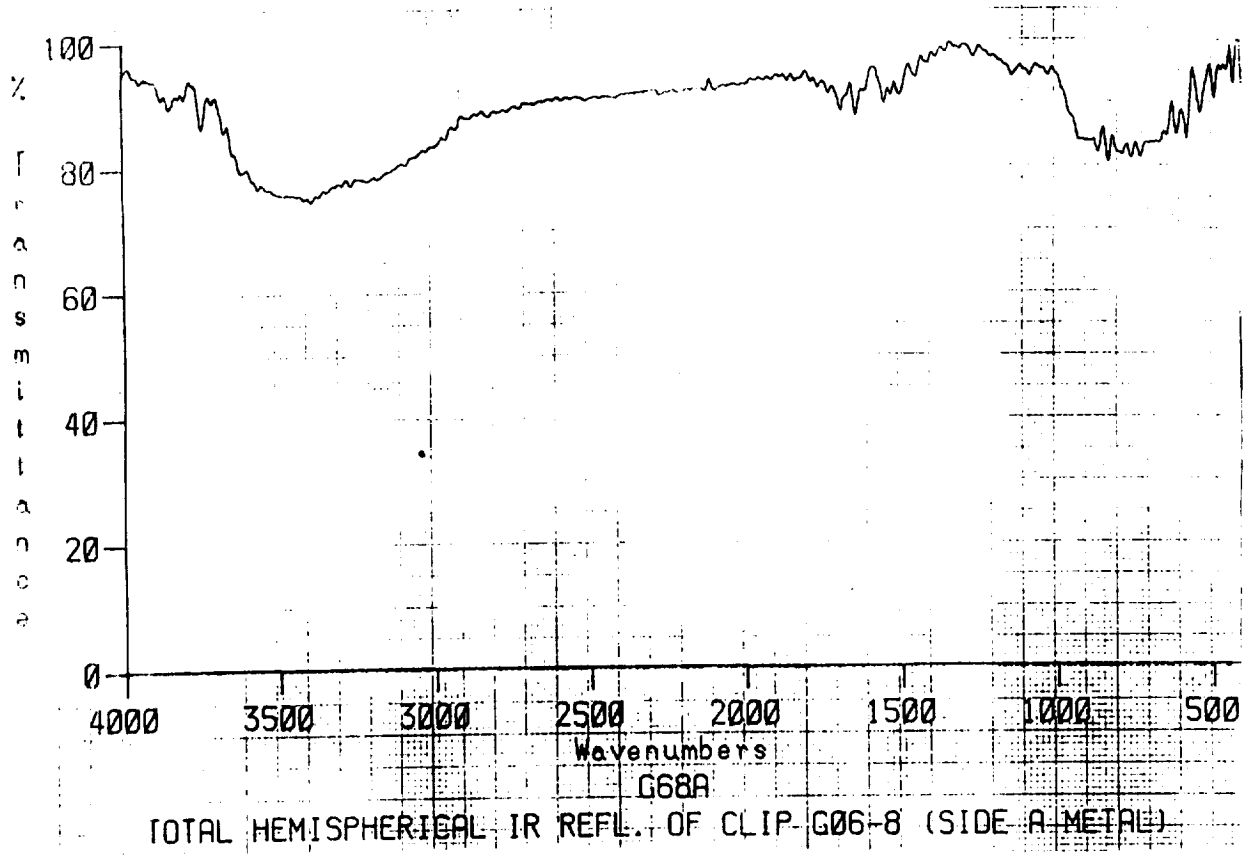

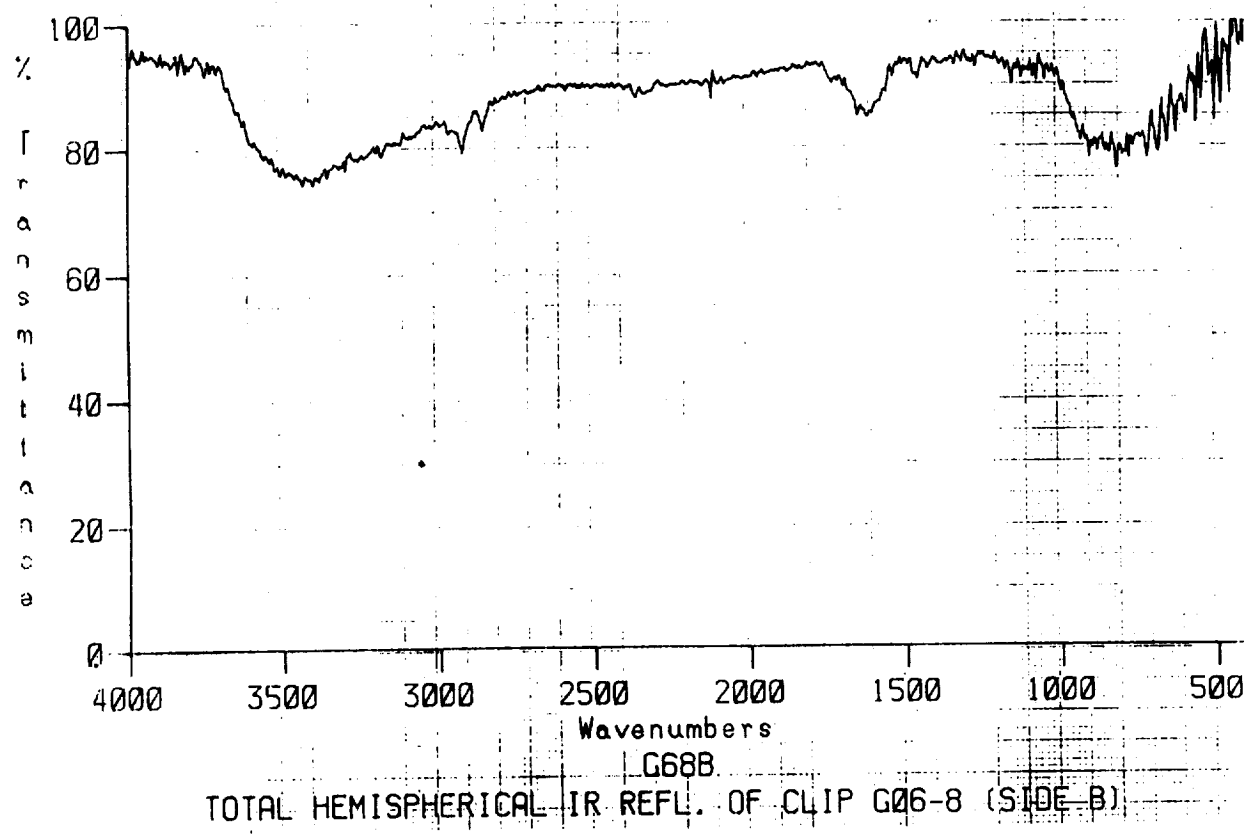

Figure A32: Total Hemispherical IR Reflectance of clip G06-8, (A) Front (B) Back.

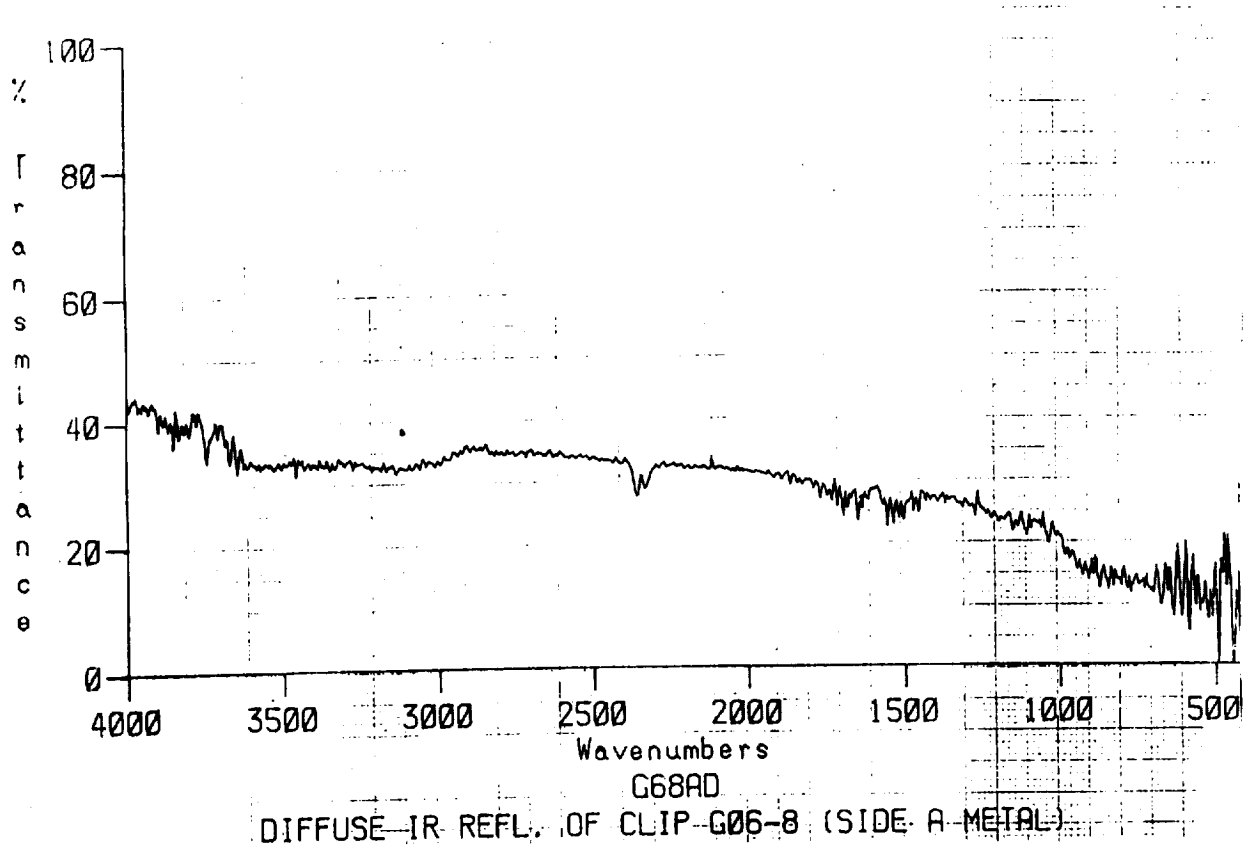

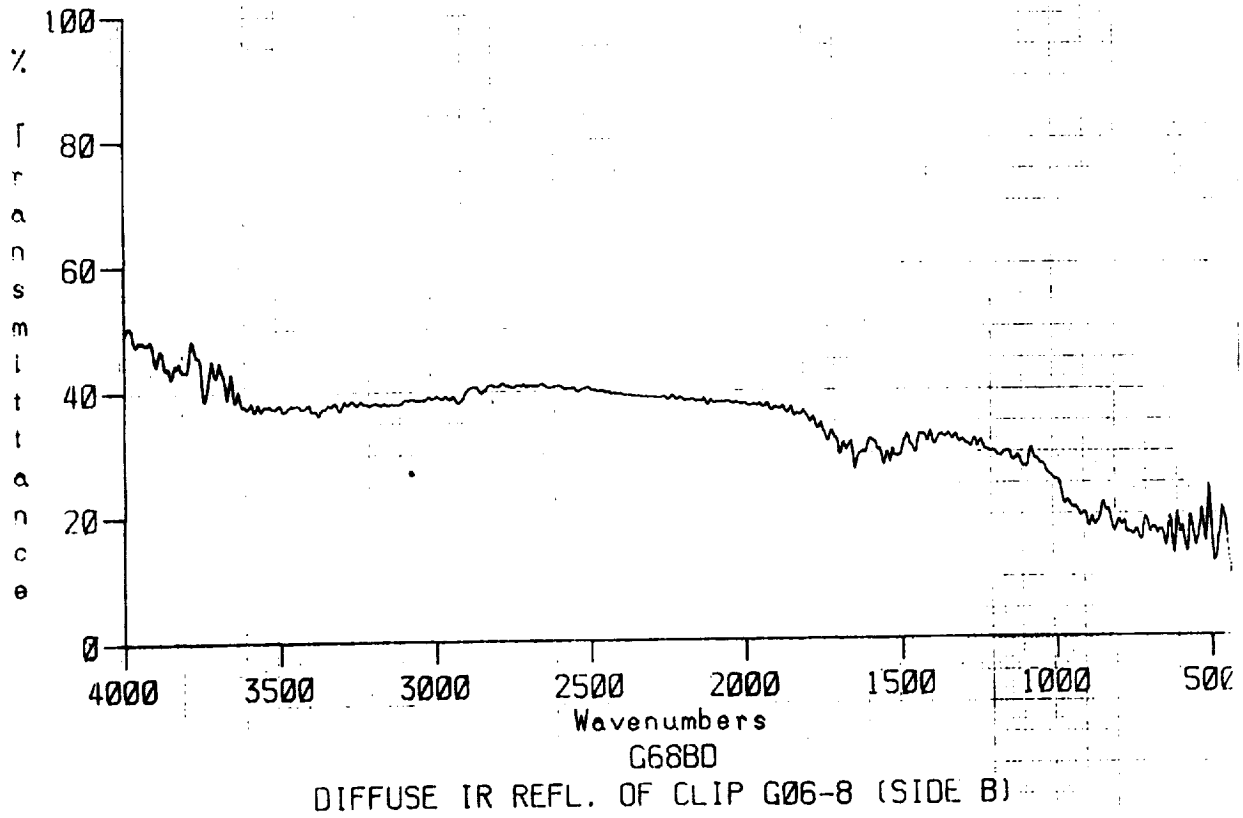

Figure A33: Diffuse IR Reflectance of clip G06-8, (A) Front (B) Back.

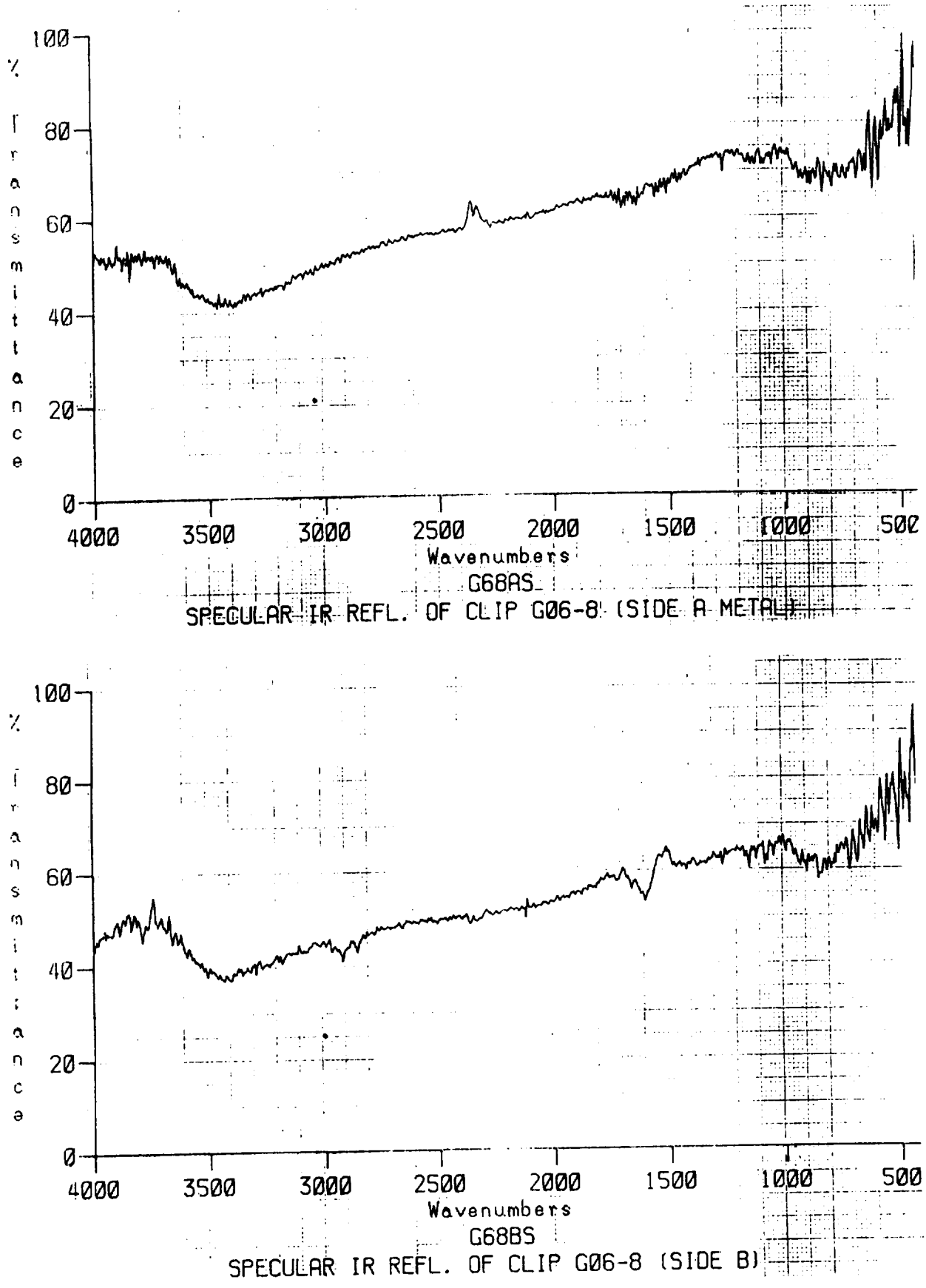

Figure A34: Specular IR Reflectance of clip G06-8, (A) Front (B) Back.

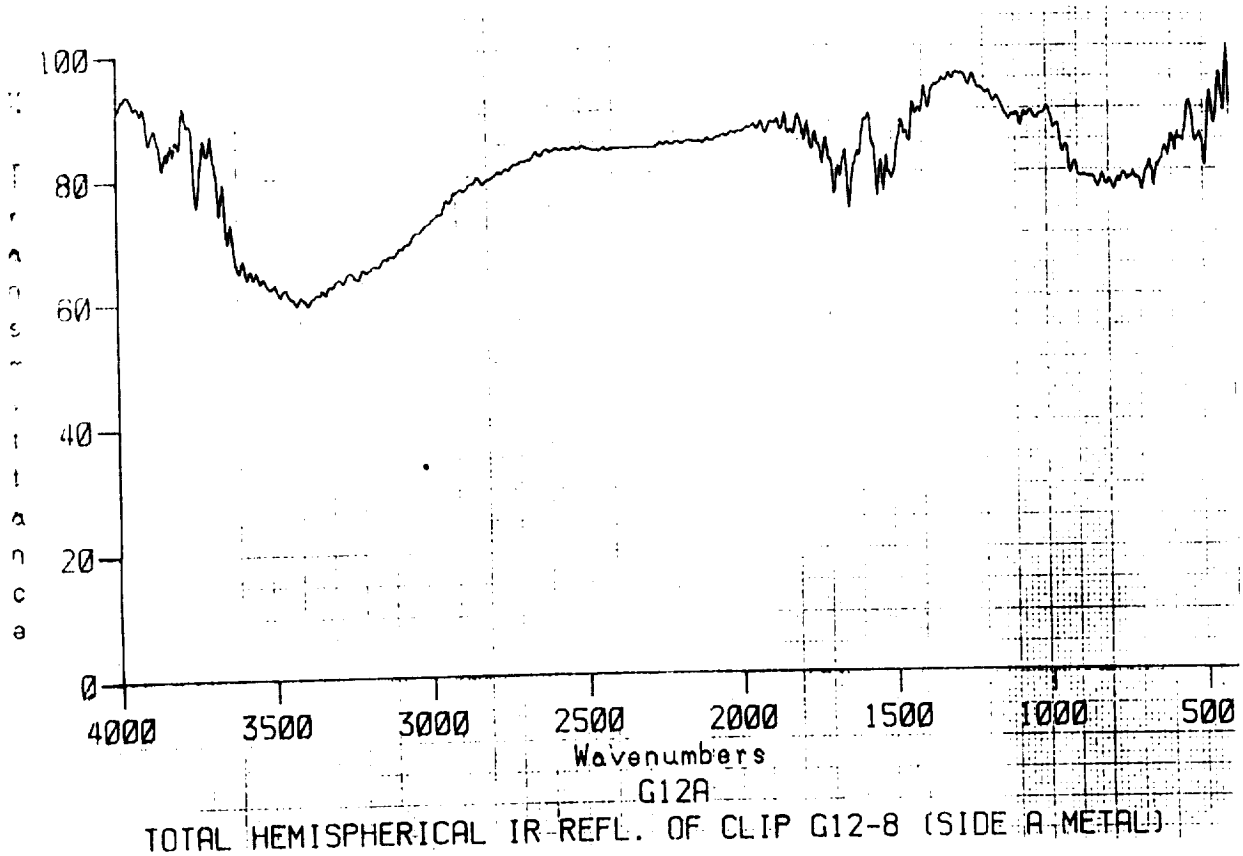

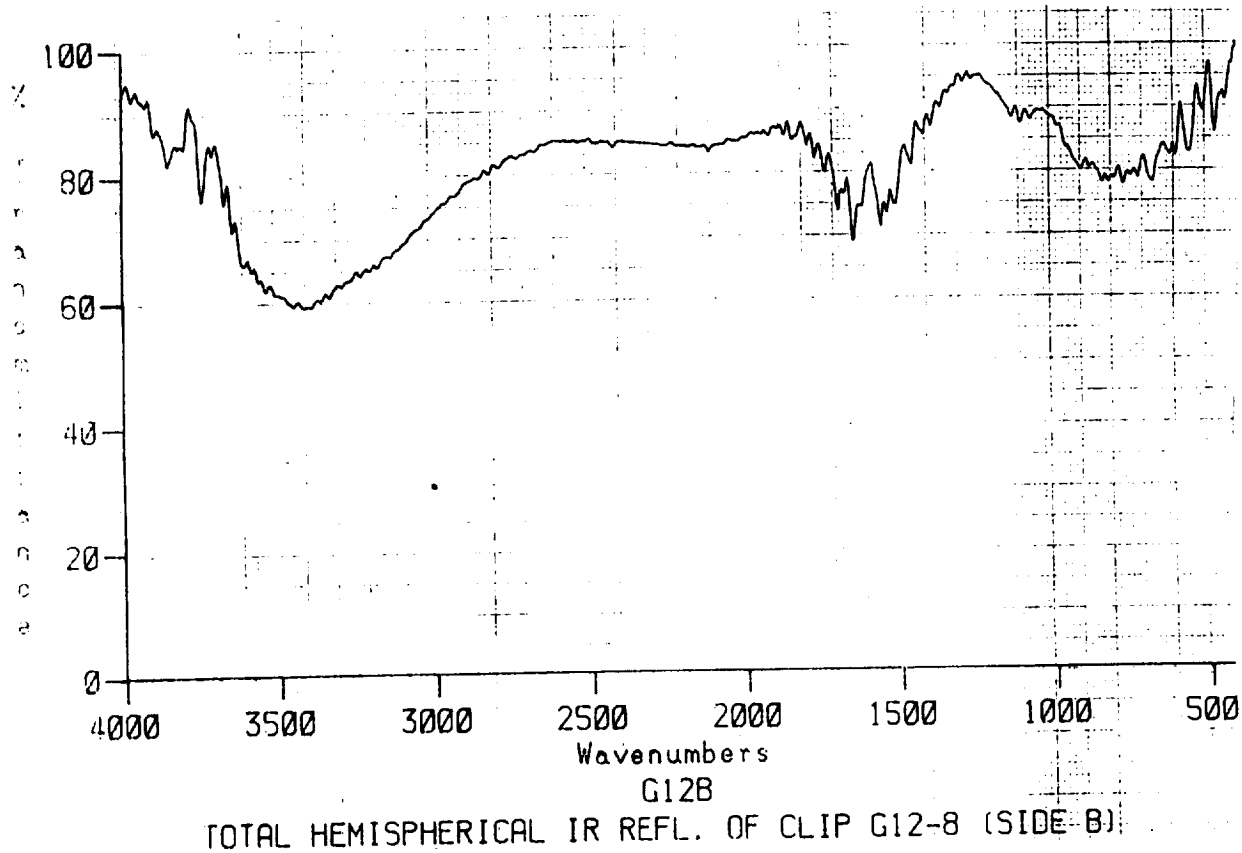

Figure A35: Total Hemispherical IR Reflectance of clip G12-8, (A) Front (B) Back.

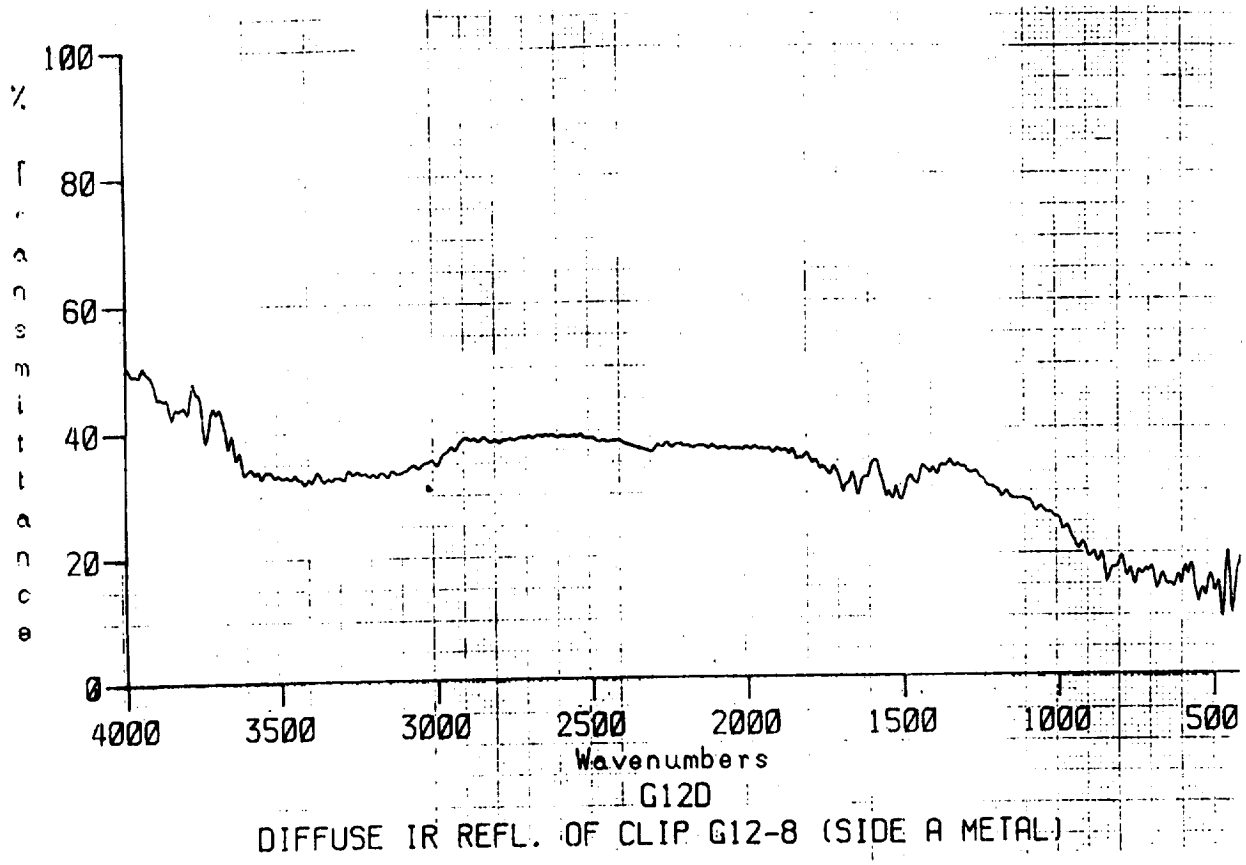

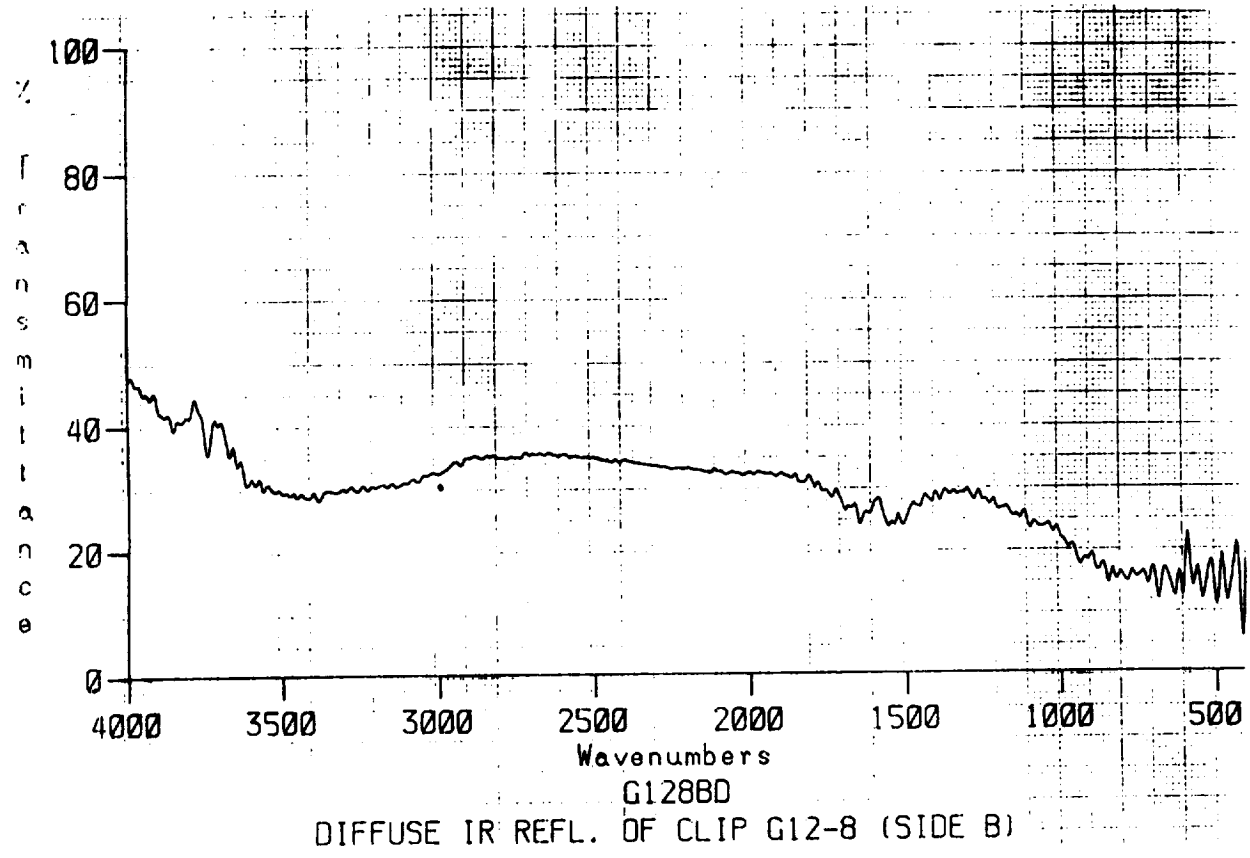

Figure A36: Diffuse IR Reflectance of clip G12-8, (A) Front (B) Back.

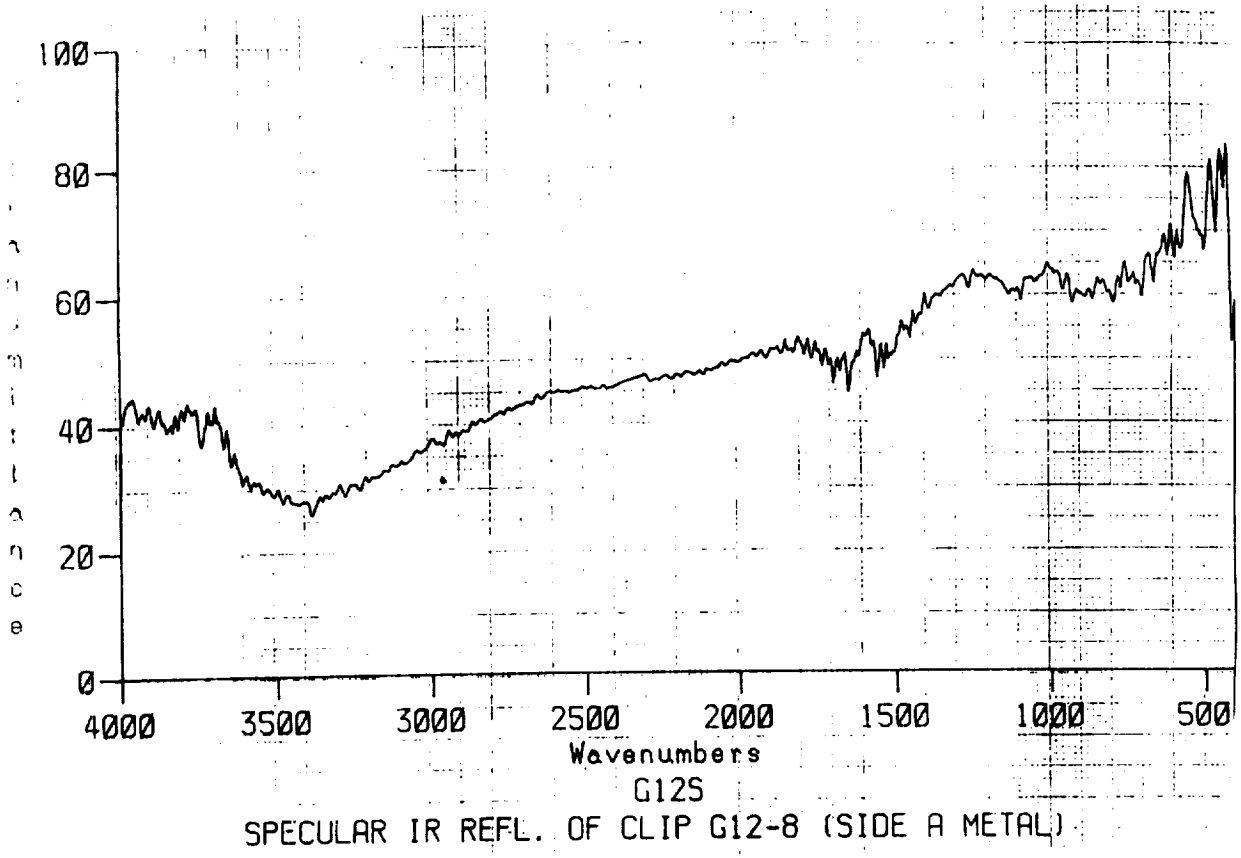

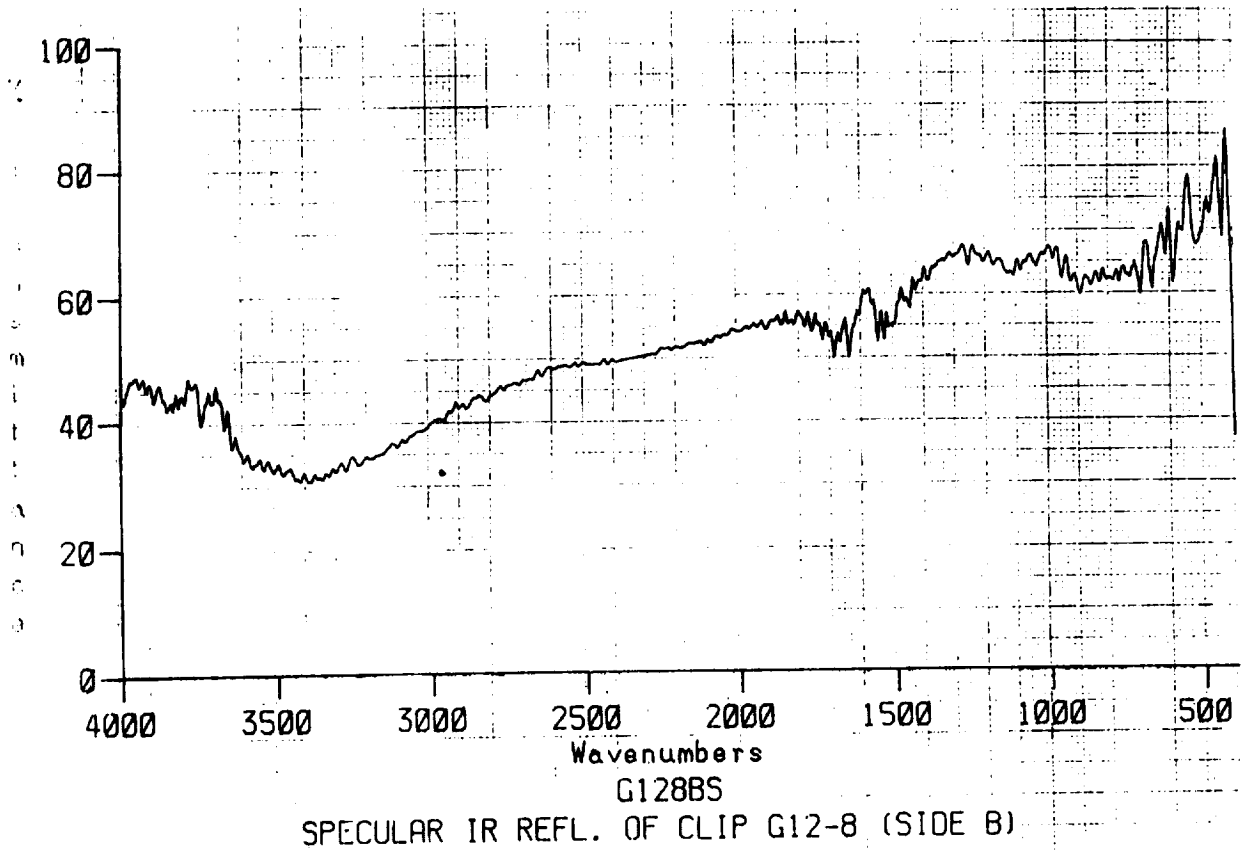

Figure A37: Specular IR Reflectance of clip G12-8, (A) Front (B) Back.

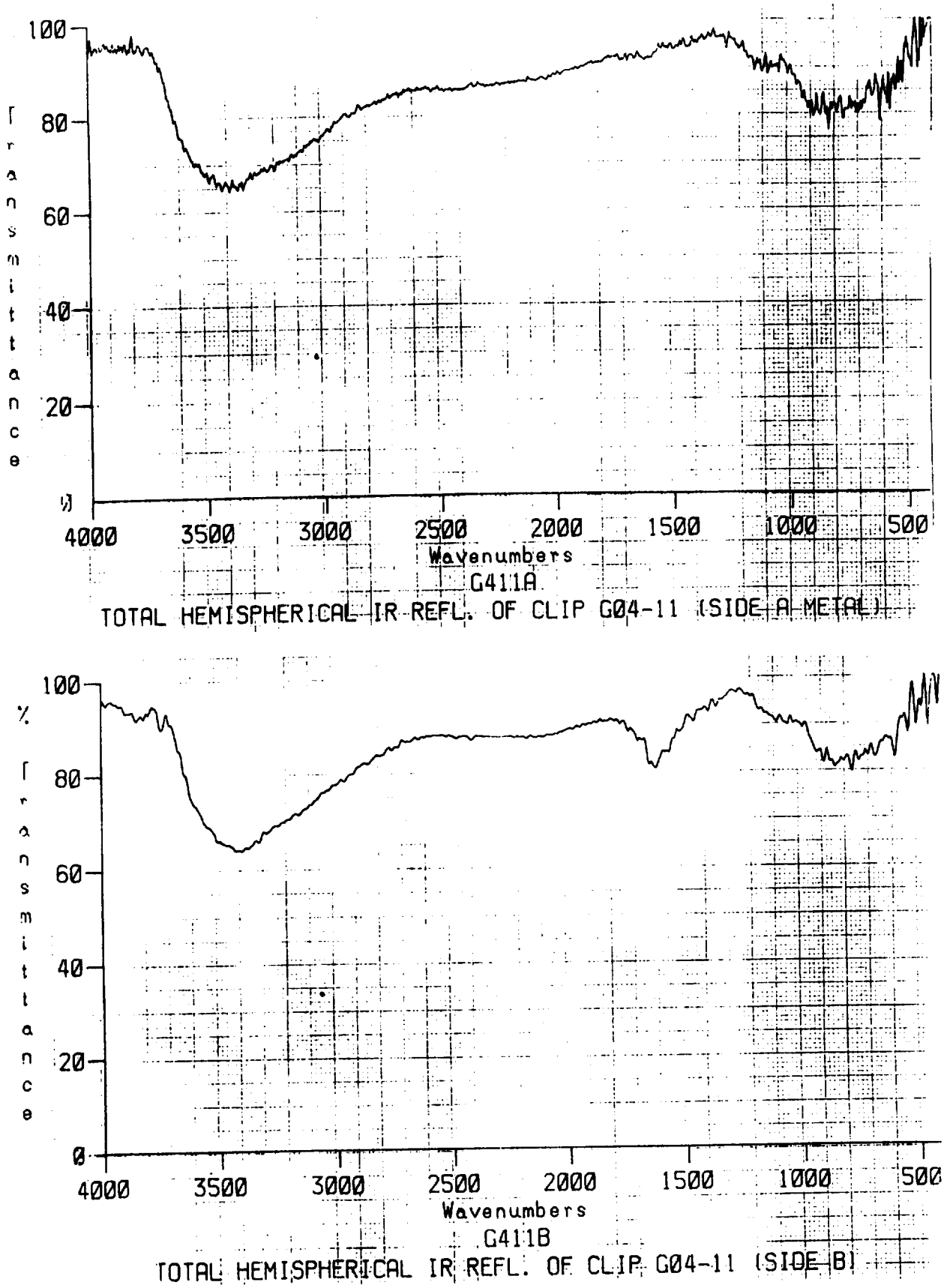

Figure A38: Total Hemispherical IR Reflectance of clip G04-11, (A) Front (B) Back.

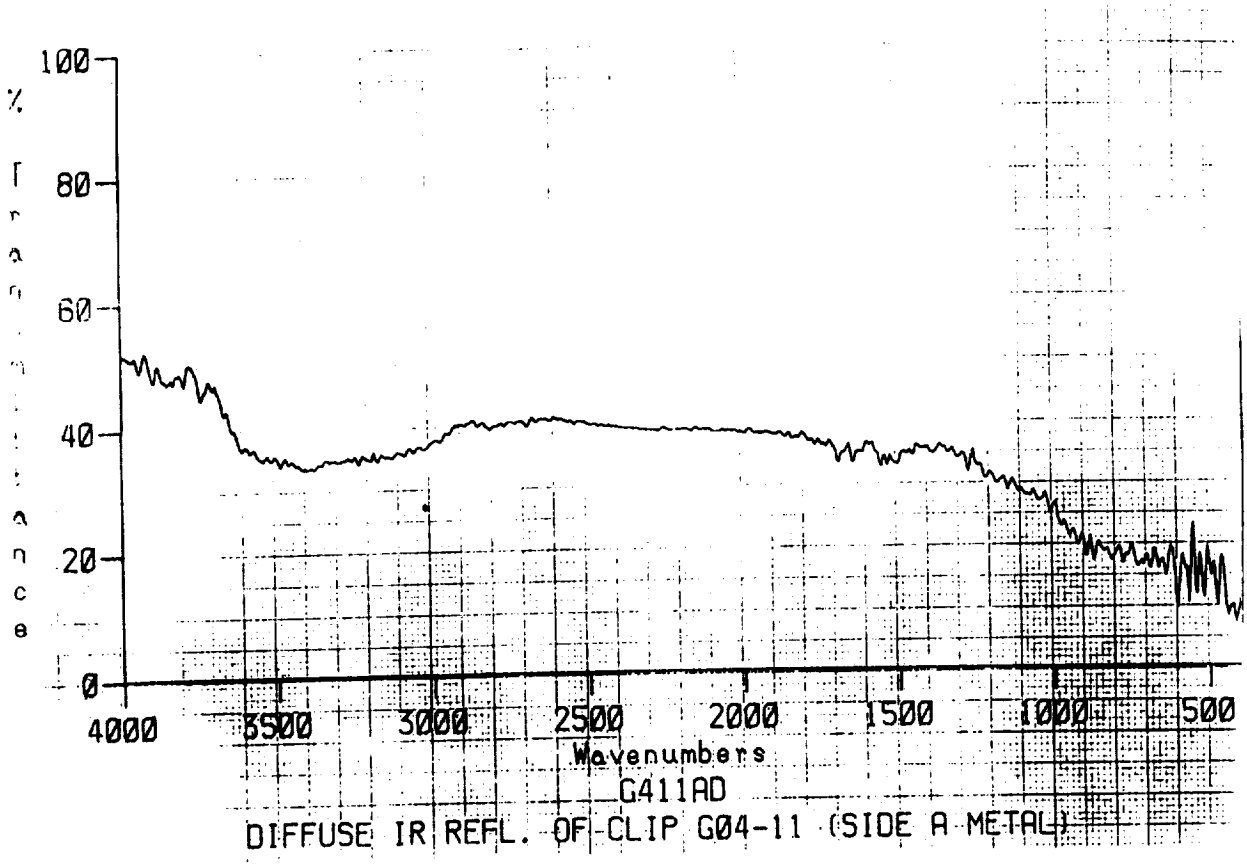

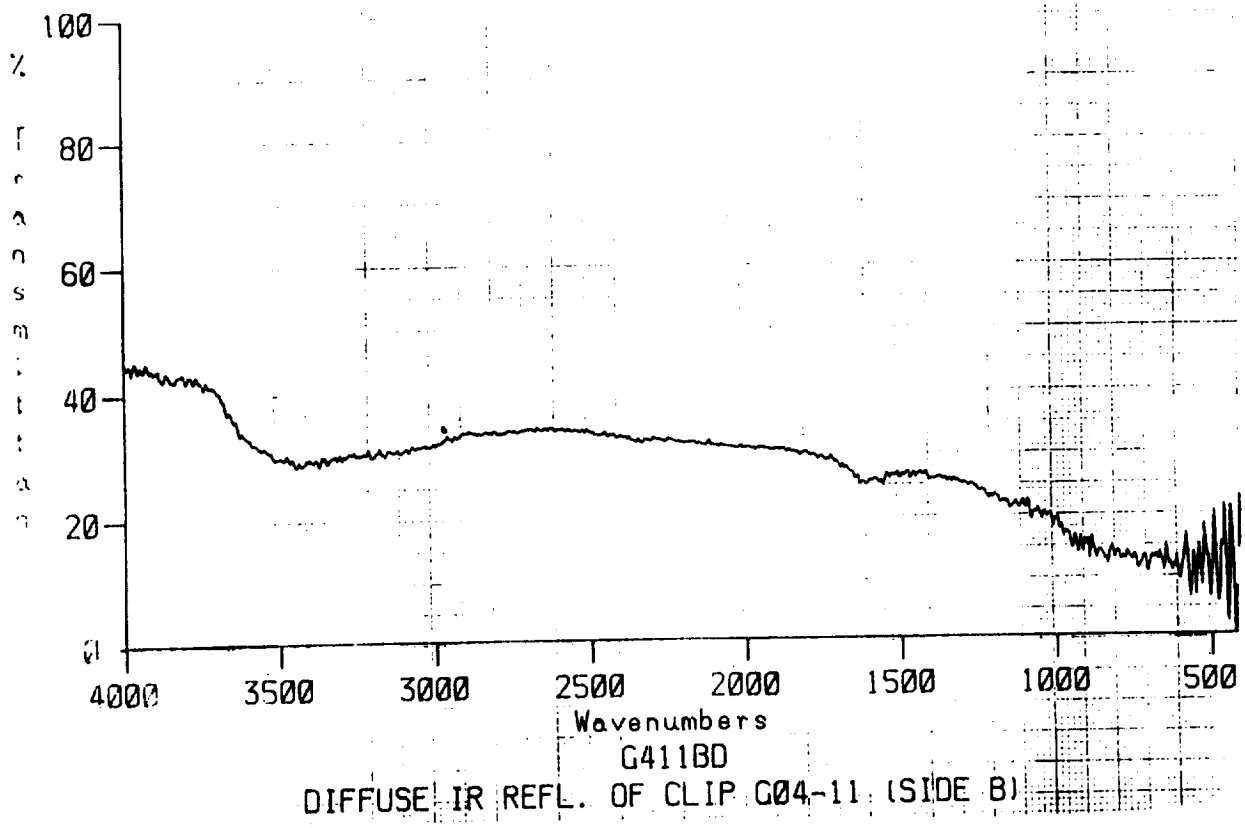

Figure A39: Diffuse IR Reflectance of clip G04-11, (A) Front (B) Back.

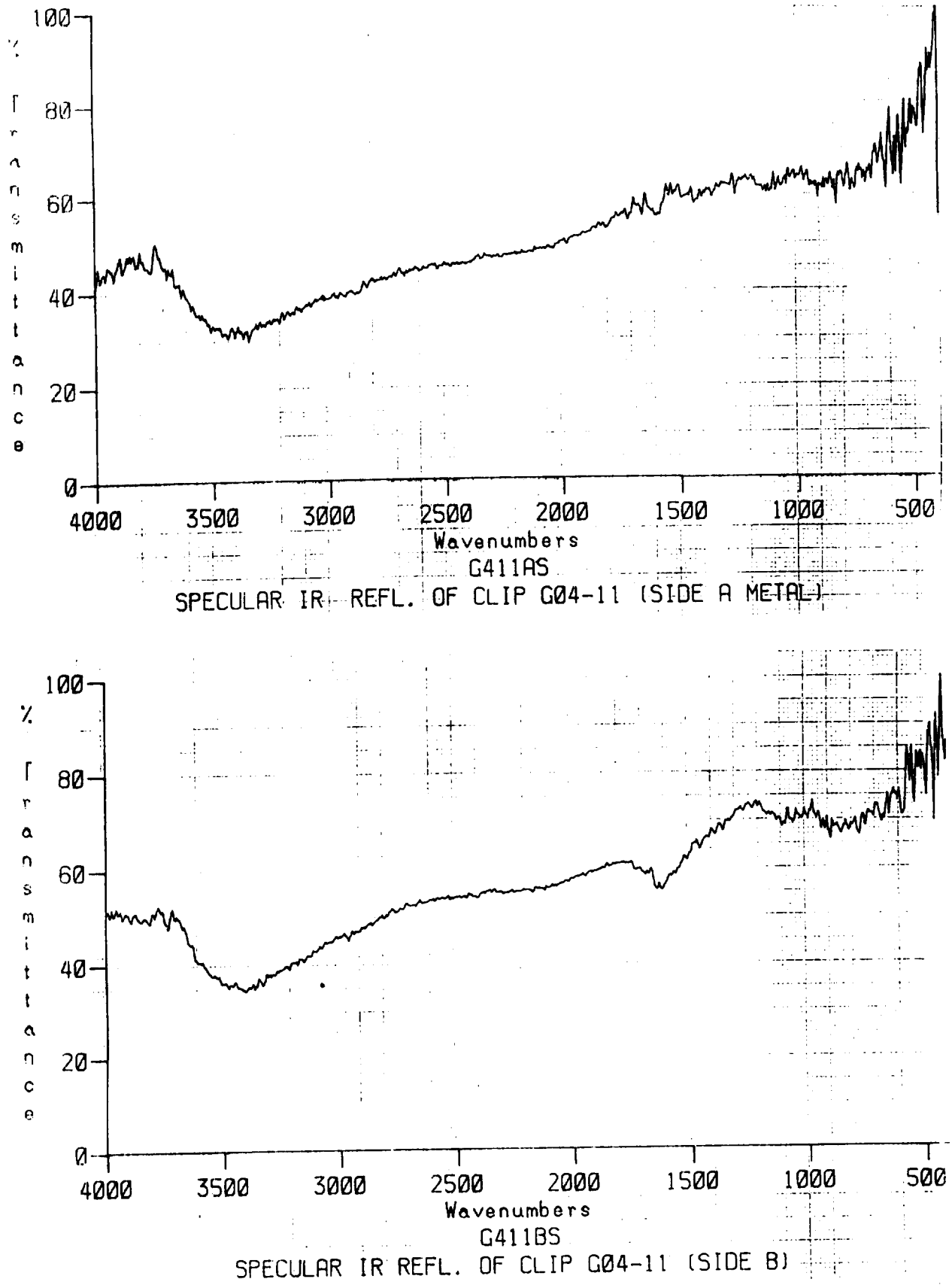

Figure A40: Specular IR Reflectance of clip G04-11, (A) Front (B) Back.

SPACE END

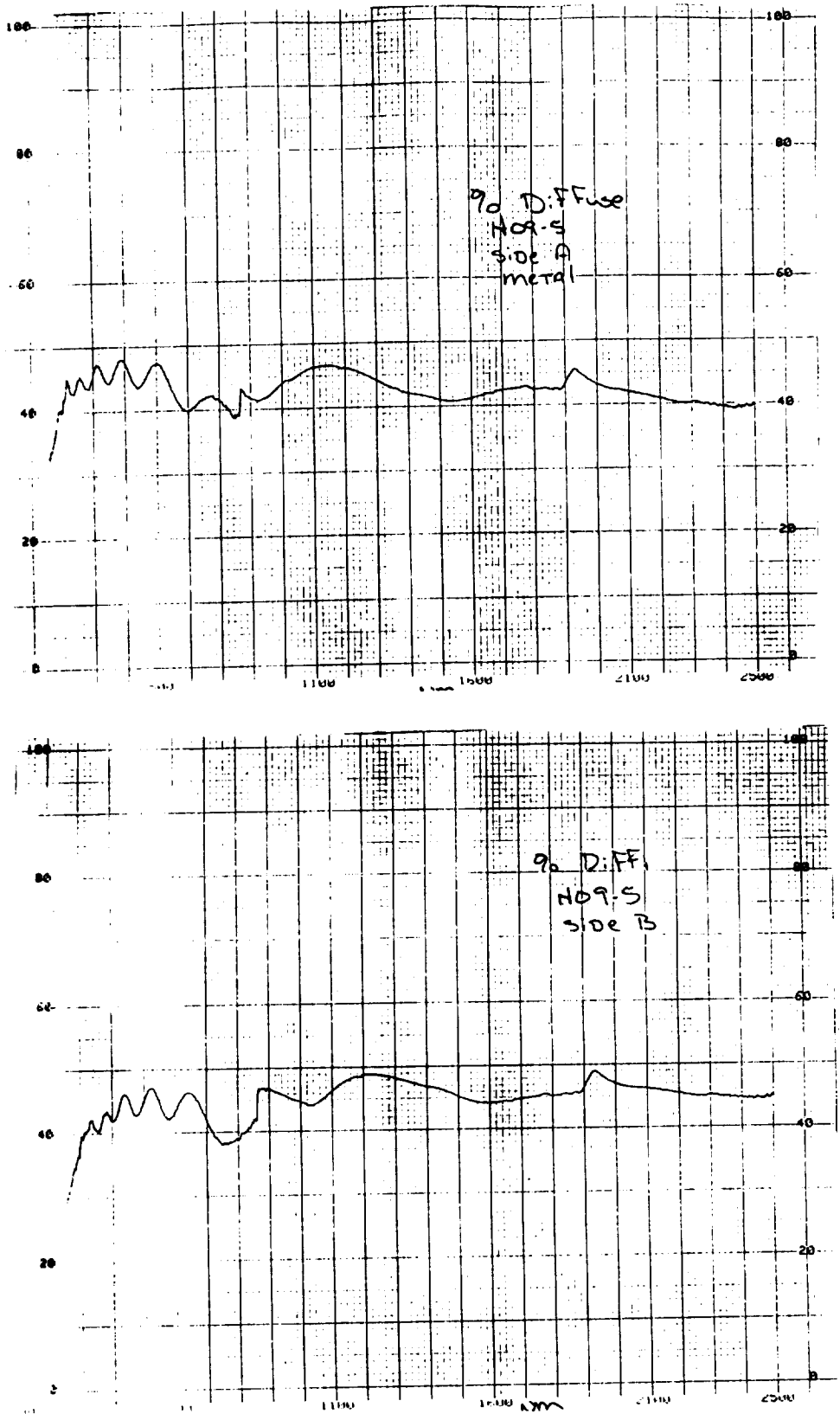

Figure A41: UV-Vis/NIR Diffuse Reflectance of clamp H 09-5, (A) Front (B) Back.

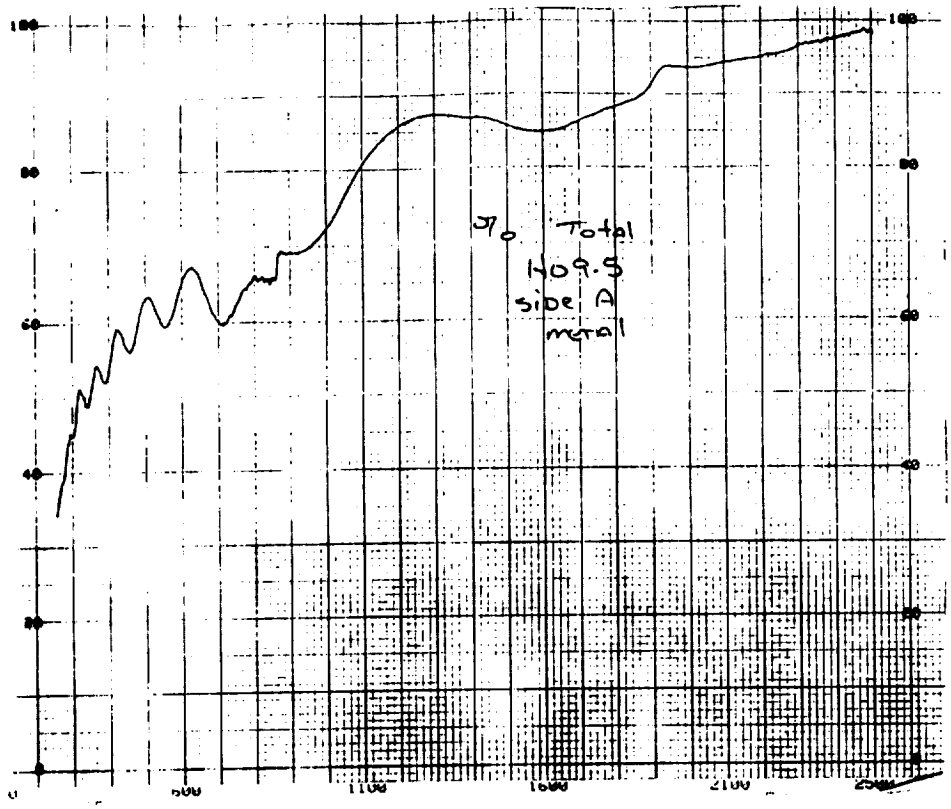

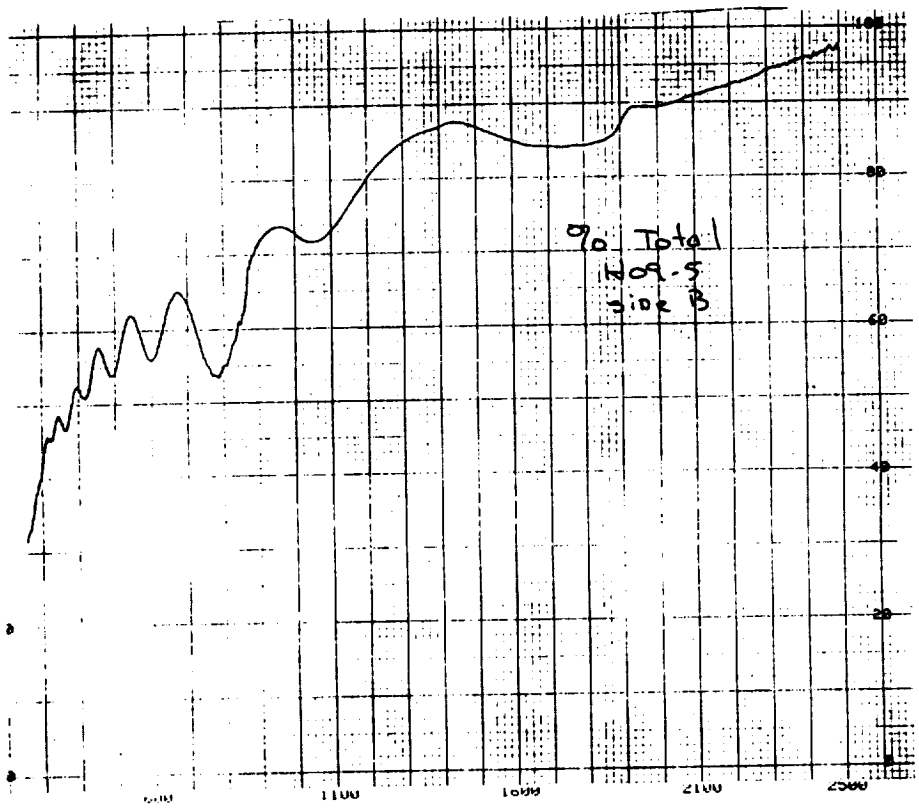

Figure A42: UV-Vis/NIR Total Reflectance of clamp H09-5, (A) Front (B) Back.

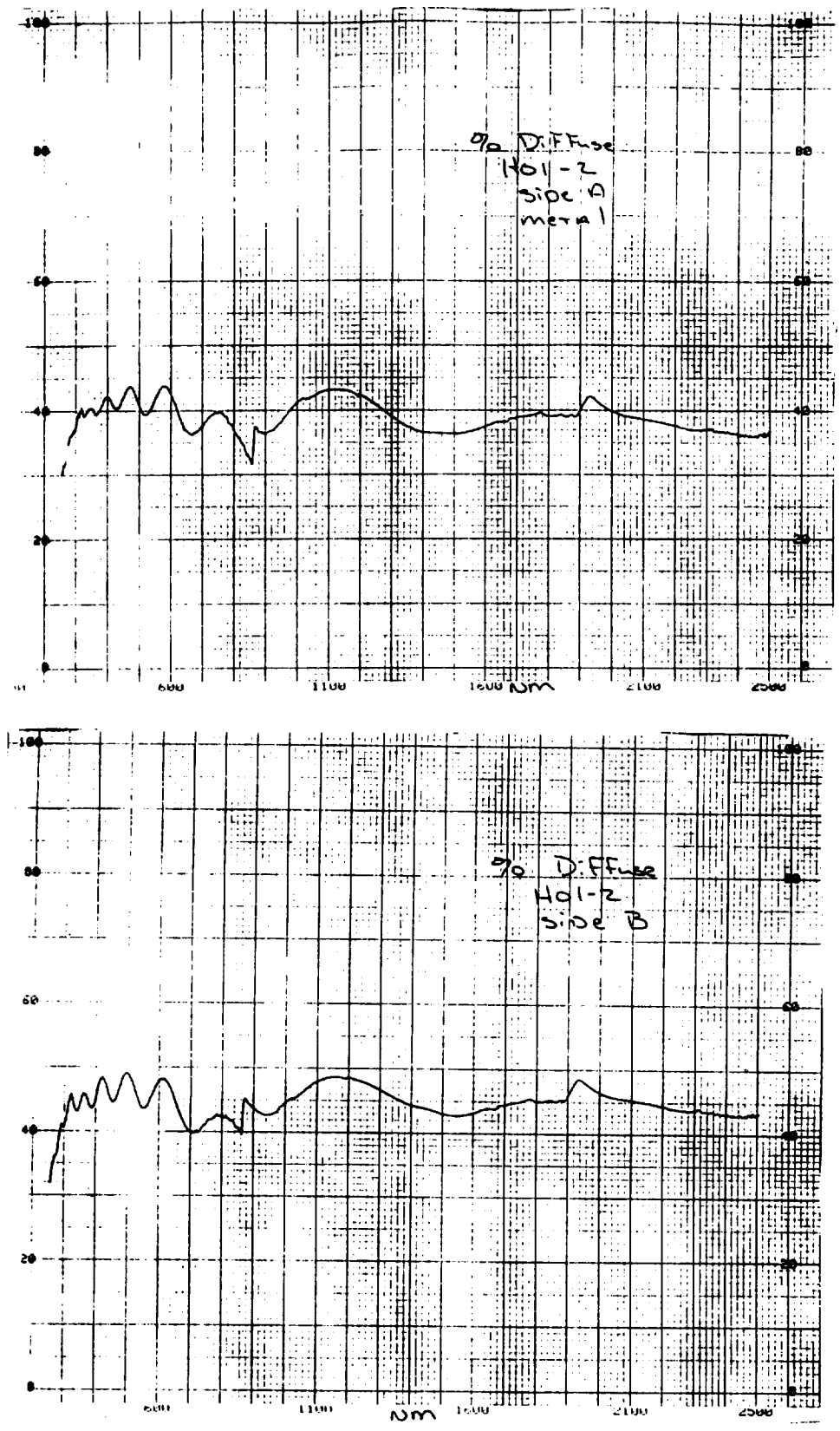

Figure A43: UV-Vis/NIR Diffuse Reflectance of clamp H01-2, (A) Front (B) Back.

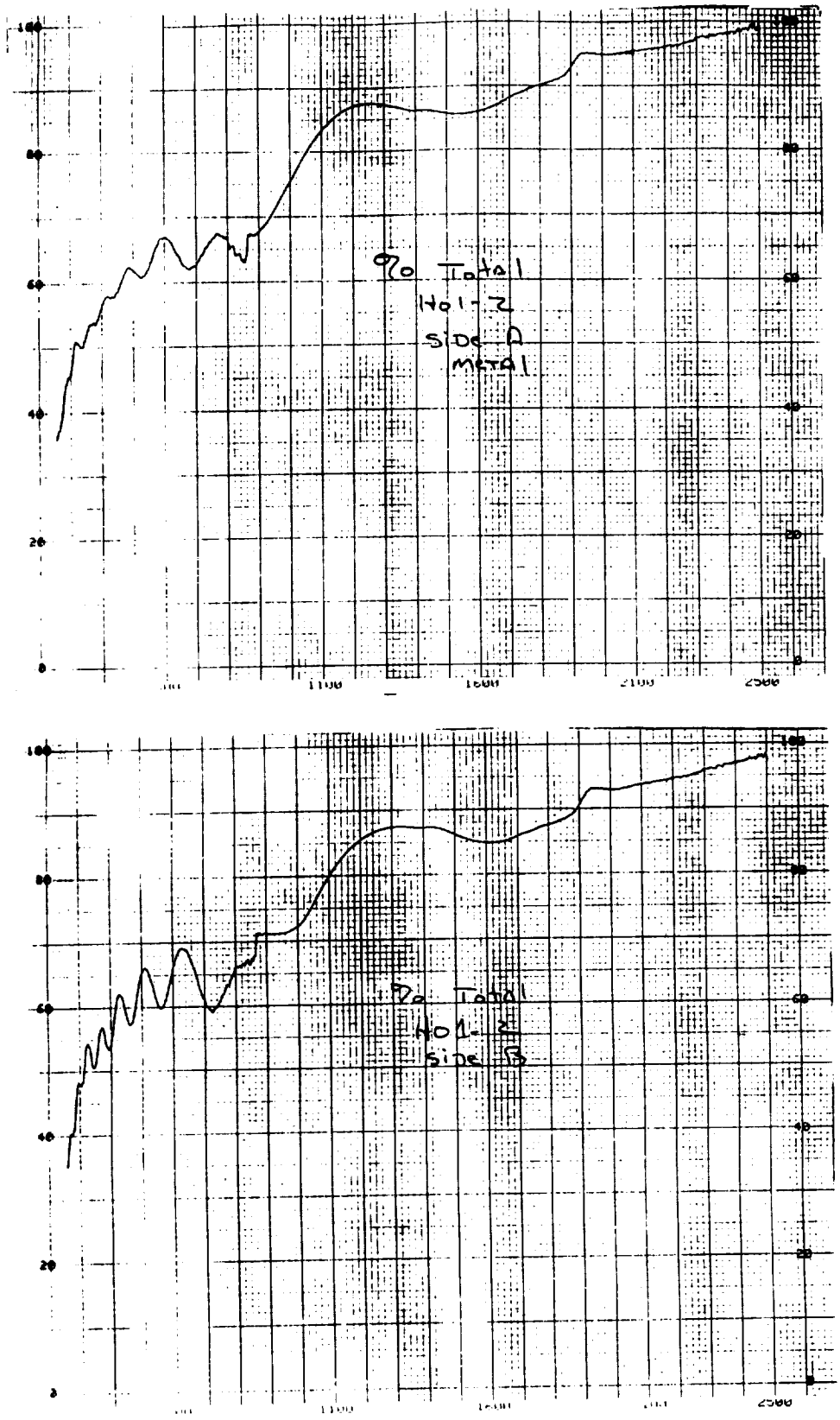

Figure A44: UV-Vis/NIR Total Reflectance of clamp H01-2, (A) Front (B) Back.

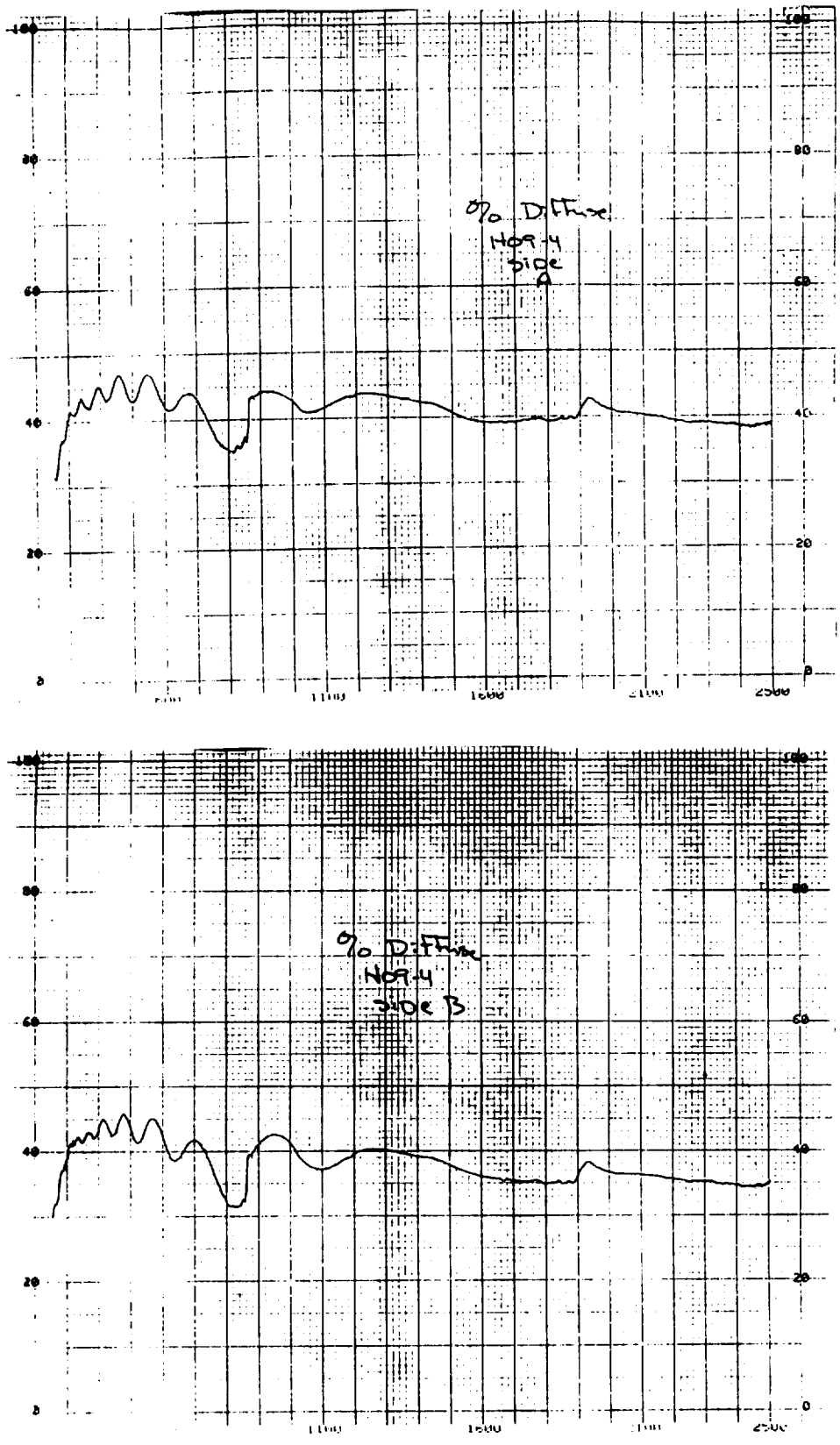

Figure A45: UV-Vis/NIR Diffuse Reflectance of clamp, H09-4, (A) Front (B) Back.

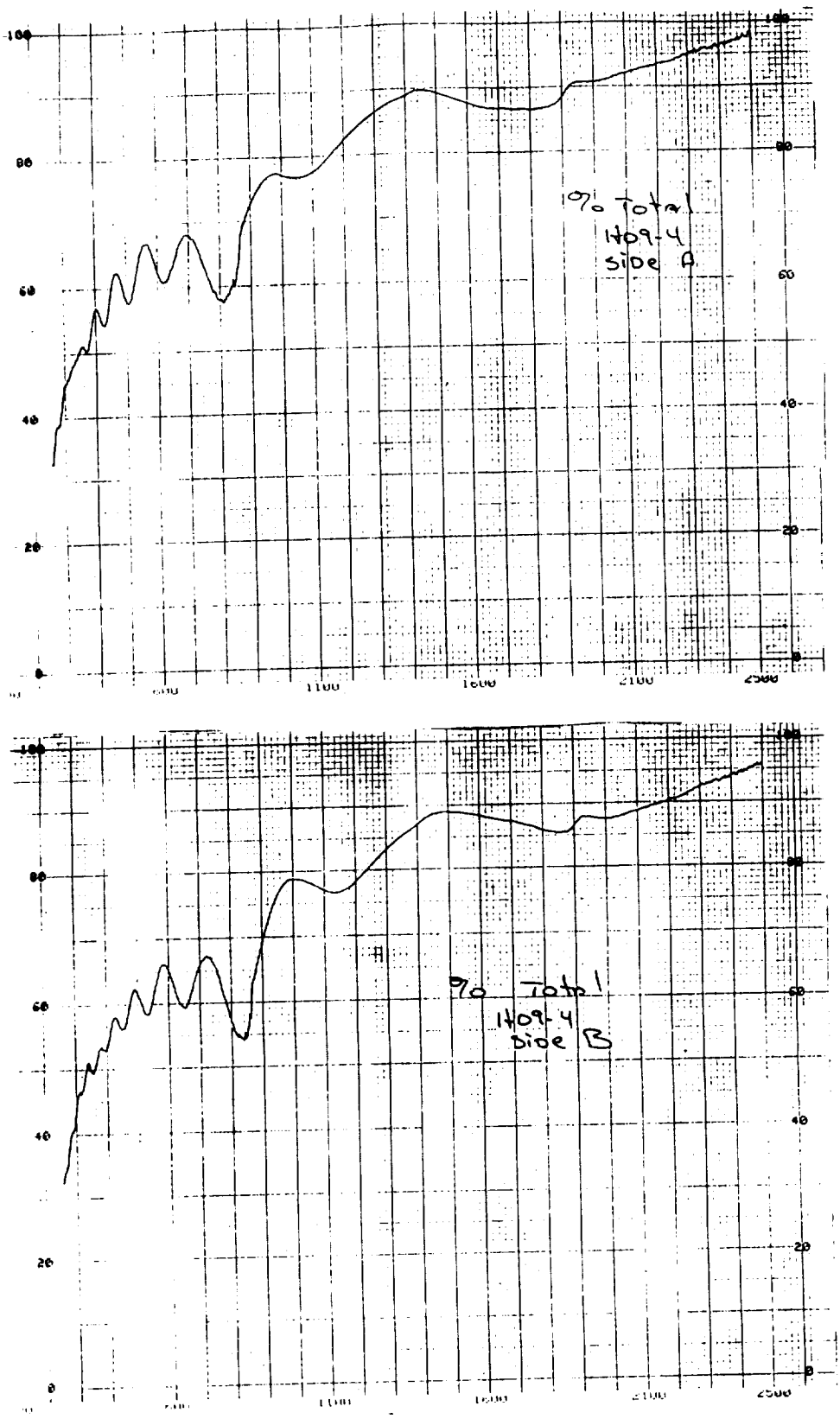

Figure A46: UV-Vis/NIR Total Reflectance of clamp, H09-4, (A) Front (B) Back.

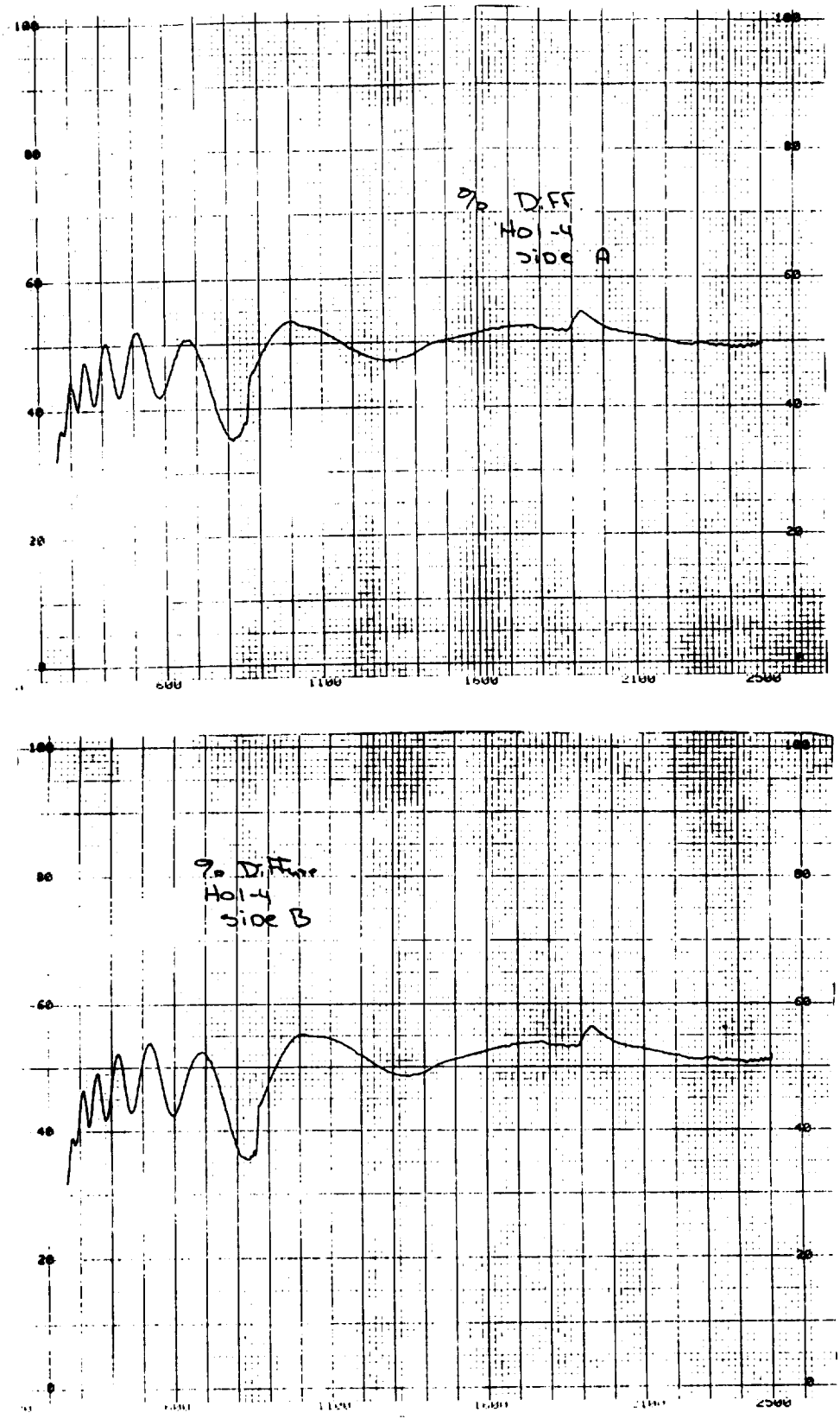

Figure A47: UV-Vis/NIR Diffuse Reflectance of clamp, H01-4, (A) Front (B) Back.

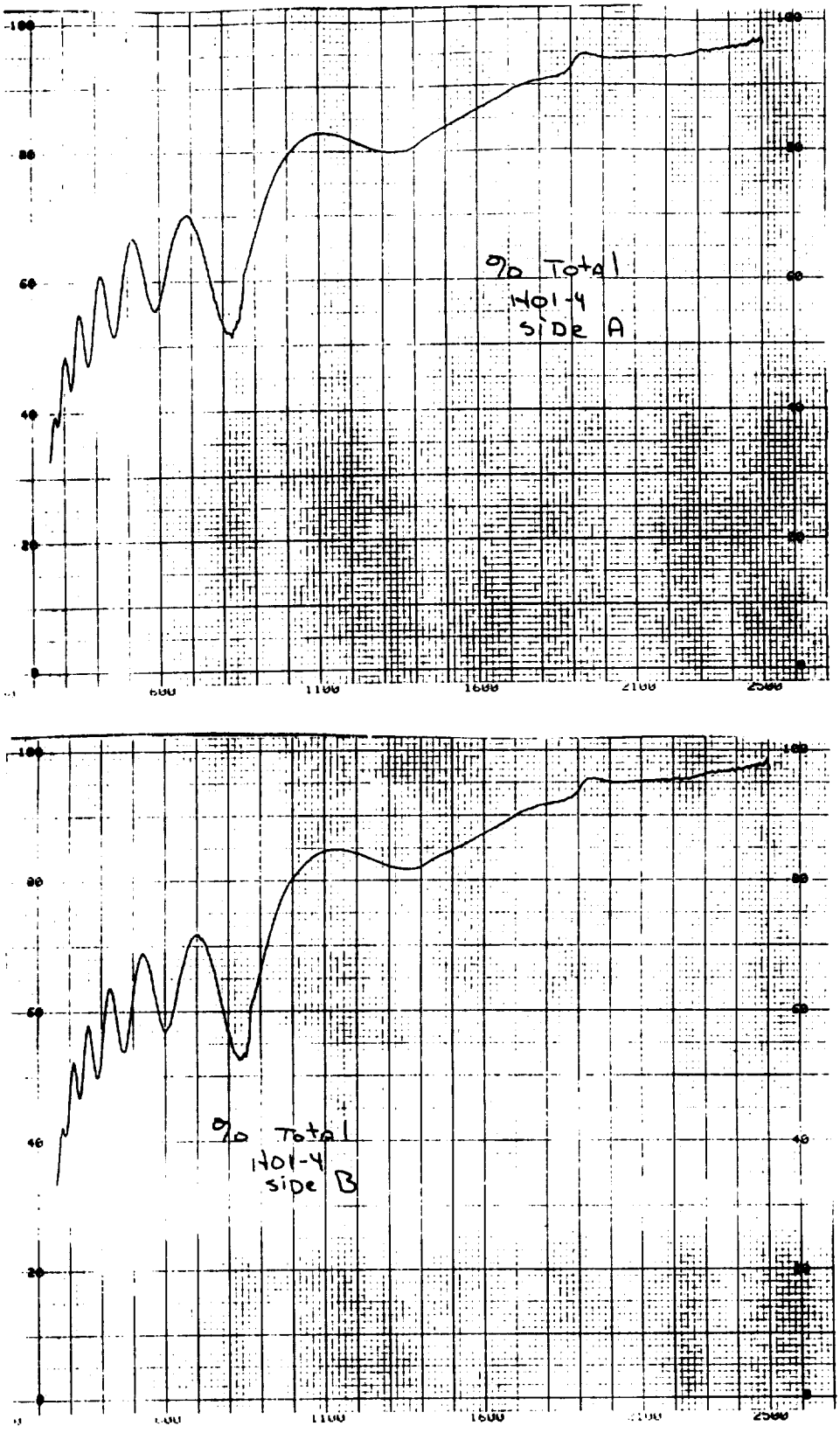

Figure A48: UV-Vis/NIR Total Reflectance of clamp, H01-4, (A) Front (B) Back.

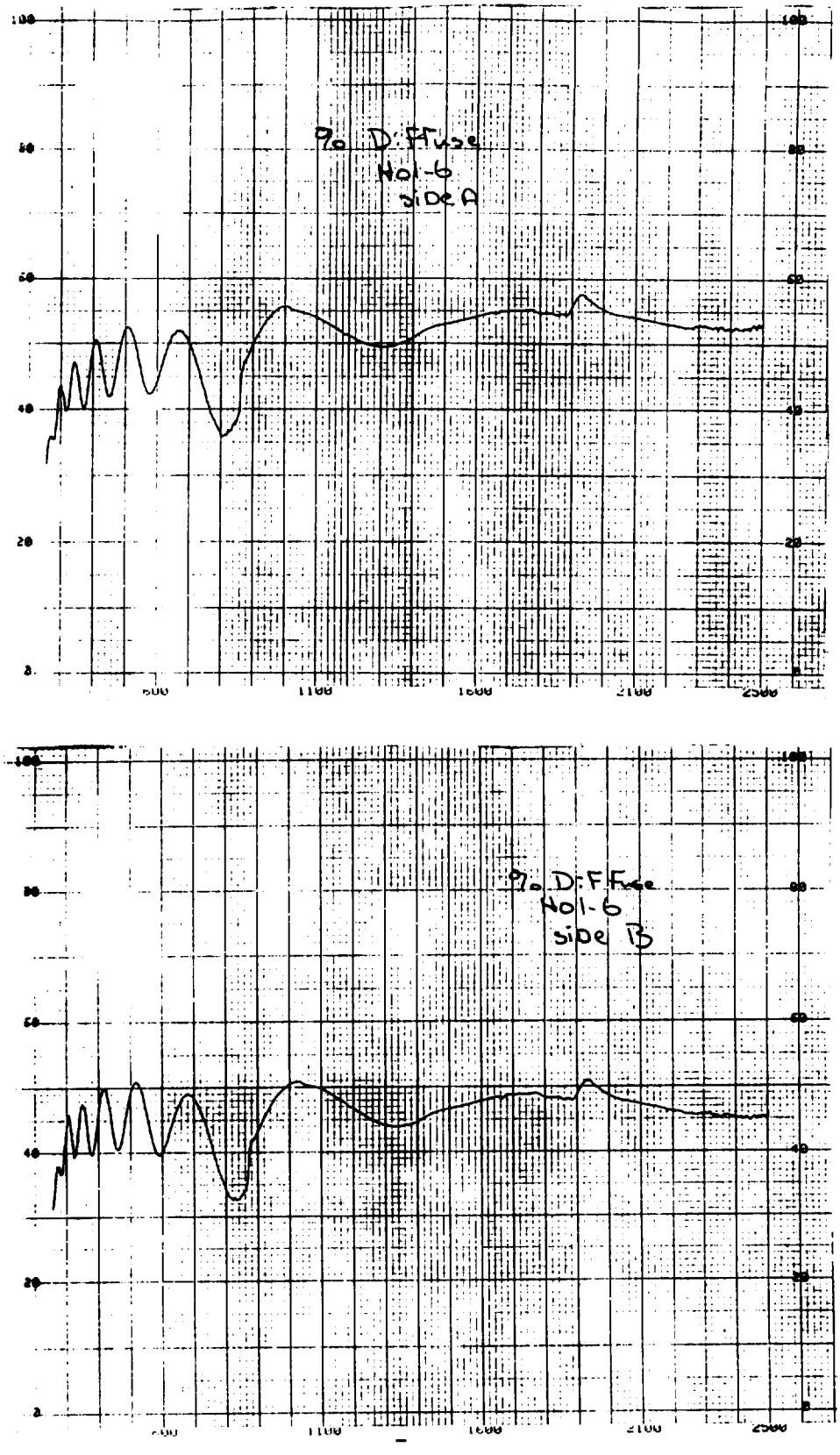

Figure A49: UV-Vis/NIR Diffuse Reflectance of clamp H01-6, (A) Front (B) Back.

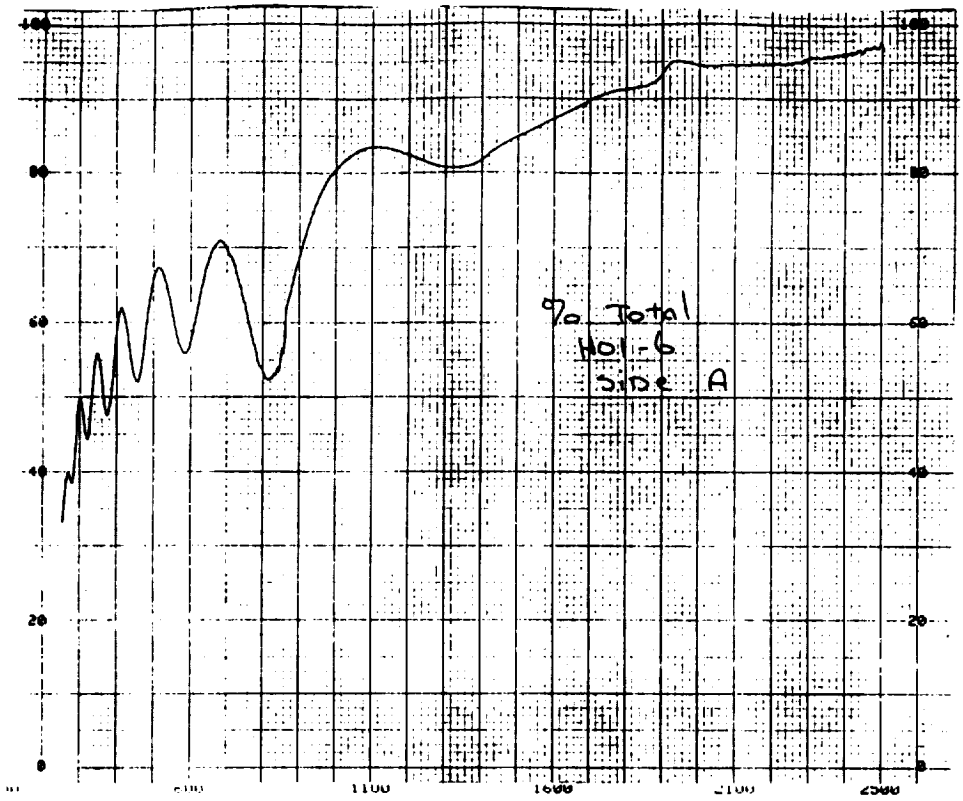

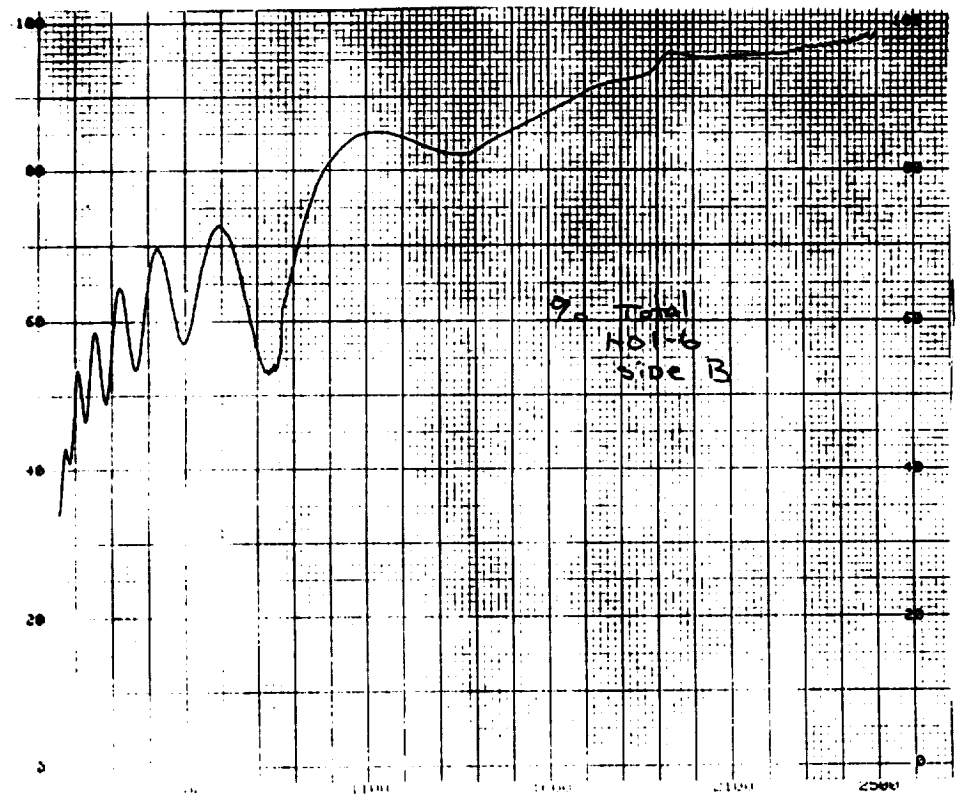

Figure A50: UV-Vis/NIR Total Reflectance of clamp H01-6, (A) Front (B) Back.

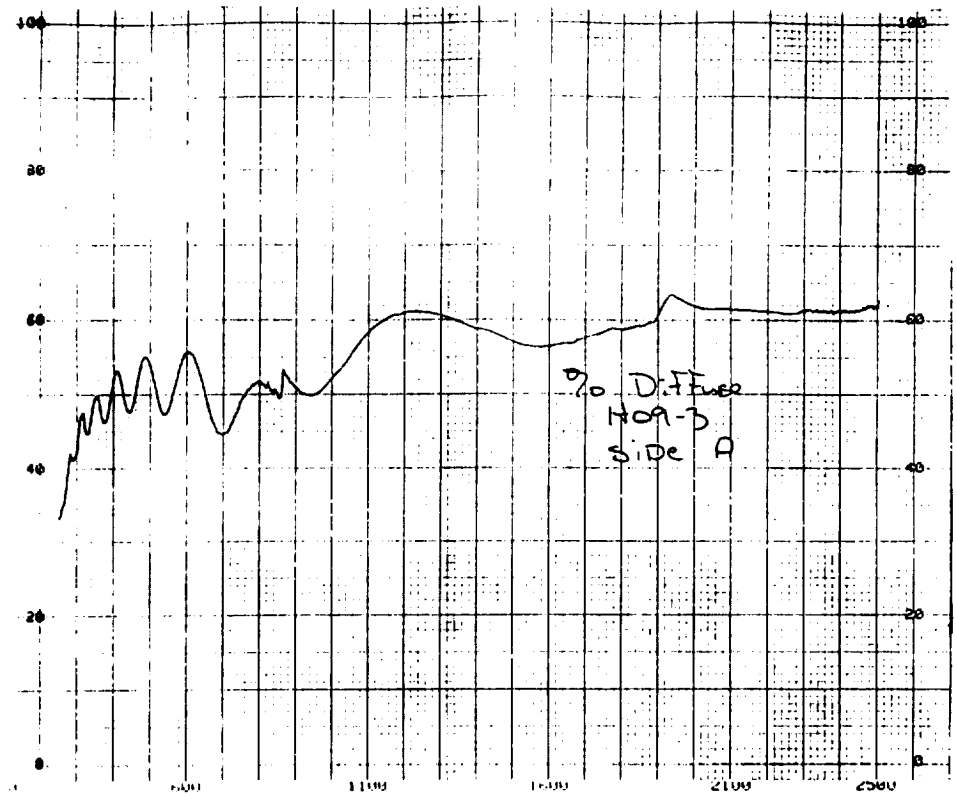

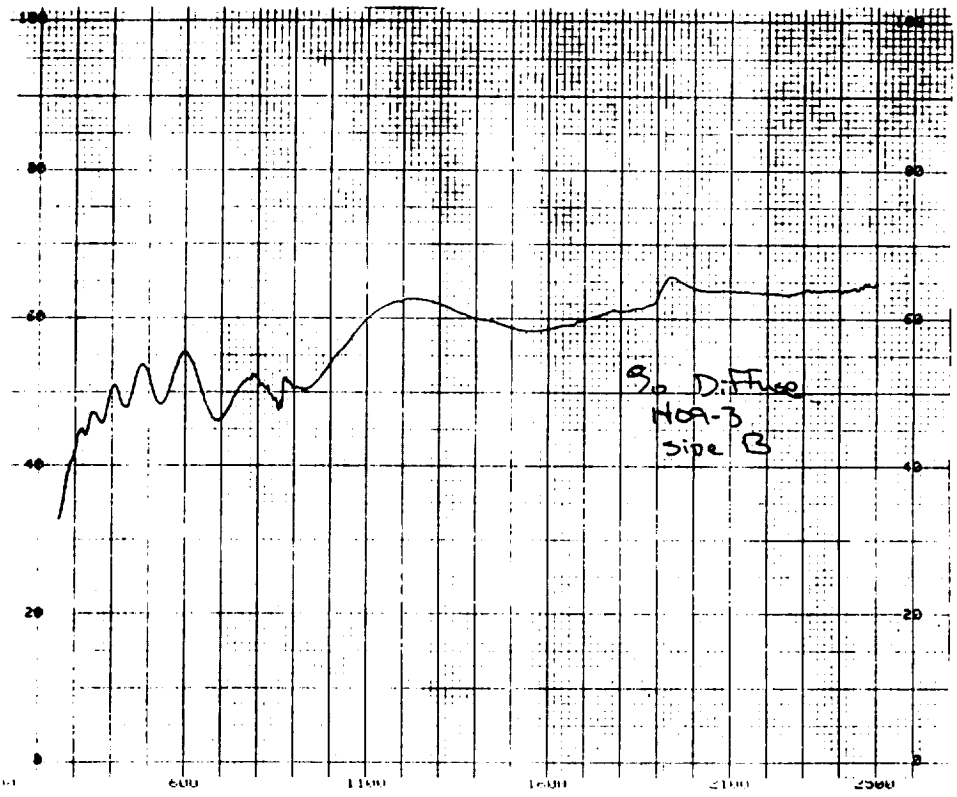

Figure A51: UV-Vis/NIR Diffuse Reflectance of clamp H09-3, (A) Front (B) Back.

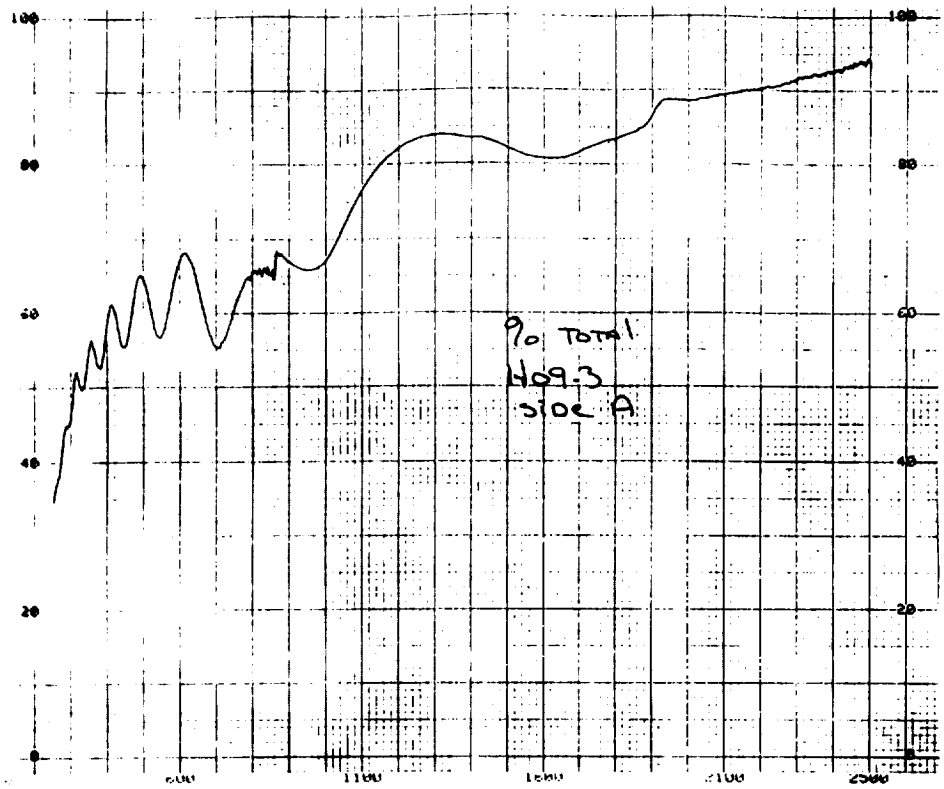

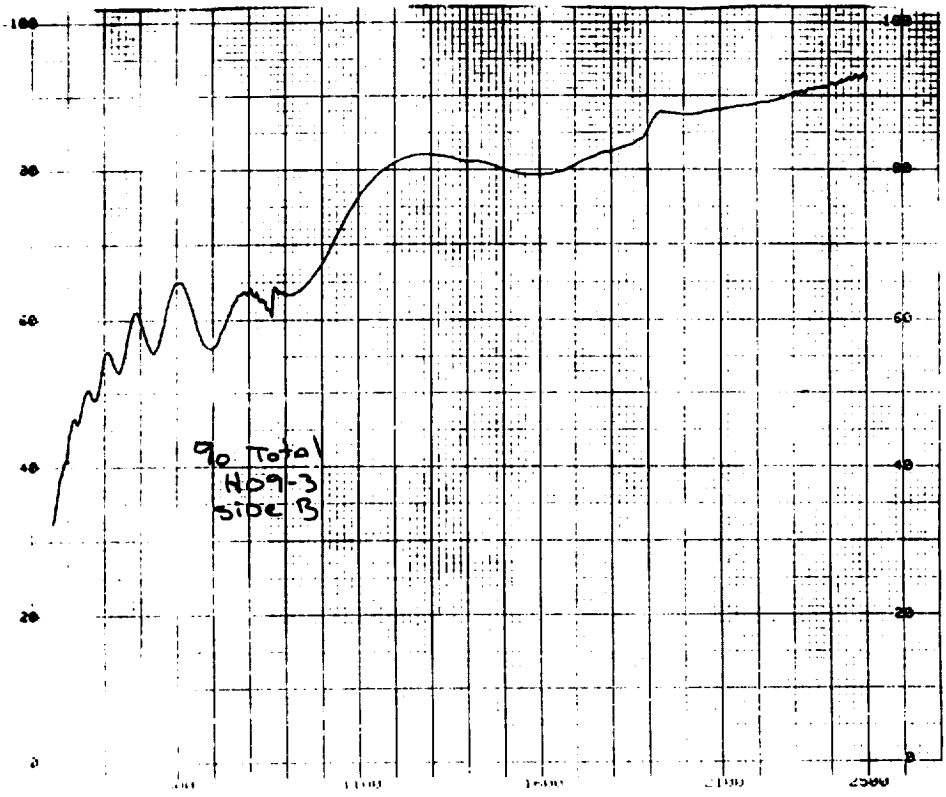

Figure A52: UV-Vis/NIR Total Reflectance of clamp H09-3, (A) Front (B) Back.

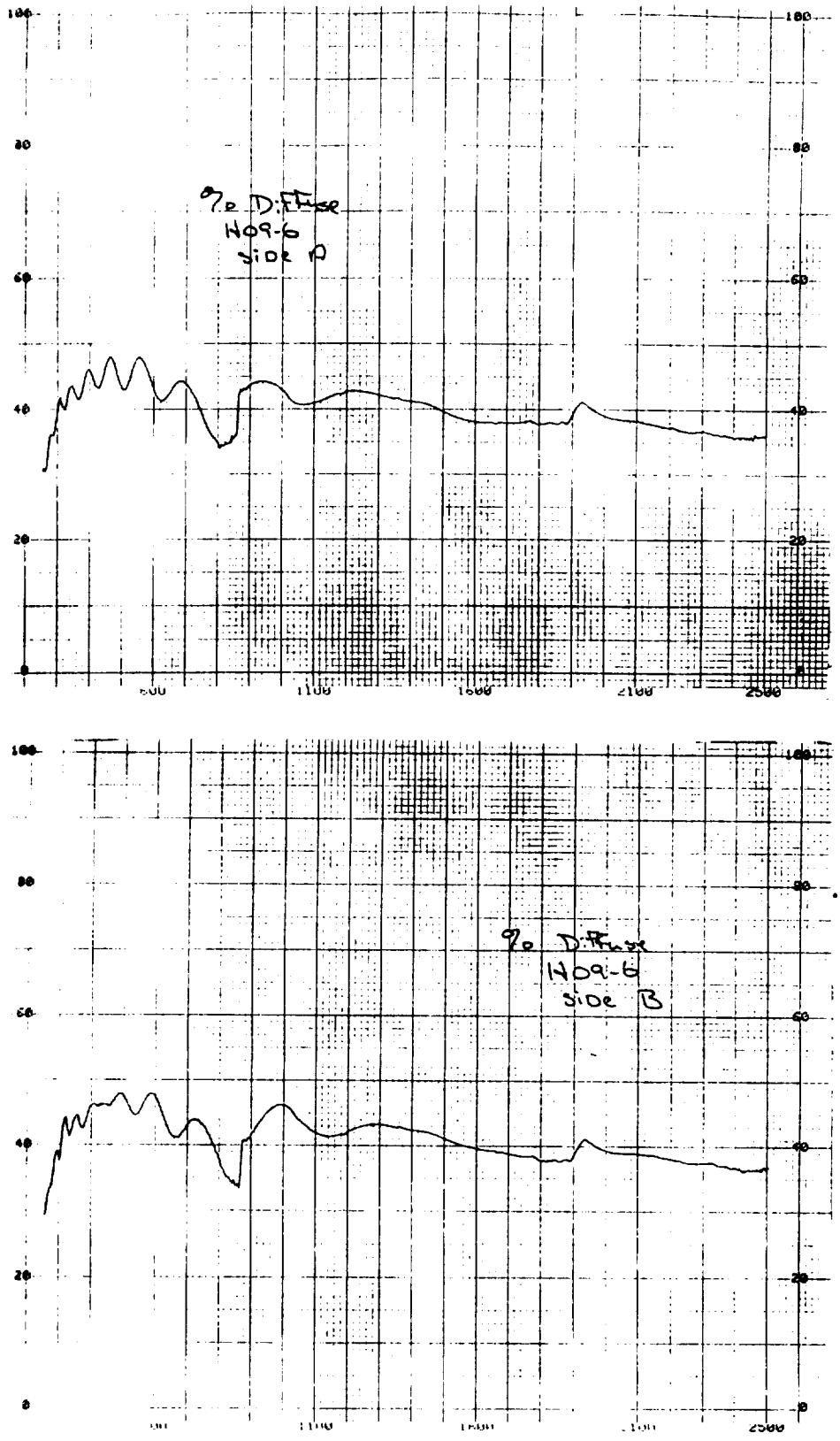

Figure A53: UV-Vis/NIR Diffuse Reflectance of clamp H09-6, (A) Front (B) Back.

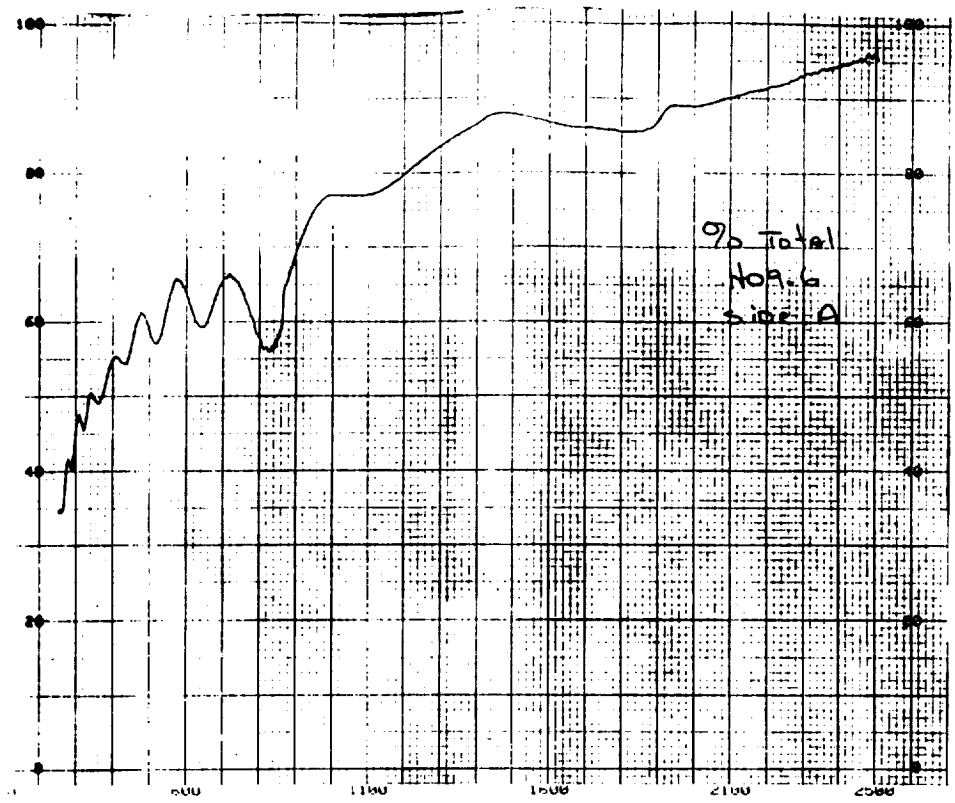

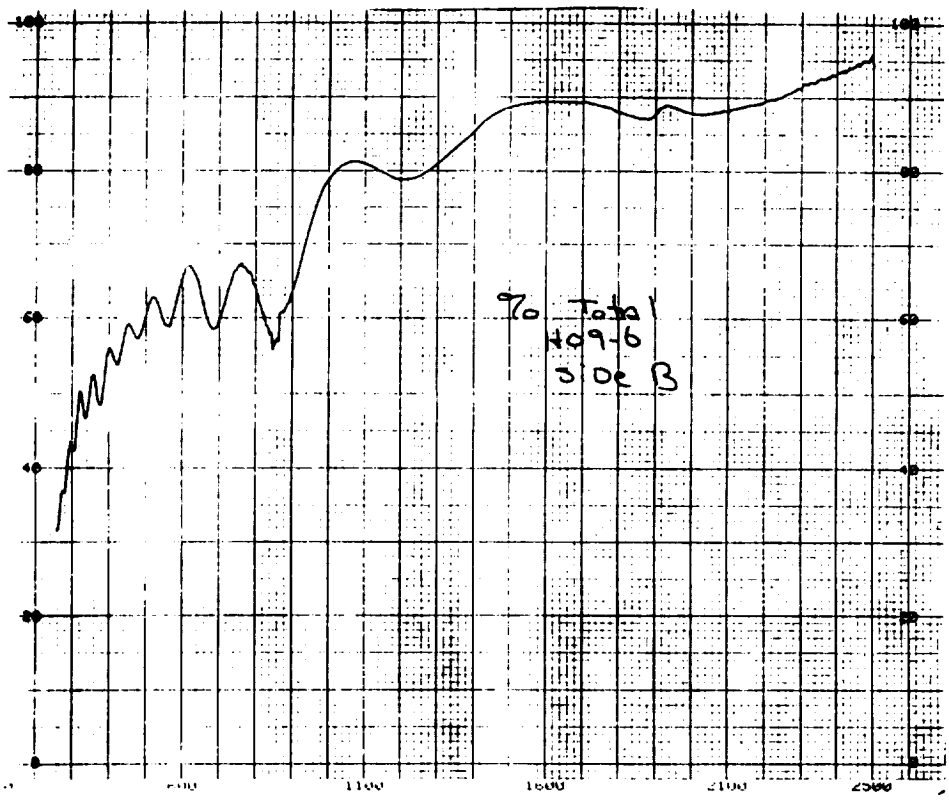

Figure A54: UV-Vis/NIR Total Reflectance of clamp H09-6, (A) Front (B) Back.

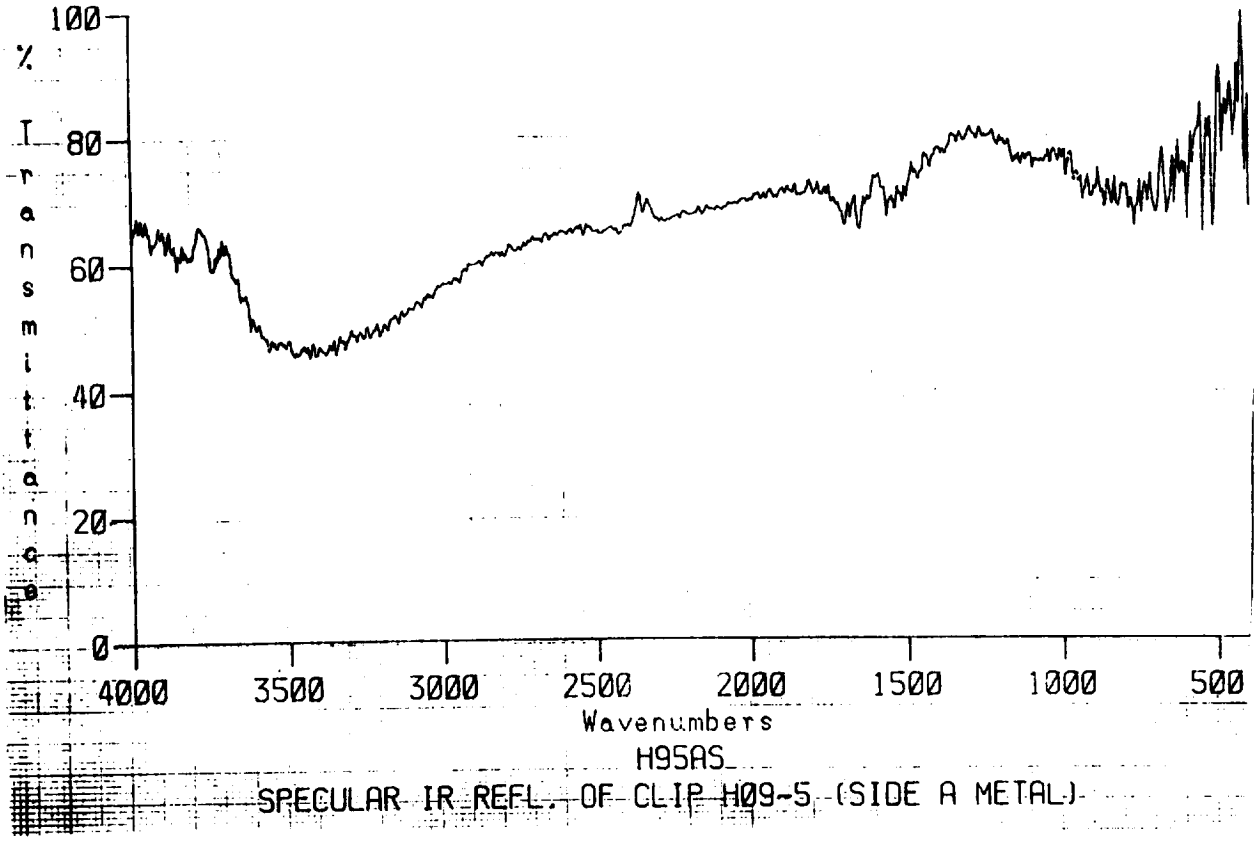

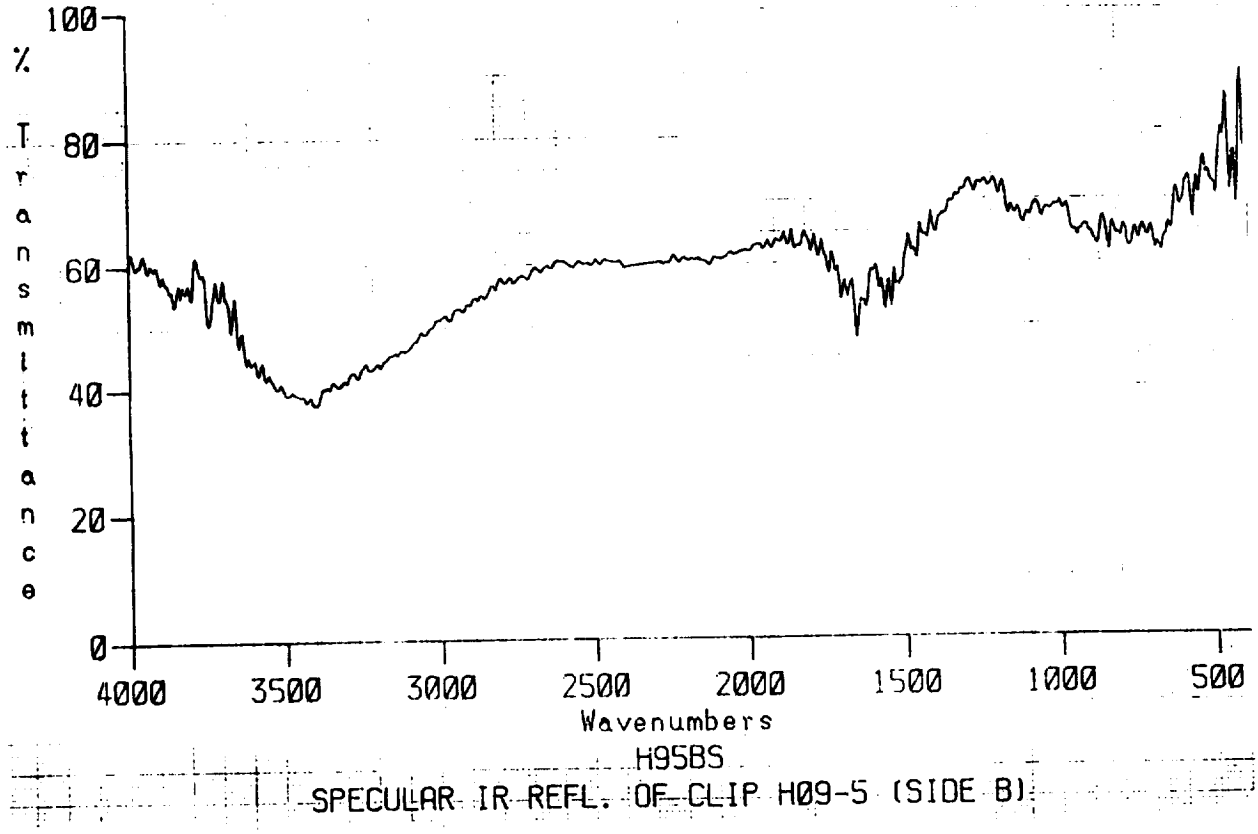

Figure A55: Specular IR Reflectance of clip H09-5, (A) Front (B) Back.

C-2

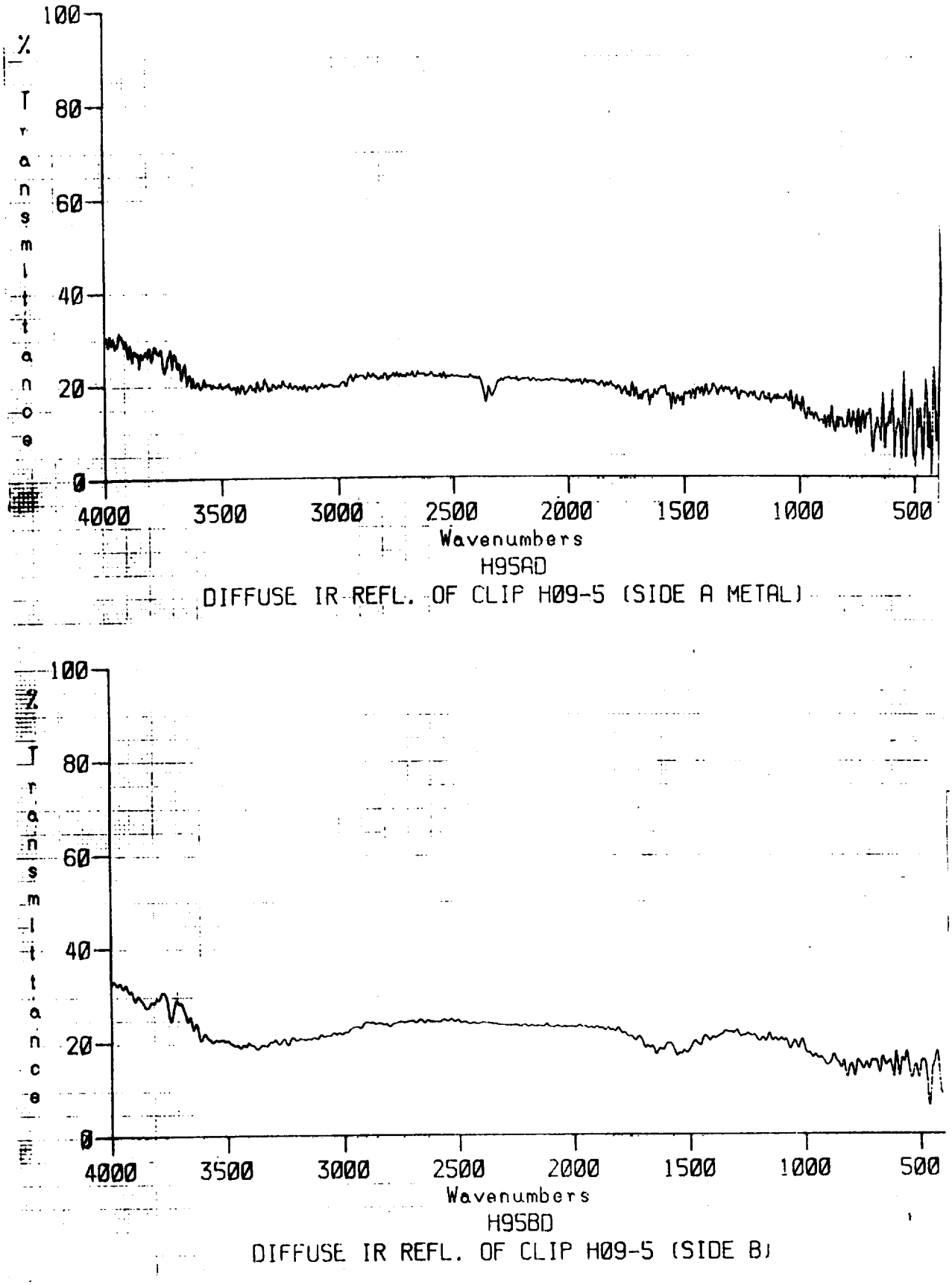

Figure A56: Diffuse IR Reflectance of clip H09-5, (A) Front (B) Back.

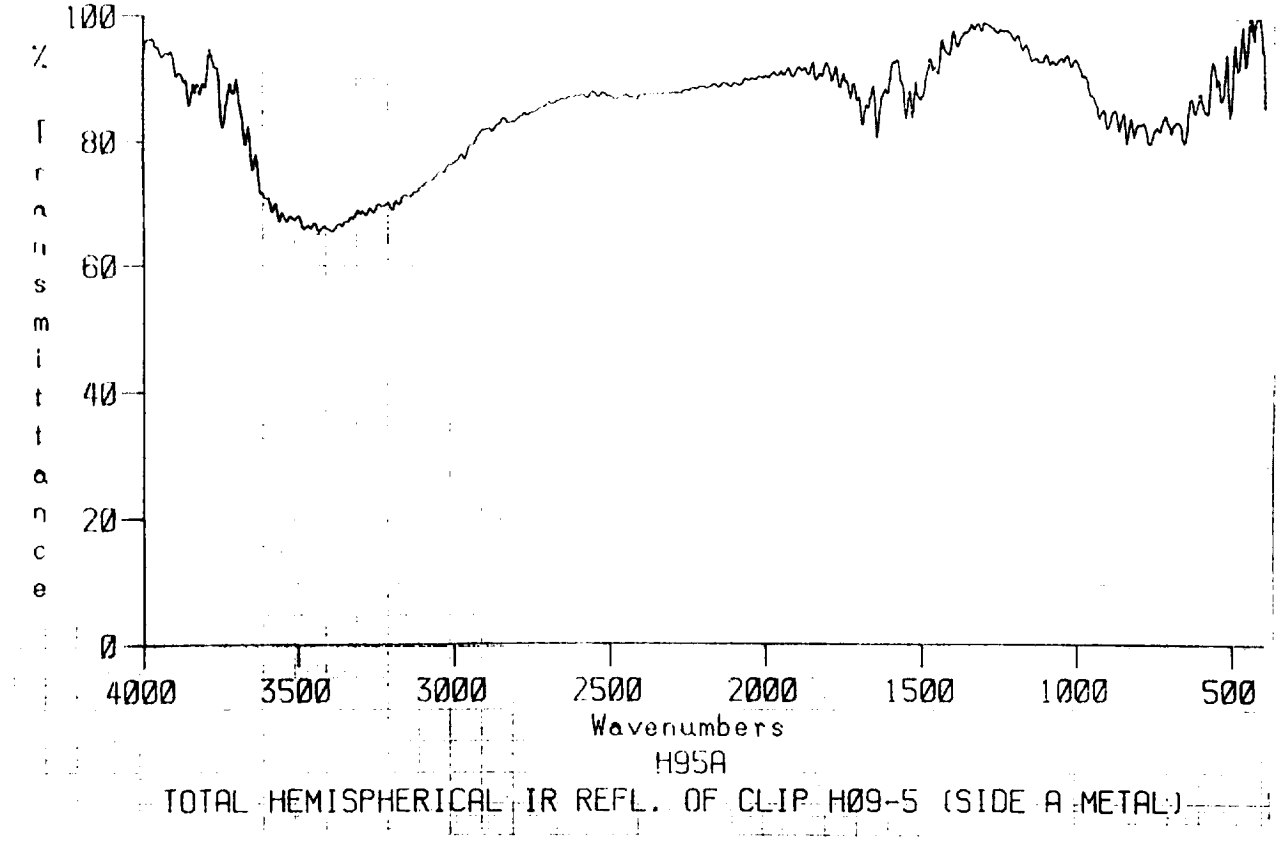

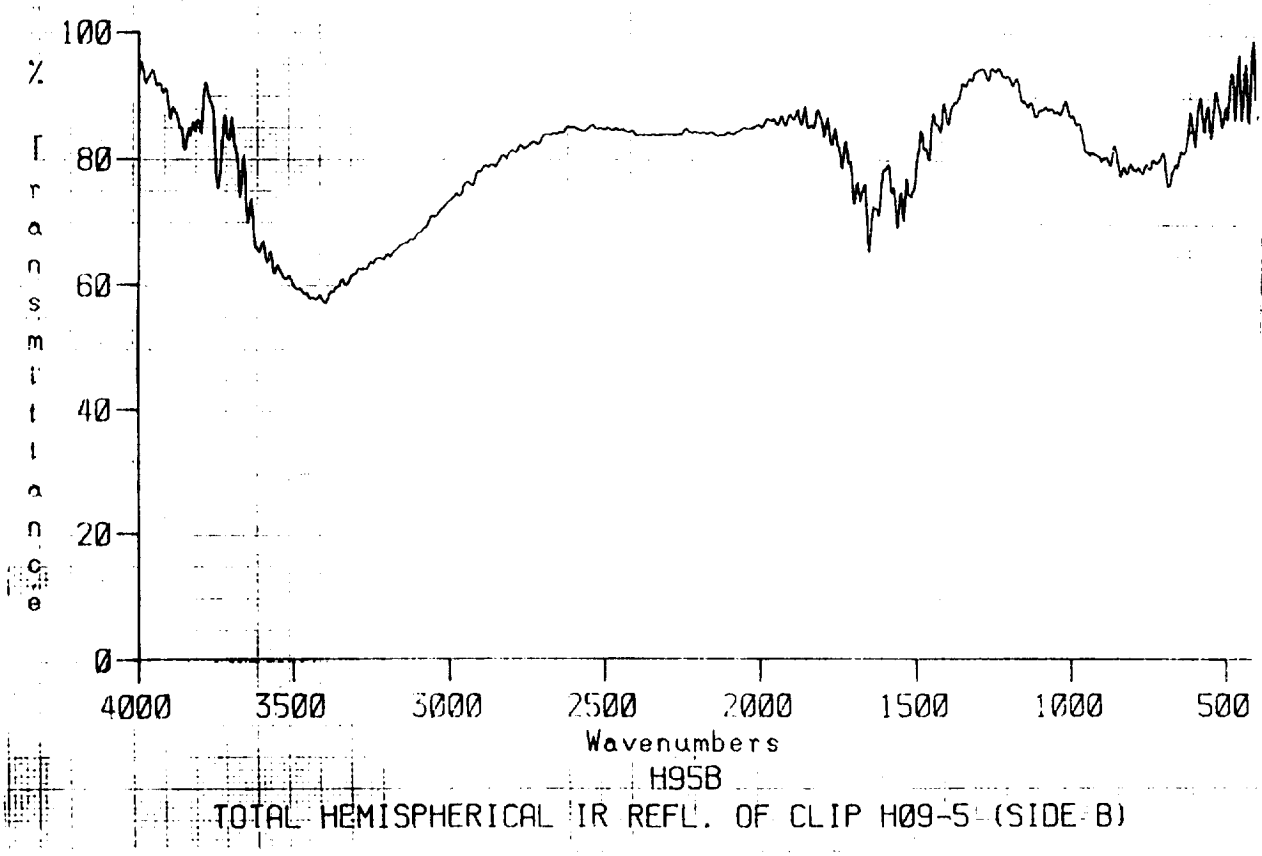

Figure A57: Total Hemispherical IR Reflectance of clip H09-5, (A) Front (B) Back.

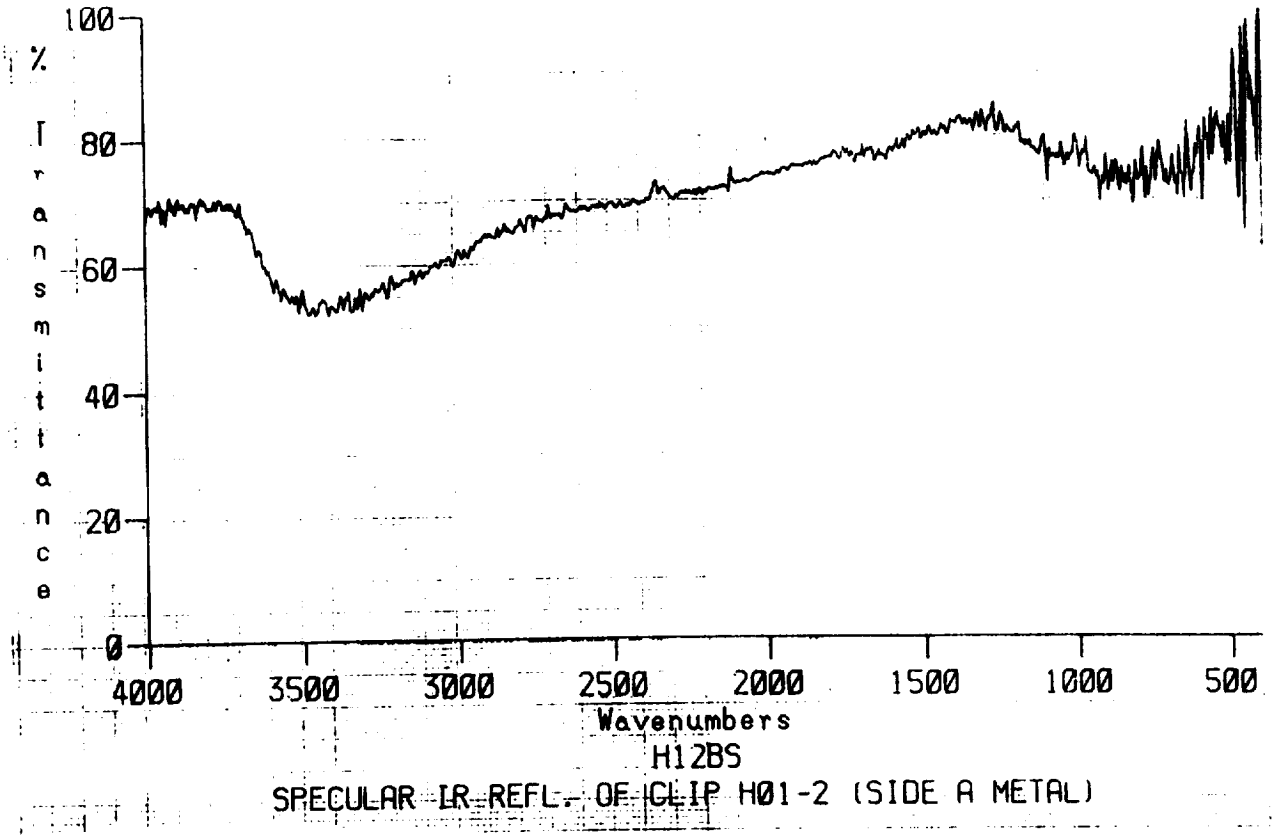

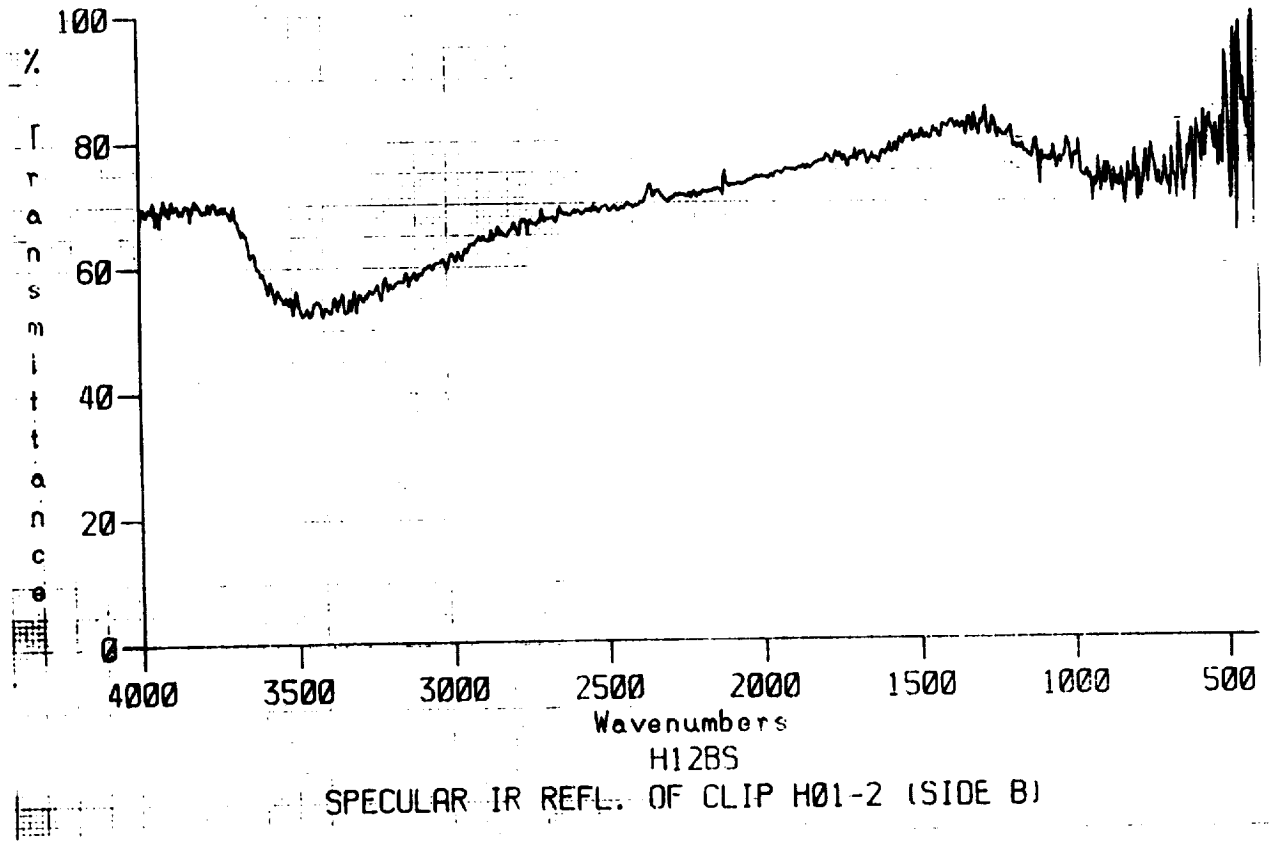

Figure A58: Specular IR Reflectance of clip H01-2, (A) Front (B) Back.

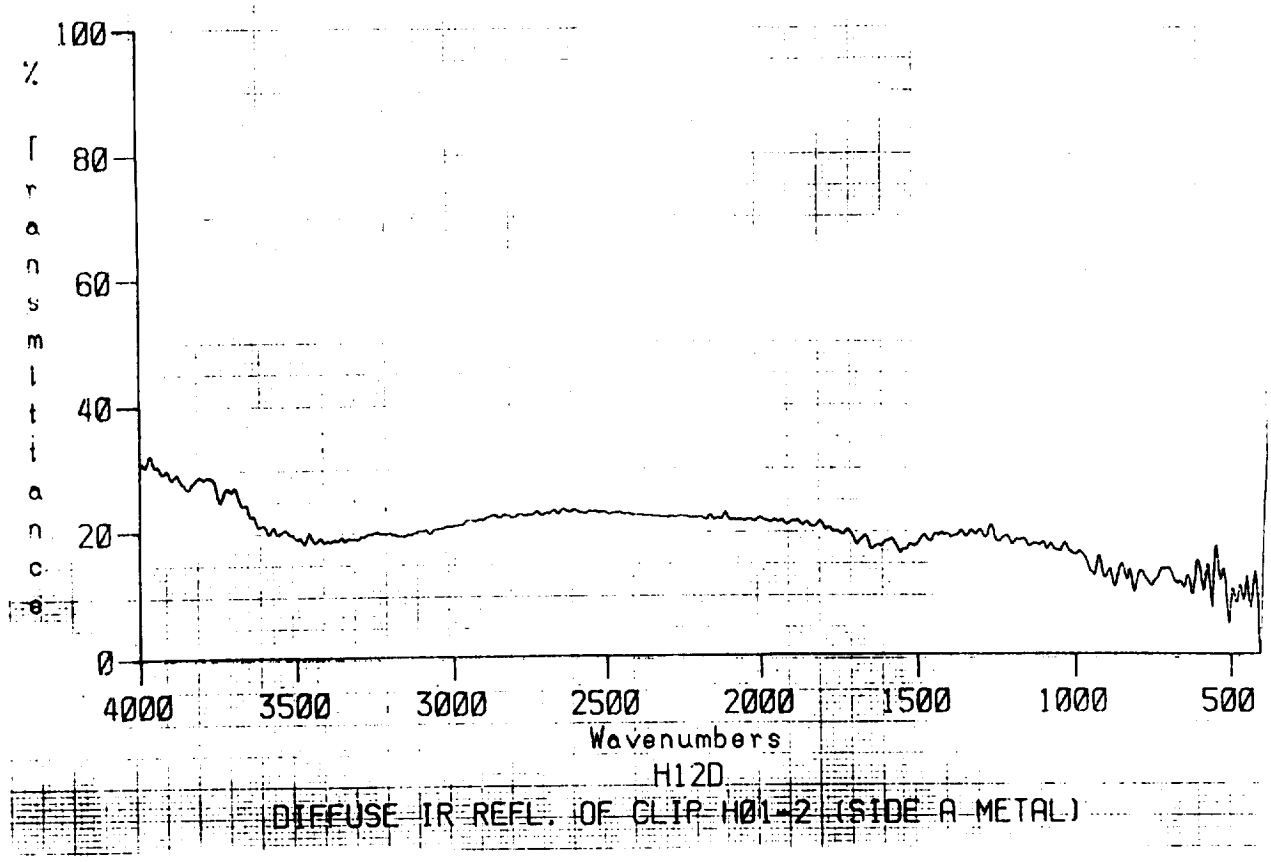

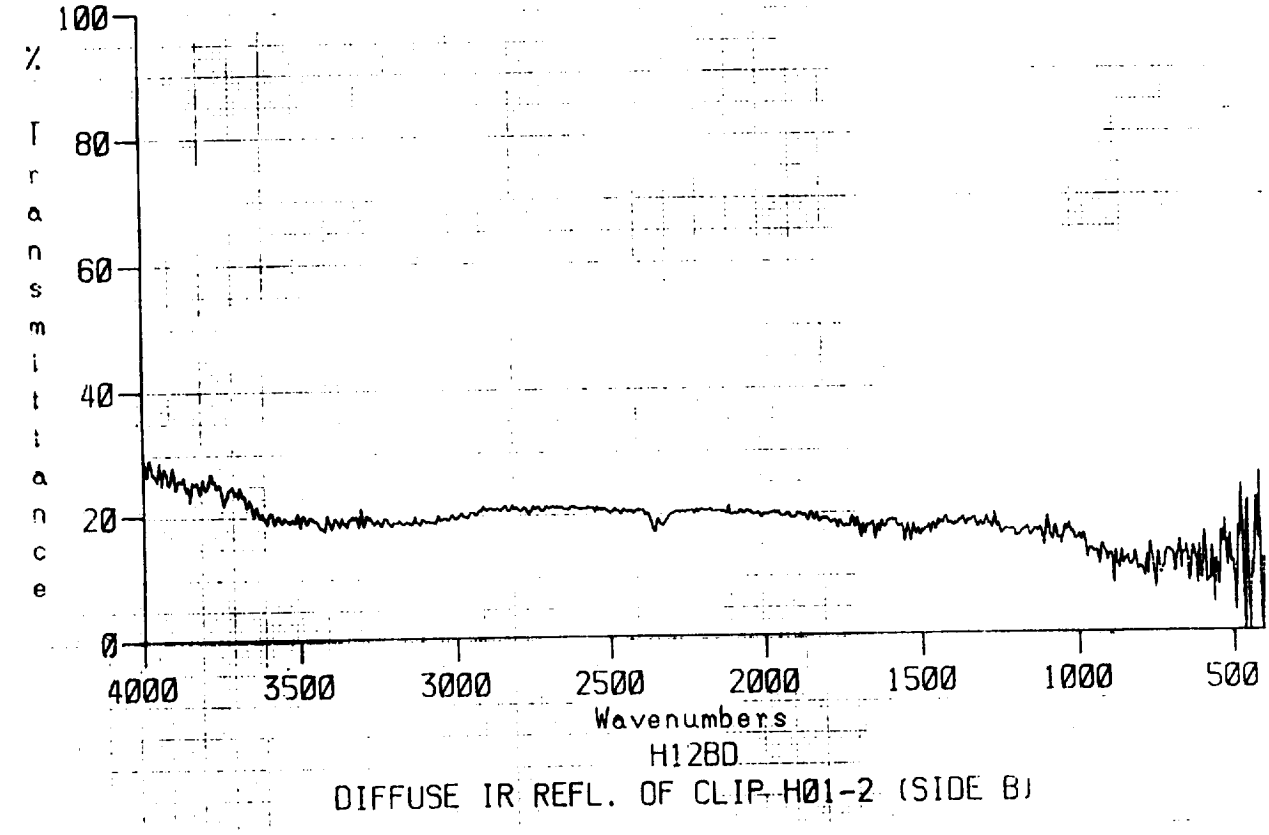

Figure A59: Diffuse IR Reflectance of clip H01-2, (A) Front (B) Back.

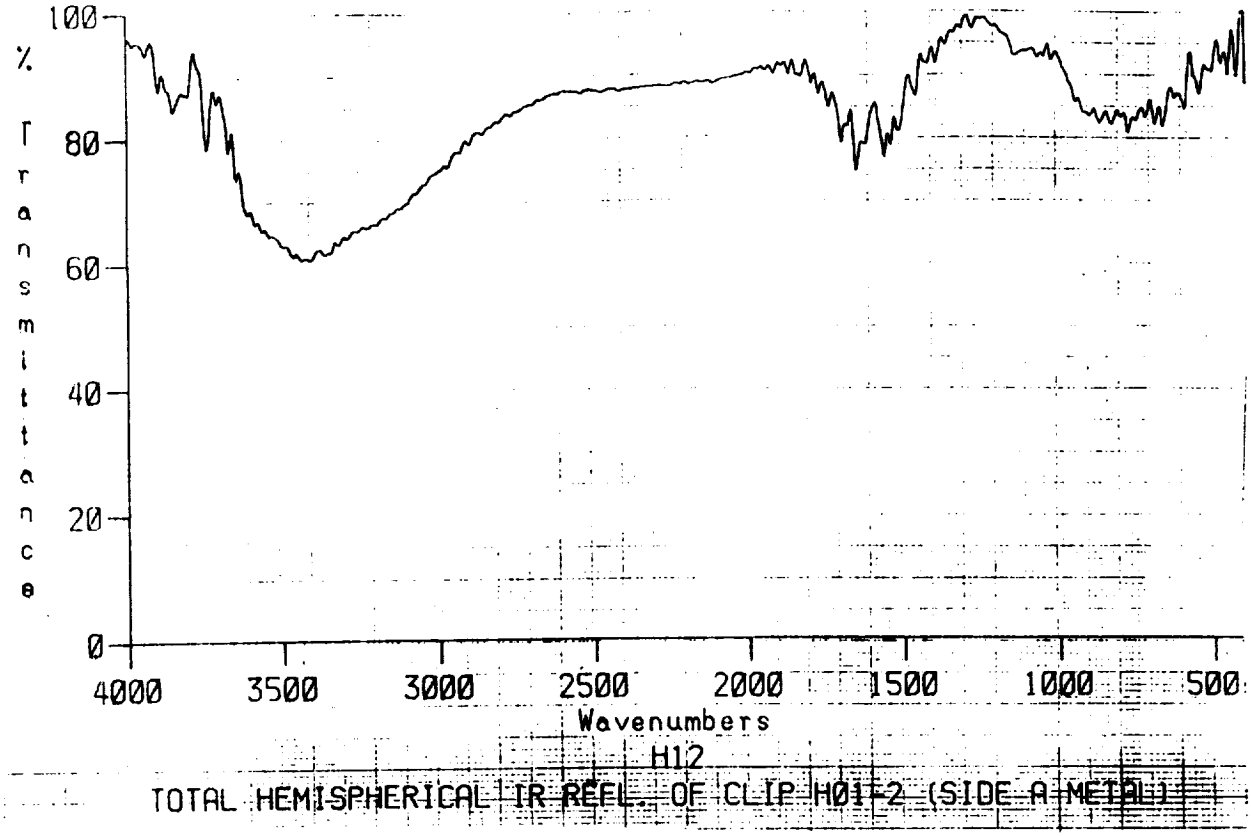

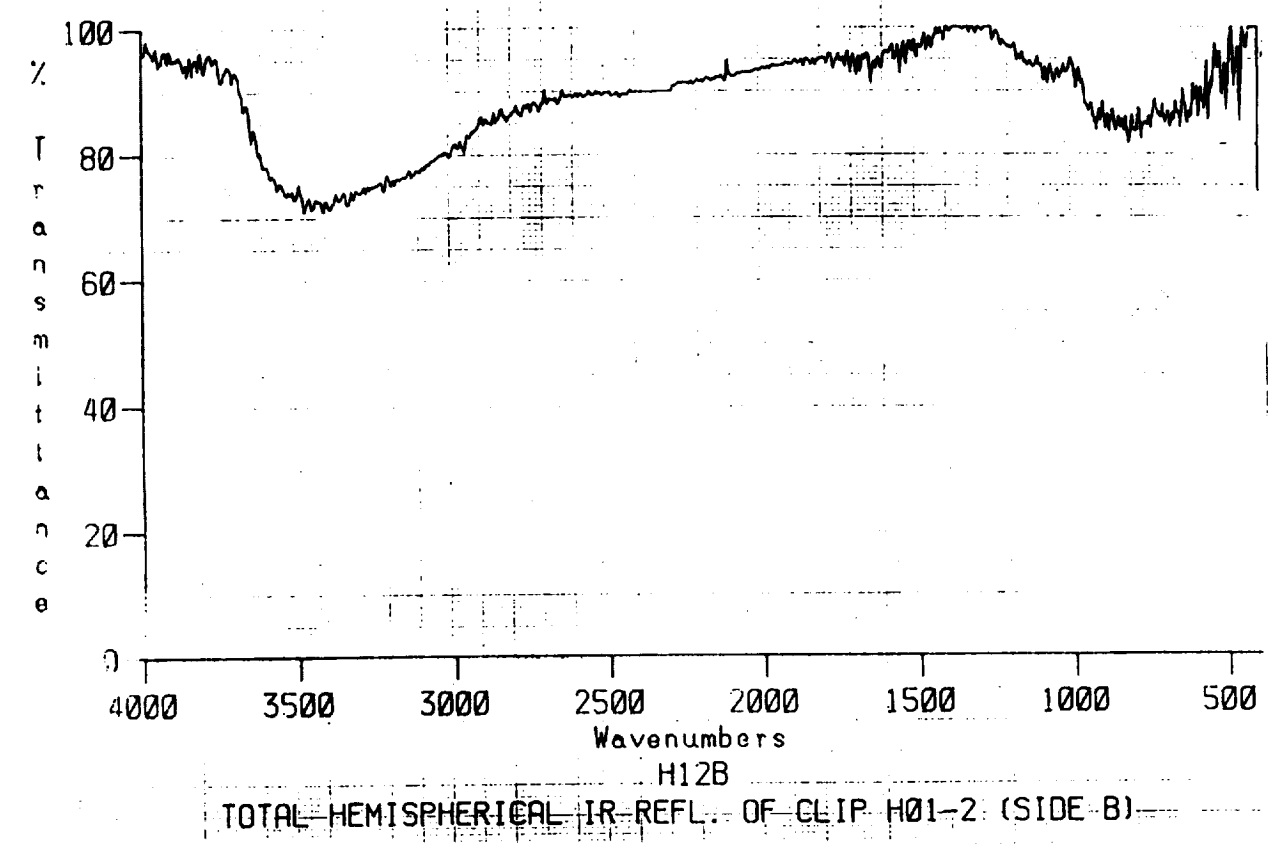

Figure A60: Total Hemispherical IR Reflectance of clip H01-2, (A) Front (B) Back.

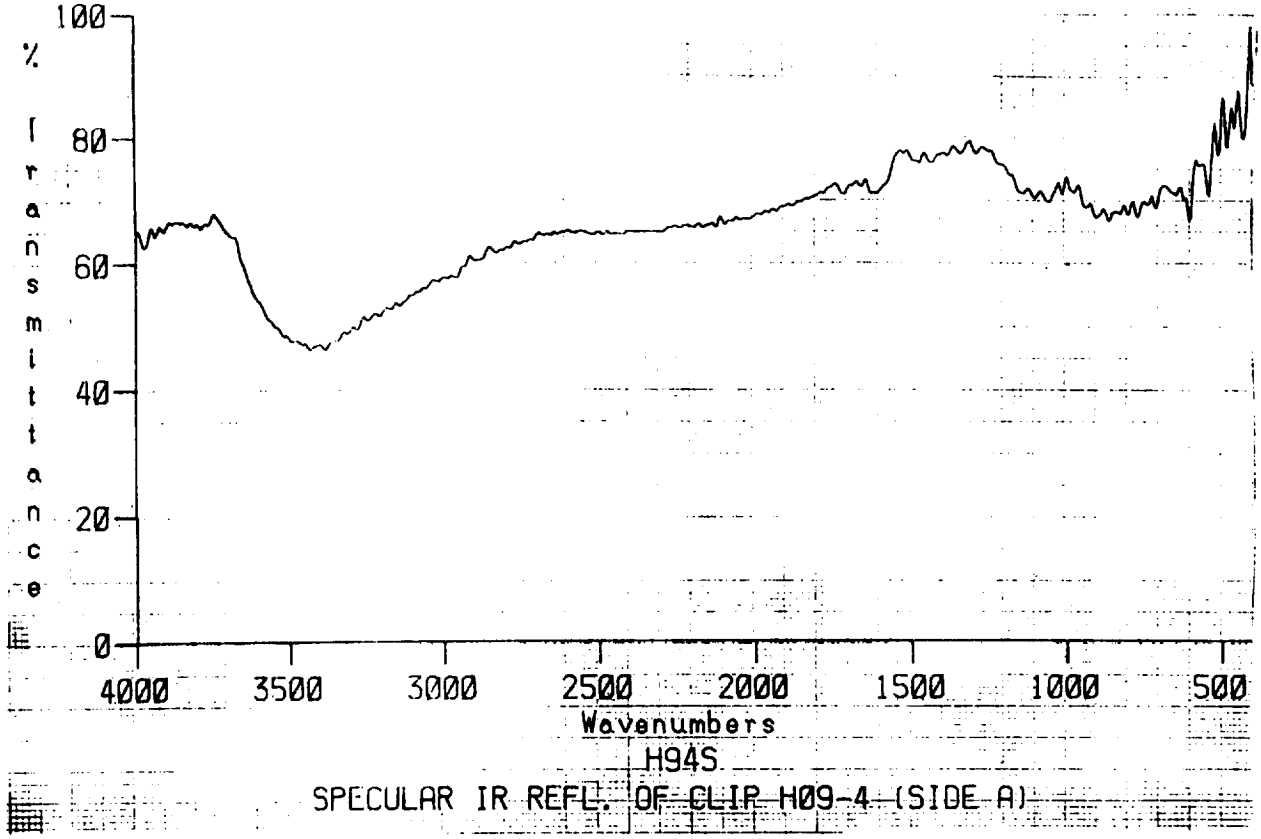

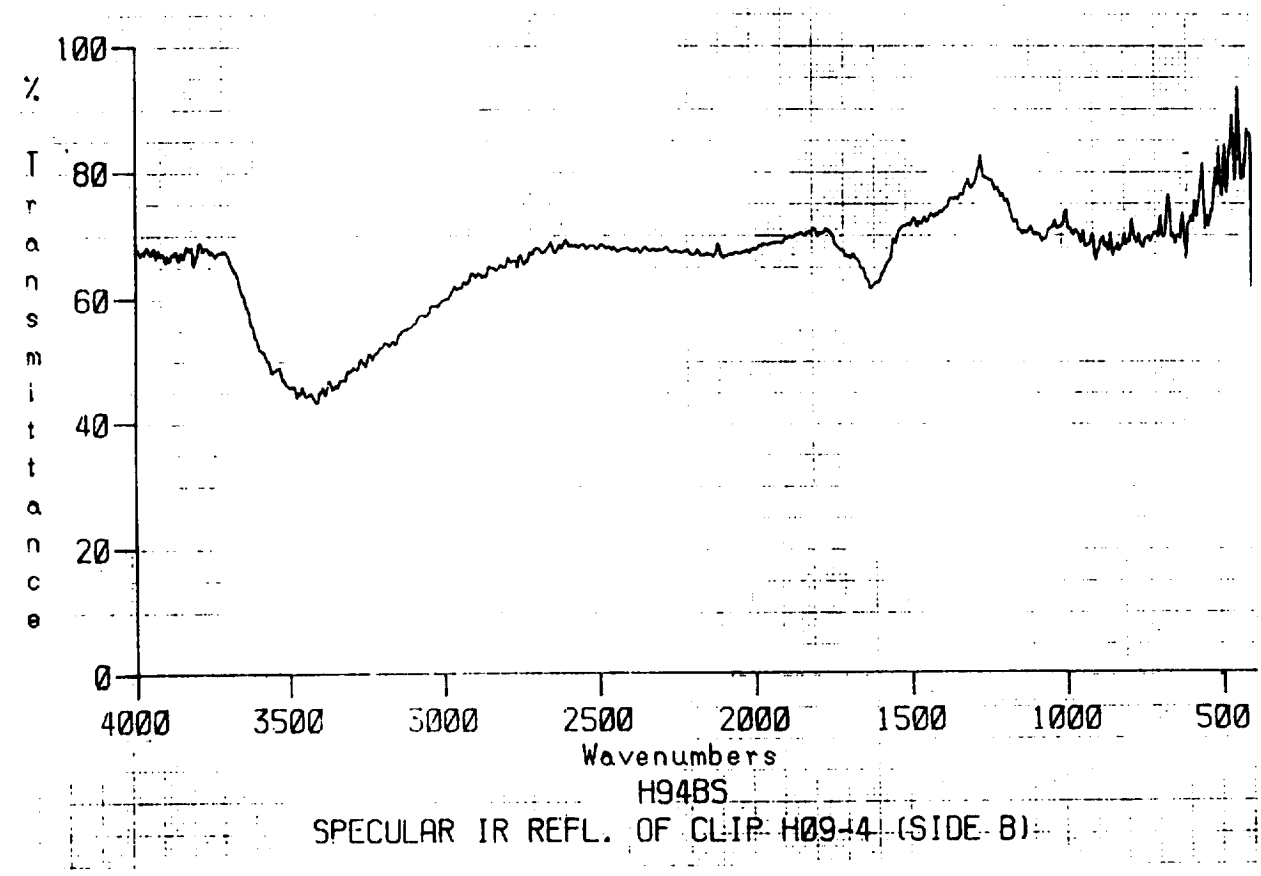

Figure A61: Specular IR Reflectance of clip H09-4, (A) Front (B) Back.

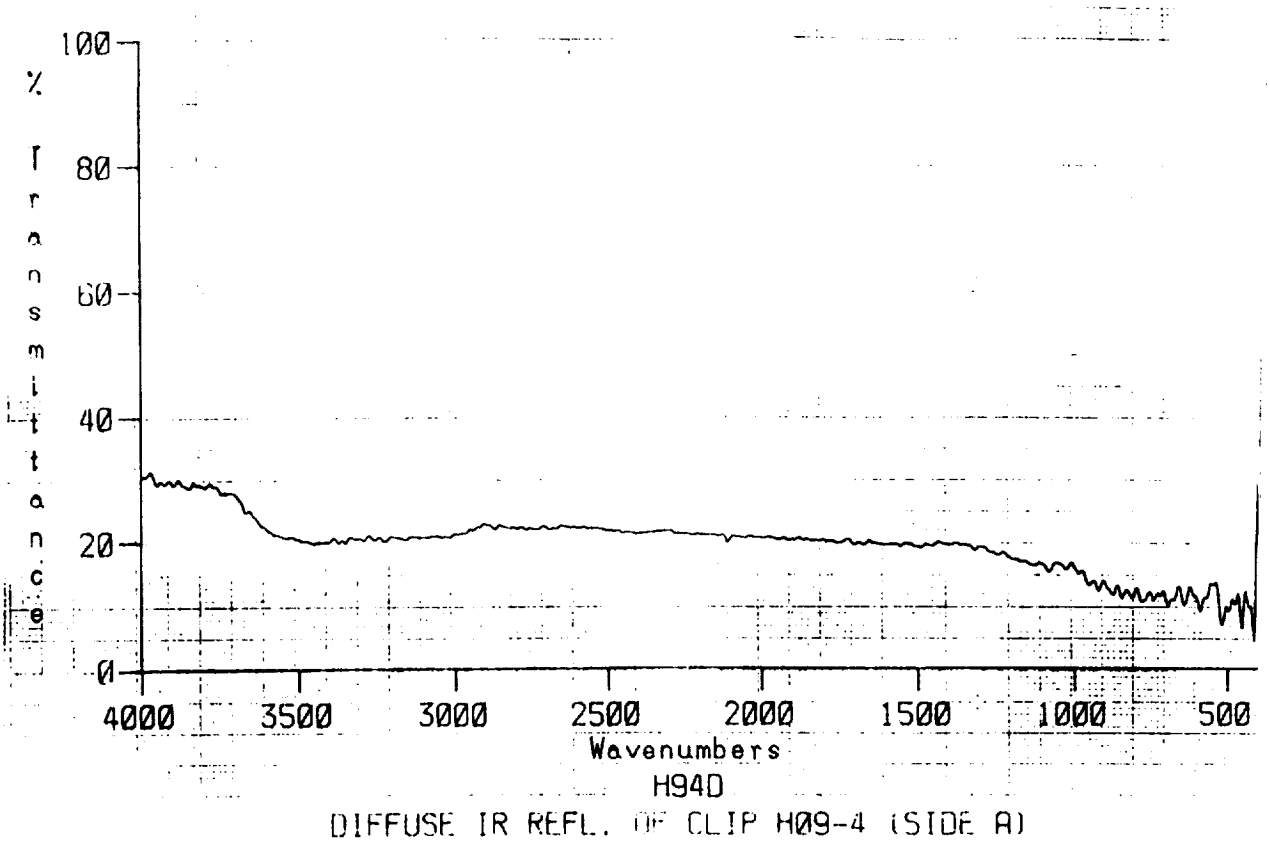

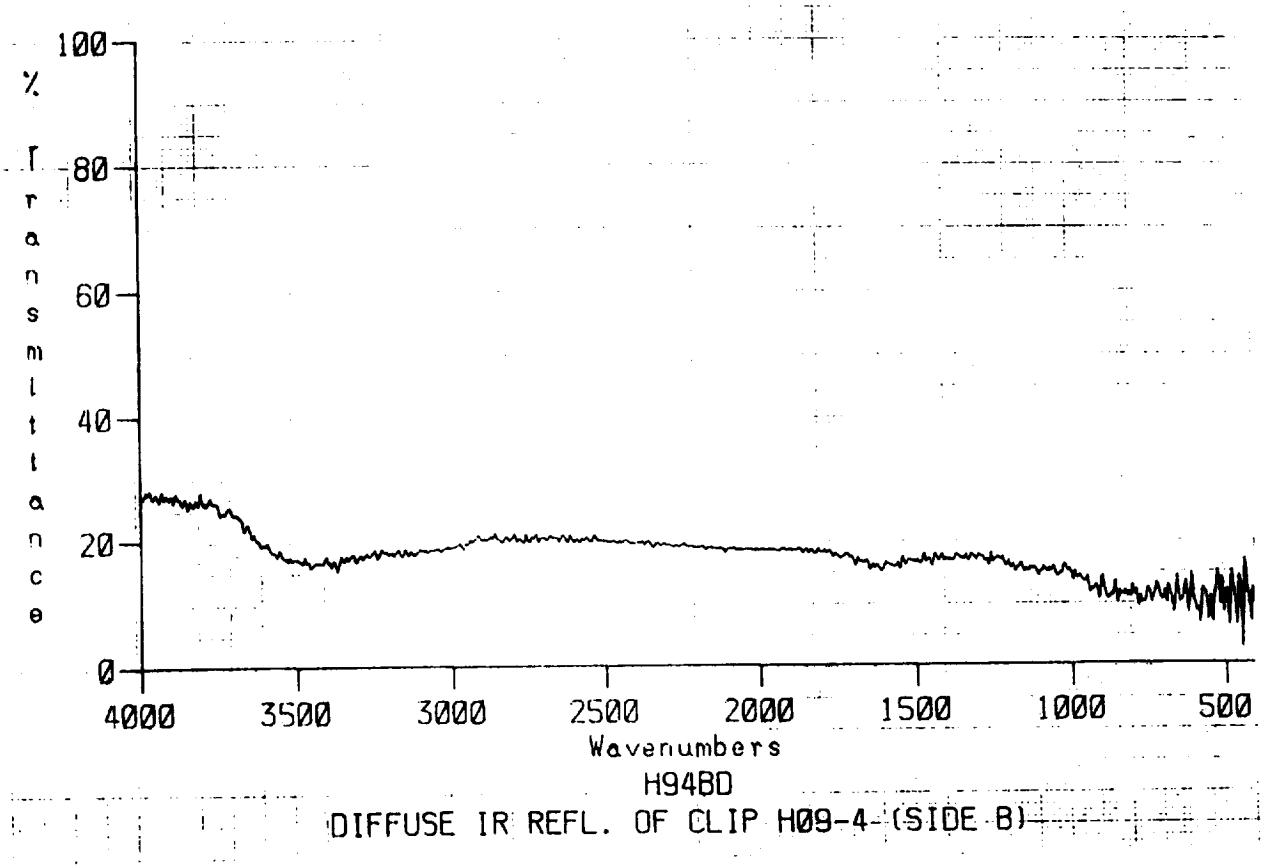

Figure A62: Diffuse IR Reflectance of clip H09-4, (A) Front (B) Back.

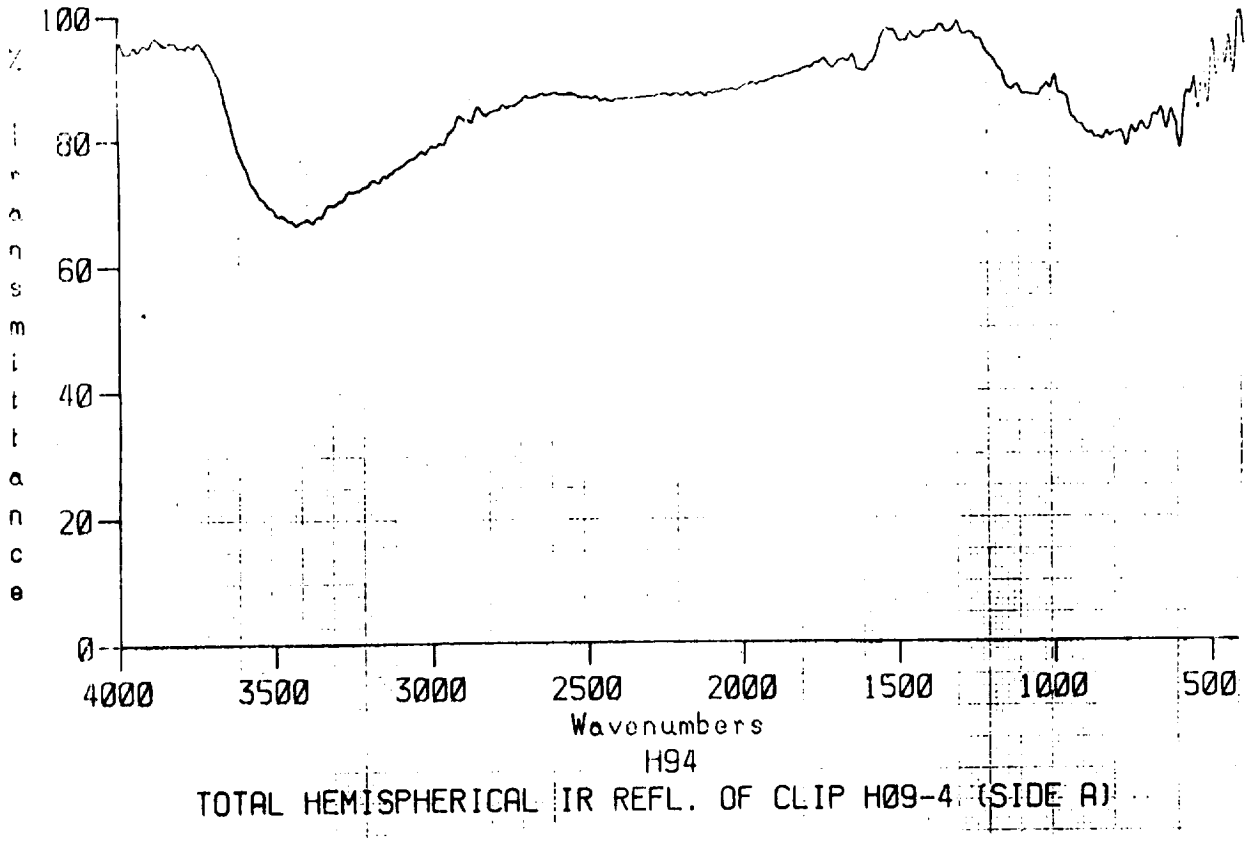

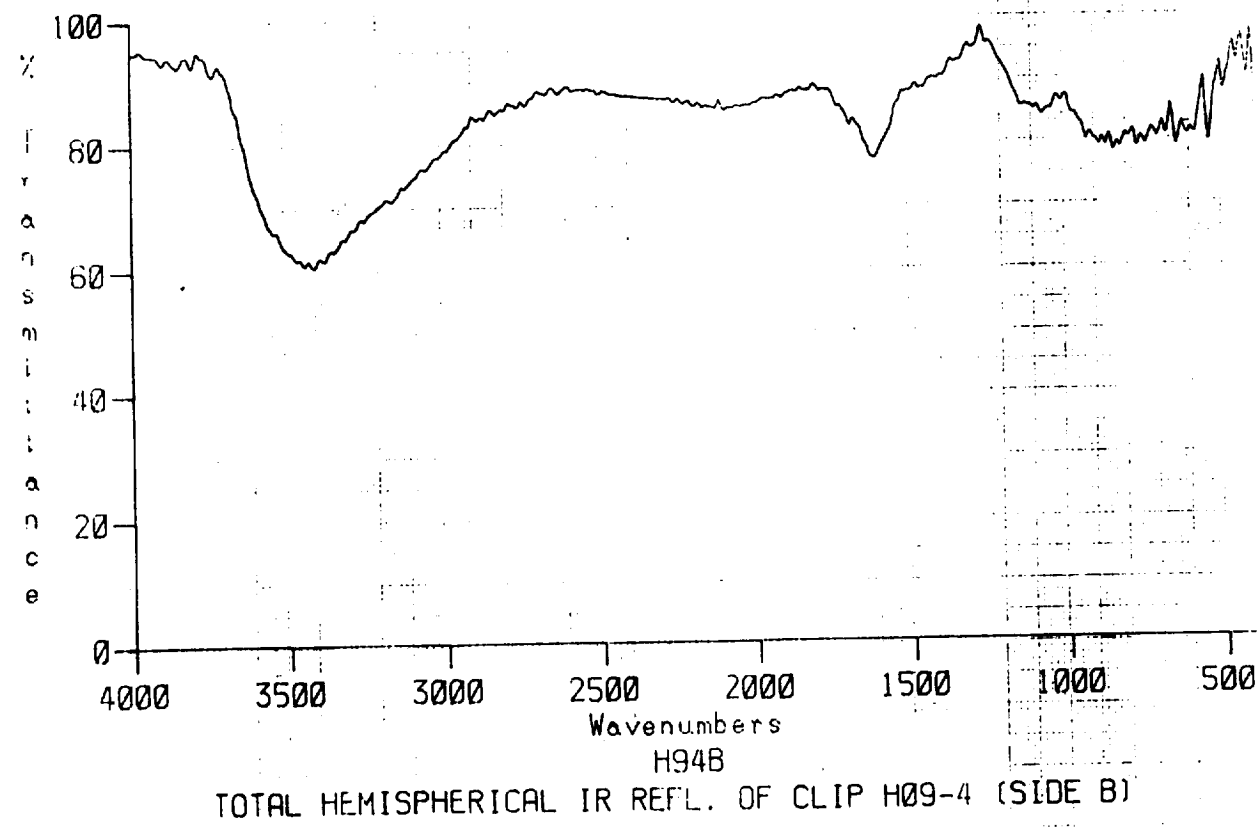

Figure A63: Total Hemispherical IR Reflectance of clip H09-4, (A) Front (B) Back.

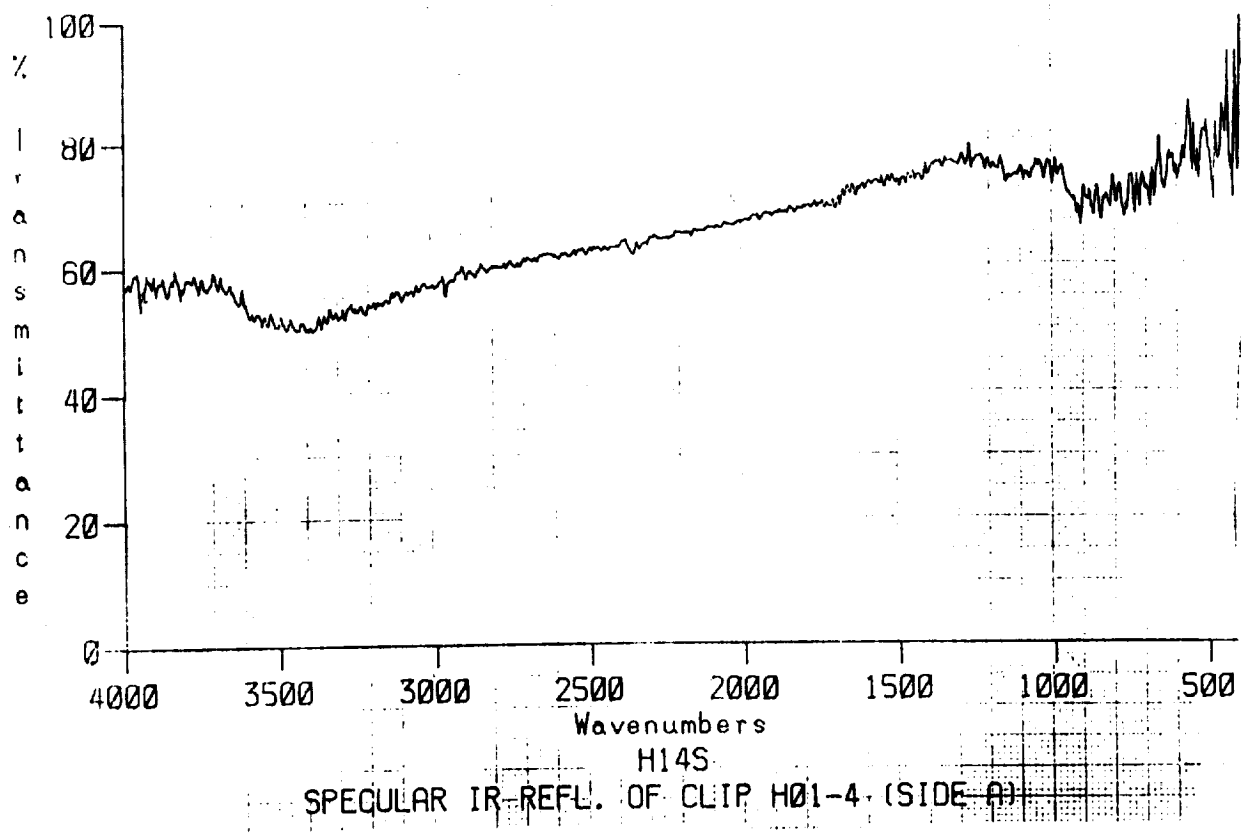

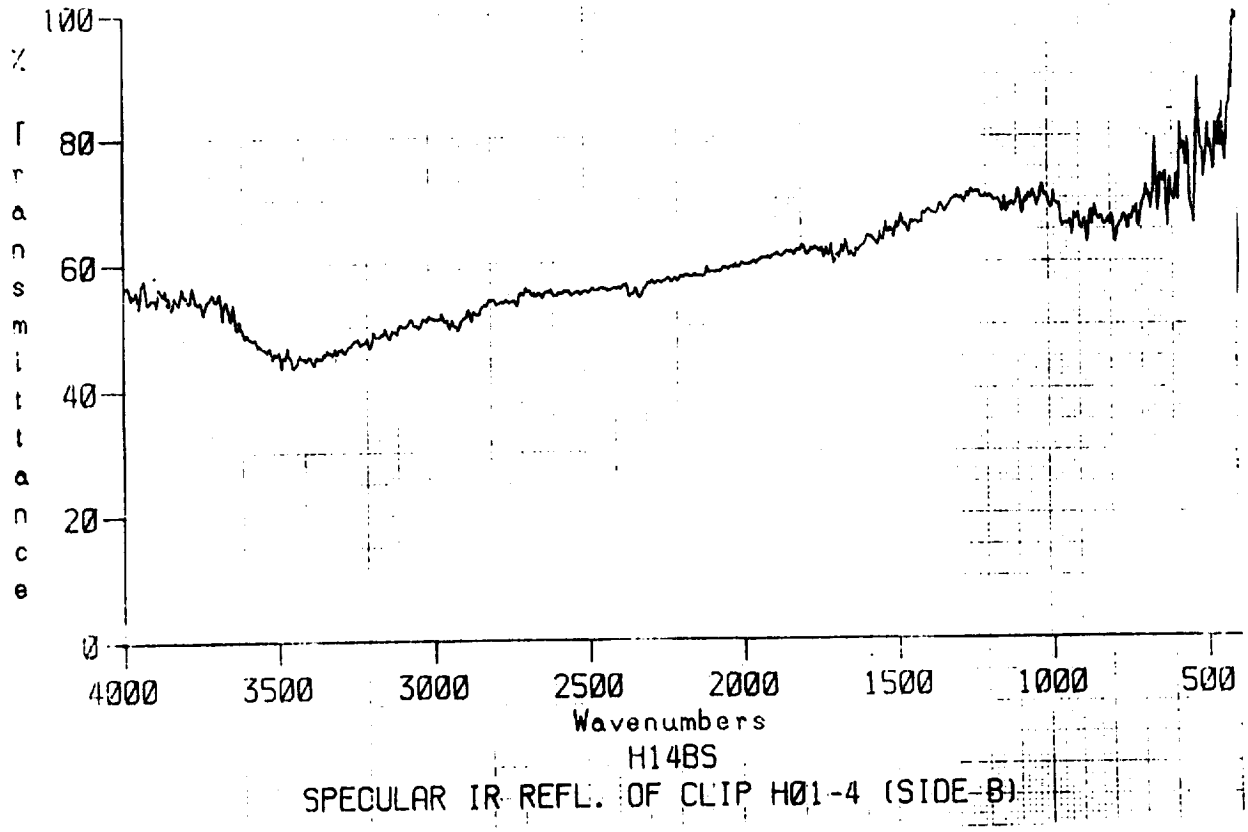

Figure A64: Specular IR Reflectance of clip H01-4, (A) Front (B) Back.

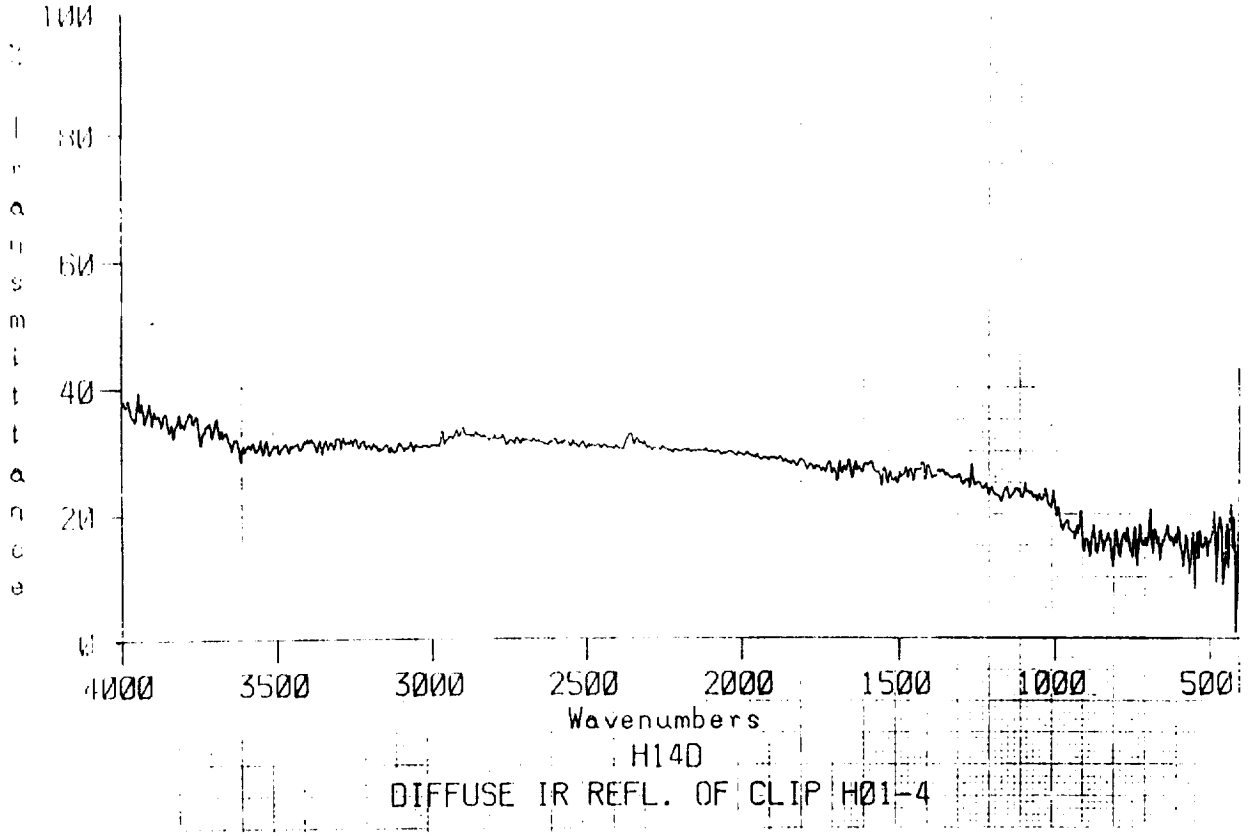

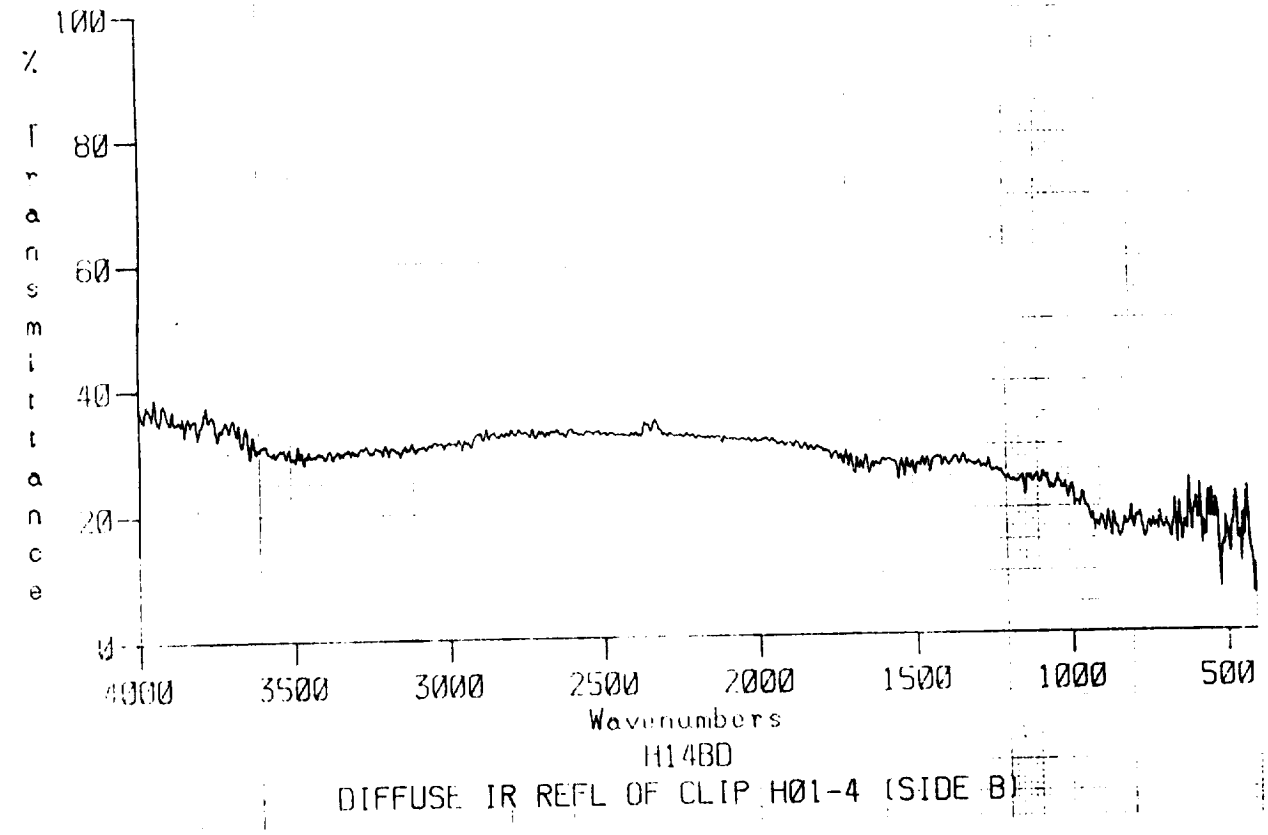

Figure A65: Diffuse IR Reflectance of clip H01-4, (A) Front (B) Back.

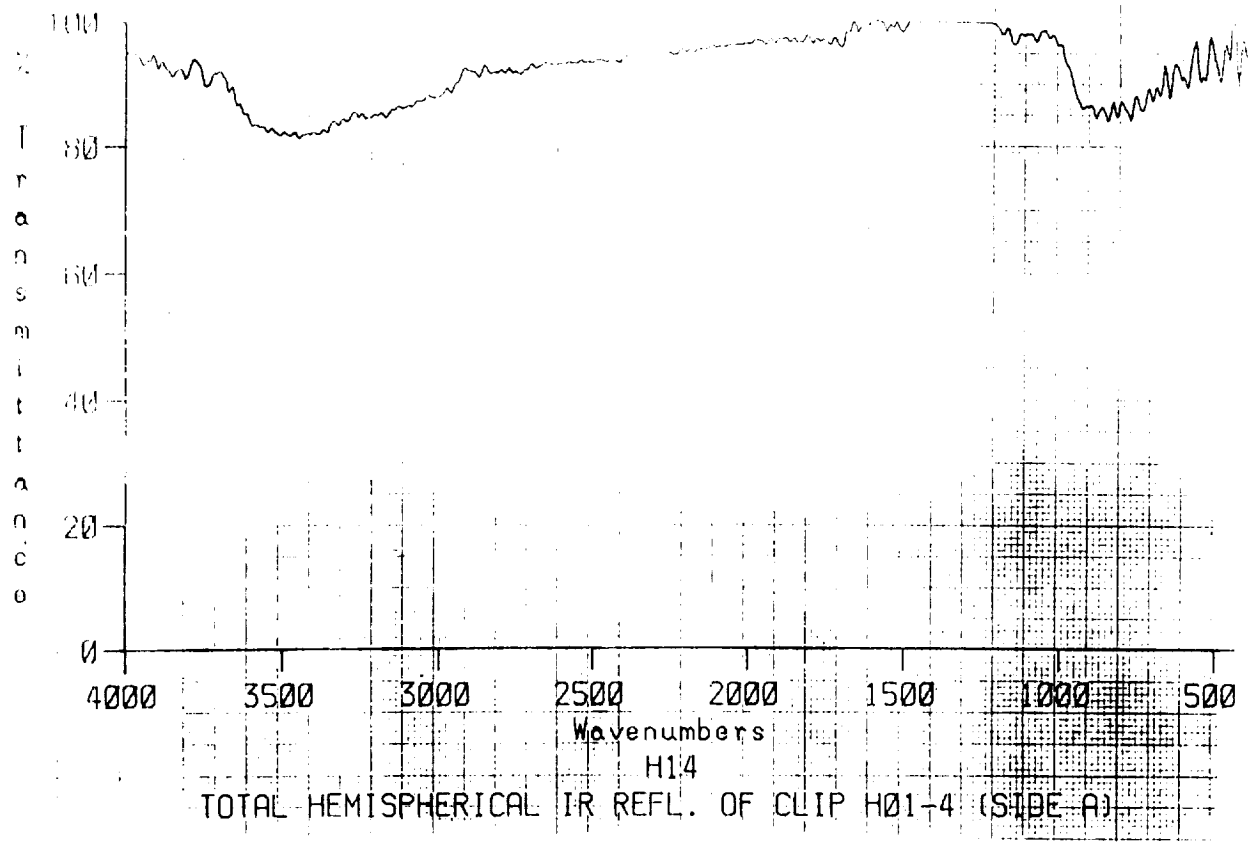

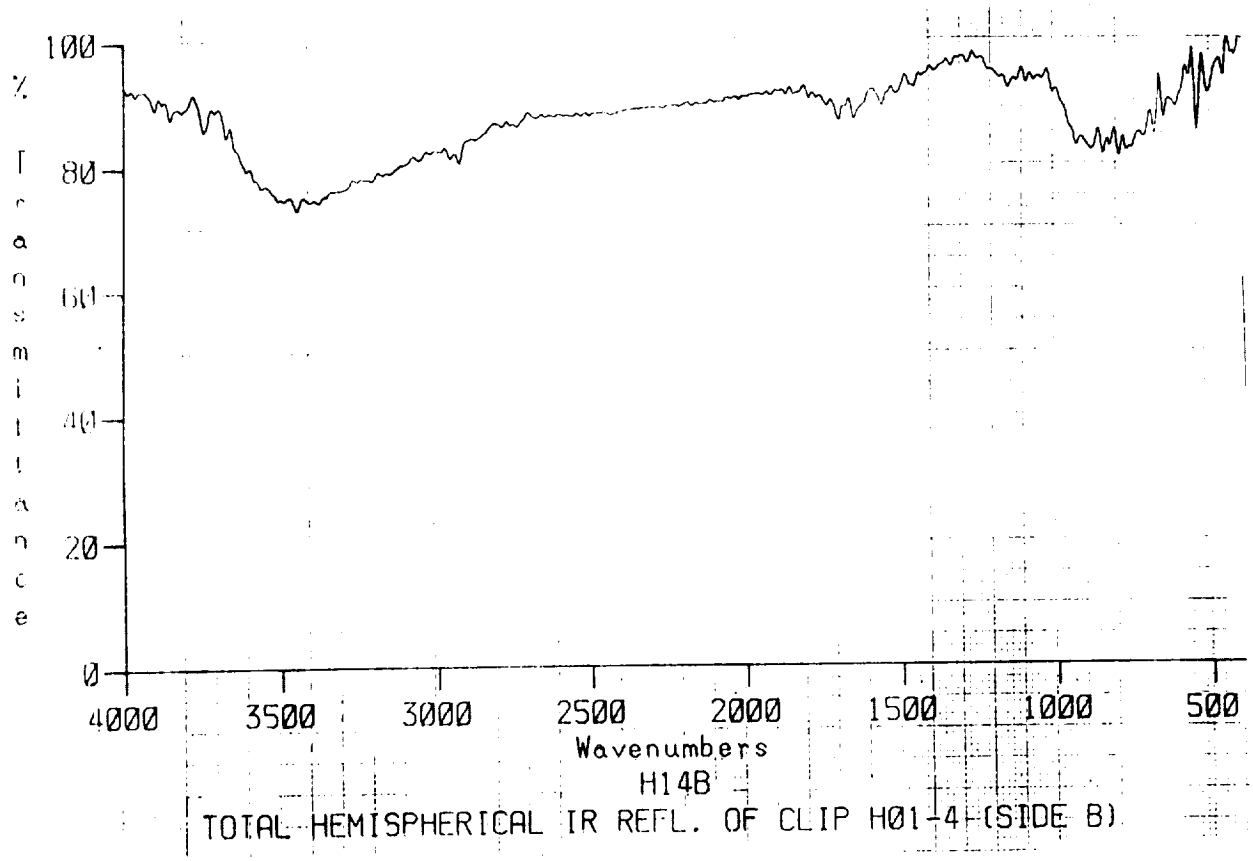

Figure A66: Total Hemispherical IR Reflectance of clip H01-4, (A) Front (B) Back.

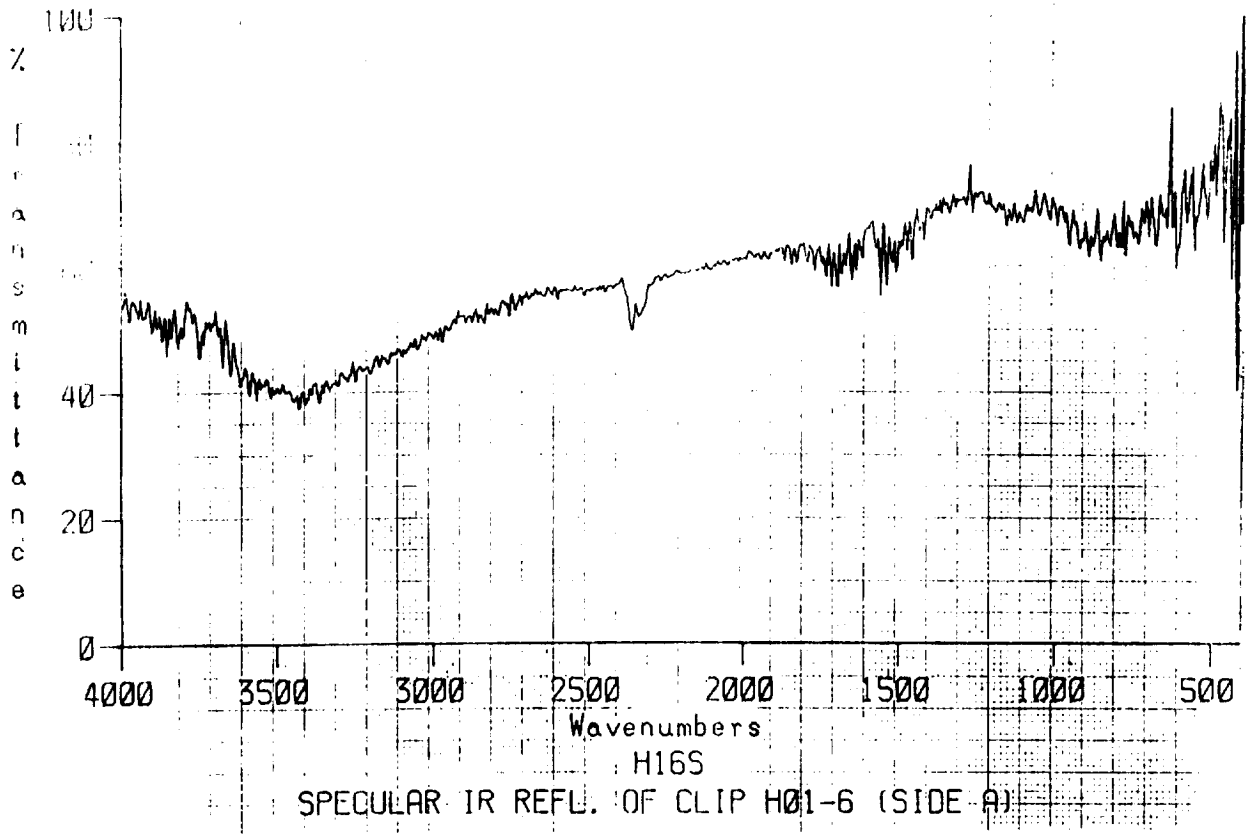

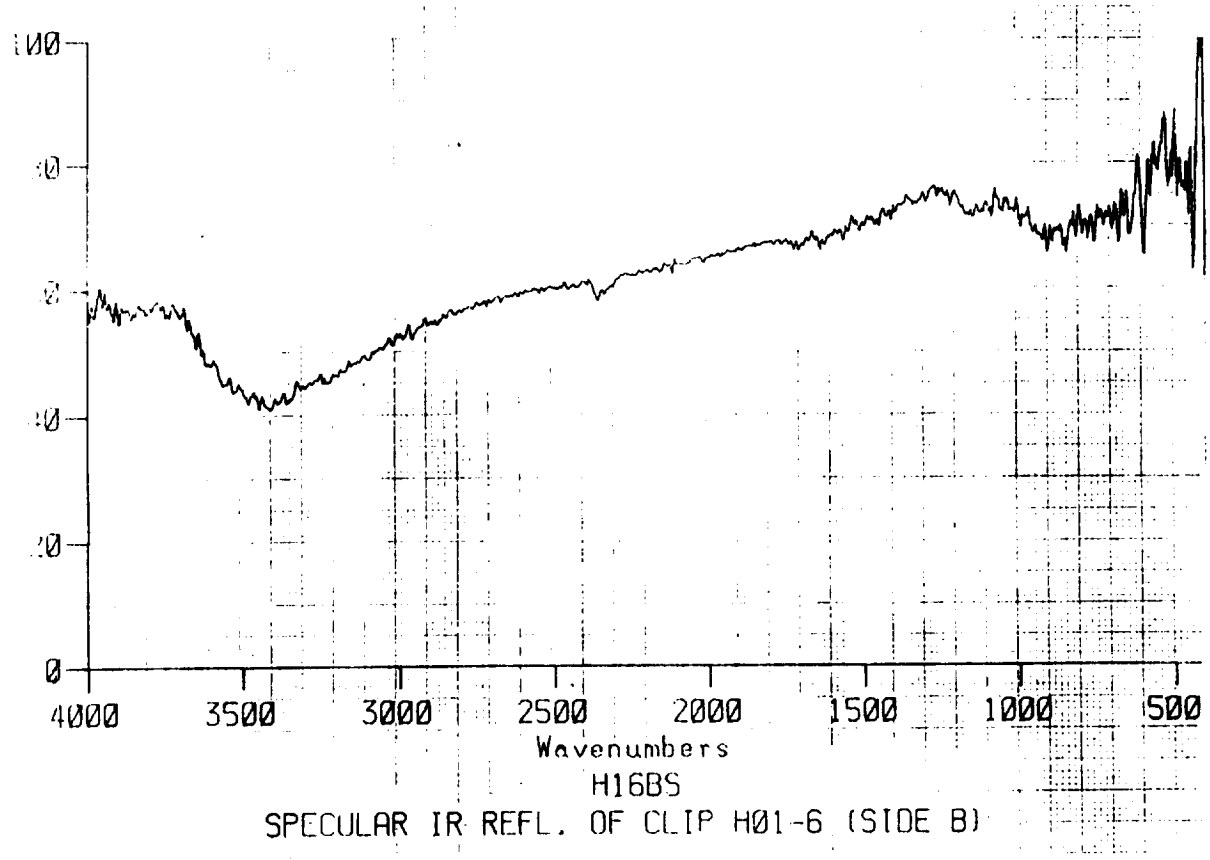

Figure A67: Specular IR Reflectance of clip H01-6, (A) Front (B) Back.

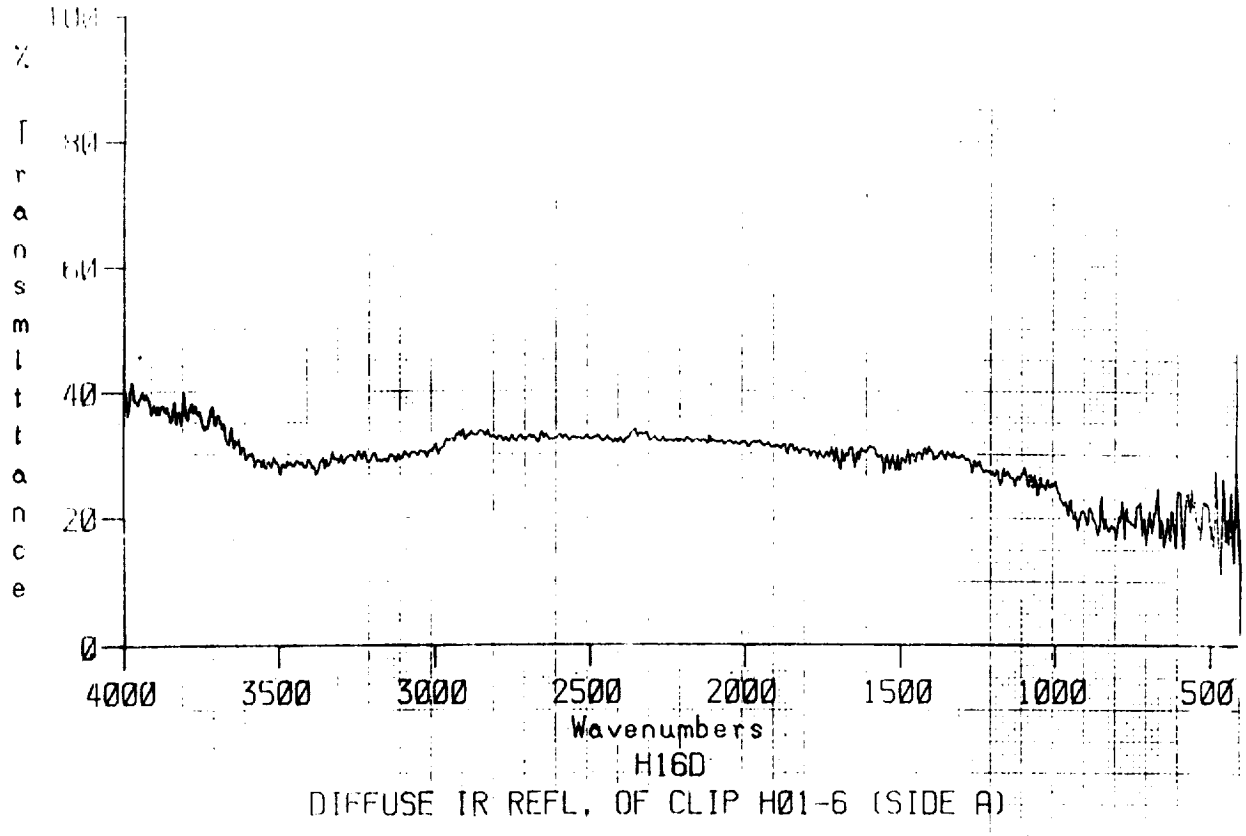

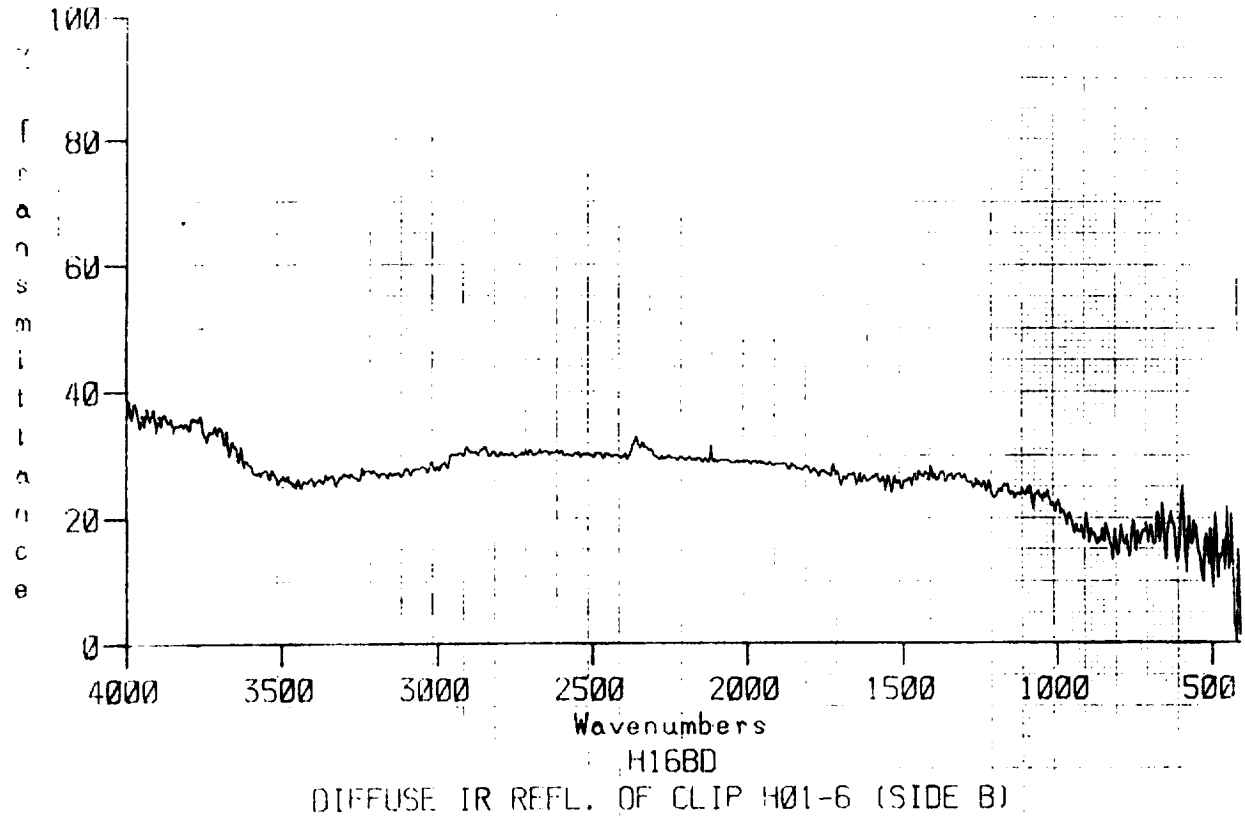

Figure A68: Diffuse IR Reflectance of clip H01-6, (A) Front (B) Back.

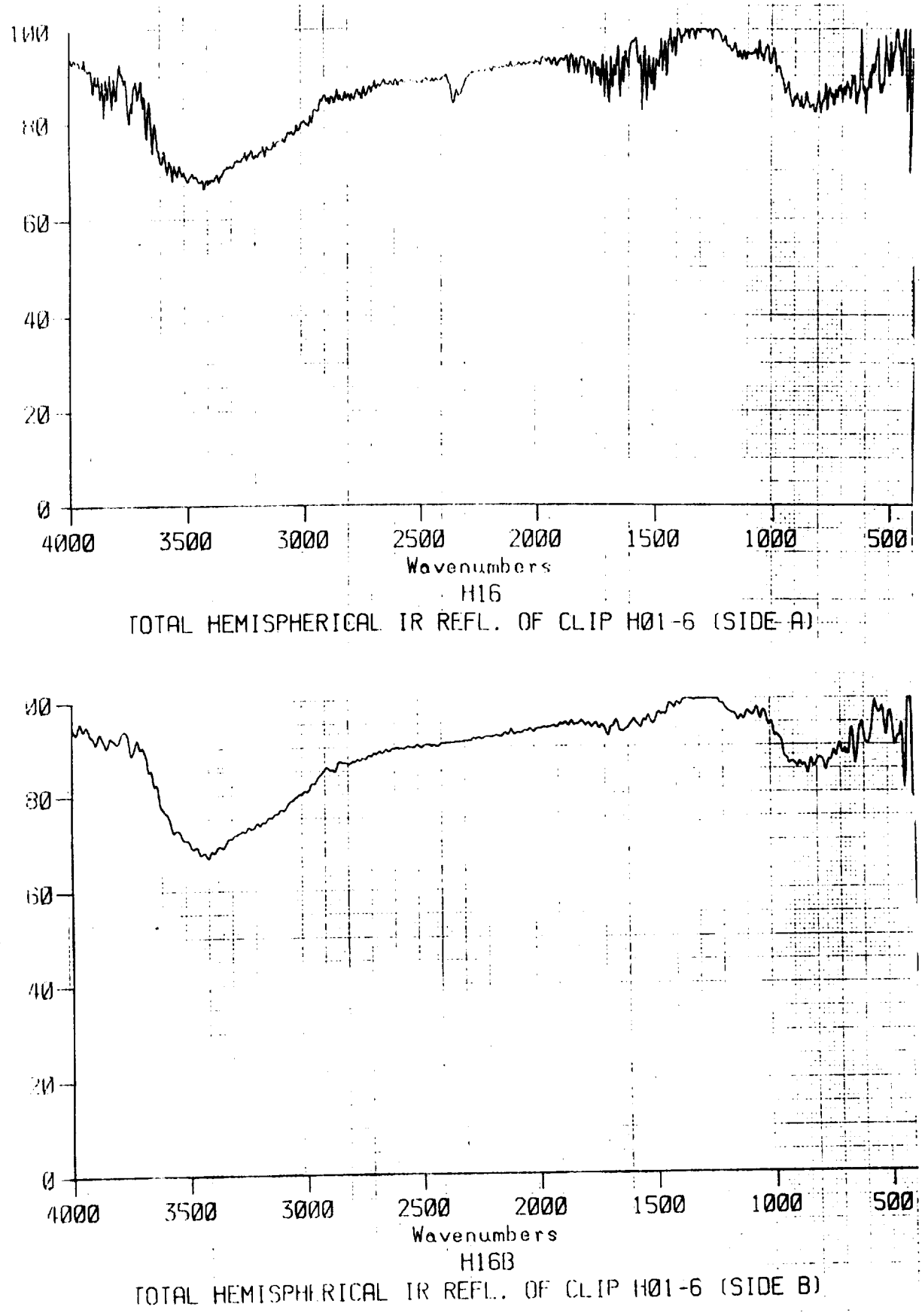

Figure A69: Total Hemispherical IR Reflectance of clip H01-6, (A) Front (B) Back.

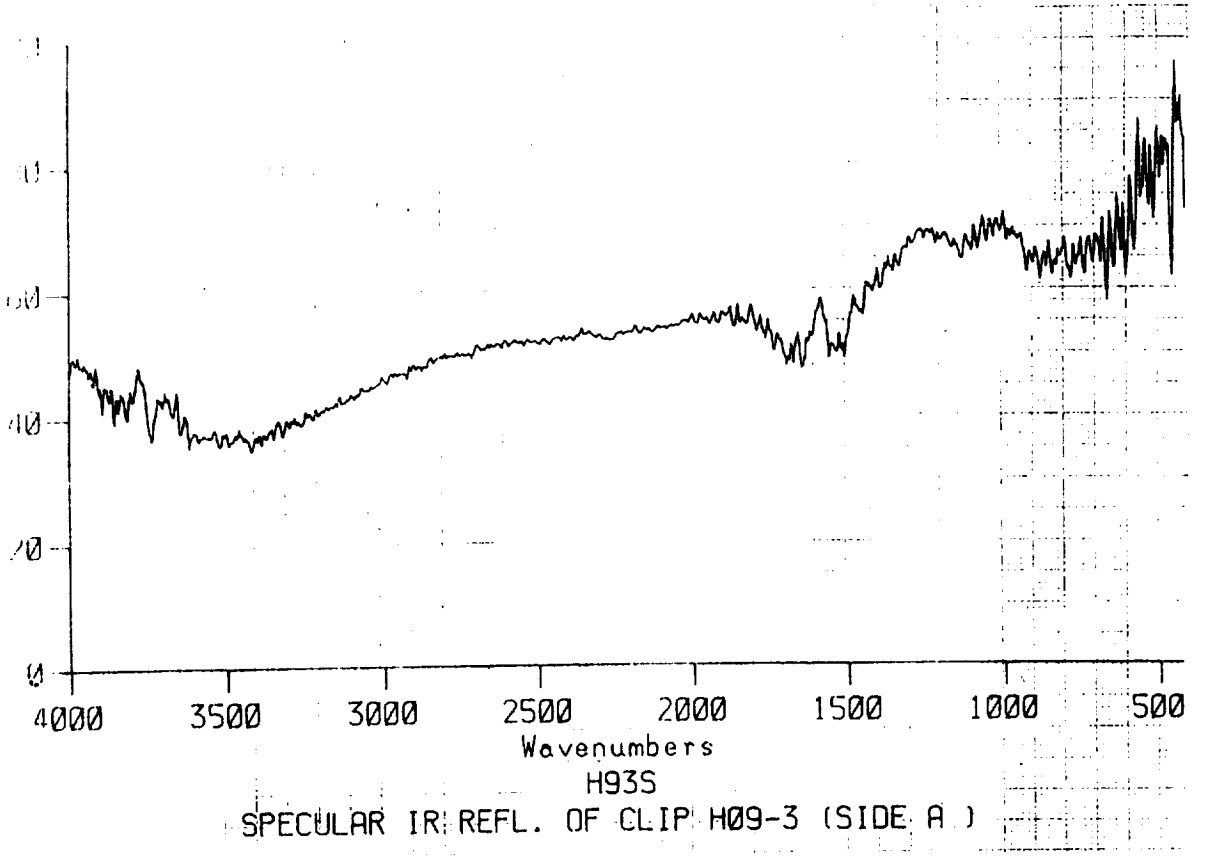

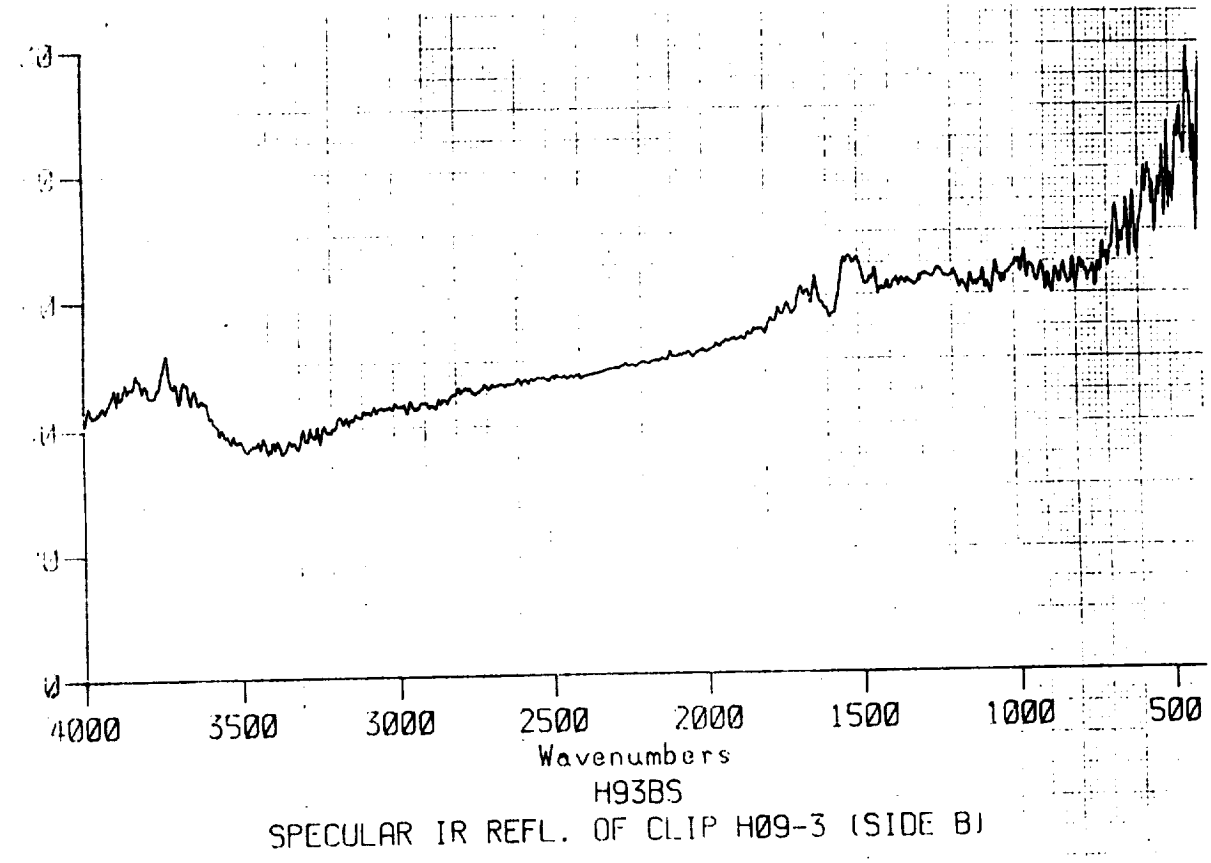

Figure A70: Specular IR Reflectance of clip H09-3, (A) Front (B) Back.

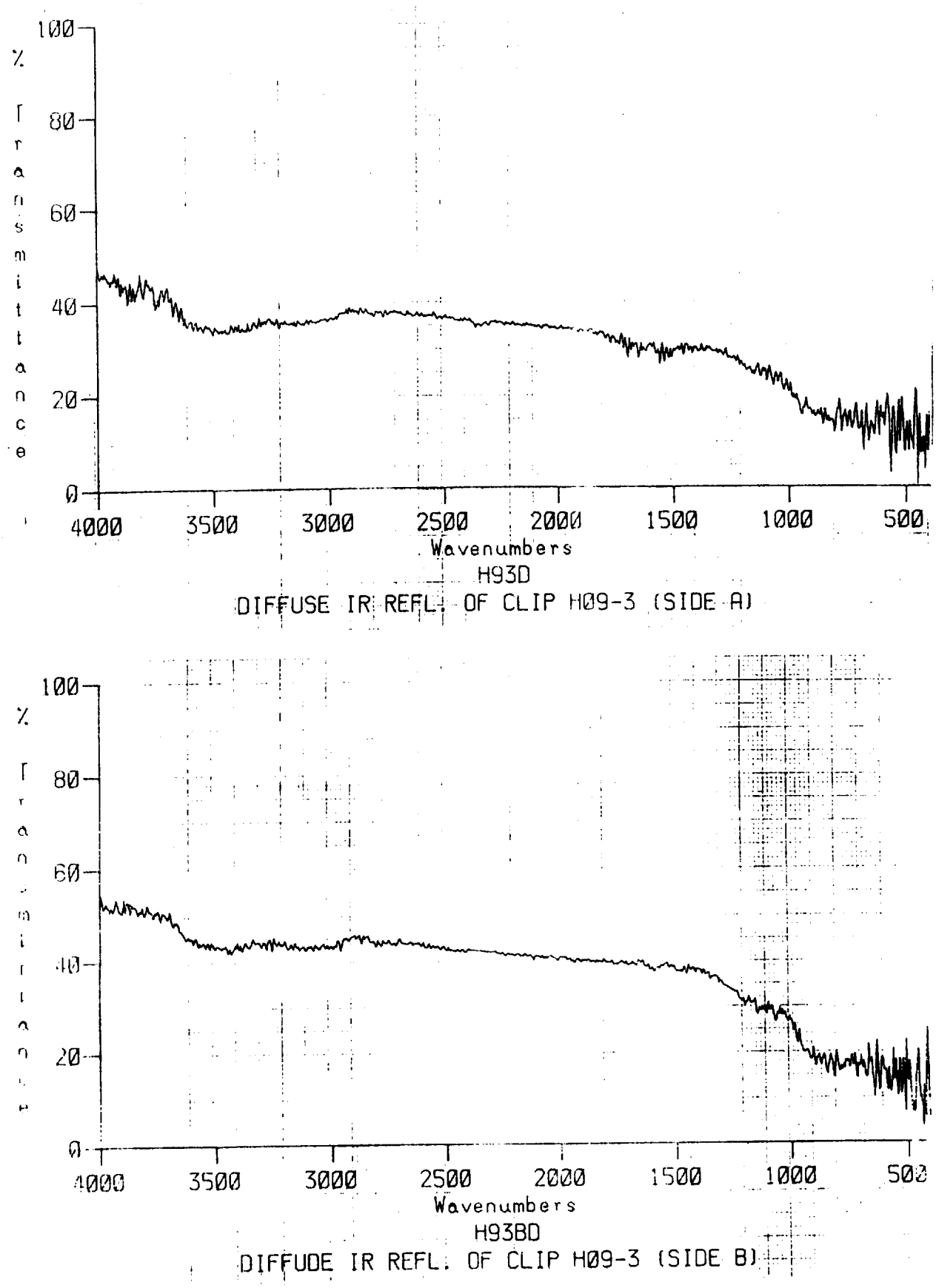

Figure A71: Diffuse IR Reflectance of clip H09-3, (A) Front (B) Back.

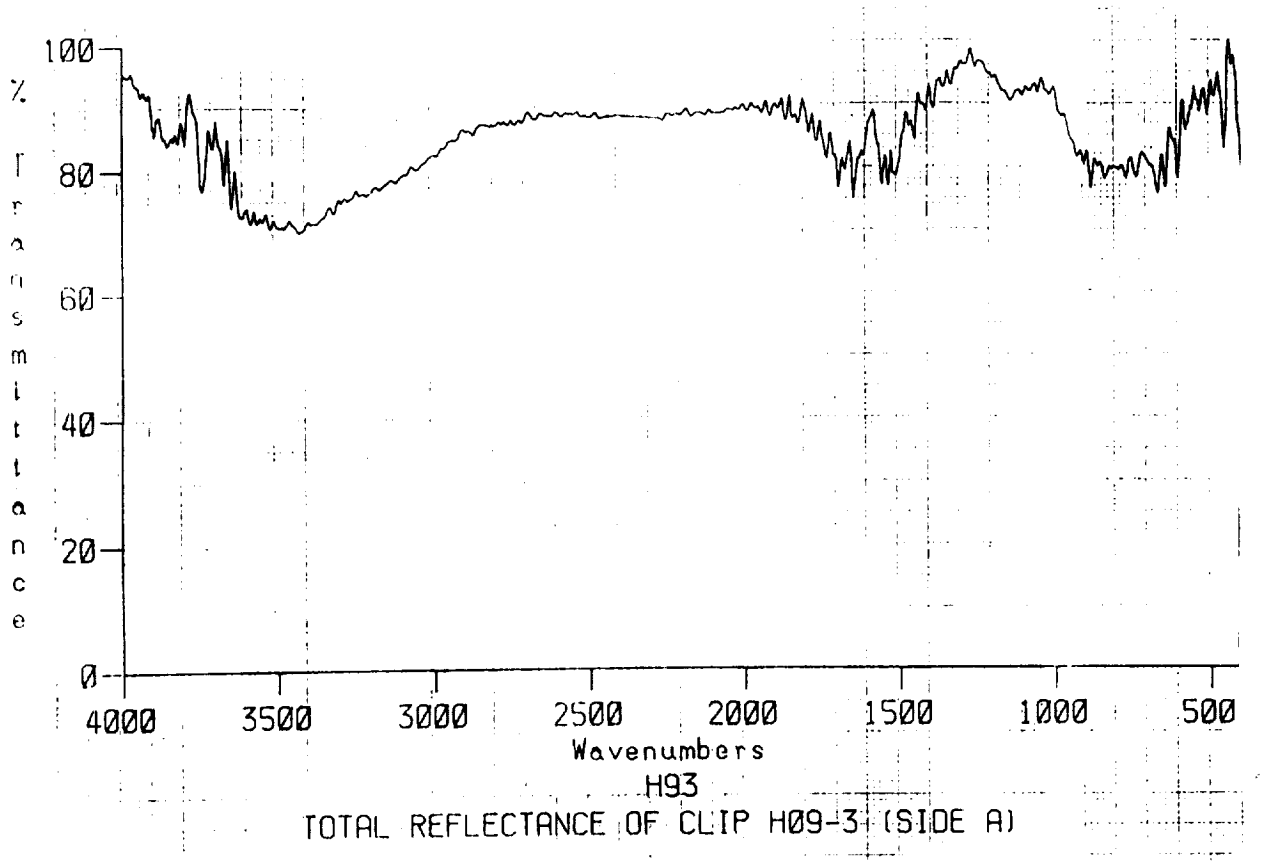

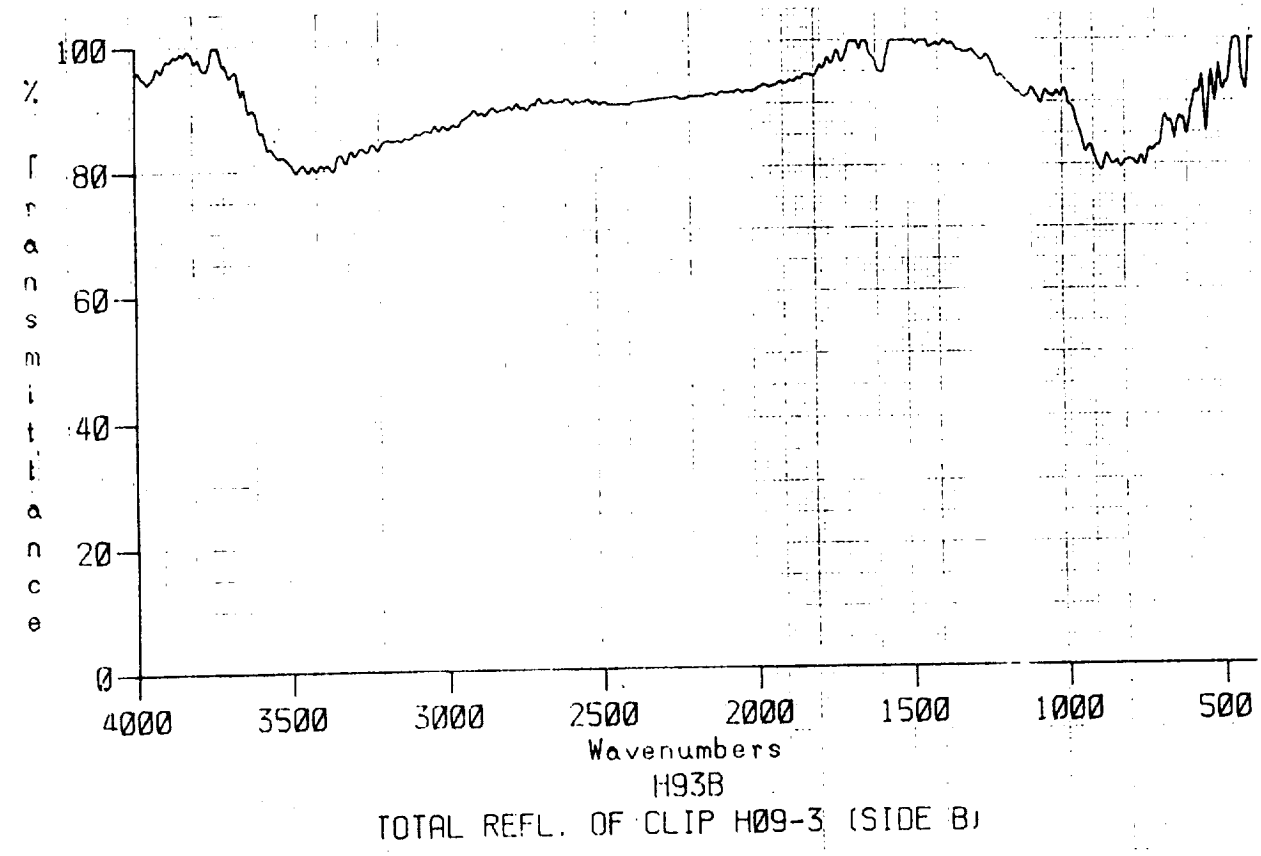

Figure A72: Total Reflectance of clip H09-3, (A) Front (B) Back.

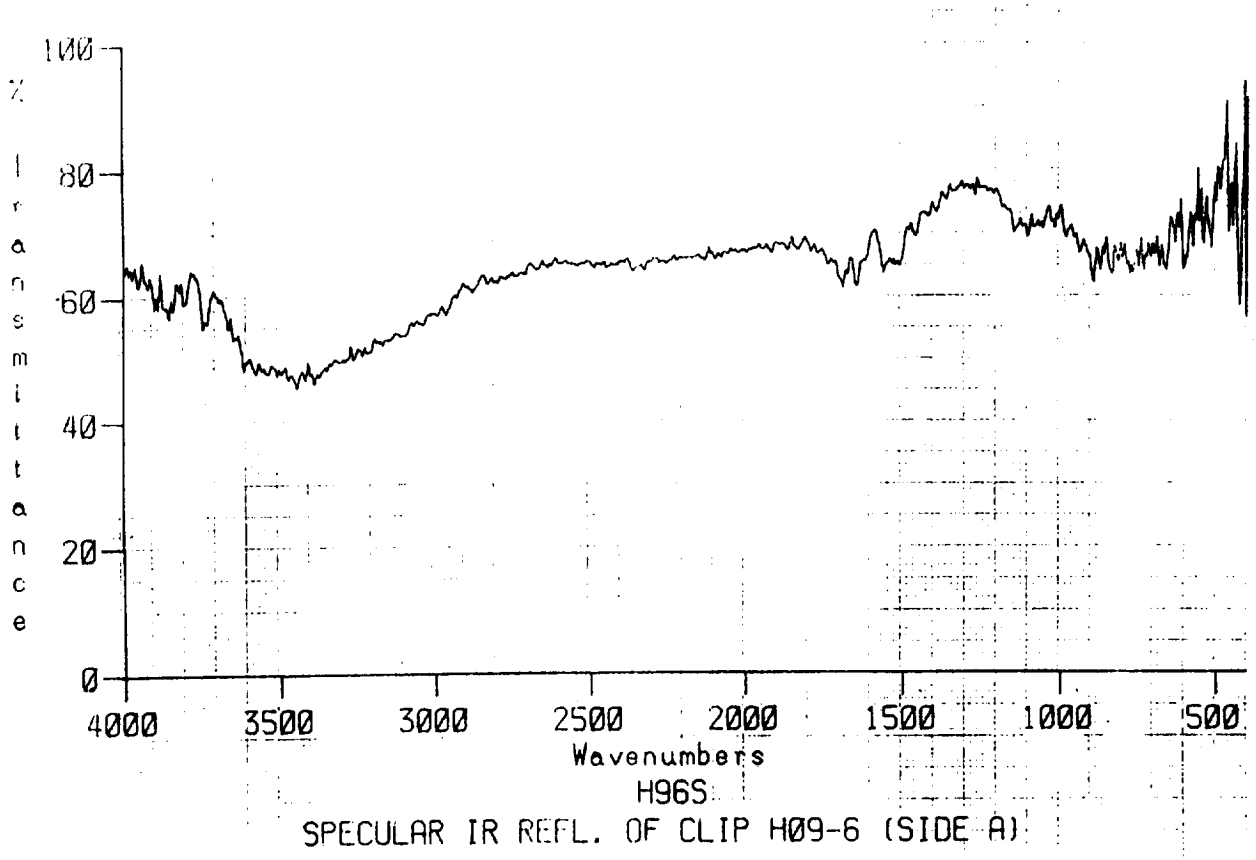

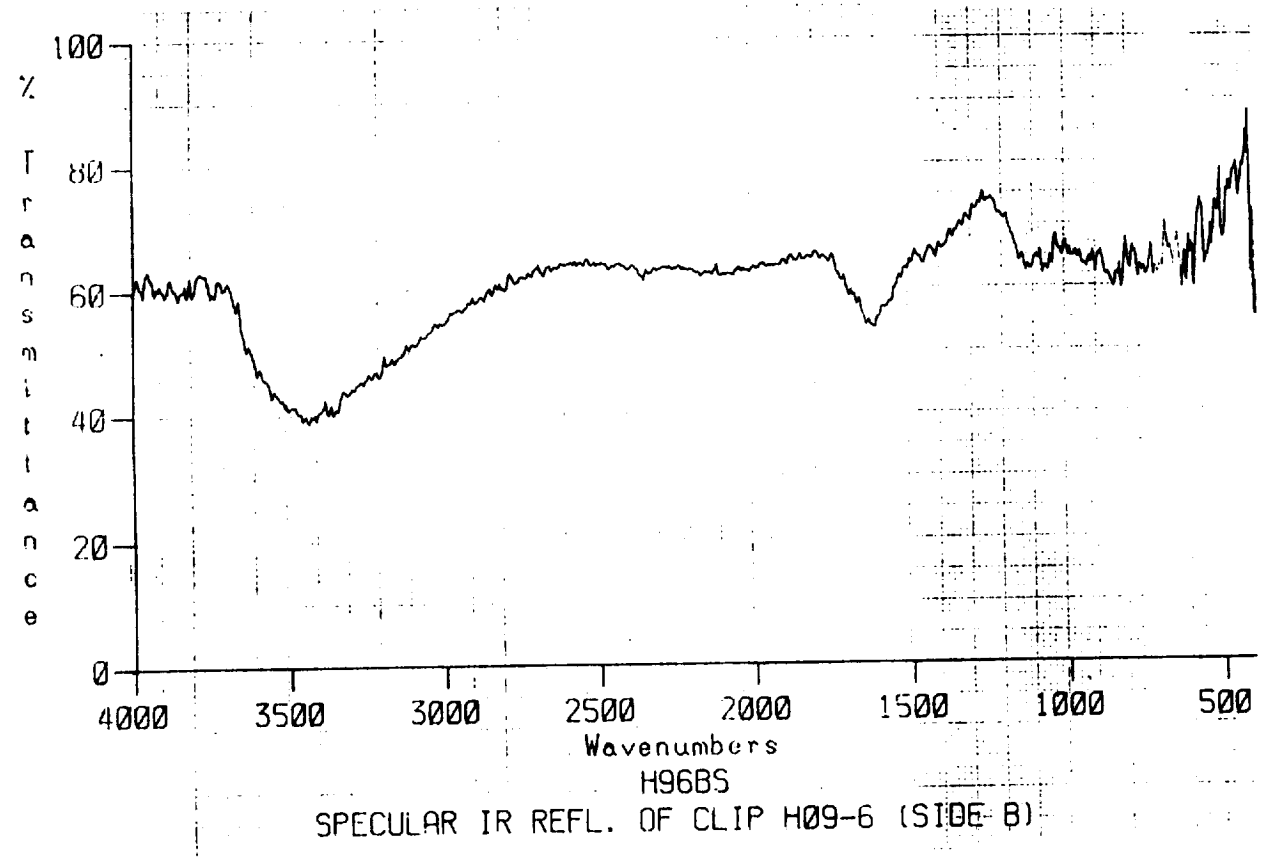

Figure A73: Specular IR Reflectance of clip H09-6, (A) Front (B) Back.

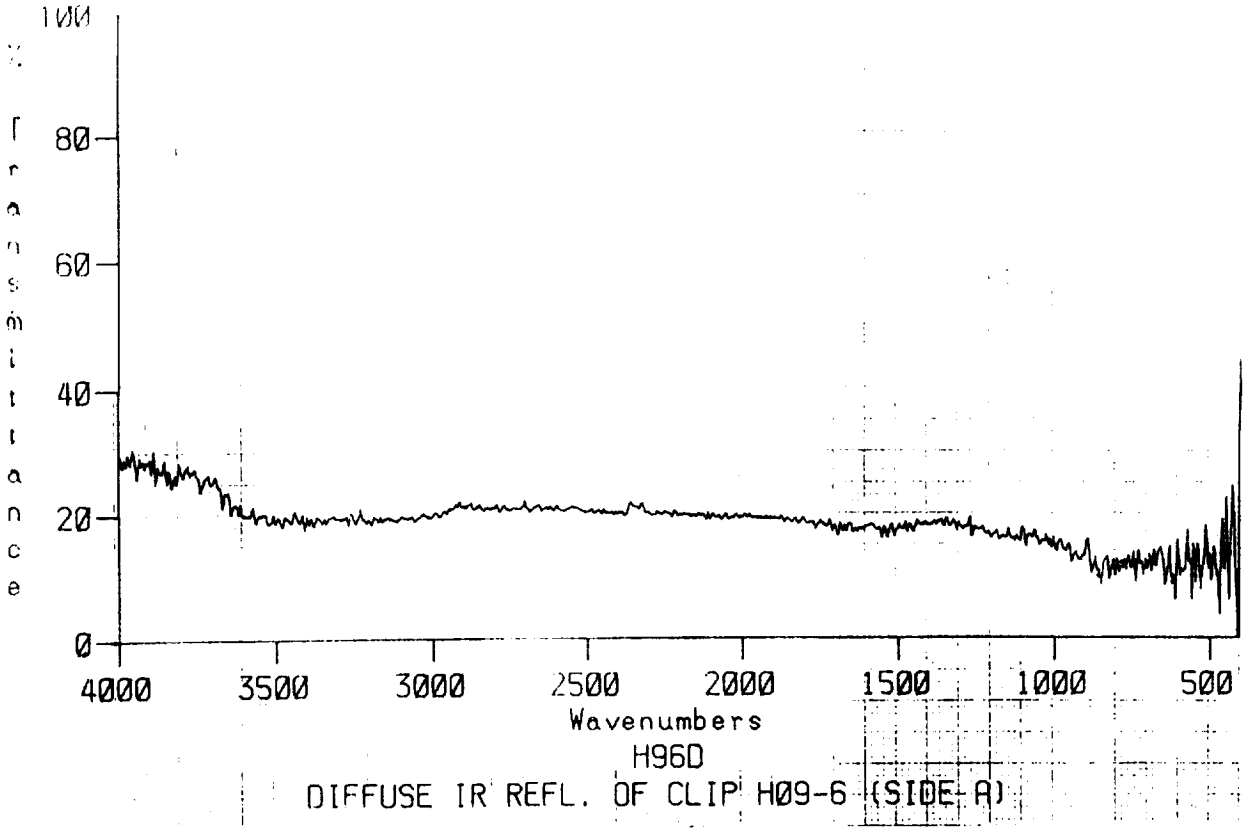

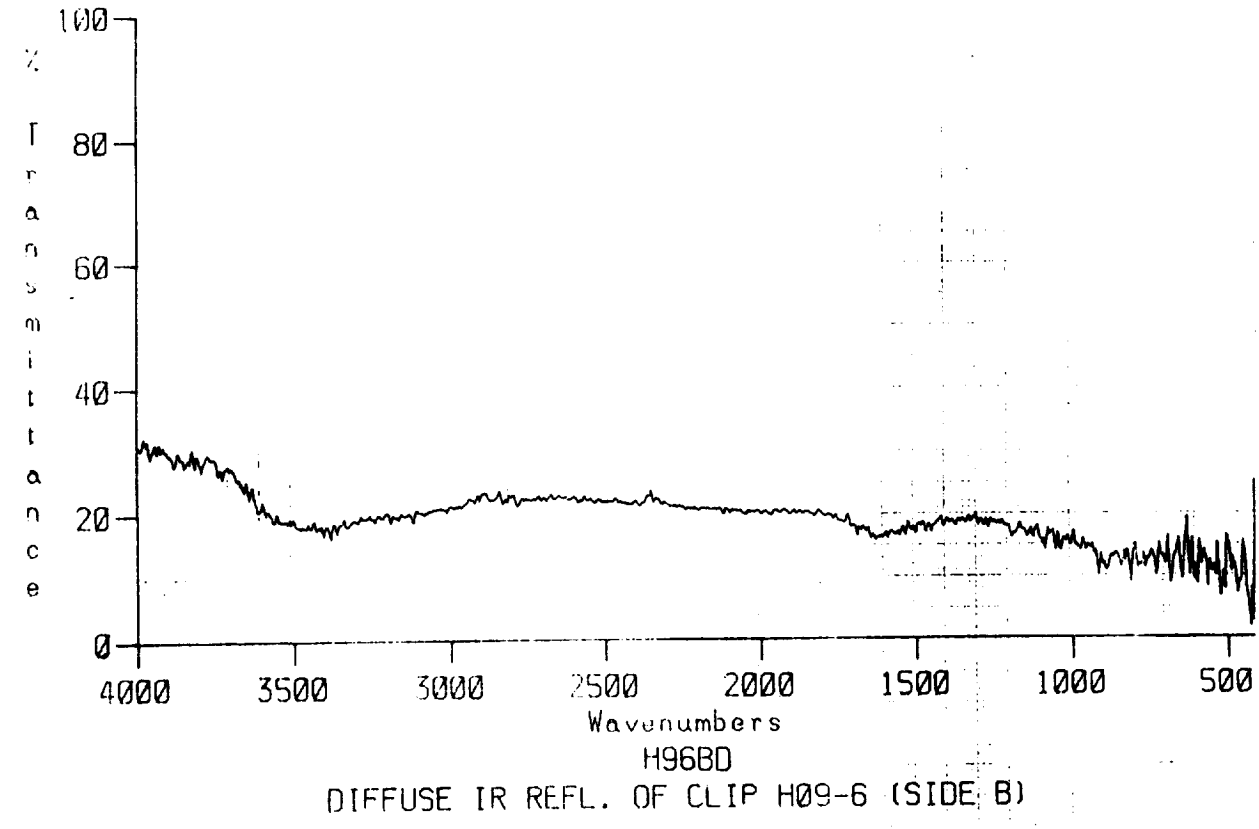

Figure A74: Diffuse IR Reflectance of clip H09-6, (A) Front (B) Back.

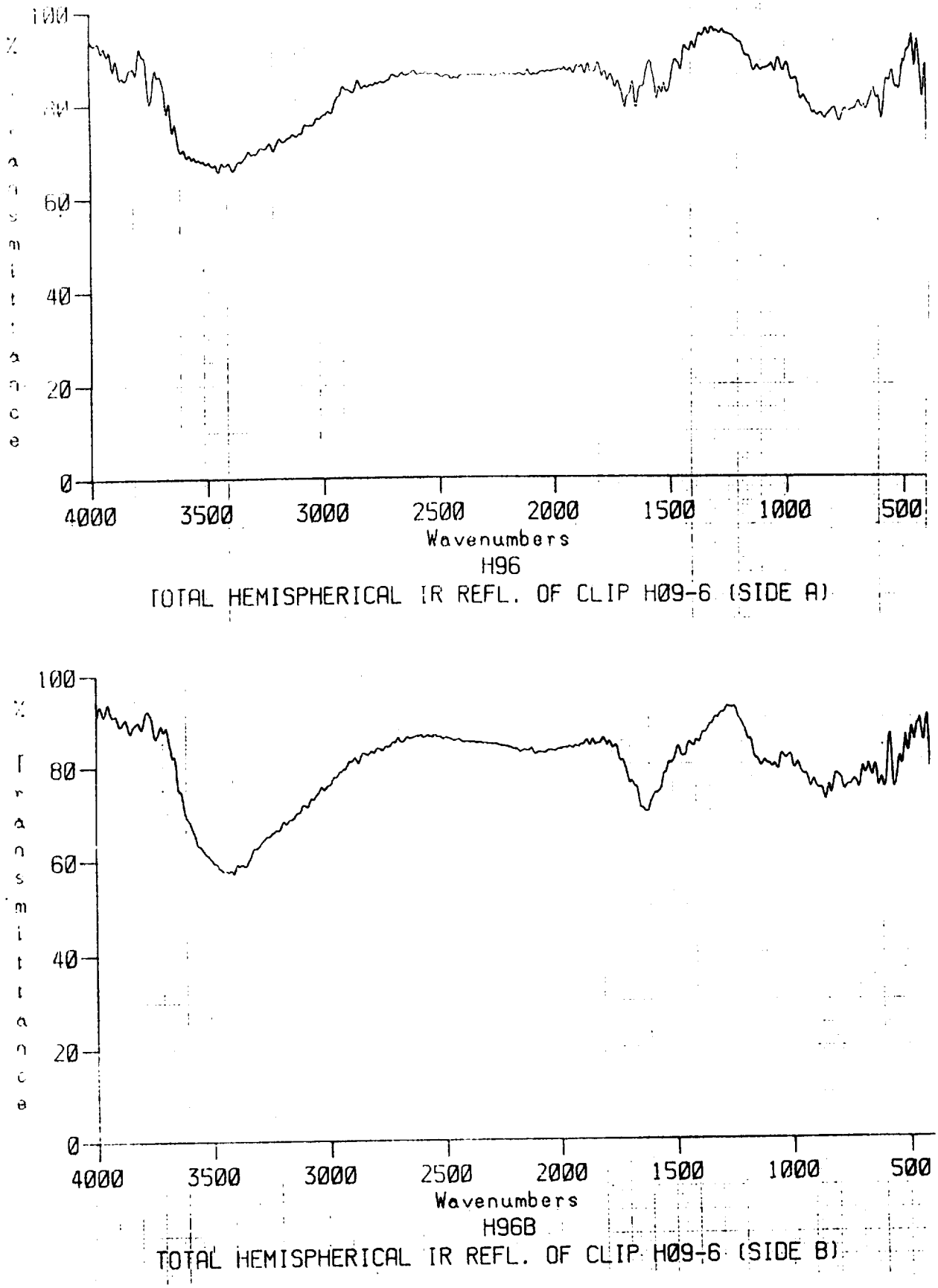

Figure A75: Total Hemispherical IR Reflectance of clip H09-6, (A) Front (B) Back.

LEADING EDGE

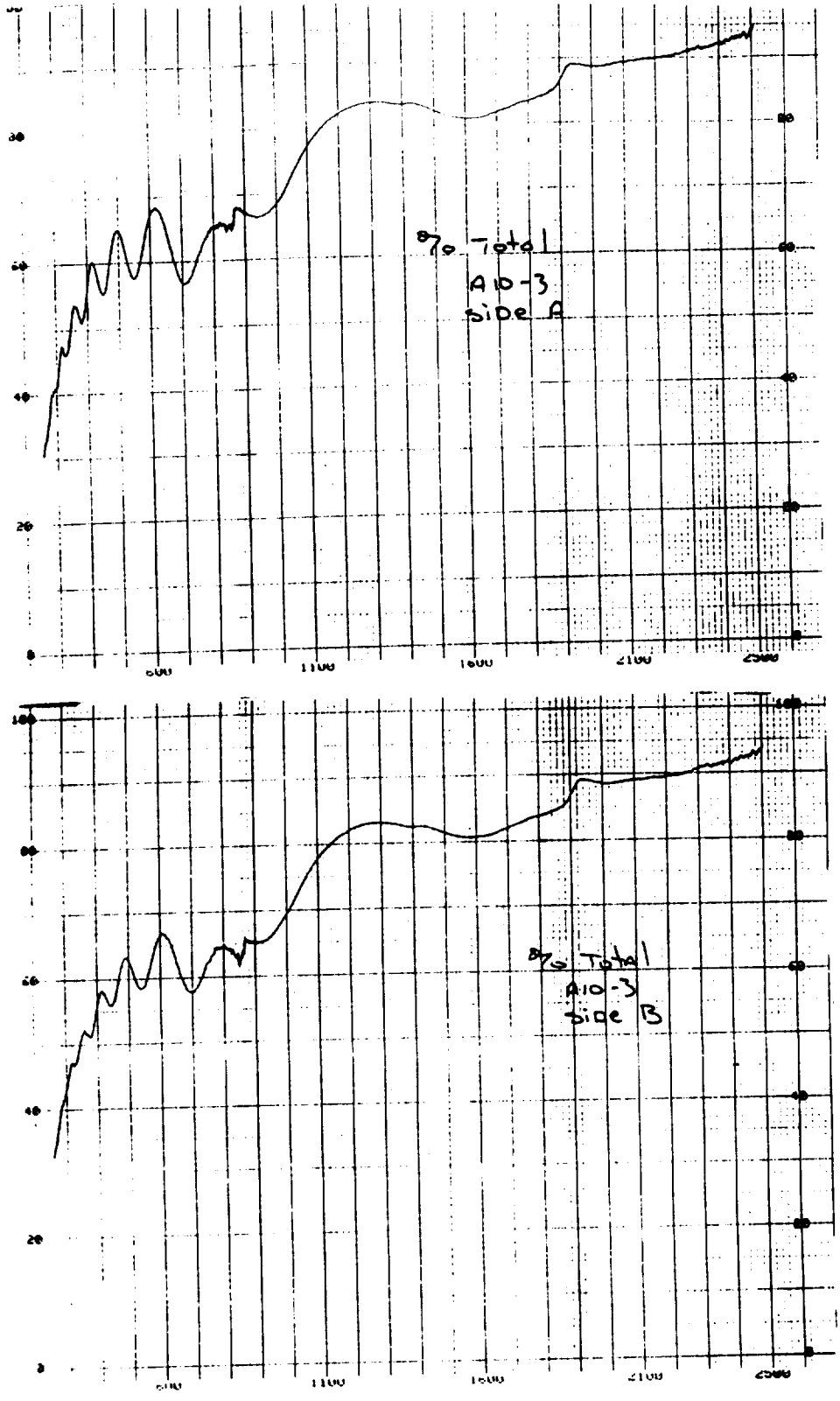

Figure A76: UV-Vis/NIR Total Reflectance of clamp A10-3, (A) Front (B) Back.

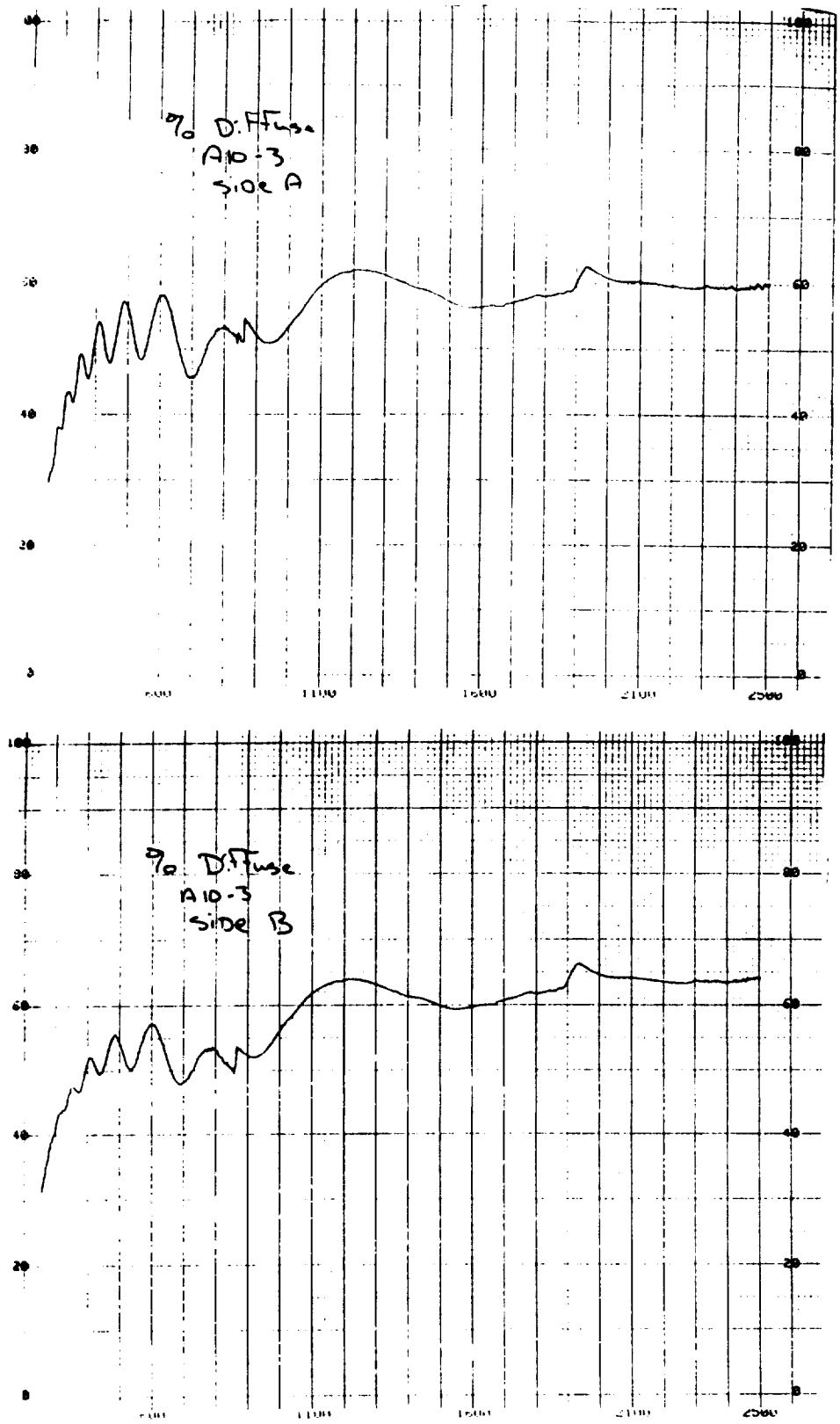

Figure A77: UV-Vis/NIR Diffuse Reflectance of clamp A10-3, (A) Front (B) Back.

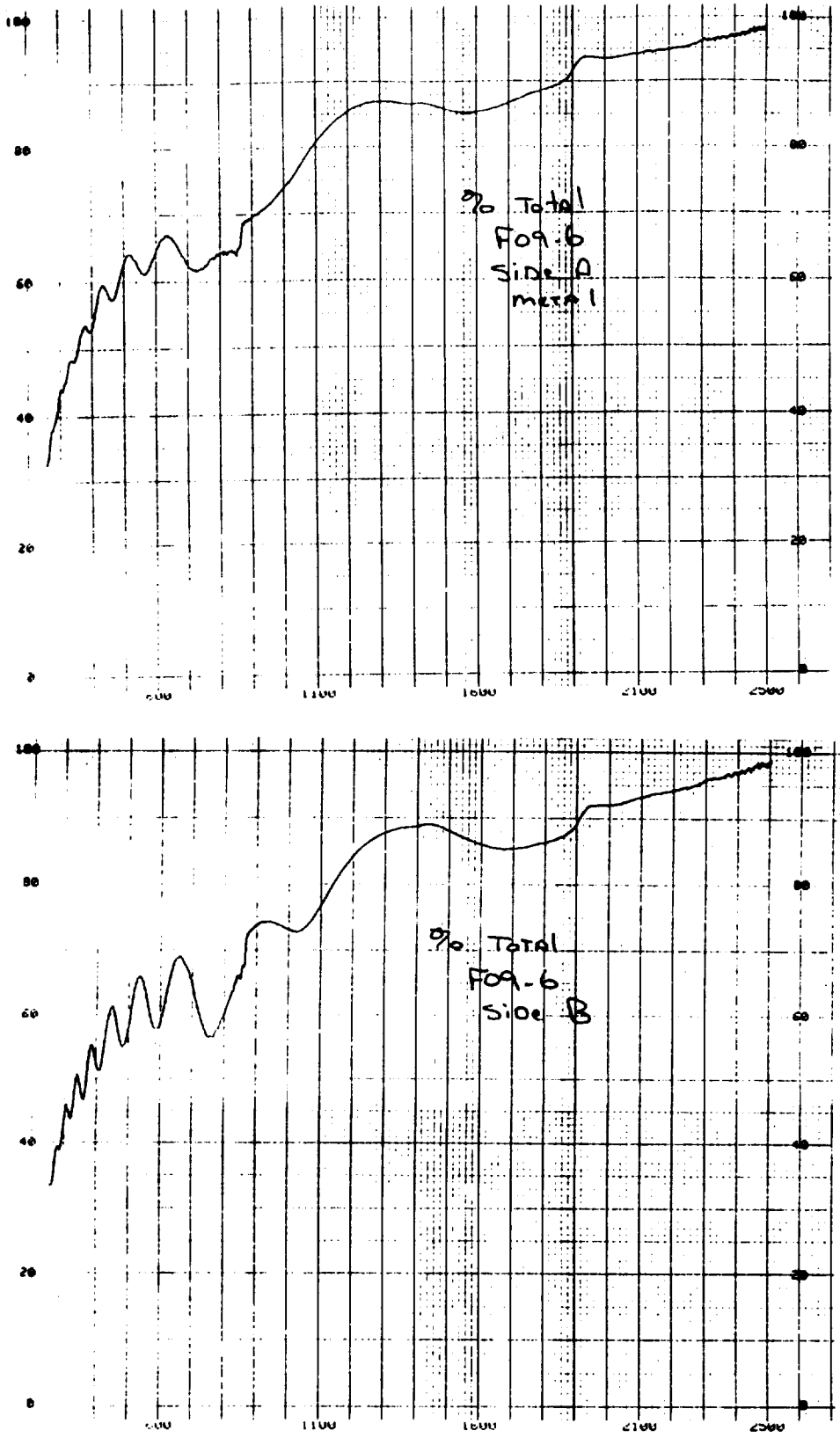

Figure A78: UV-Vis/NIR Total Reflectance of clamp F09-6, (A) Front (B) Back.

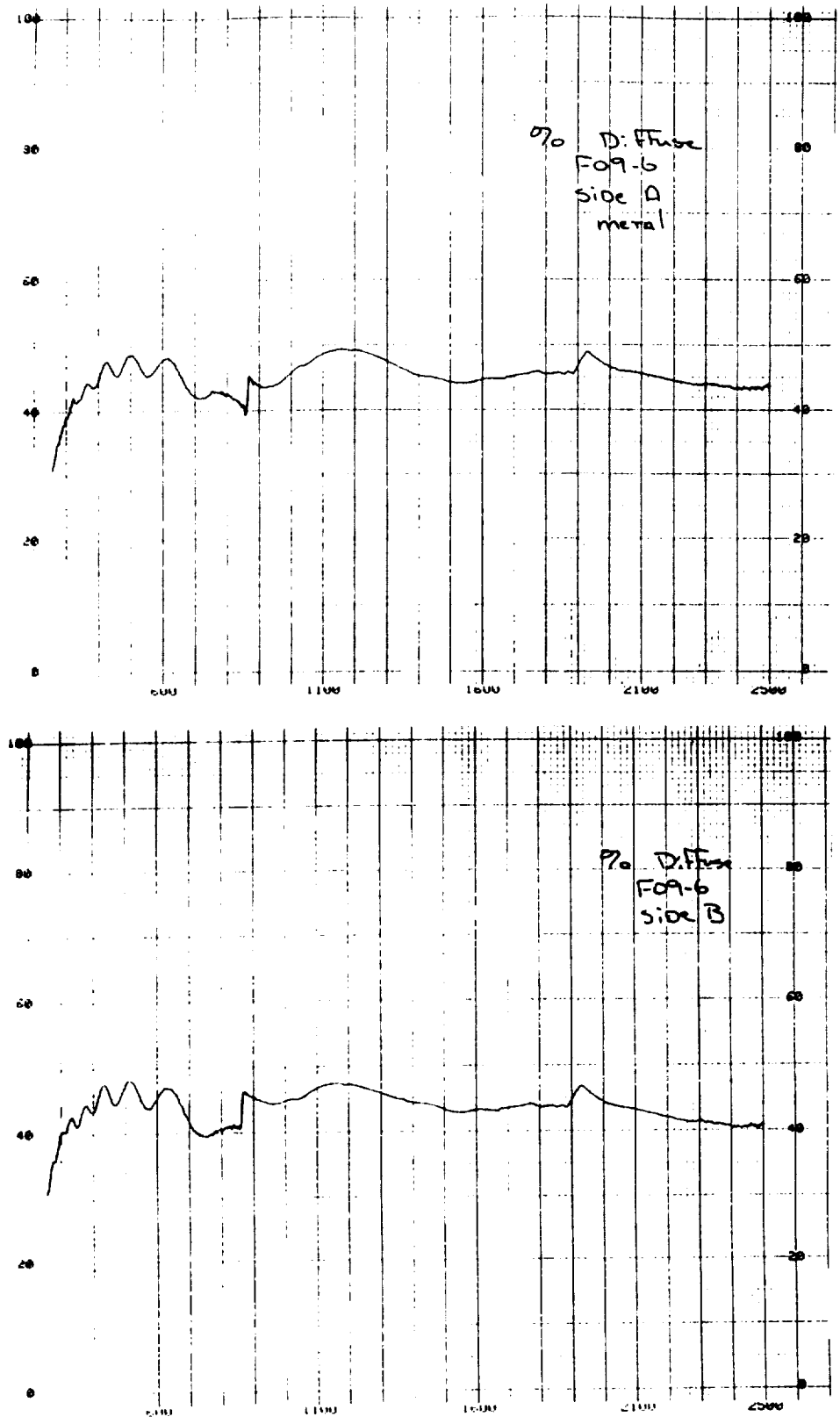

Figure A79: UV-Vis/NIR Diffuse Reflectance of clamp F09-6, (A) Front (B) Back.

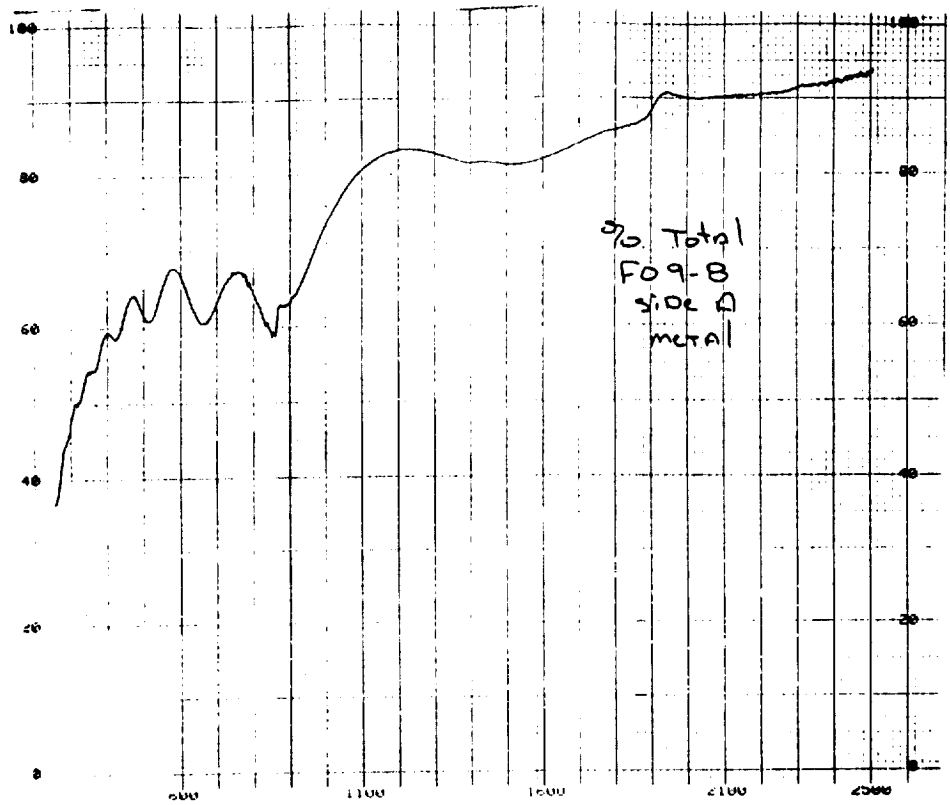

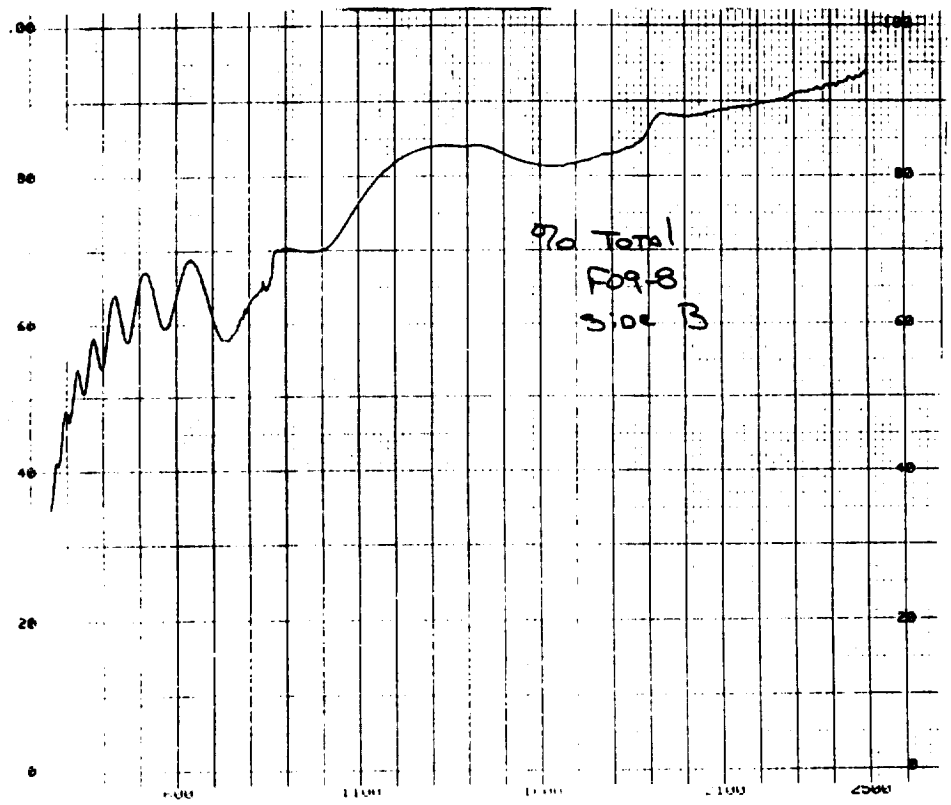

Figure A80: UV-Vis/NIR Total Reflectance of clamp F09-8, (A) Front (B) Back.

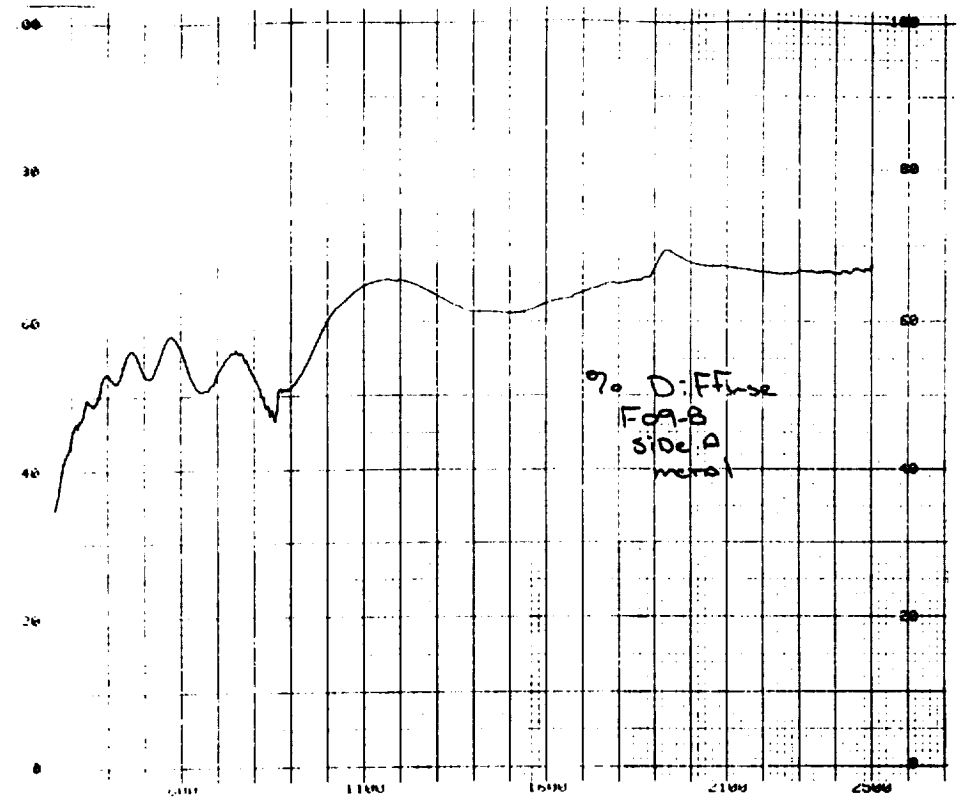

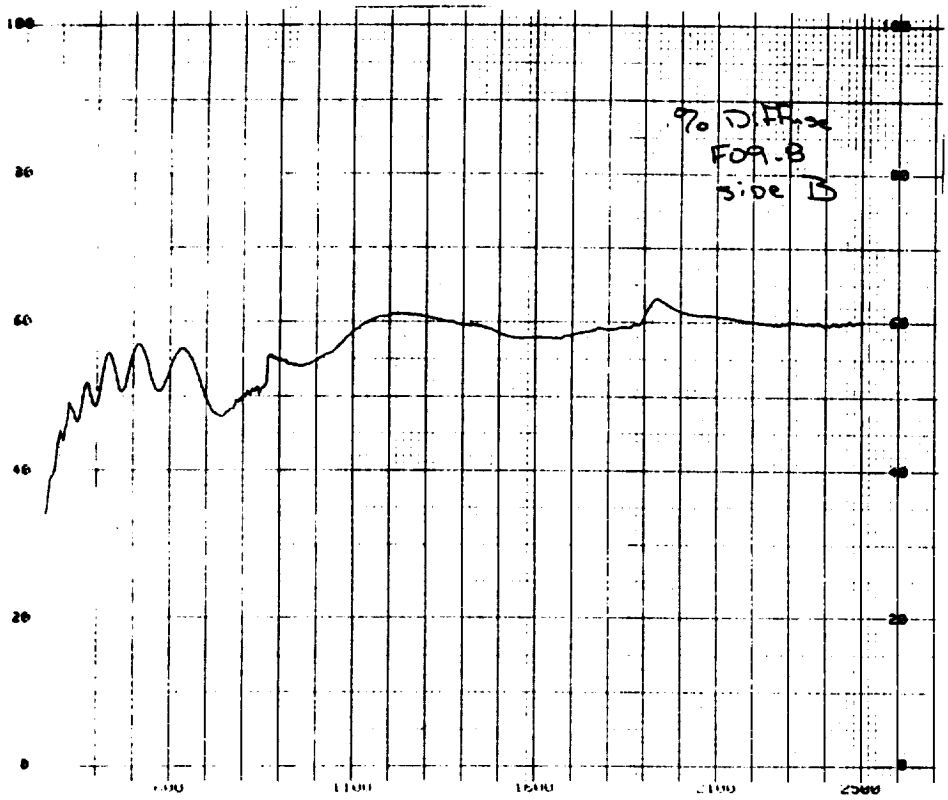

Figure A81: UV-Vis/NIR Diffuse Reflectance of clamp F09-8, (A) Front (B) Back.

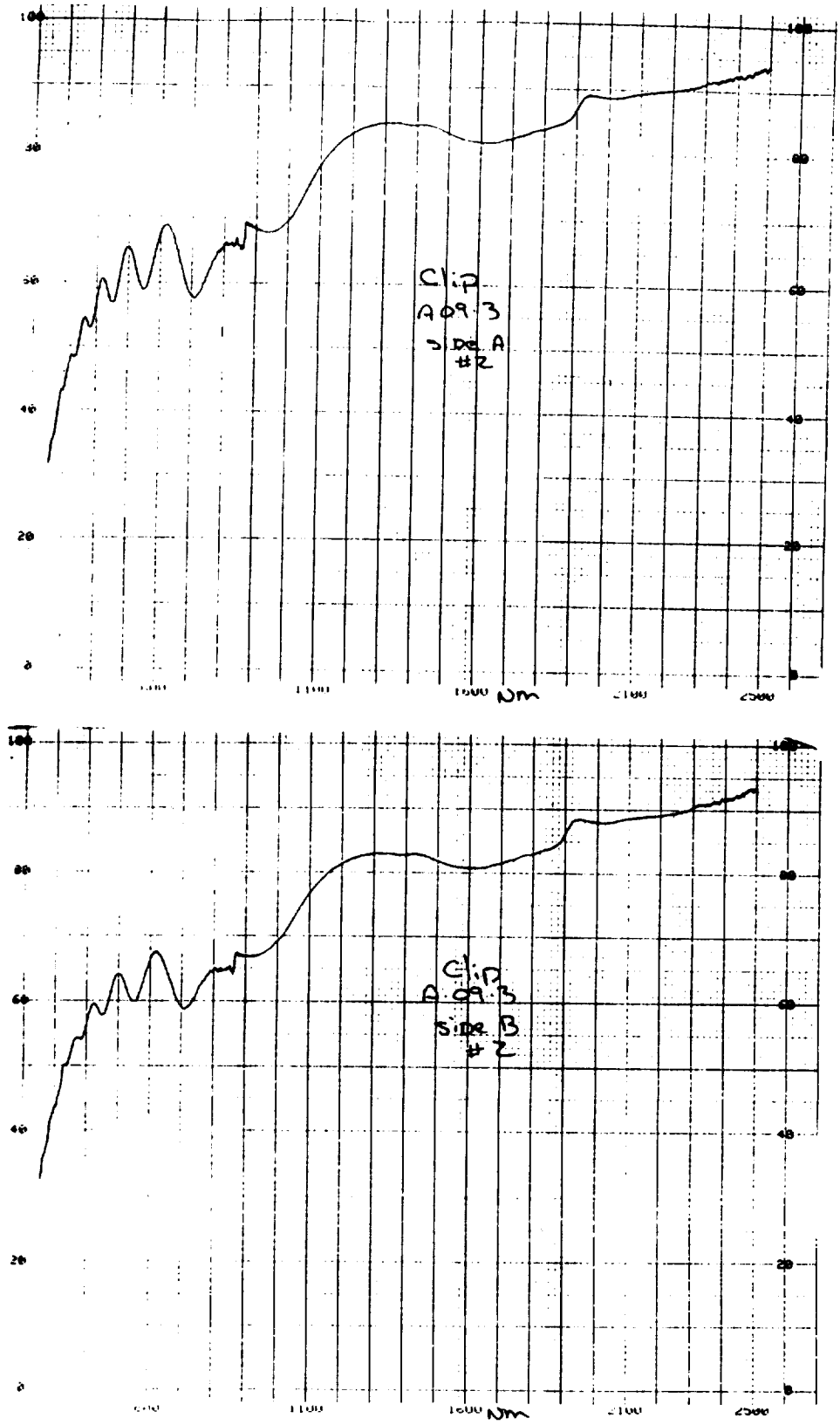

Figure A82: UV-Vis/NIR Total Reflectance of clip A09-3. (A) Front (B) Back.

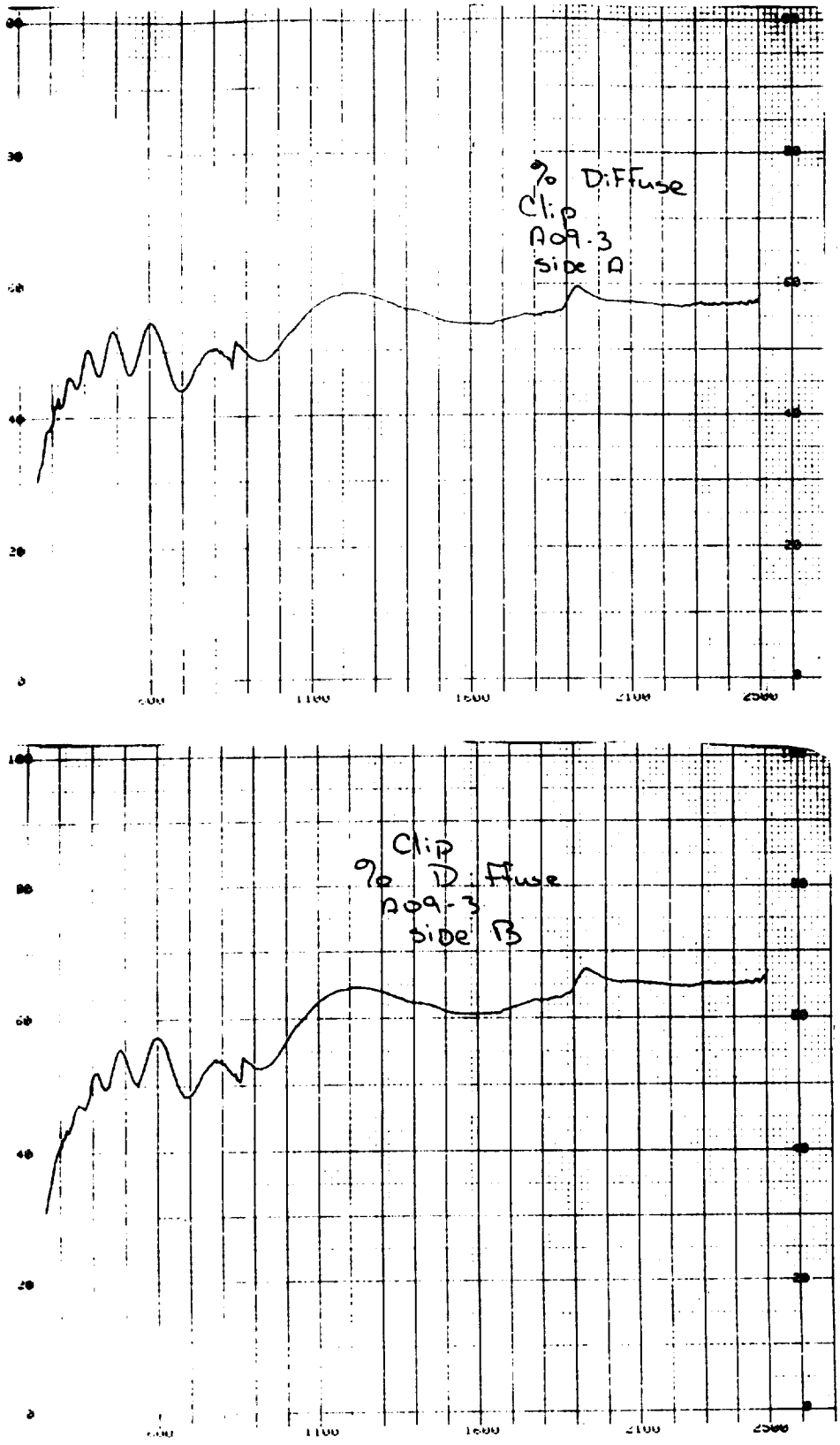

Figure A83: UV-Vis/NIR Diffuse Reflectance of clip A09-3, (A) Front (B) Back.

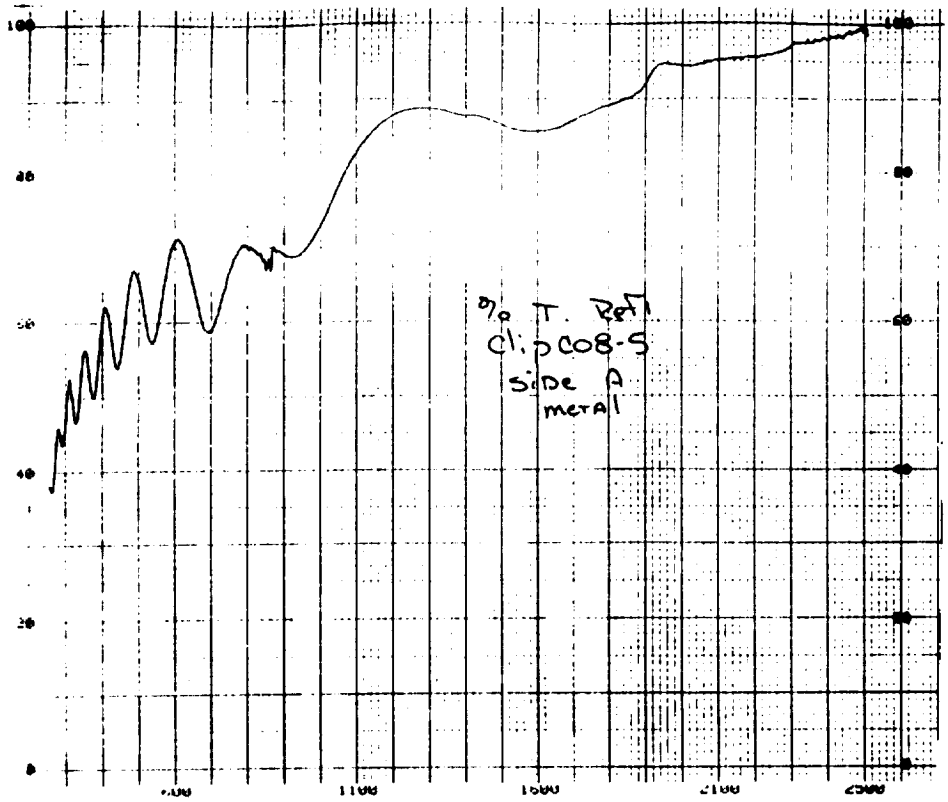

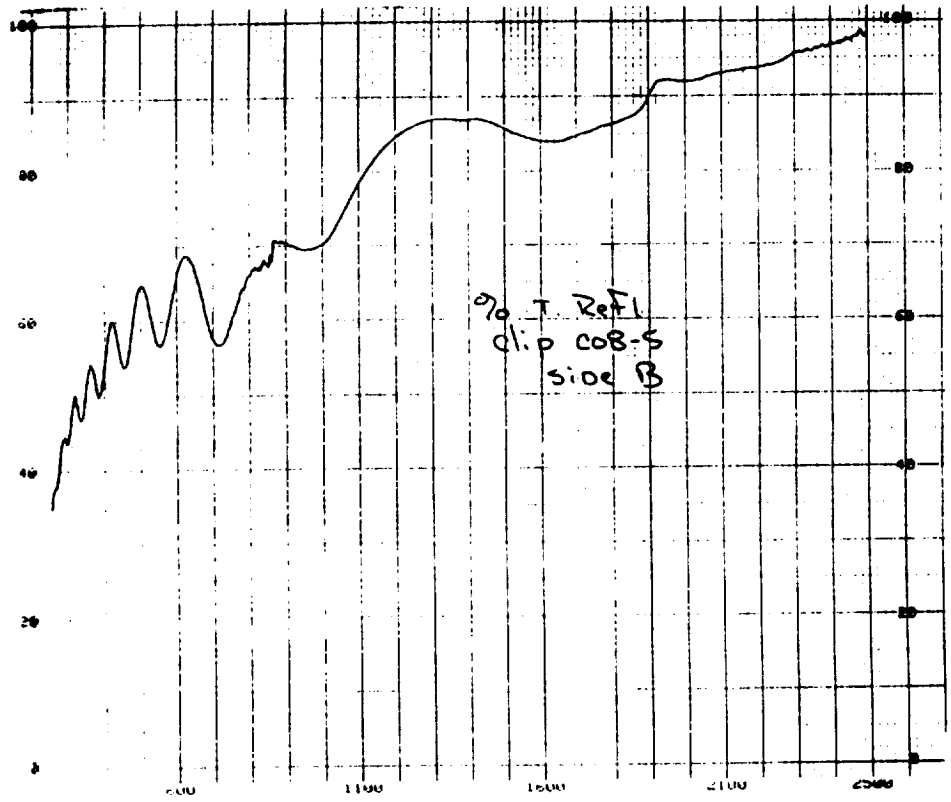

Figure A84: UV-Vis/NIR Total Reflectance of clip C08-5, (A) Front (B) Back.

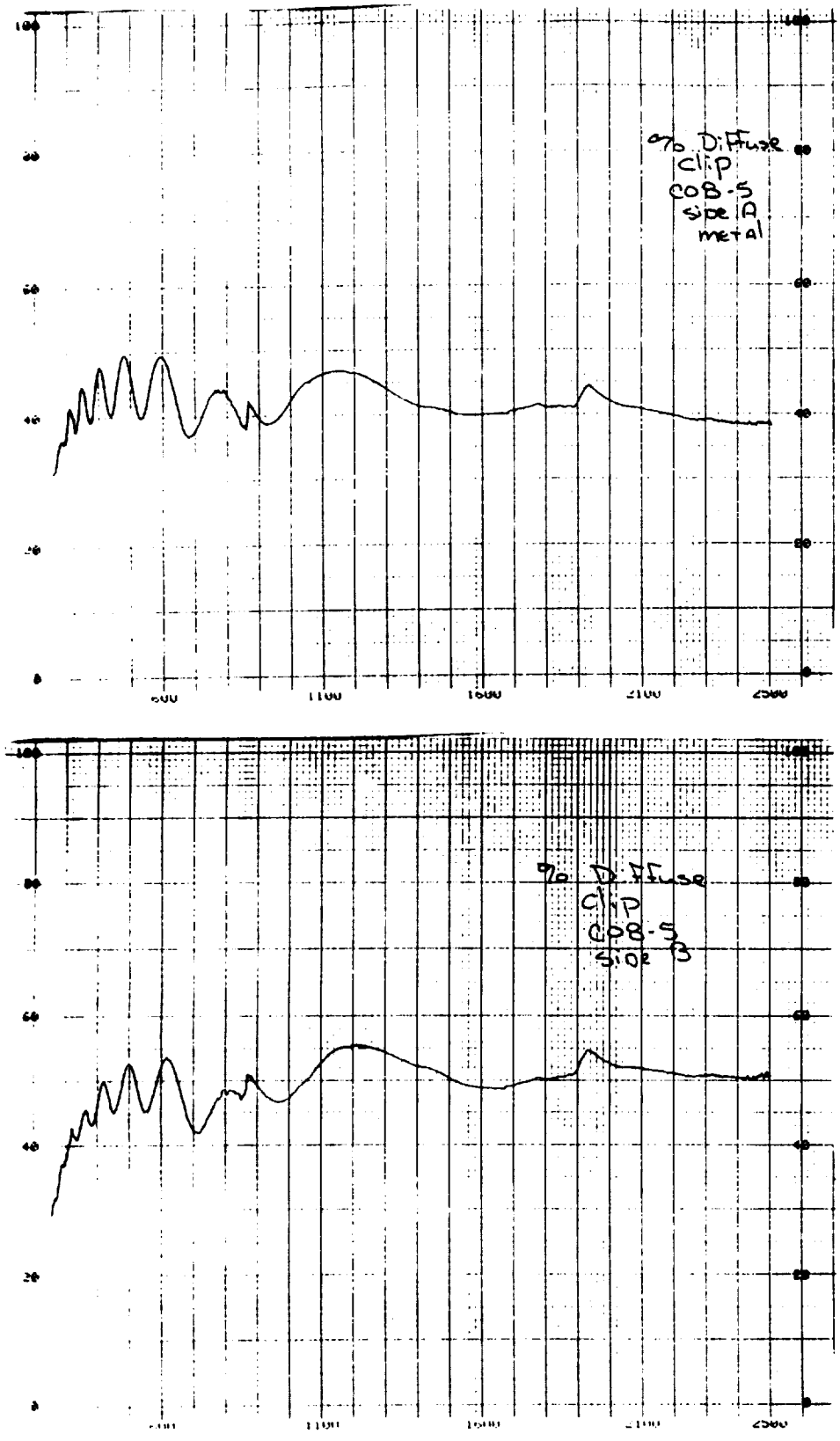

Figure A85: UV-Vis/NIR Diffuse Reflectance of clip C08-5, (A) Front (B) Back.

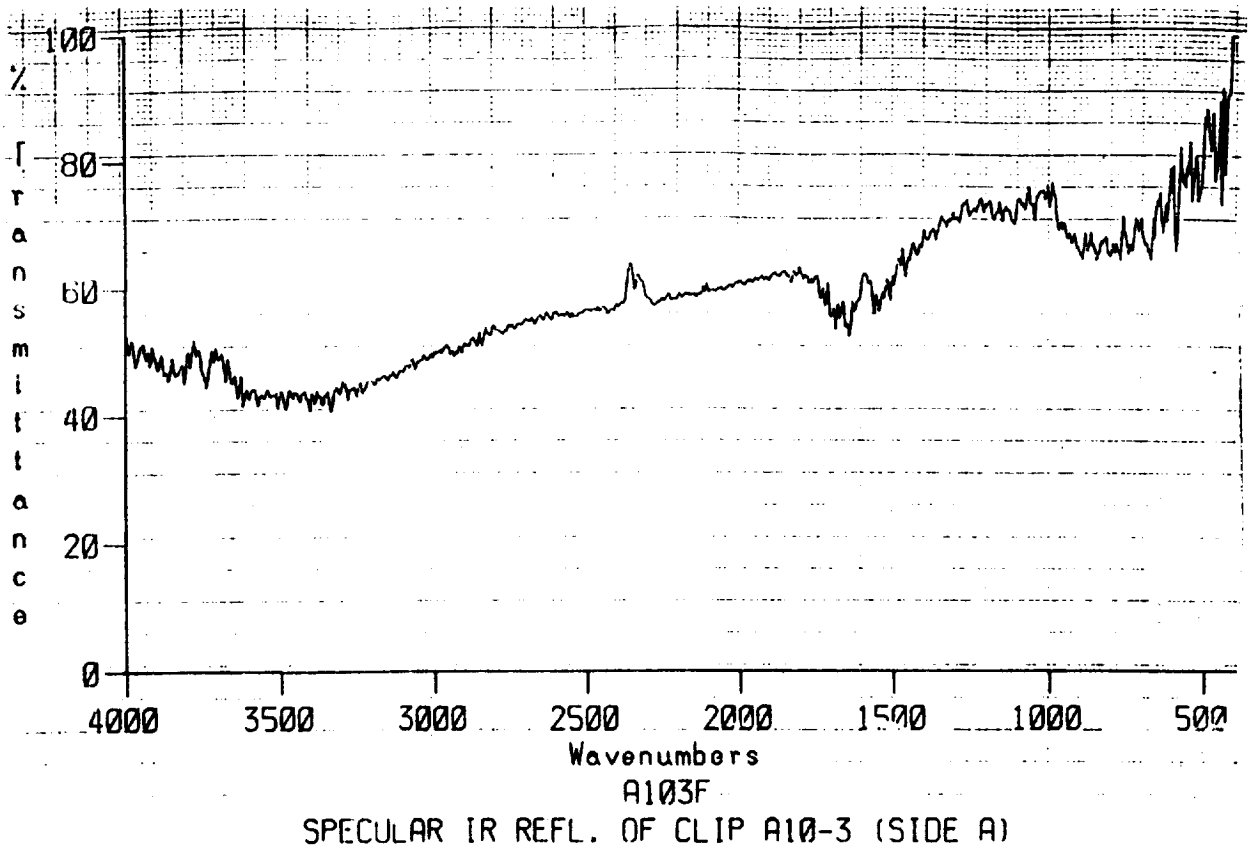

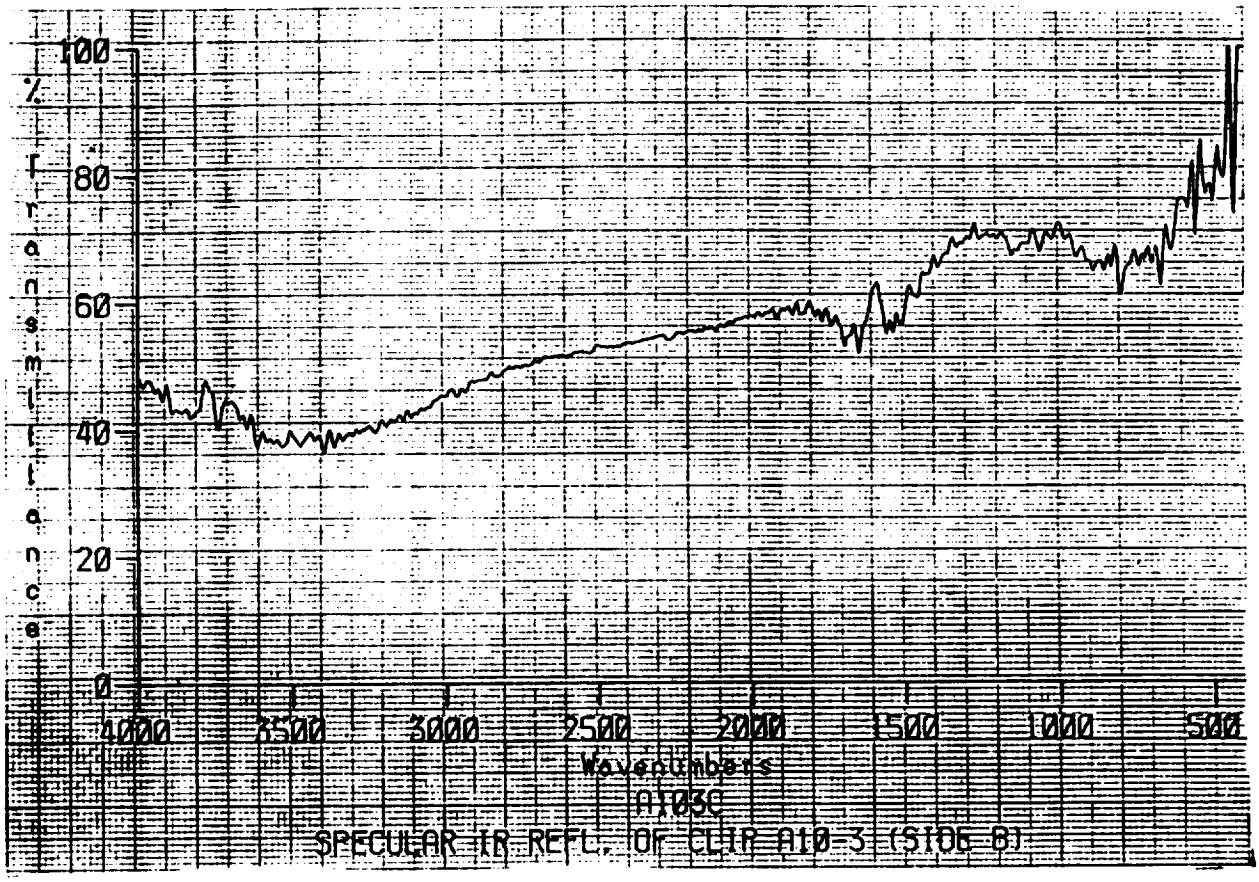

Figure A86: Specular IR Reflectance of clip A10-3, (A) Front (B) Back.

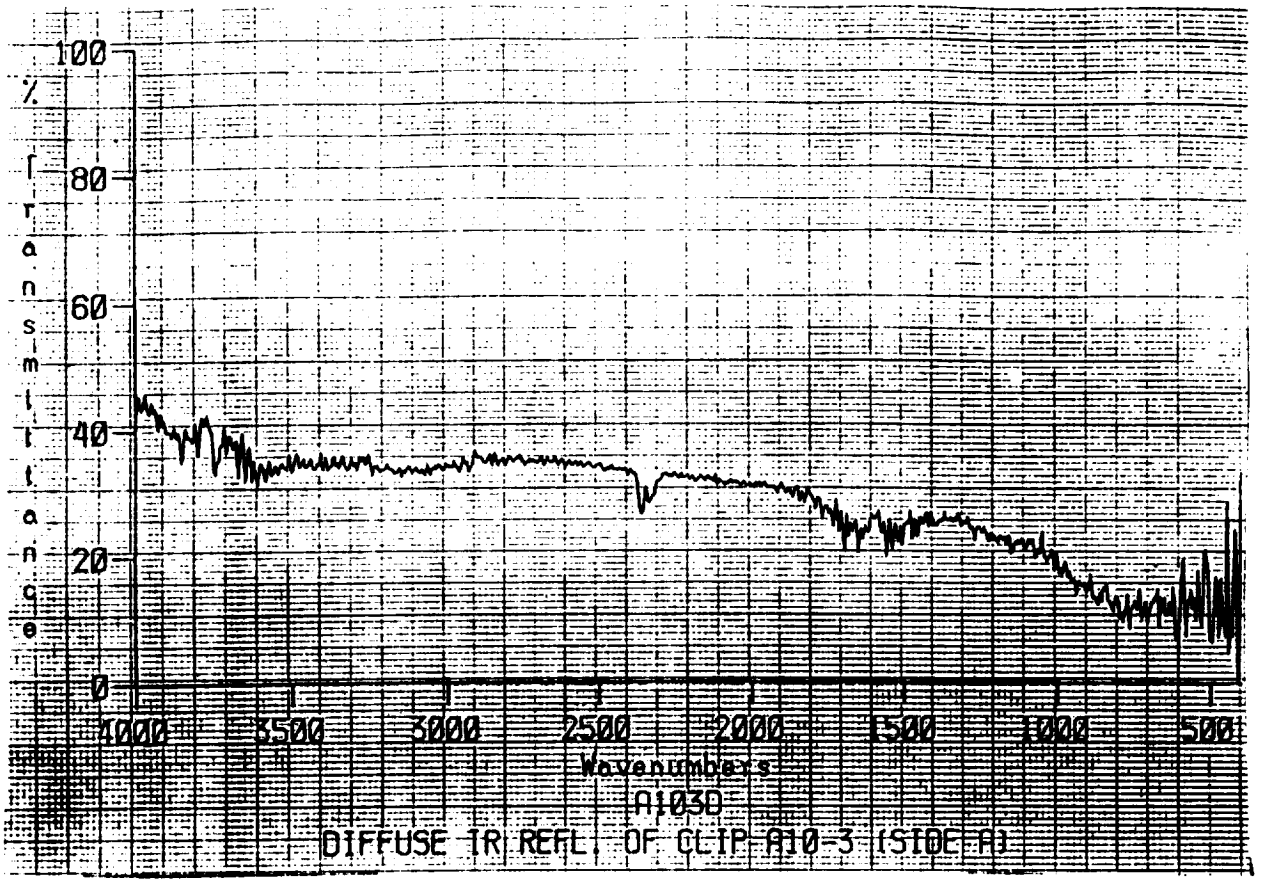

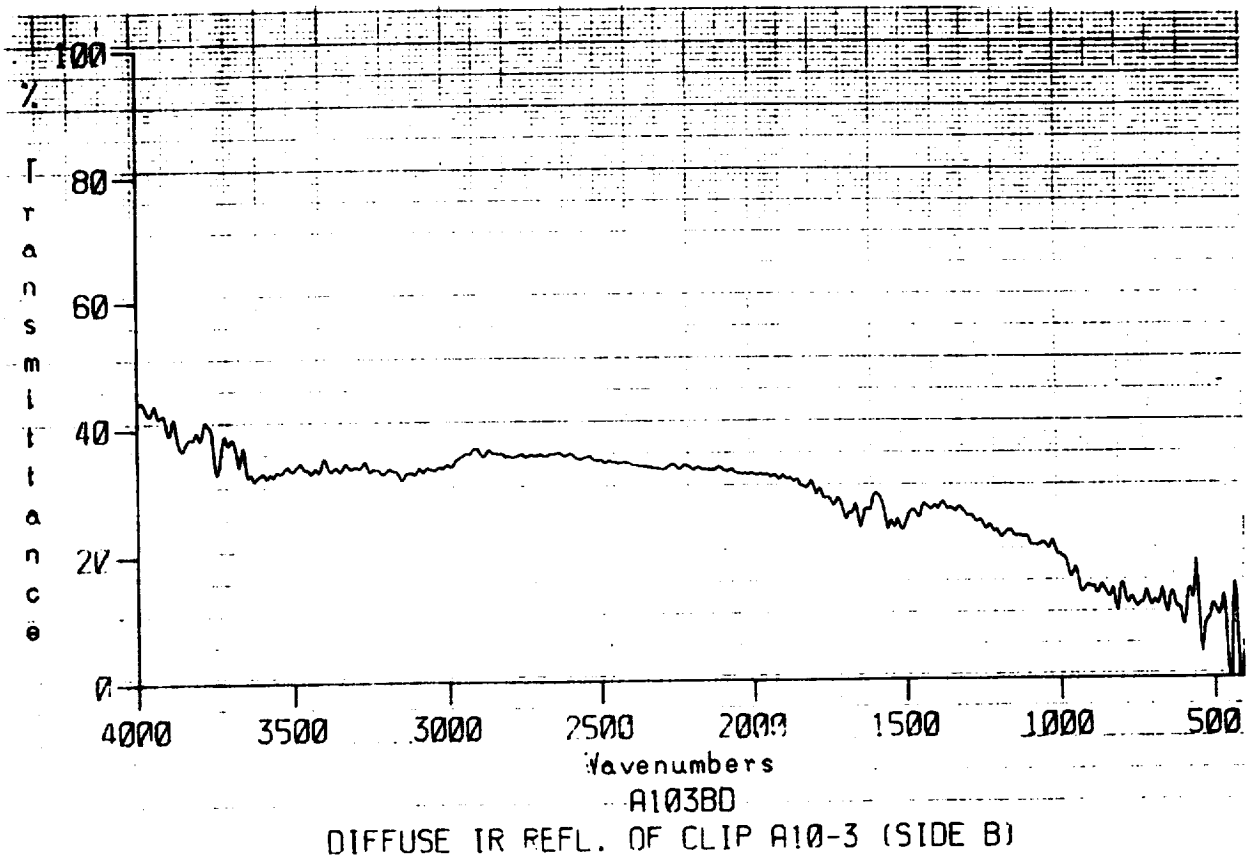

Figure A87: Diffuse IR Reflectance of clip A10-3, (A) Front (B) Back.

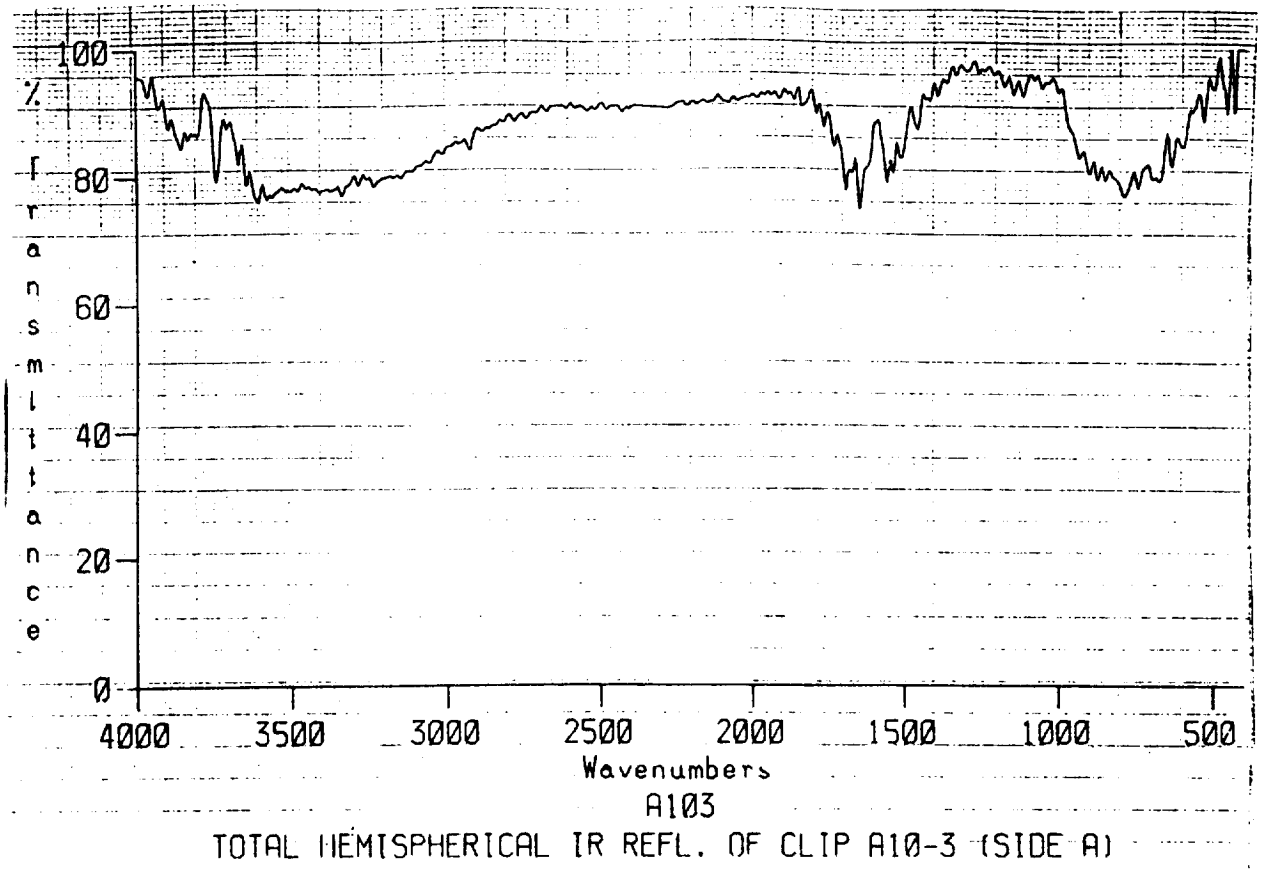

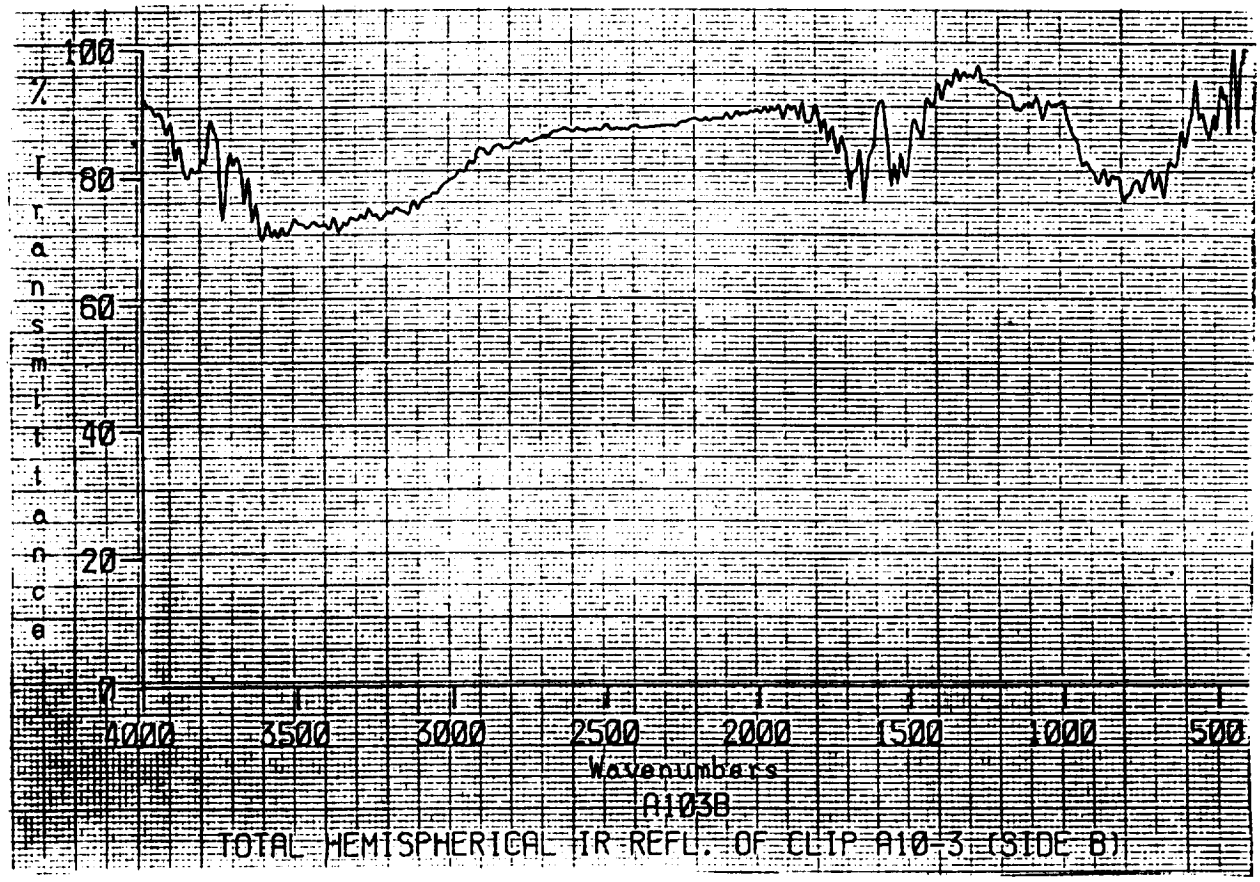

Figure A88: Total Hemispherical IR Reflectance of clip A10-3, (A) Front (B) Back

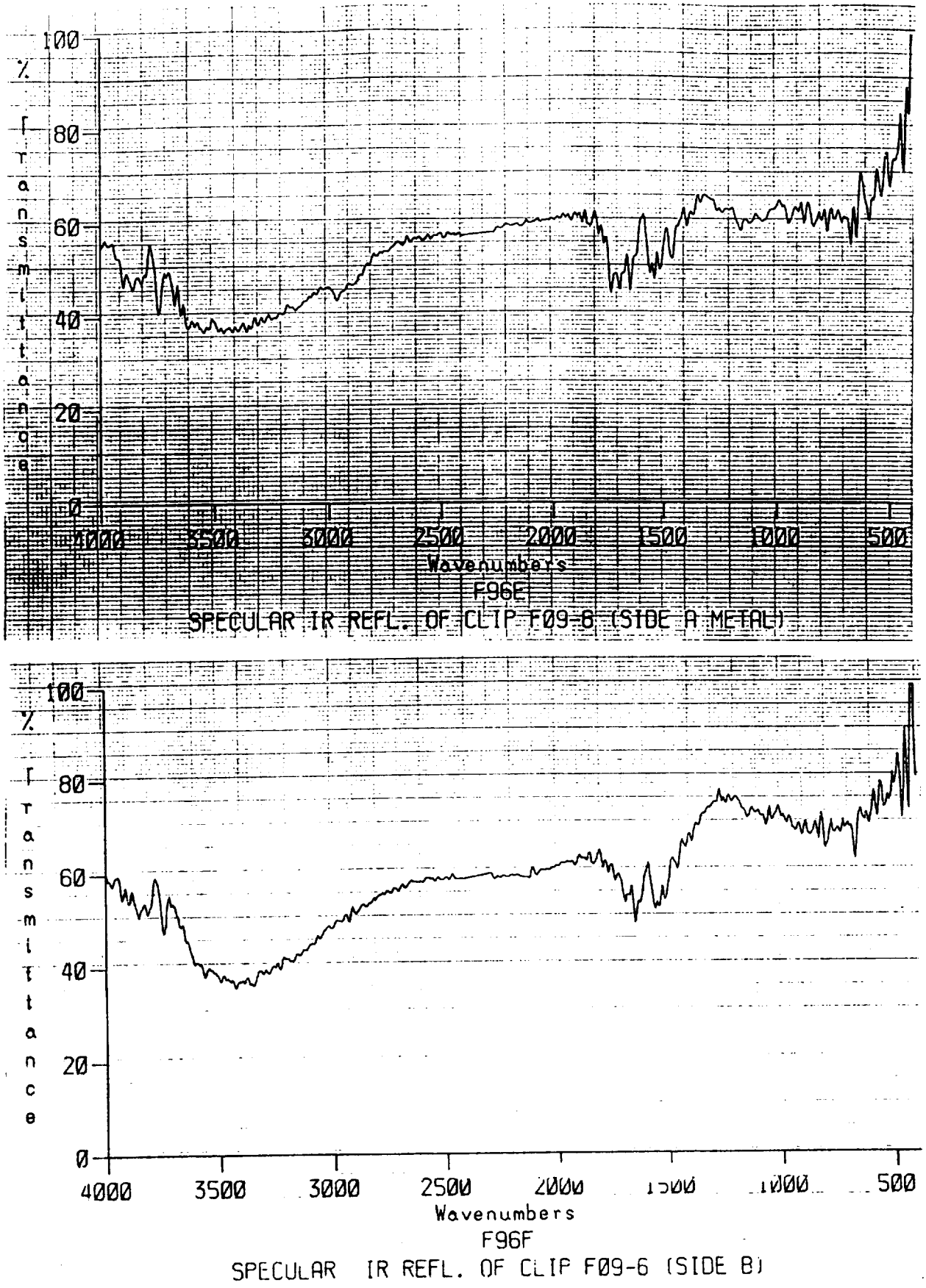

Figure A89: Specular IR Reflectance of clip F09-6, (A) Front (B) Back.

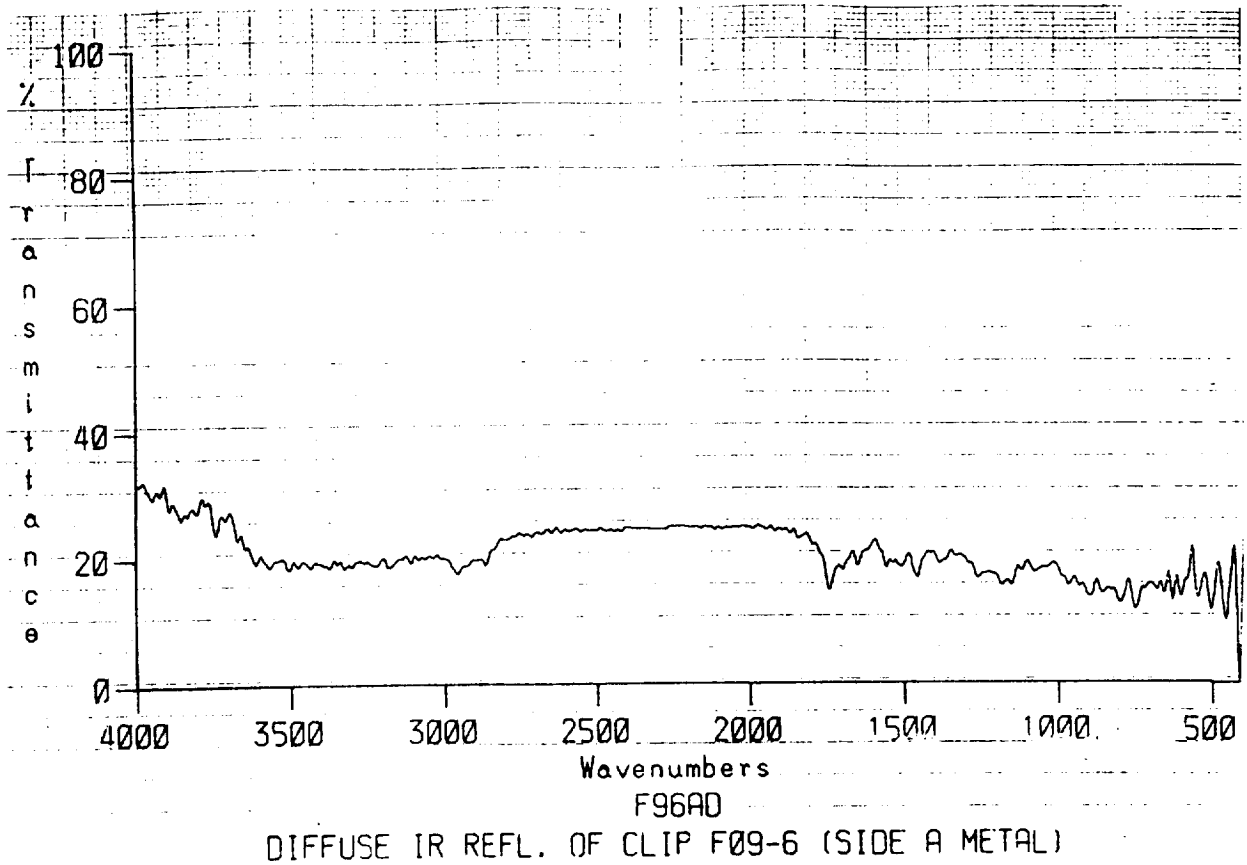

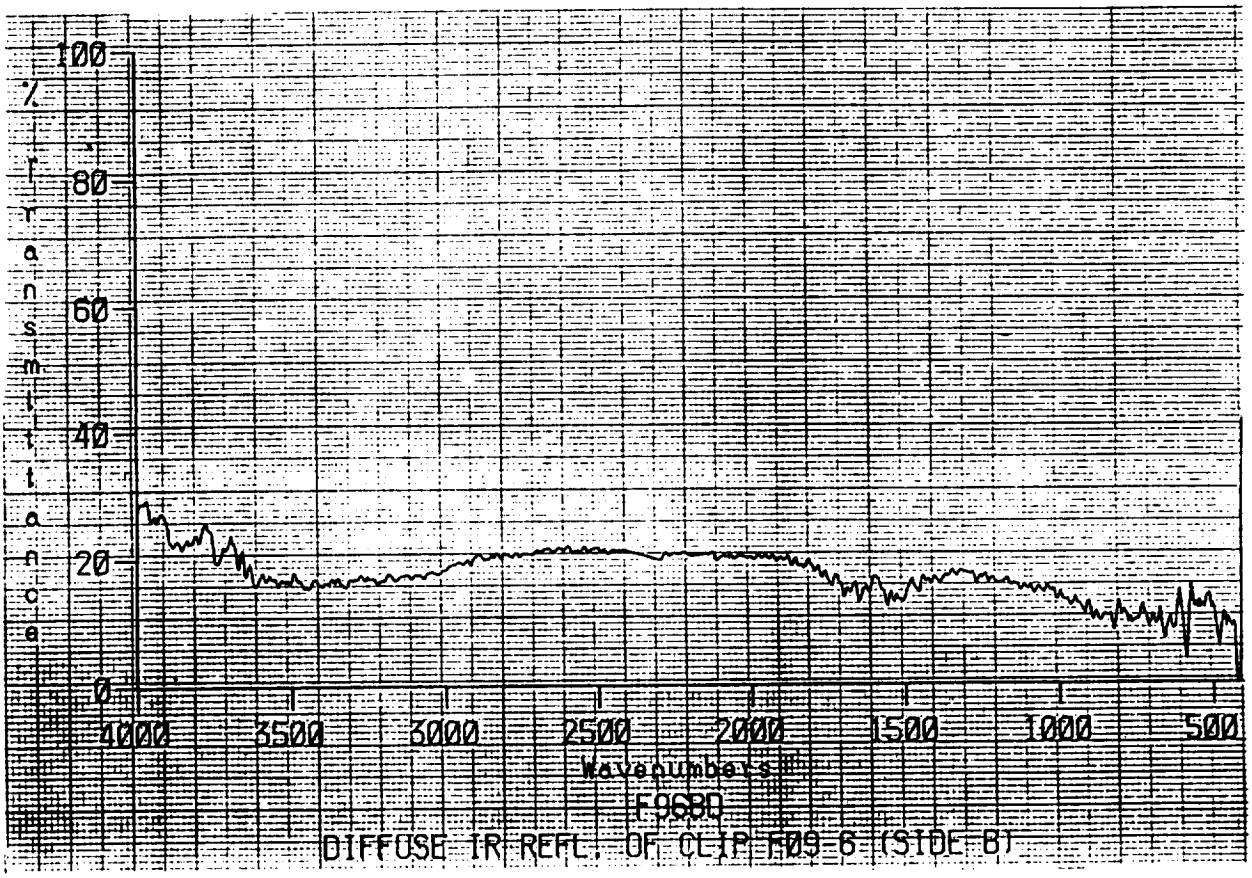

Figure A90: Diffuse IR Reflectance of Clip F09-6, (A) Front (B) Back.

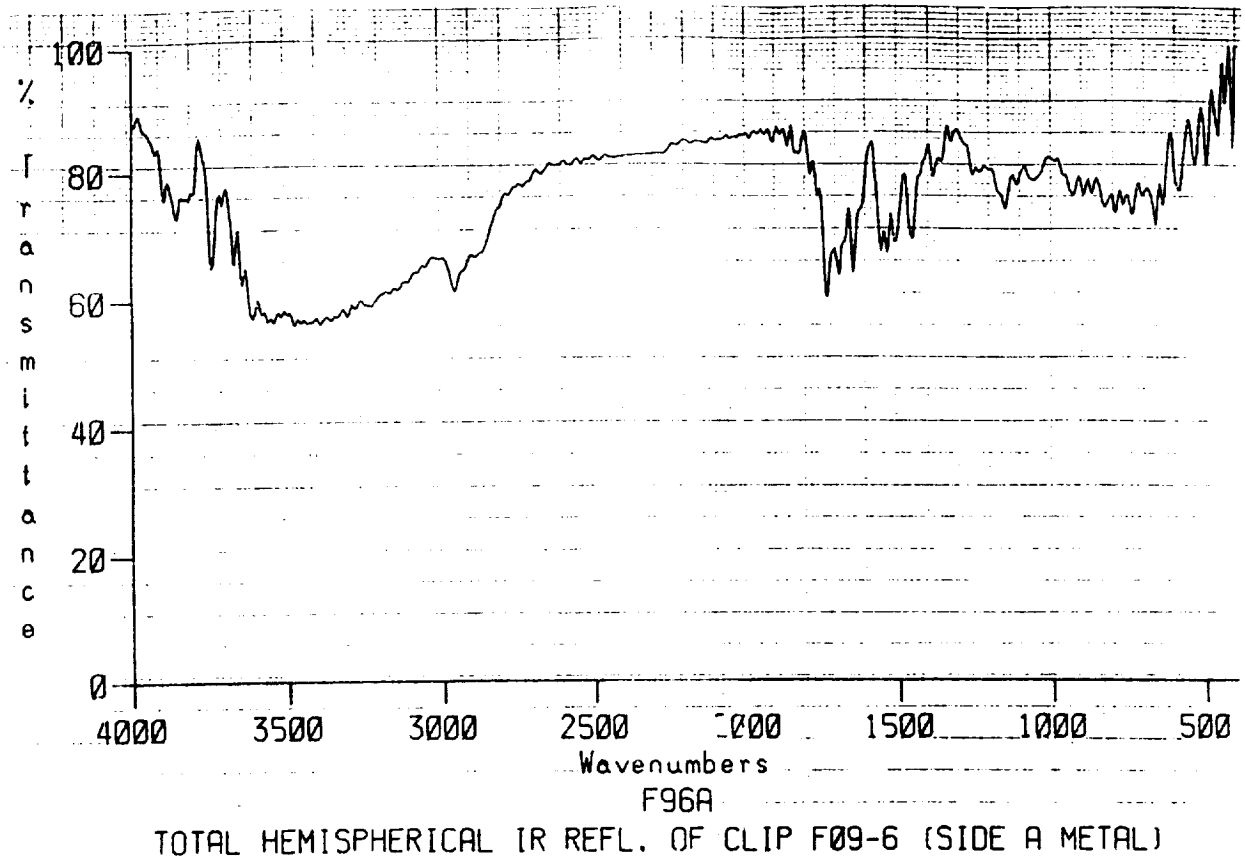

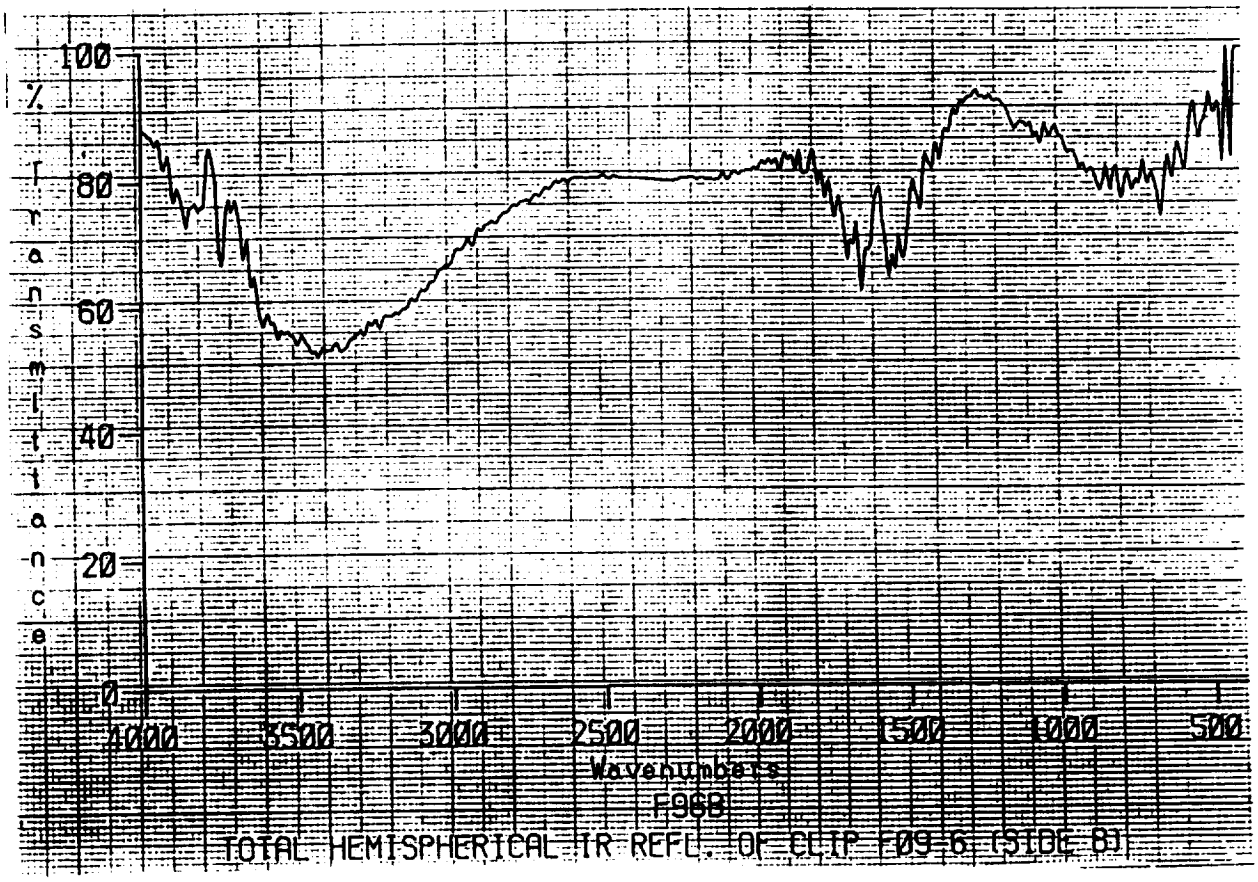

Figure A91: Total Hemispherical IR Reflectance of clip F09-6, (A) Front (B) Back.

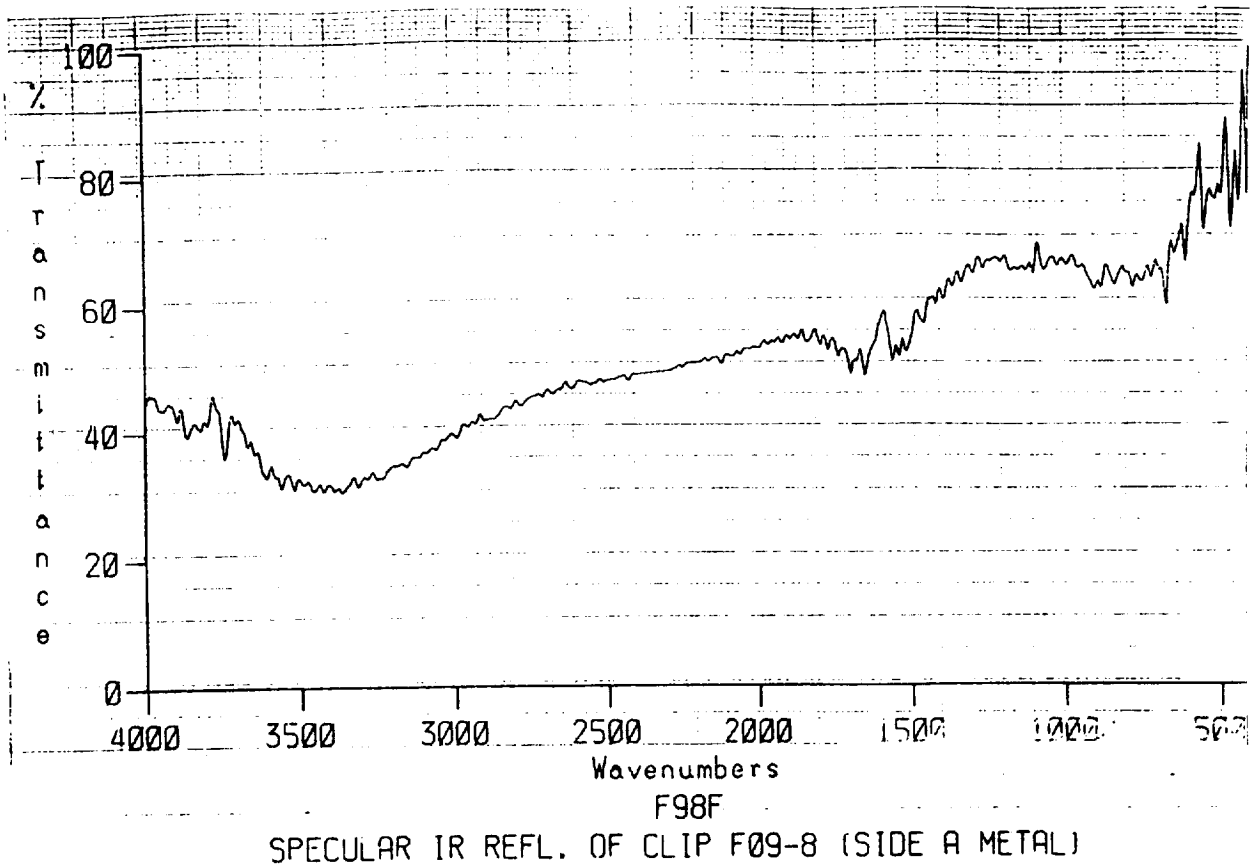

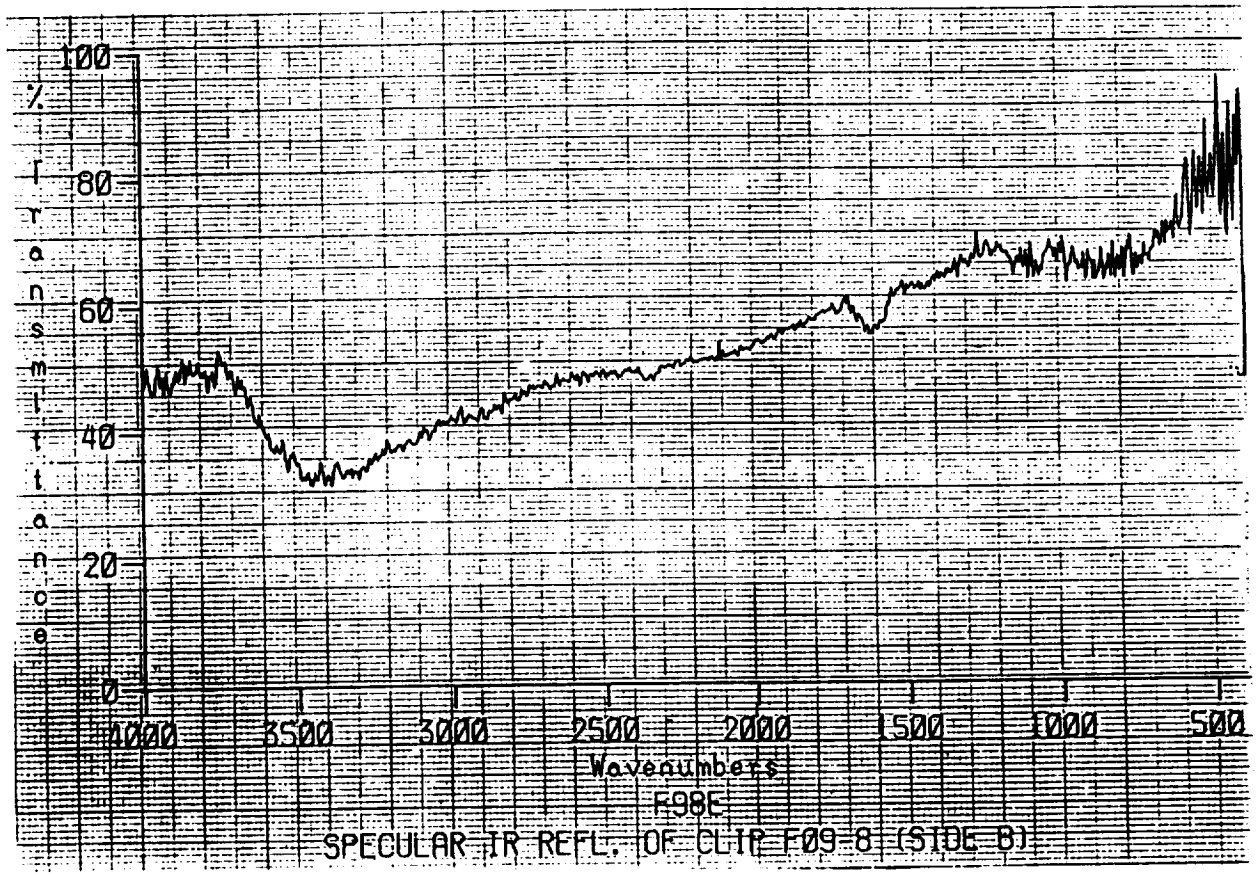

Figure A92: Specular IR Reflectance of clip F09-8, (A) Front (B) Back.

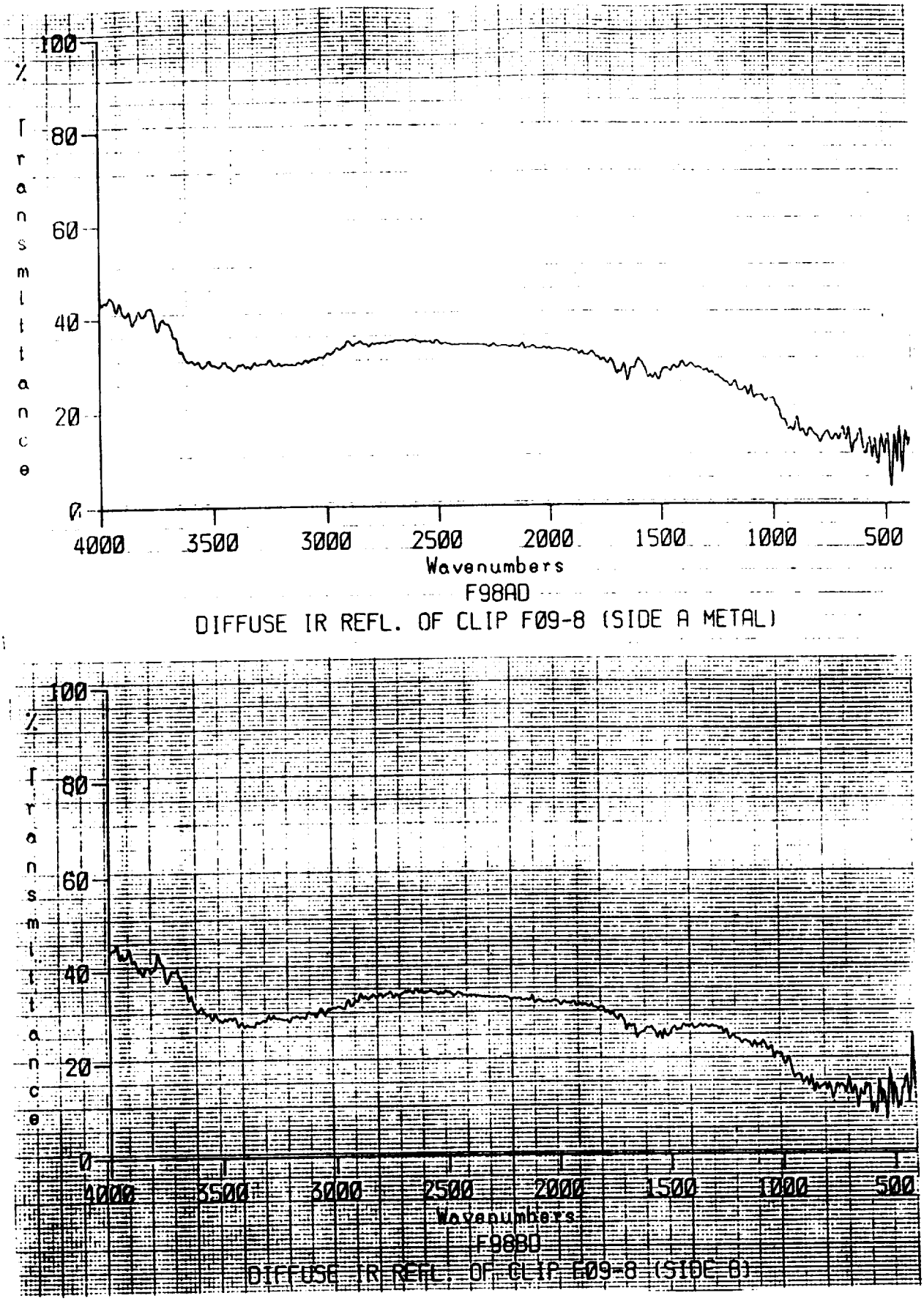

Figure A93: Diffuse IR Reflectance of clip F09-8, (A) Front (B) Back.

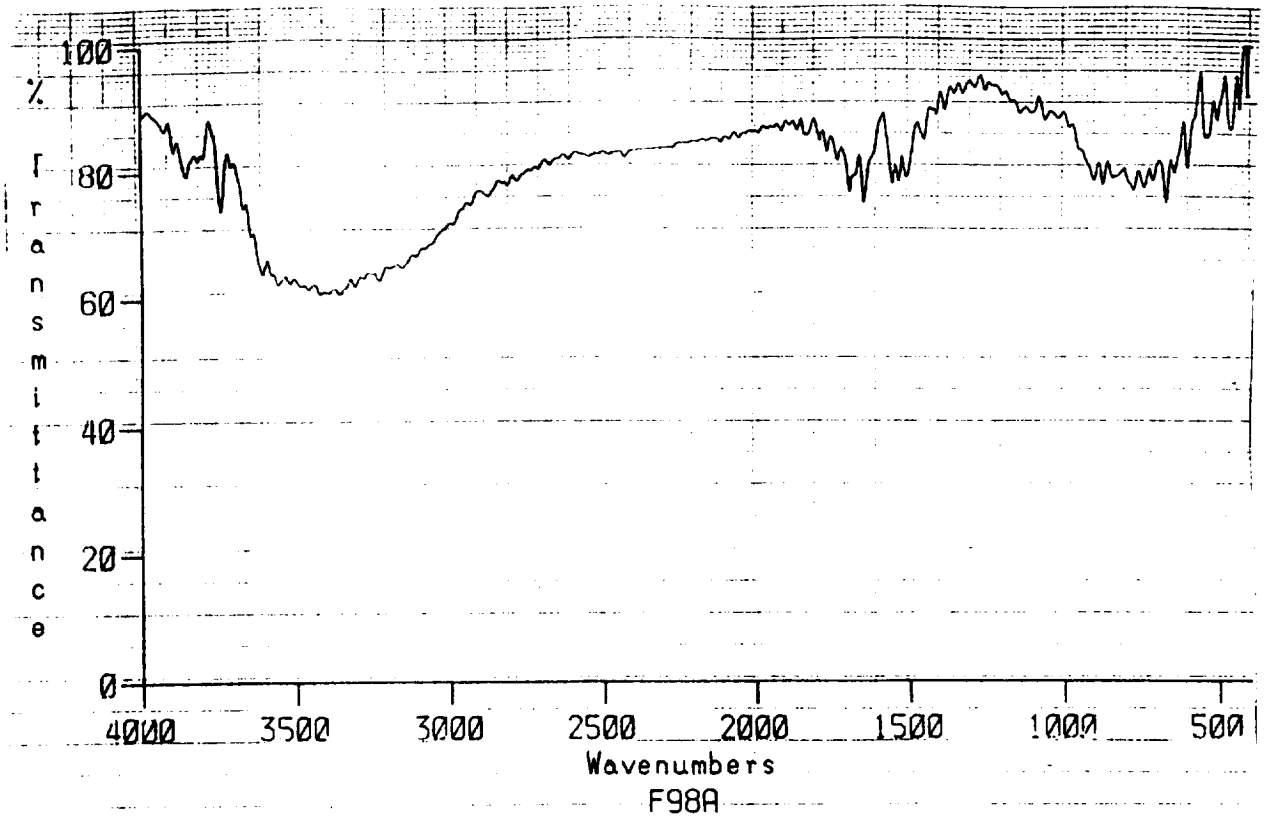

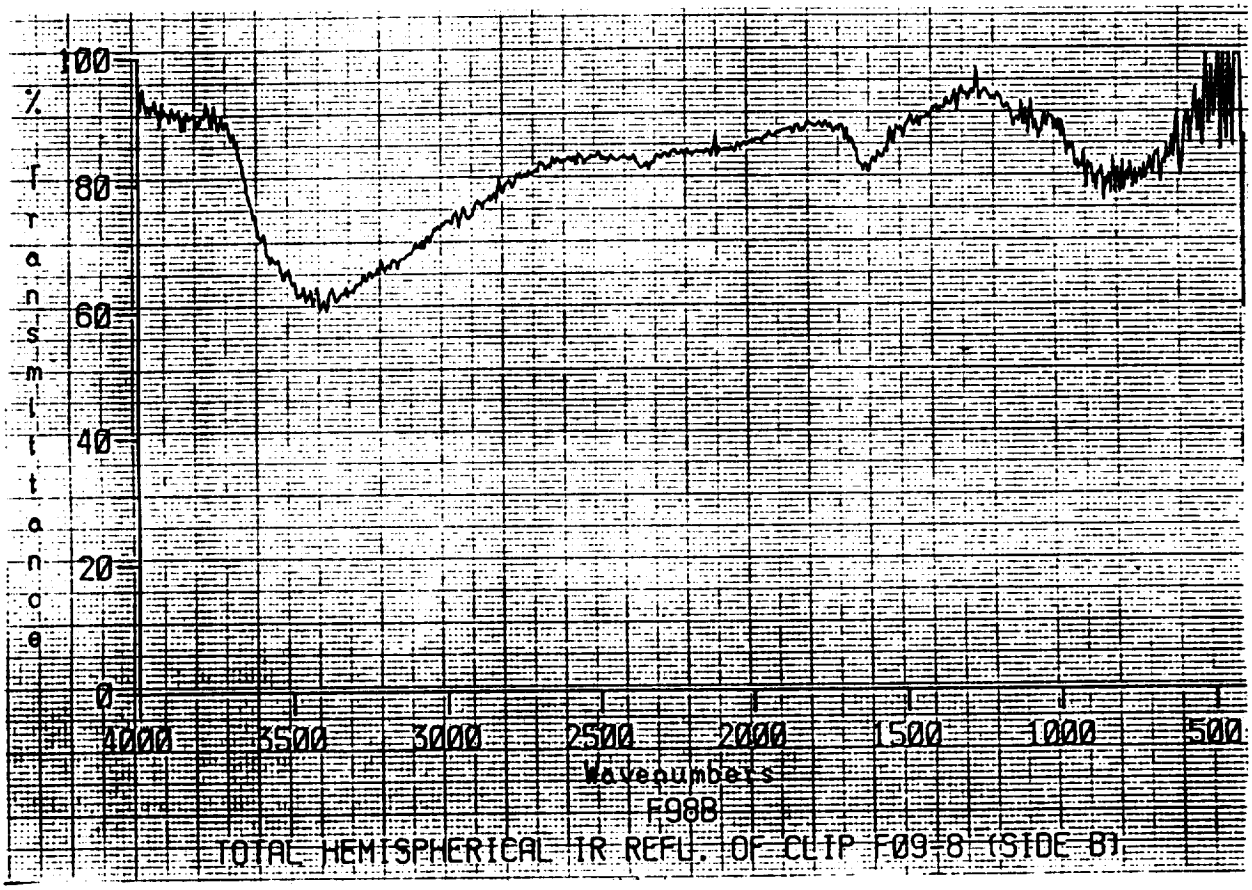

Figure A94: Total Hemispherical IR Reflectance of clip F09-8, (A) Front (B)Back.

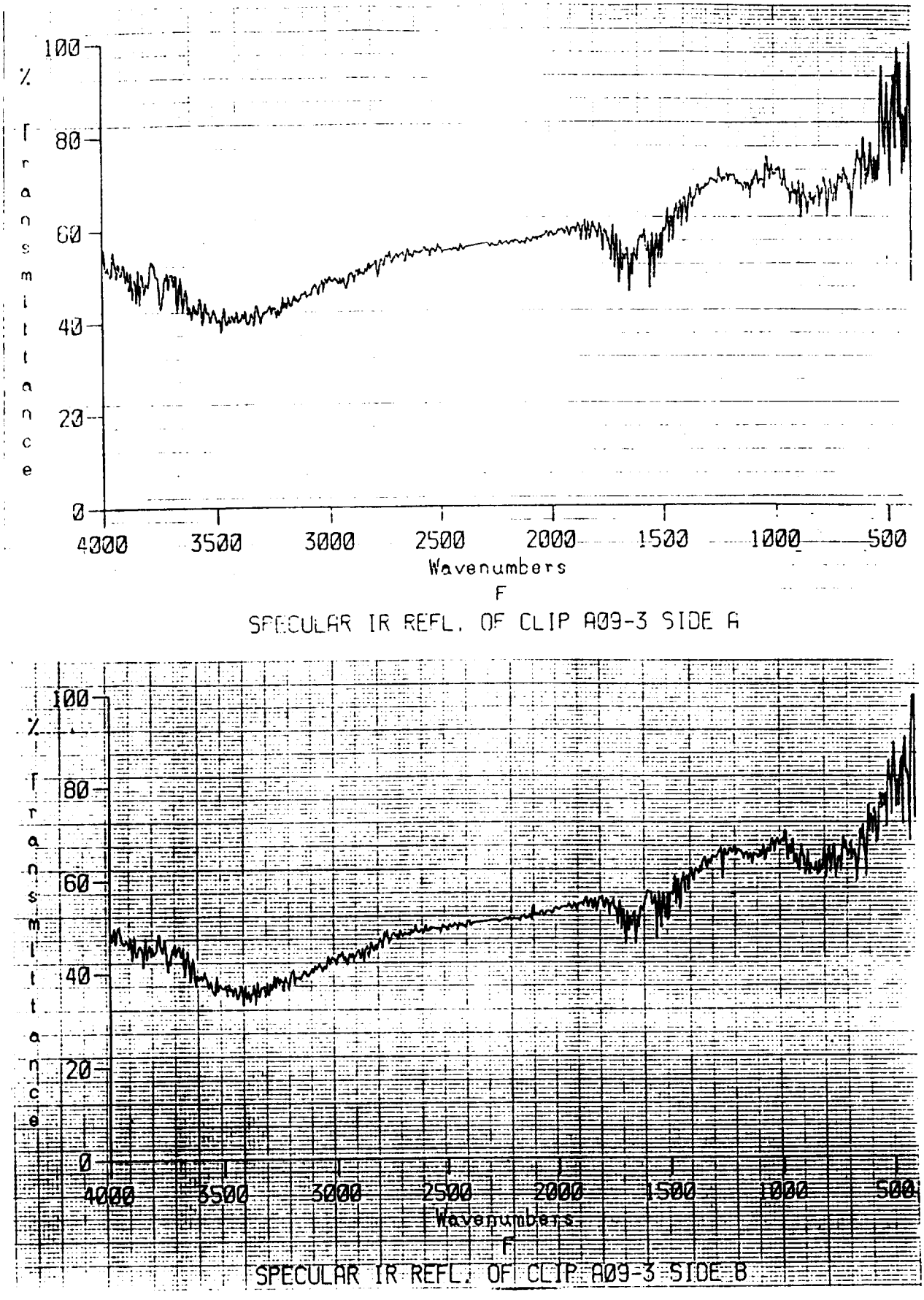

Figure A95: Specular IR Reflectance of clip A09-3, (A) Front (B) Back.

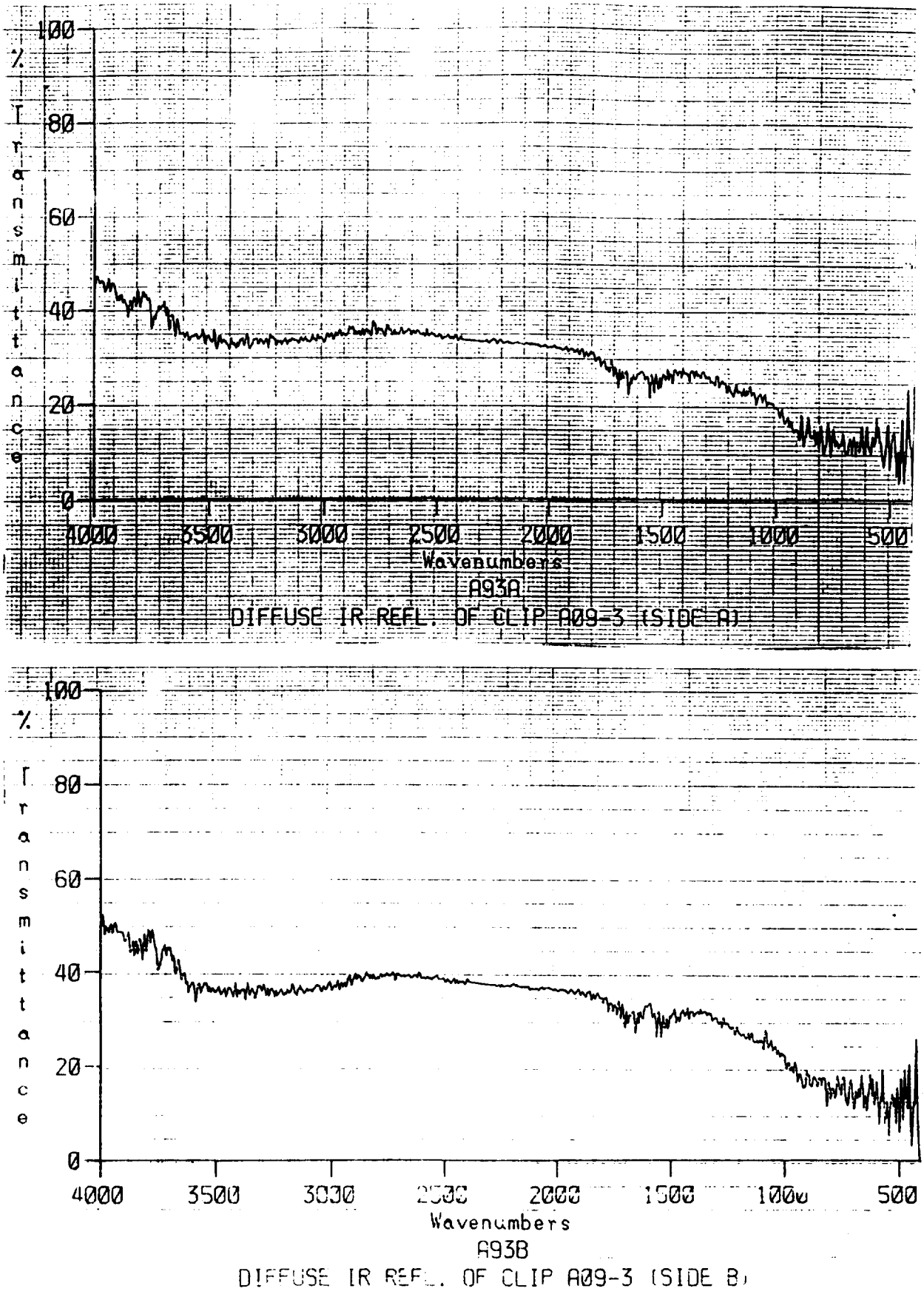

Figure A96: Diffuse IR Reflectance of A09-3, (A) Front (B) Back.

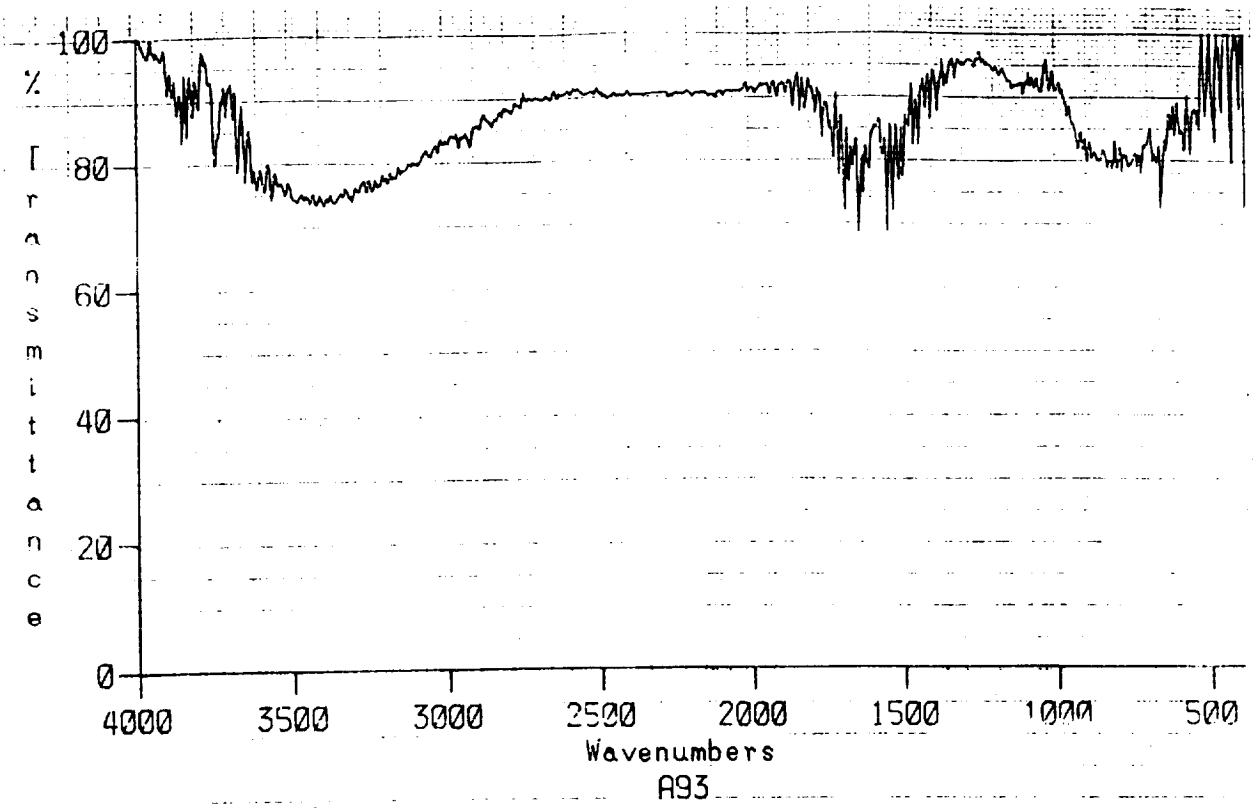

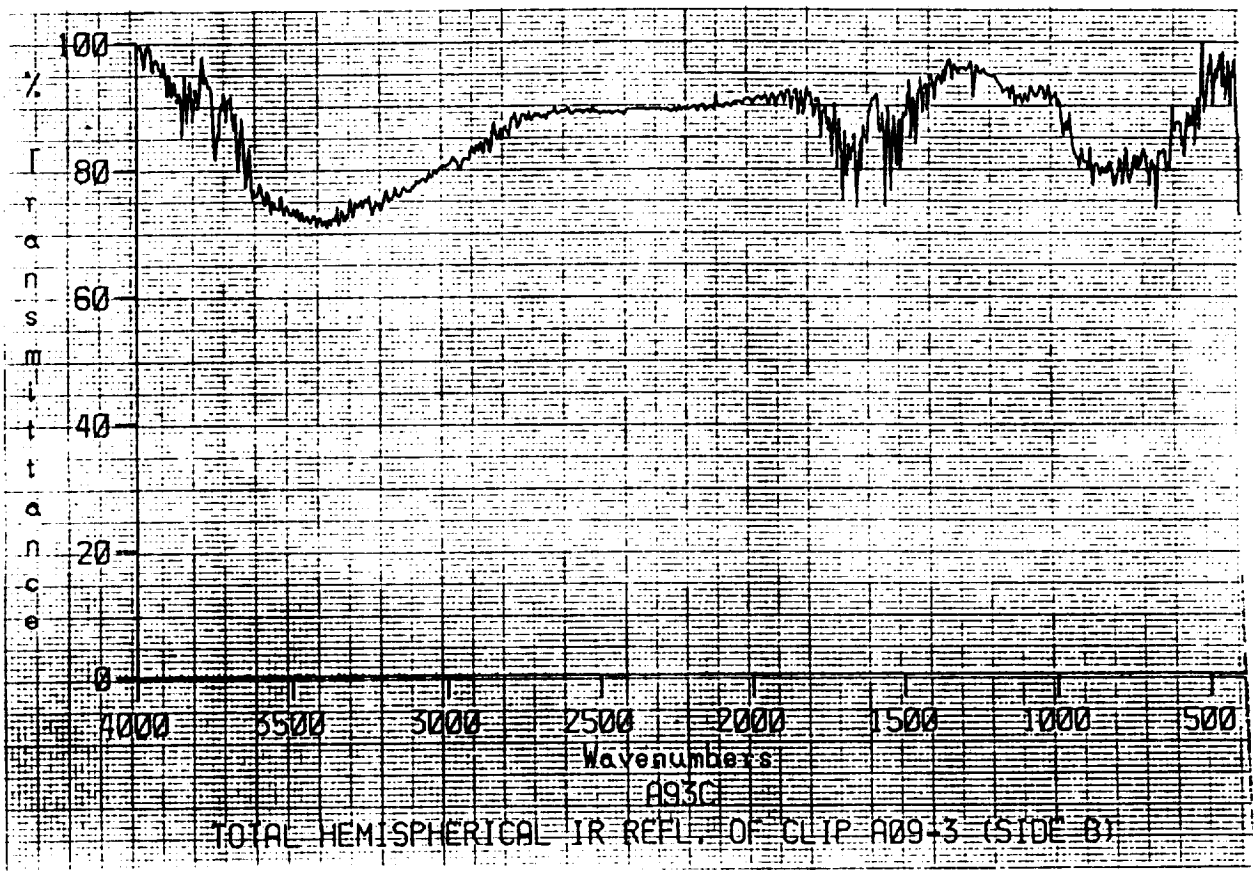

Figure A97: Total Hemispherical IR Reflectance of clip A09-3, (A) Front (B) Back.

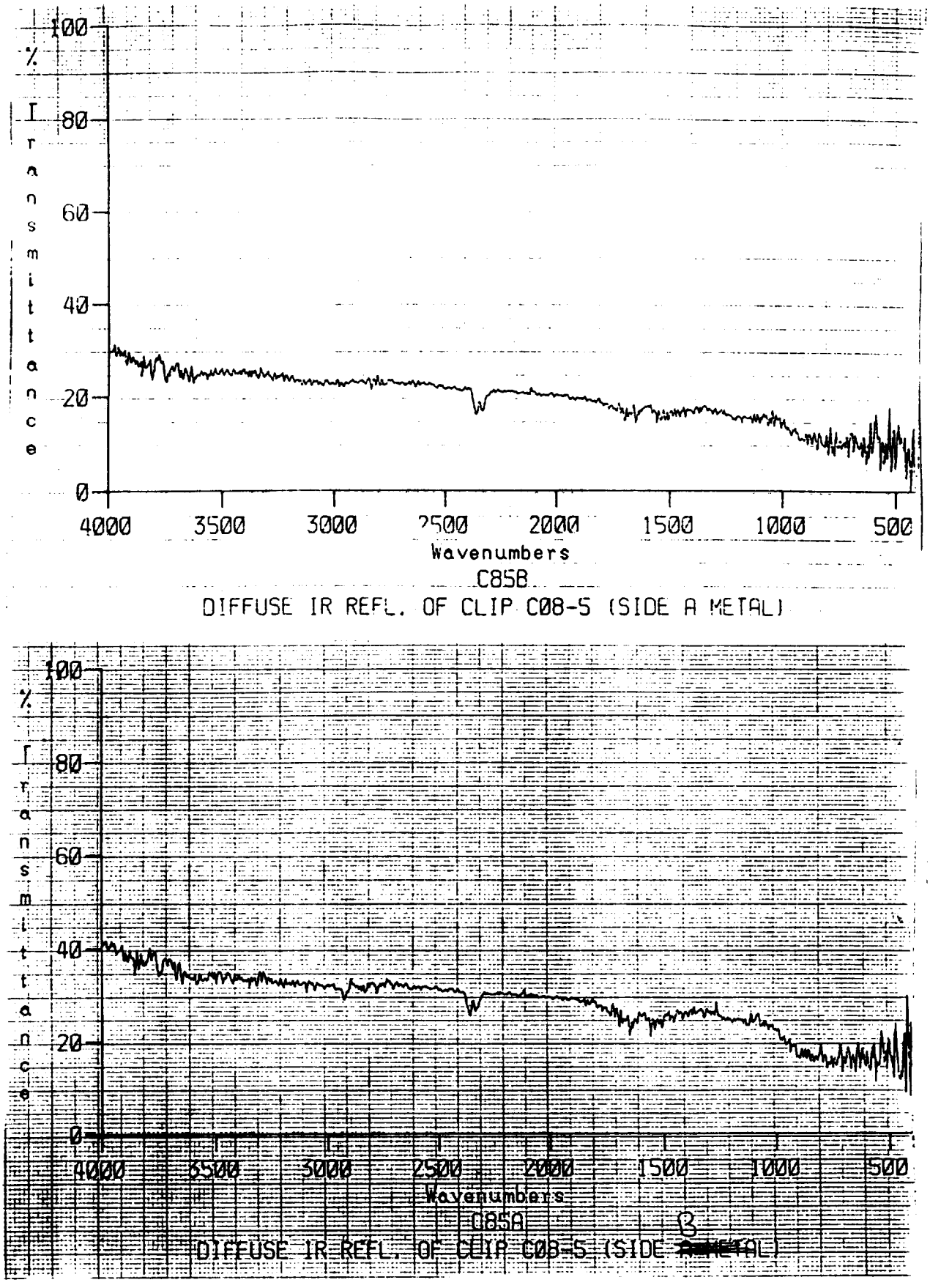

Figure A98: Diffuse IR Reflectance of clip C08-5, (A) Front (B) Back.

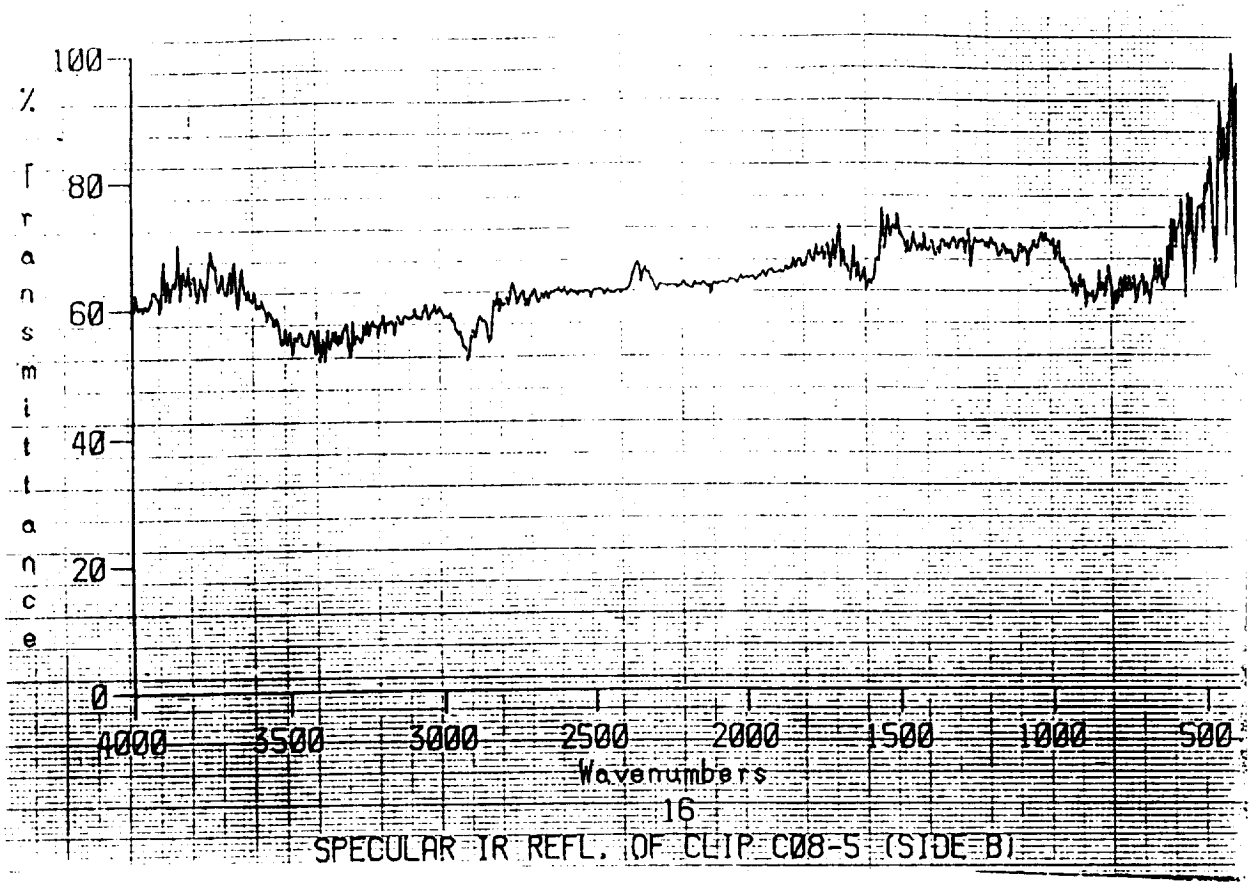

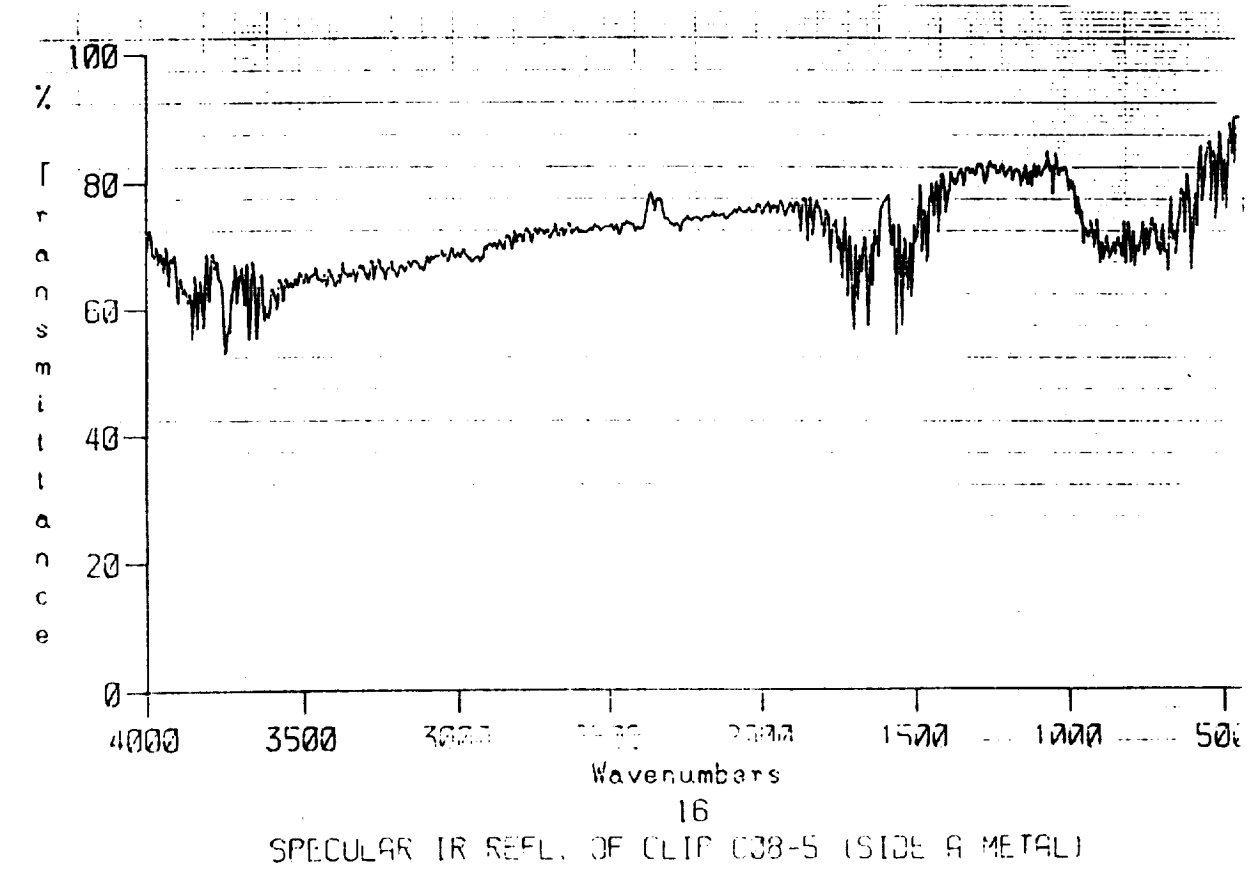

Figure A99: Specular IR Reflectance of clip C08-5, (A) Front (B) Back.

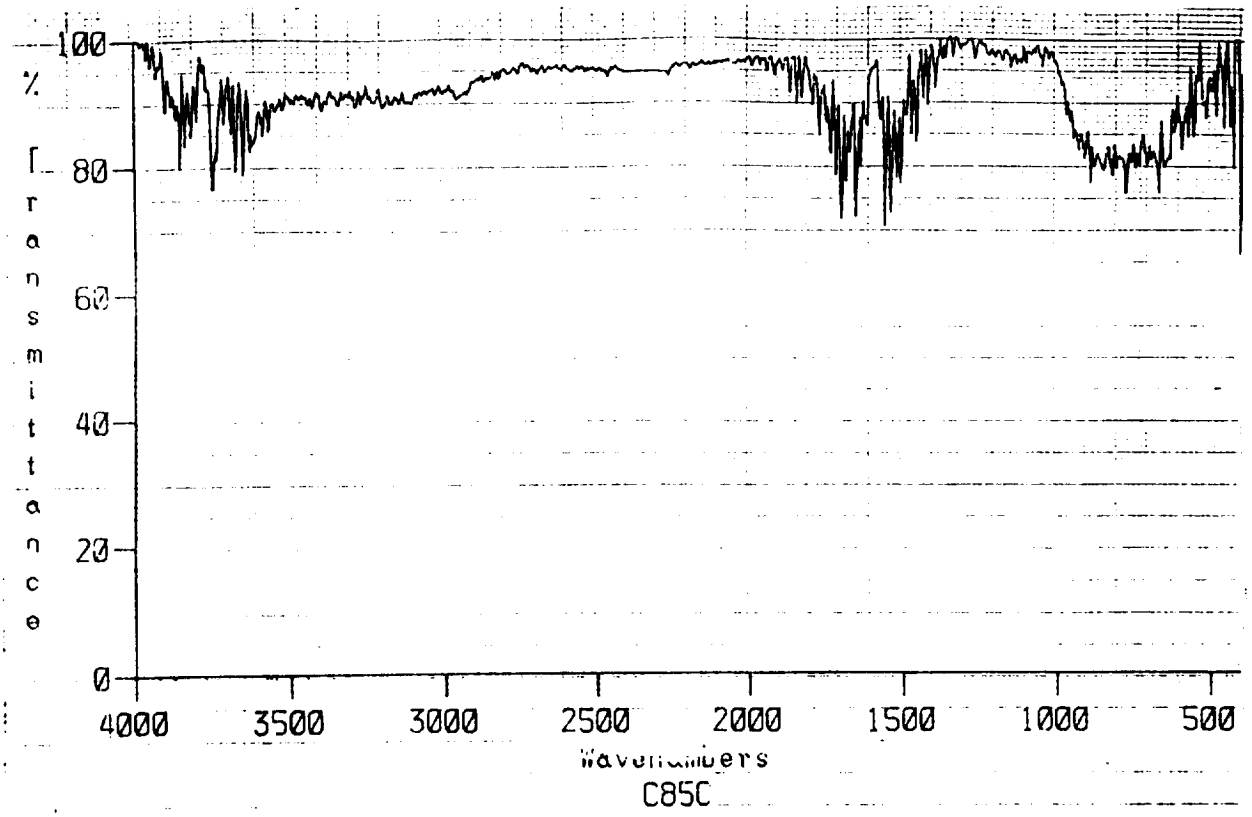

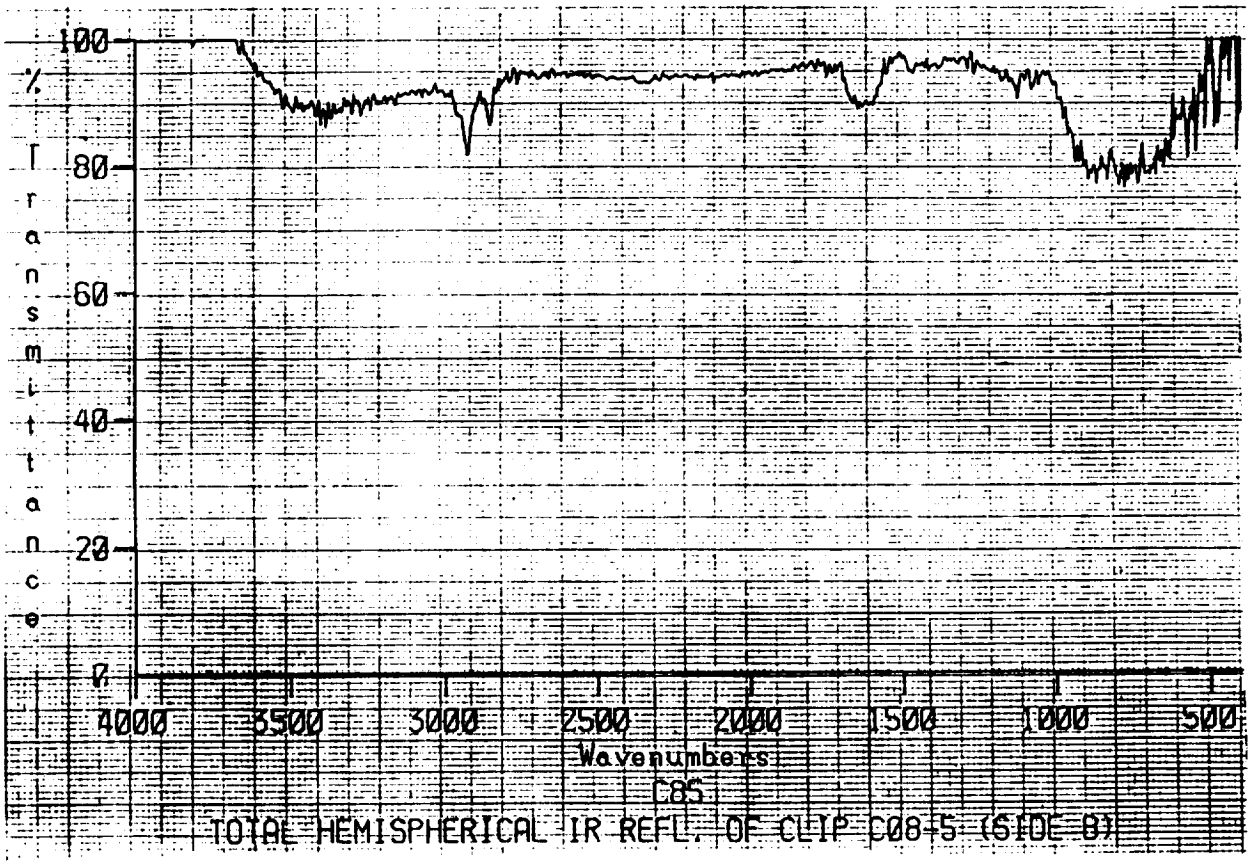

Figure A100: **Total Hemispherical IR Reflectance of clip C08-5, (A) Front (B) Back.**

TRAILING EDGE

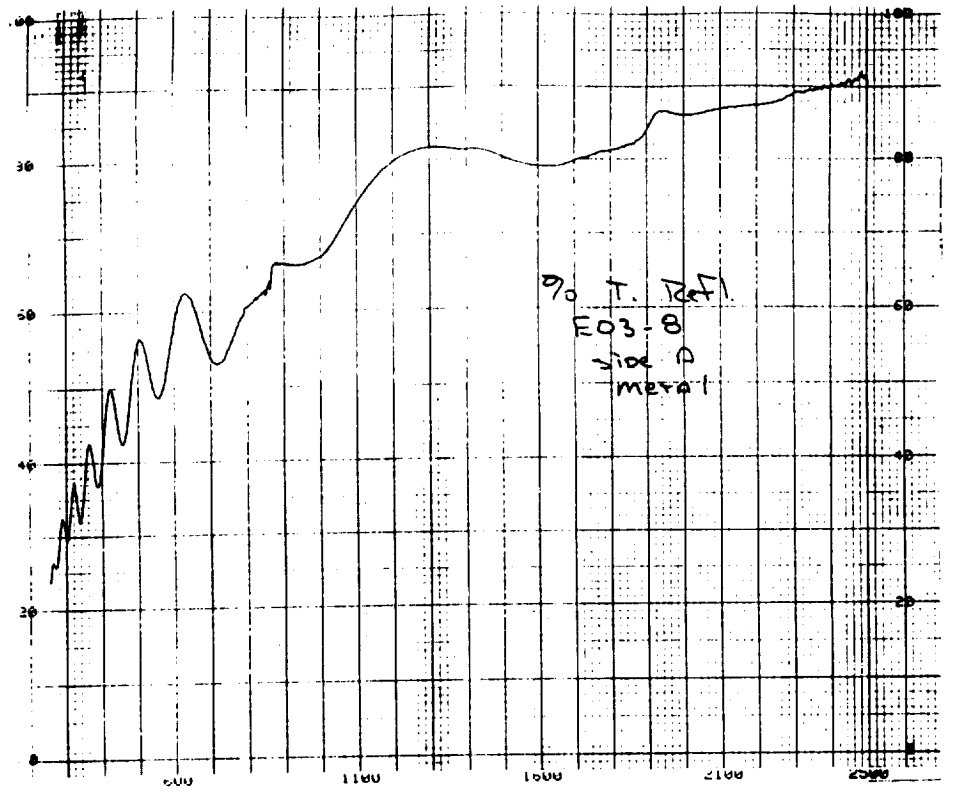

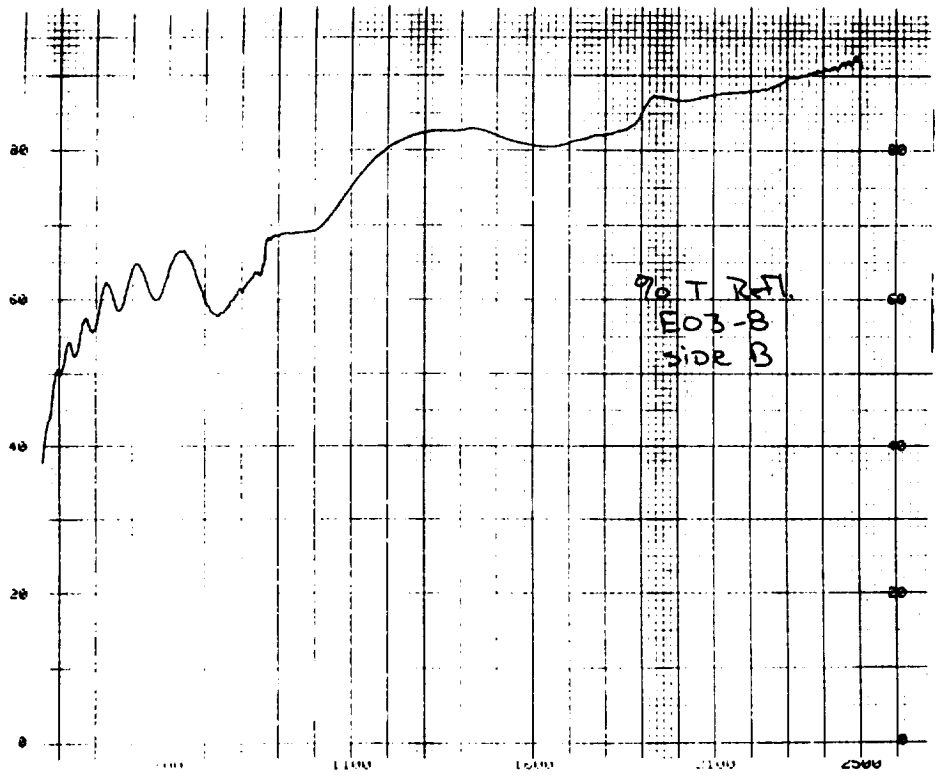

Figure A101: **UV-Vis/NIR Total Reflectance of clip E03-8, (A) Front (B) Back.**

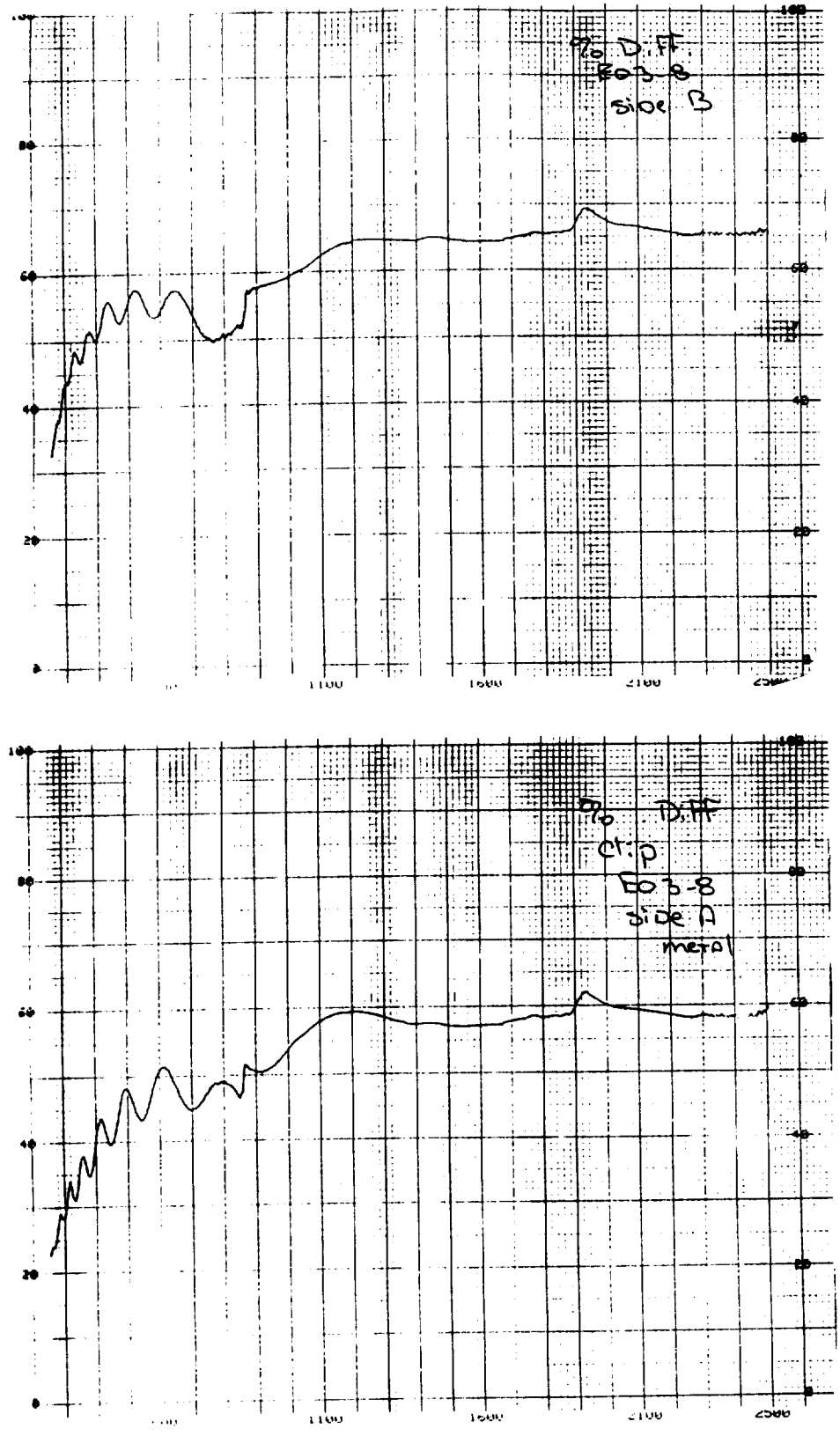

Figure A102: UV-Vis/NIR Diffuse Reflectance of clip E03-8, (A) Front (B) Back.

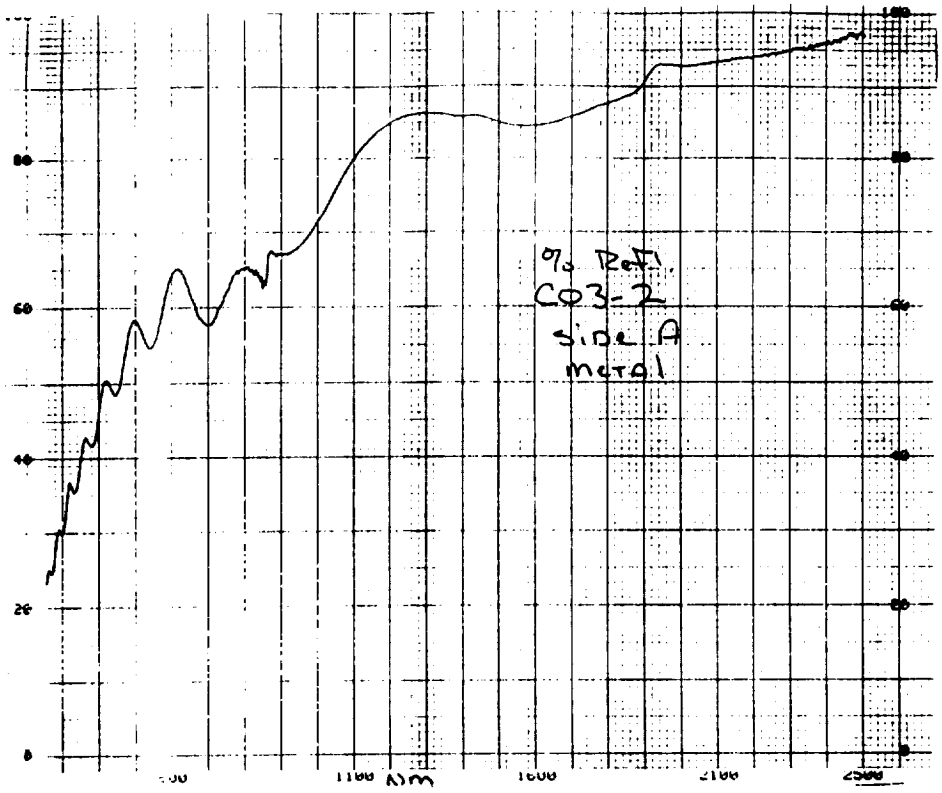

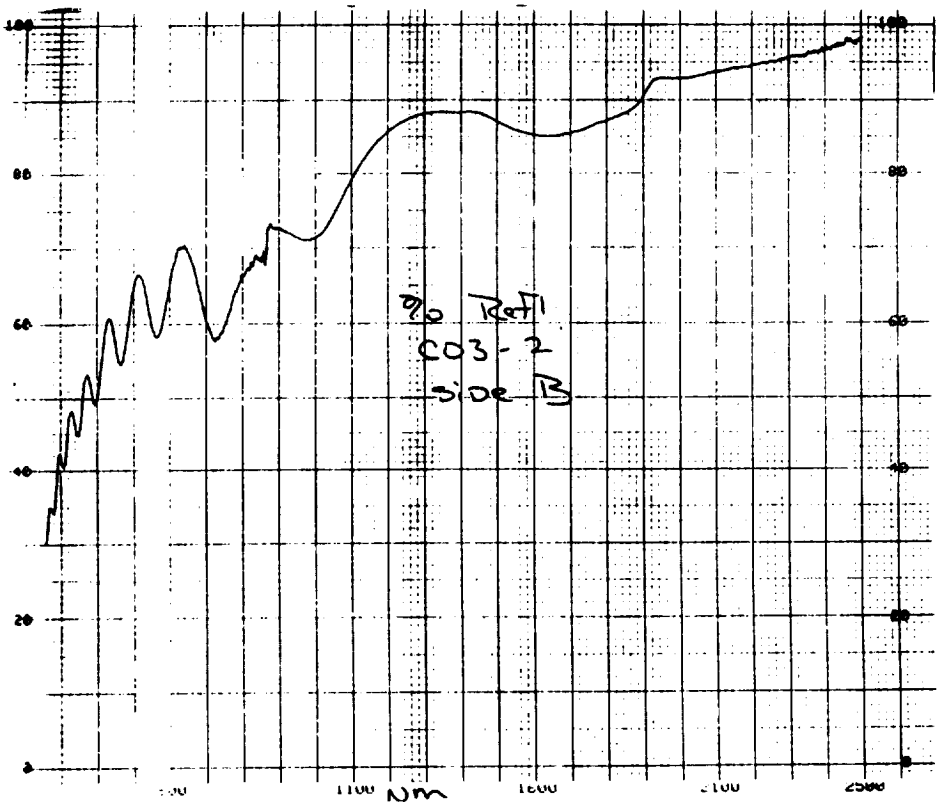

Figure A103: **UV-Vis/NIR Total Refectance of clamp C03-2, (A) Front (B) Back.**

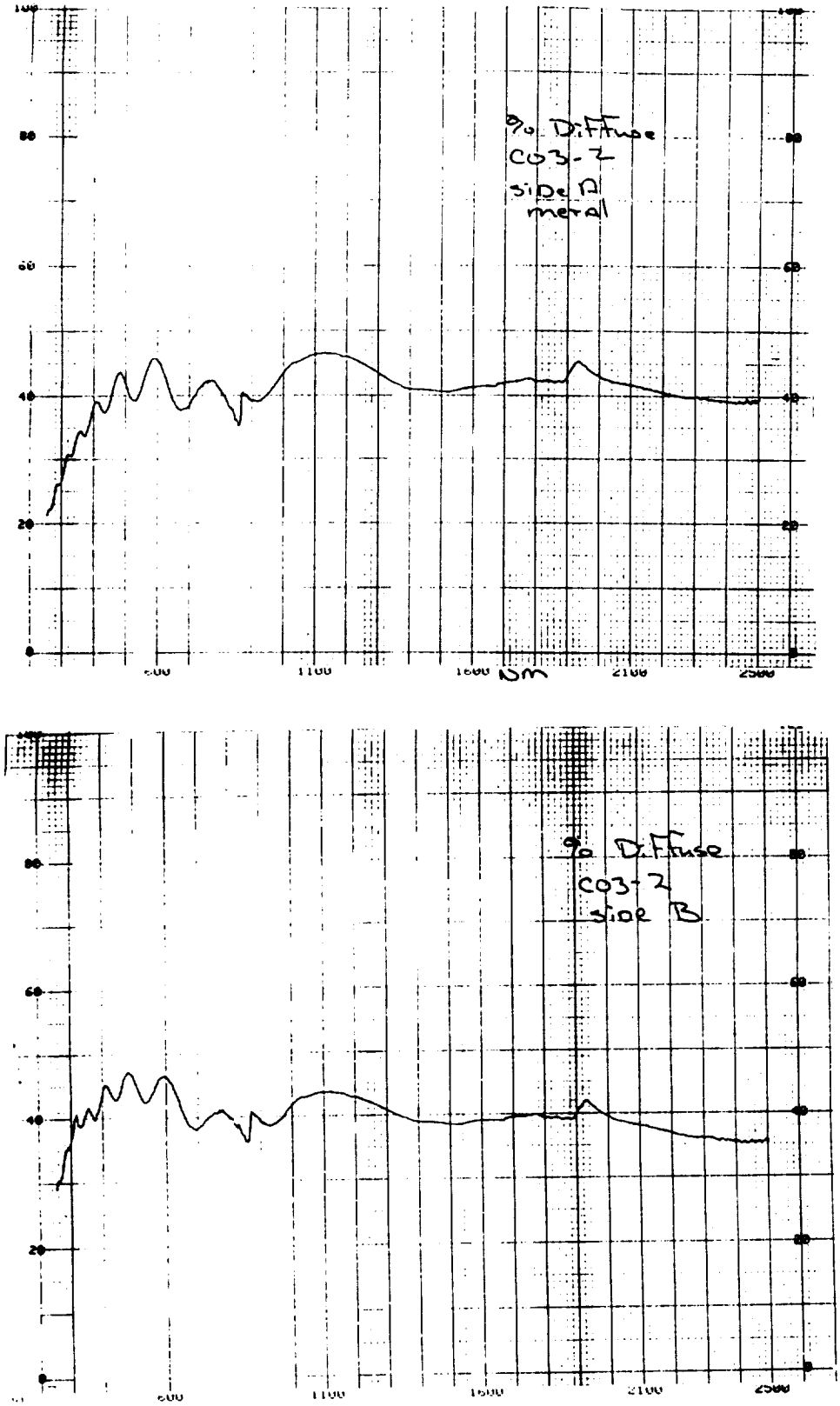

Figure A104: UV-Vis/NIR Diffuse Reflectance of clamp C03-2, (A) Front (B) Back.

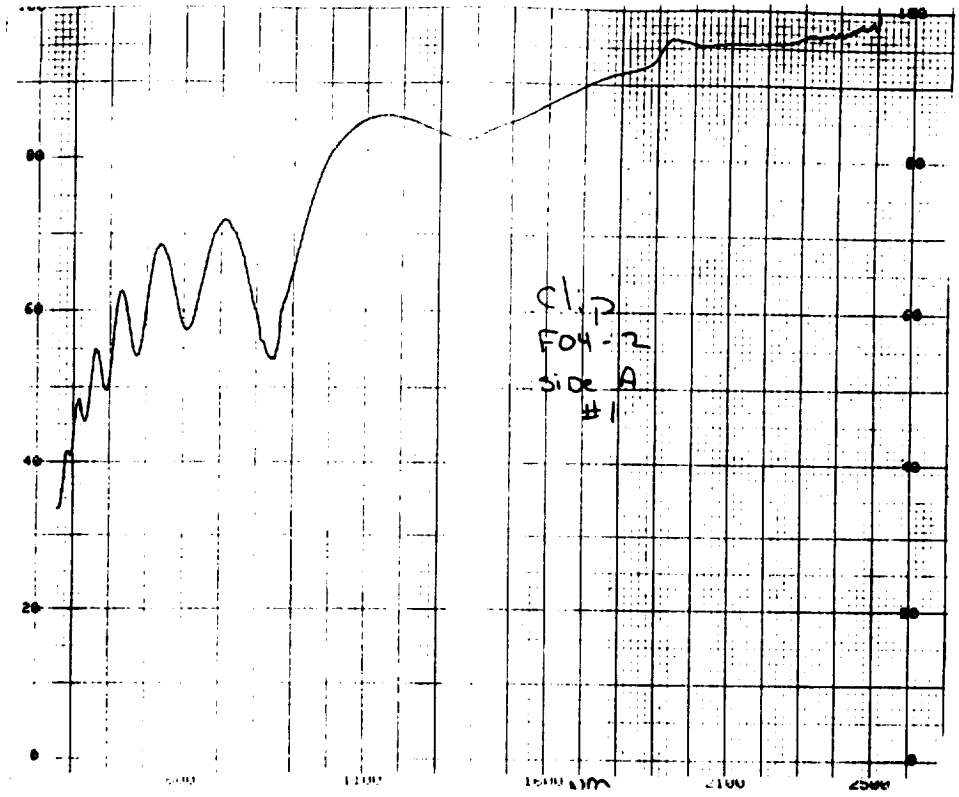

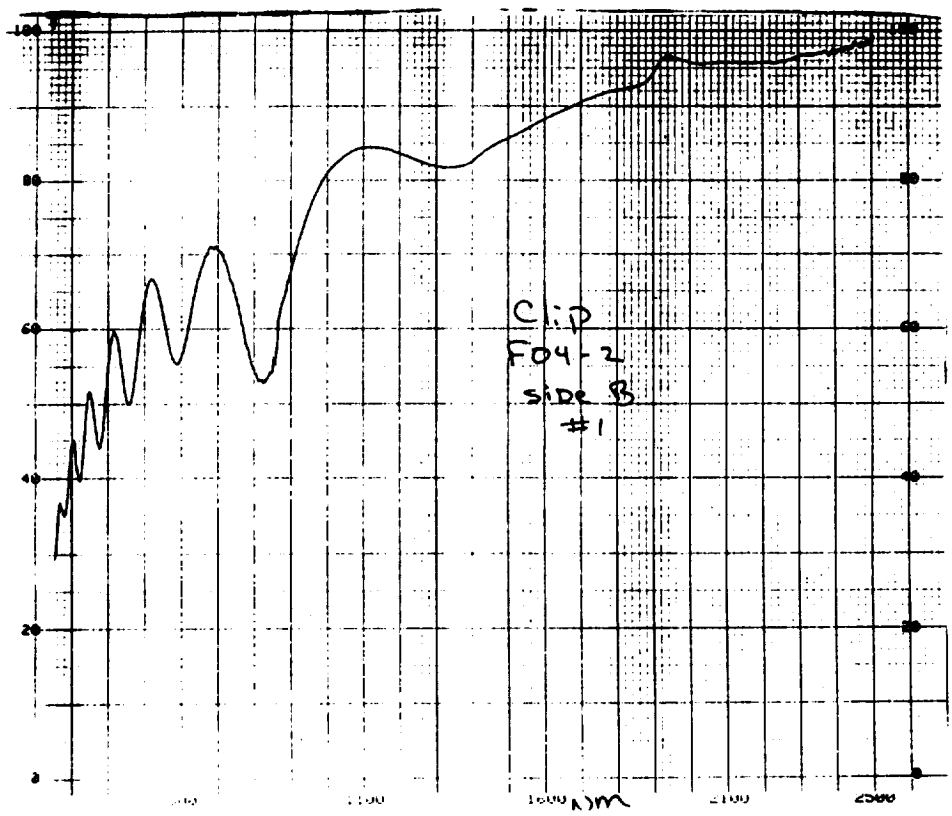

Figure A105: **UV-Vis/NIR Total Reflectance of clip F04-2, (A) Front (B) Back.**

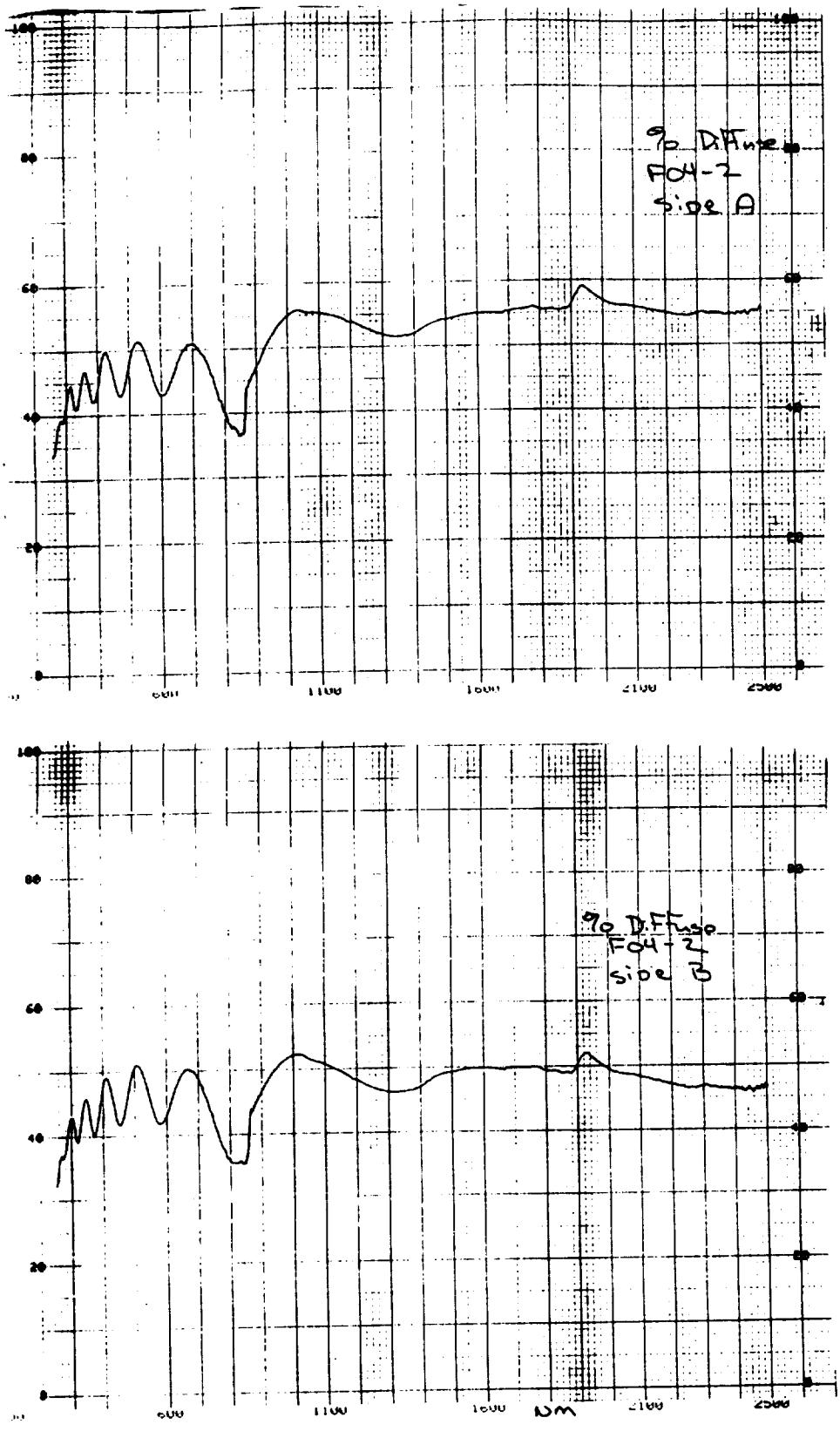

Figure A106: UV-Vis/NIR Diffuse Reflectance of clip F04-2, (A) Front (B) Back.

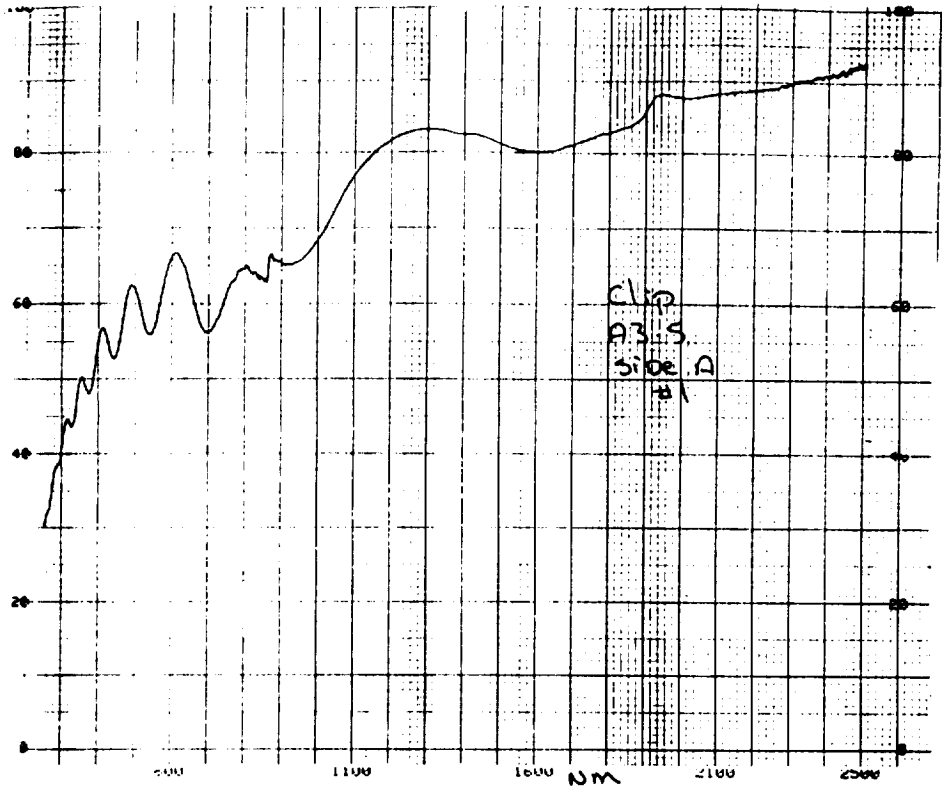

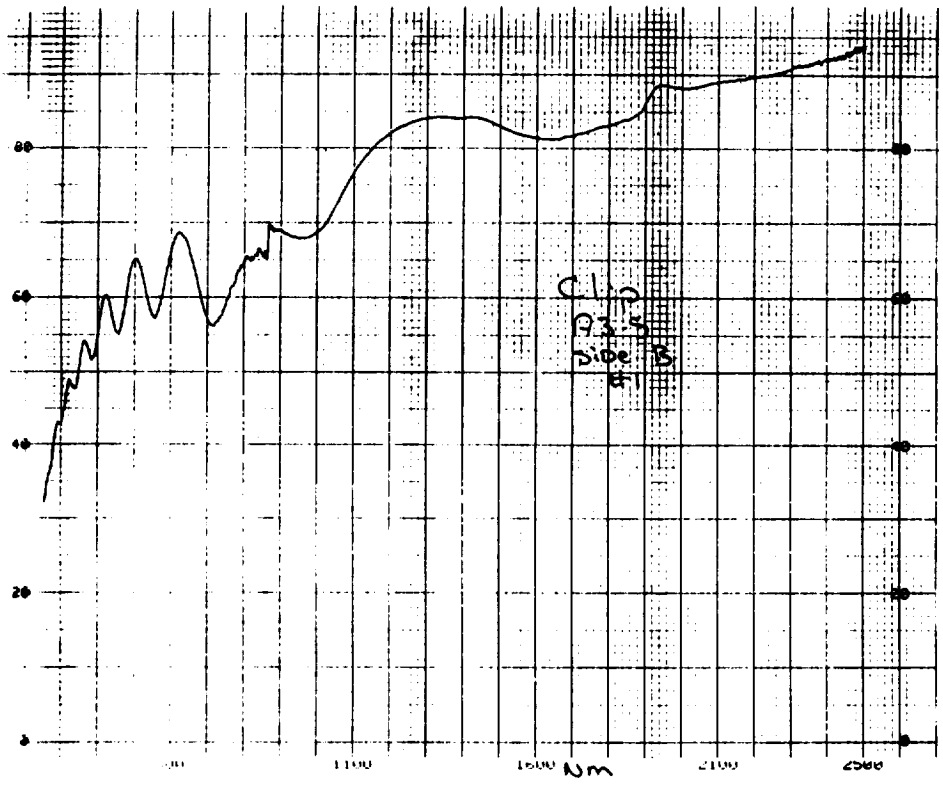

Figure A107: **UV-Vis/NIR Total Reflectance of clip A3-5, (A) Front (B) Back.**

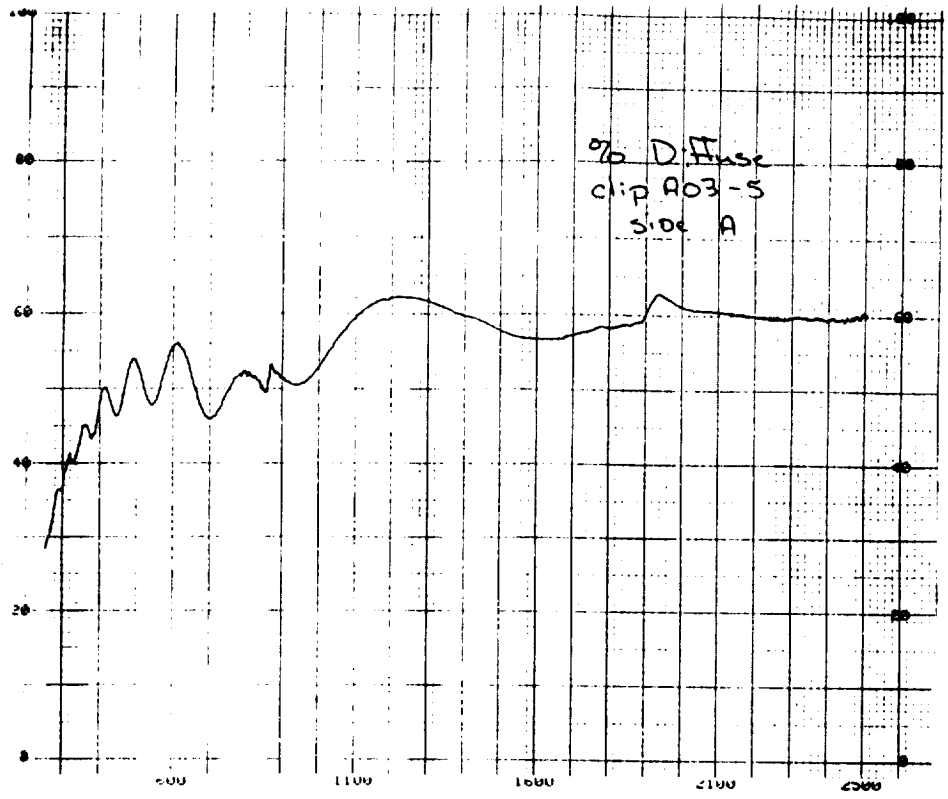

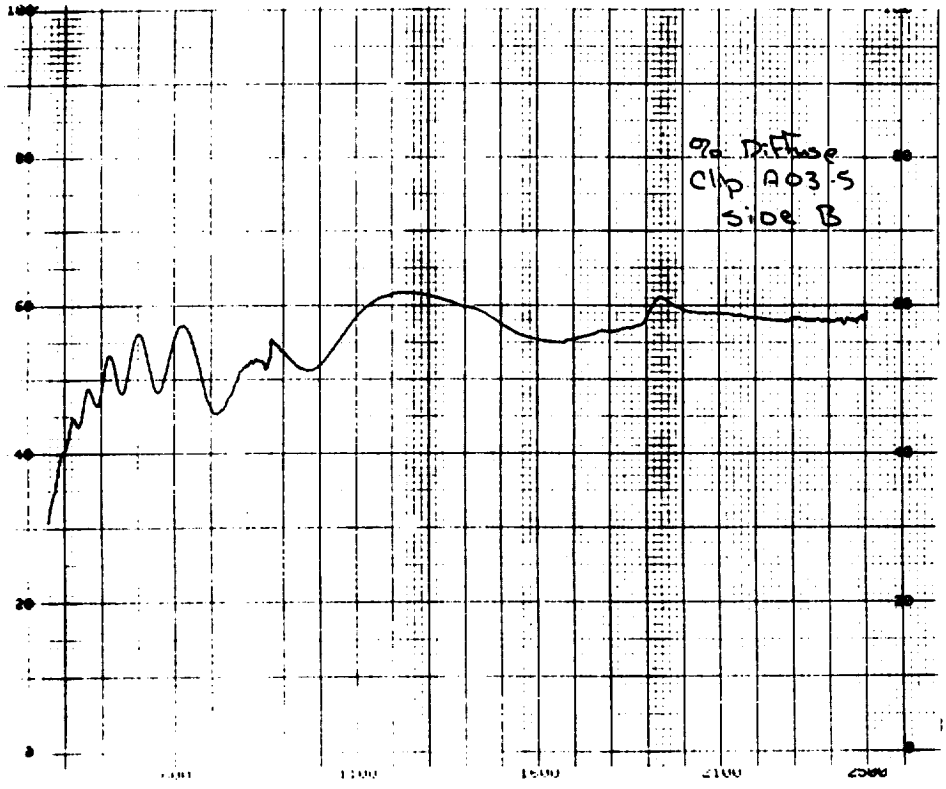

Figure A108: **UV-Vis/NIR Diffuse Reflectance of clip A03-5, (A) Front (B) Back.**

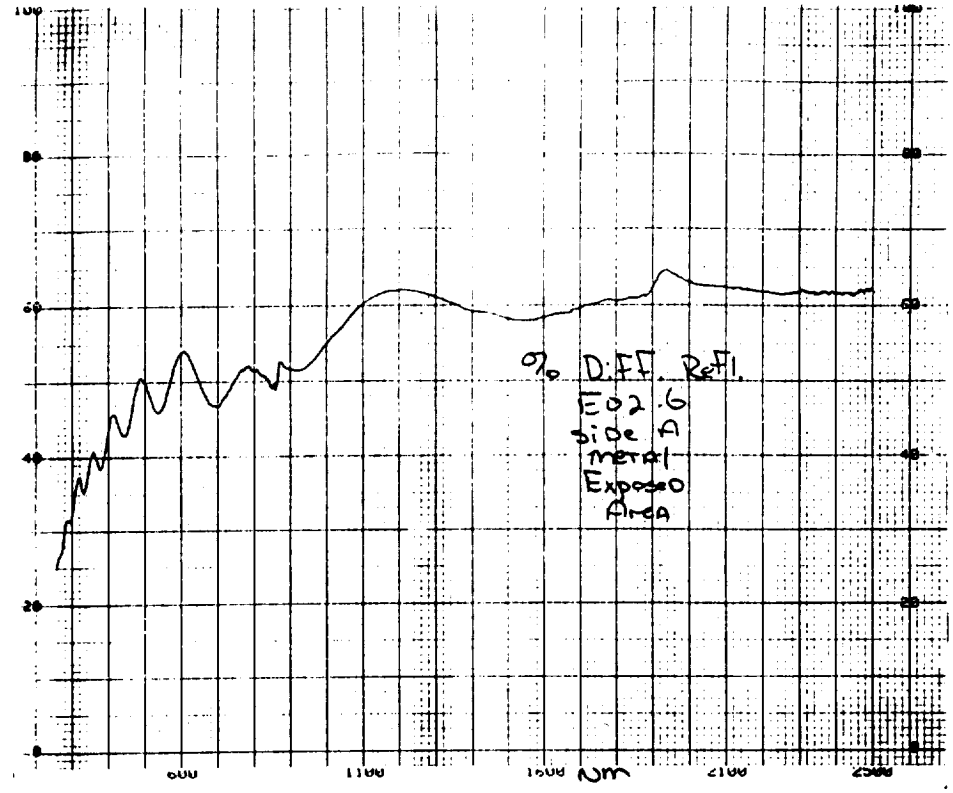

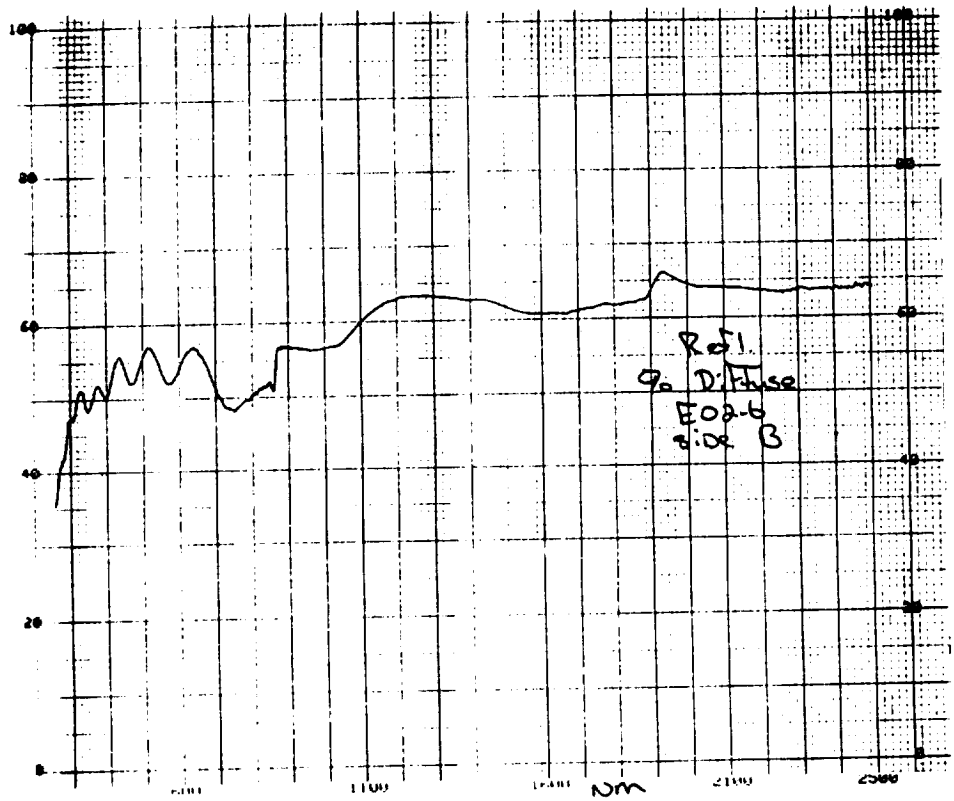

Figure A109: **UV-Vis/NIR Diffuse Reflectance of clamp E02-6, (A) Front (B) Back.**

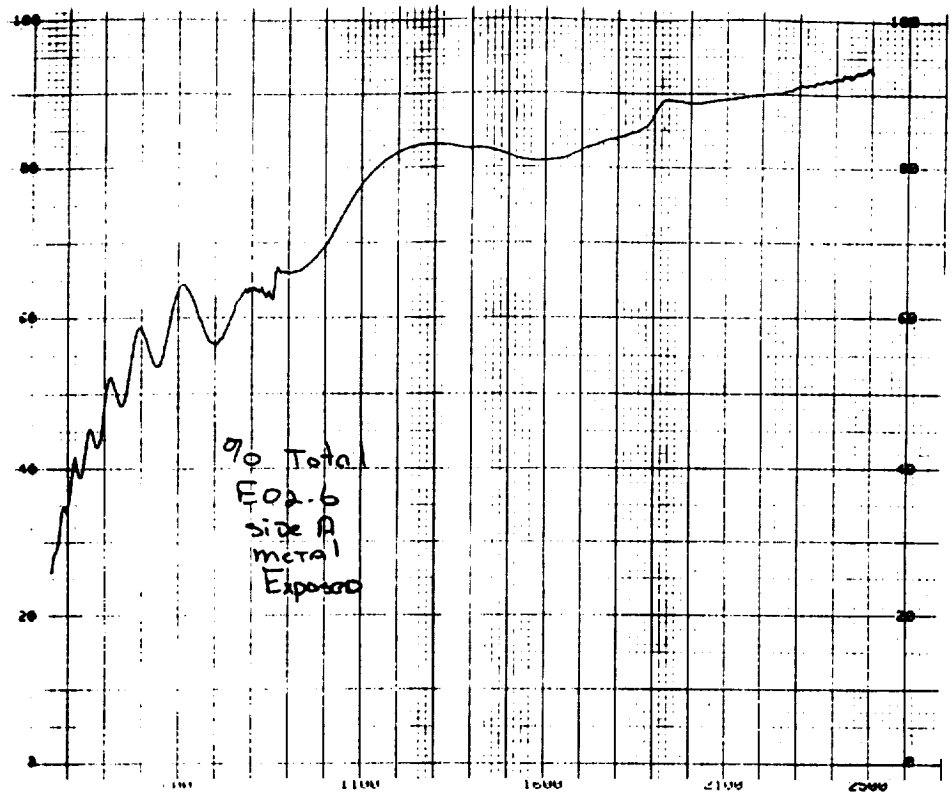

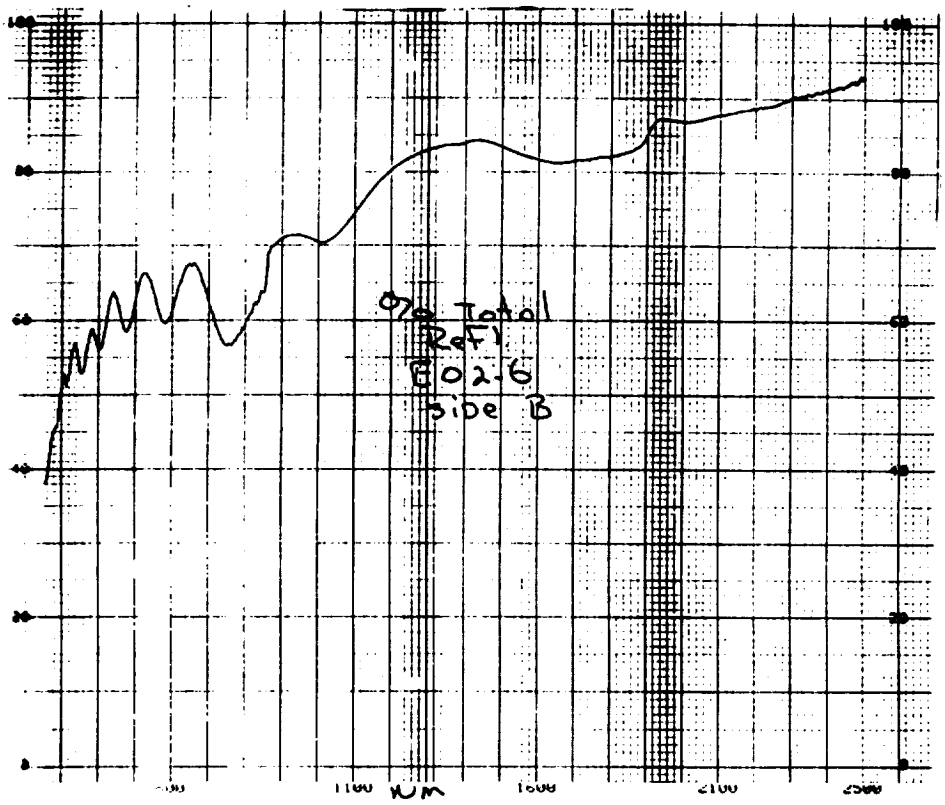

Figure A110: **UV-Vis/NIR Total Reflectance of clamp E02-6, (A) Front (B) Back.**

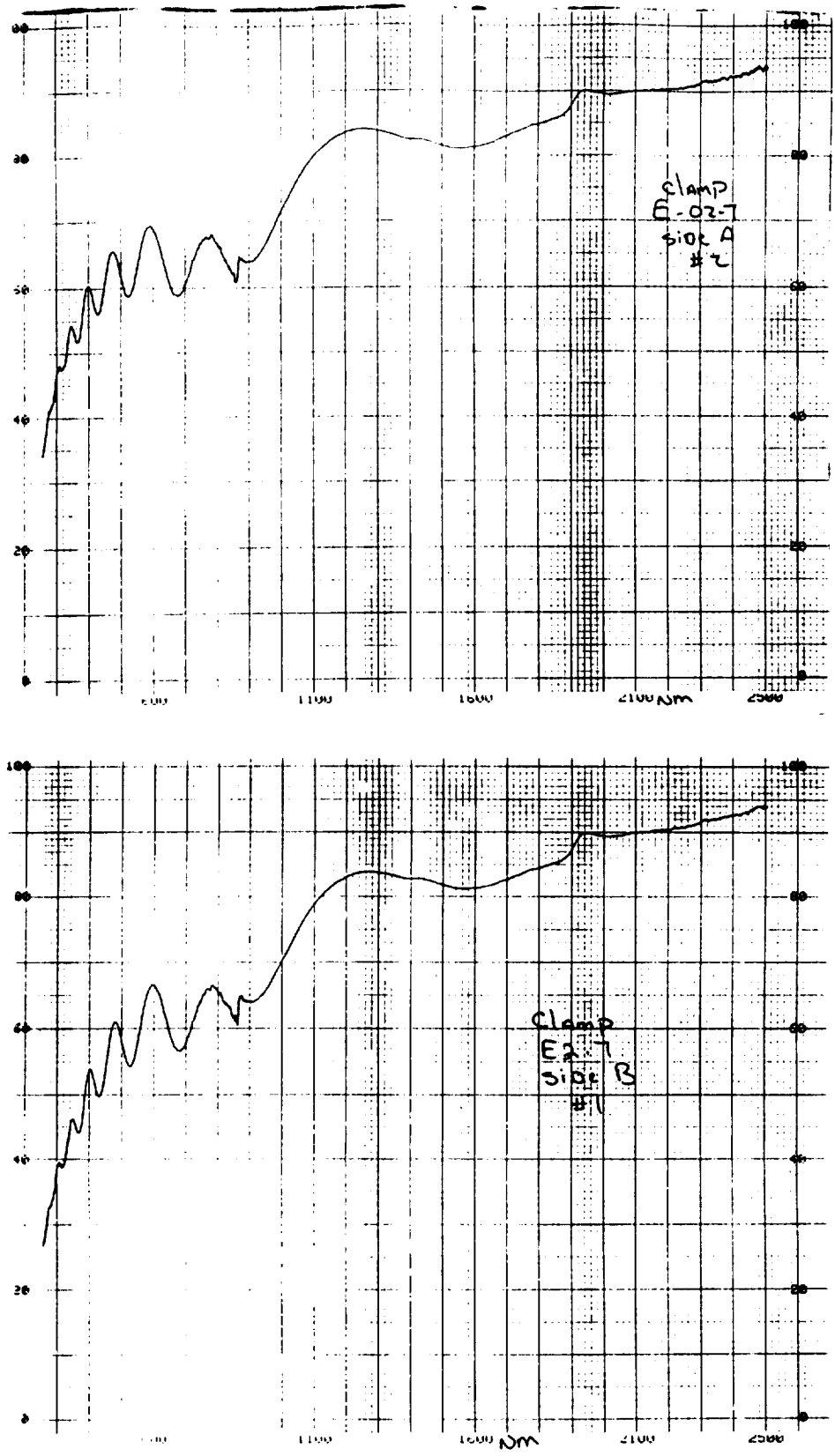

Figure A111: **UV-Vis/NIR Total Reflectance of clamp E02-7, (A) Front (B) Back.**

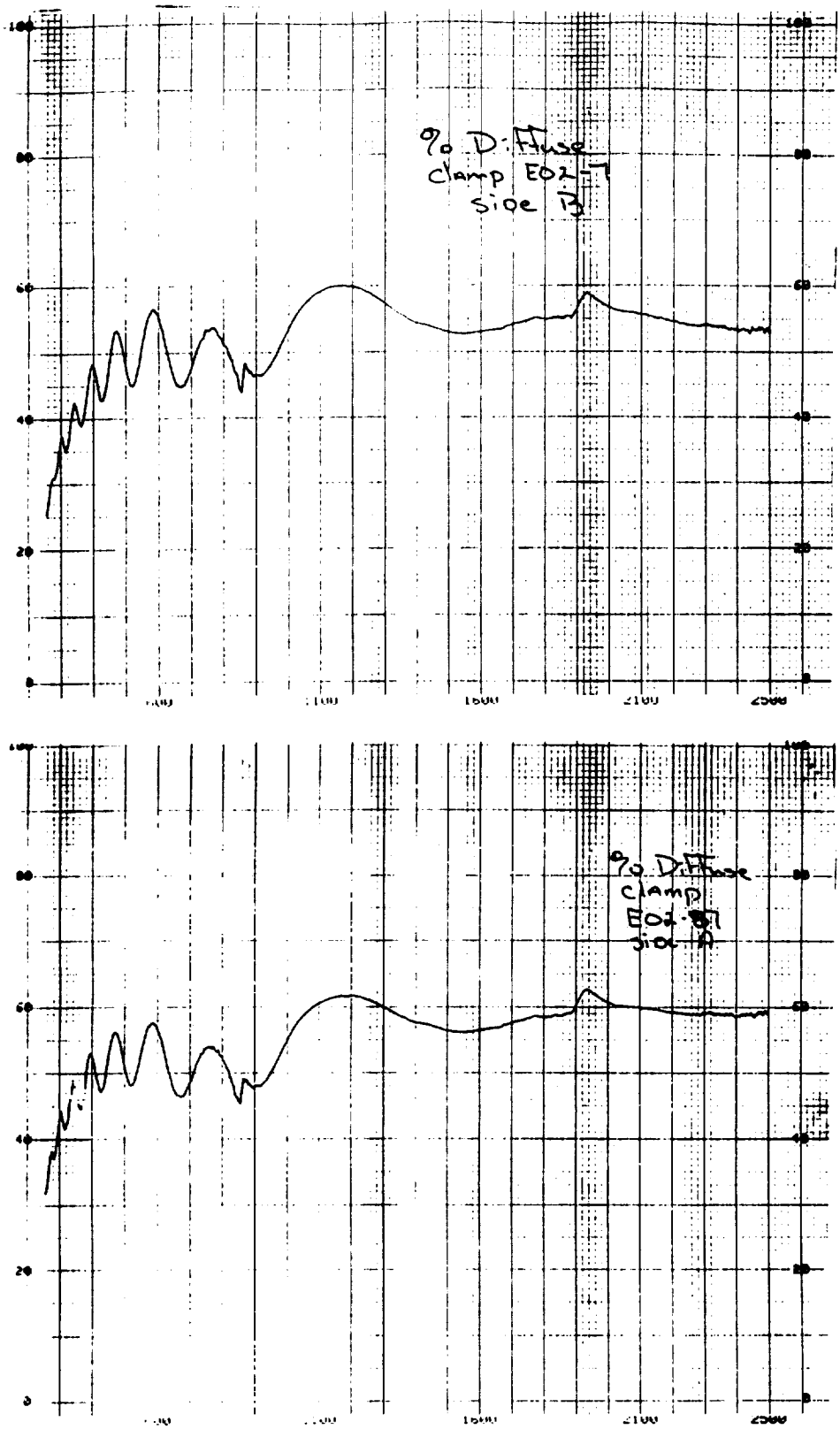

Figure A112: **UV-Vis/NIR Diffuse Reflectance of Clamp E02-7, (A) Front (B) Back.**

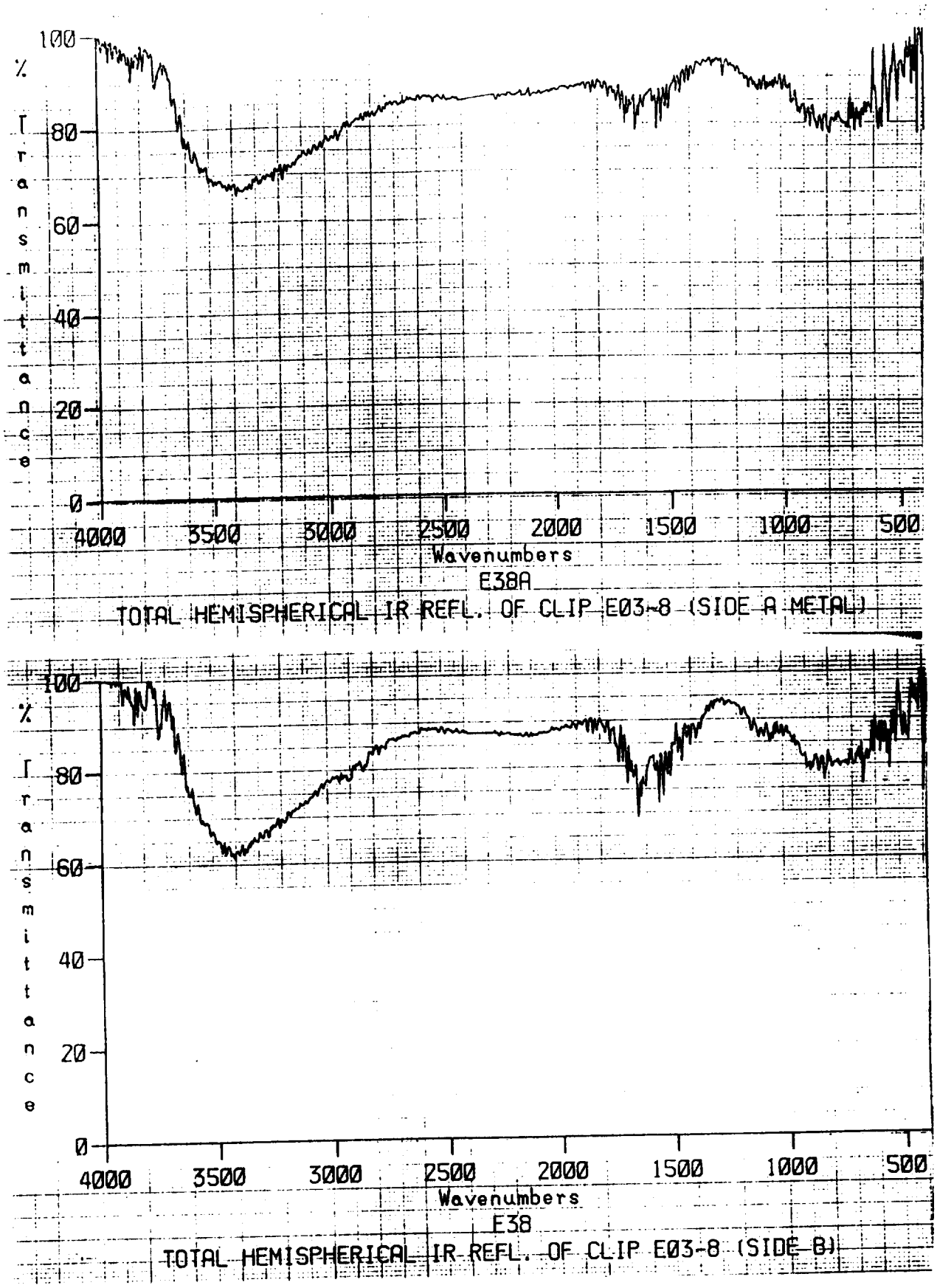

Figure A113: **Total Hemispherical IR Reflectance of clip E03-8, (A) Front (B) Back.**

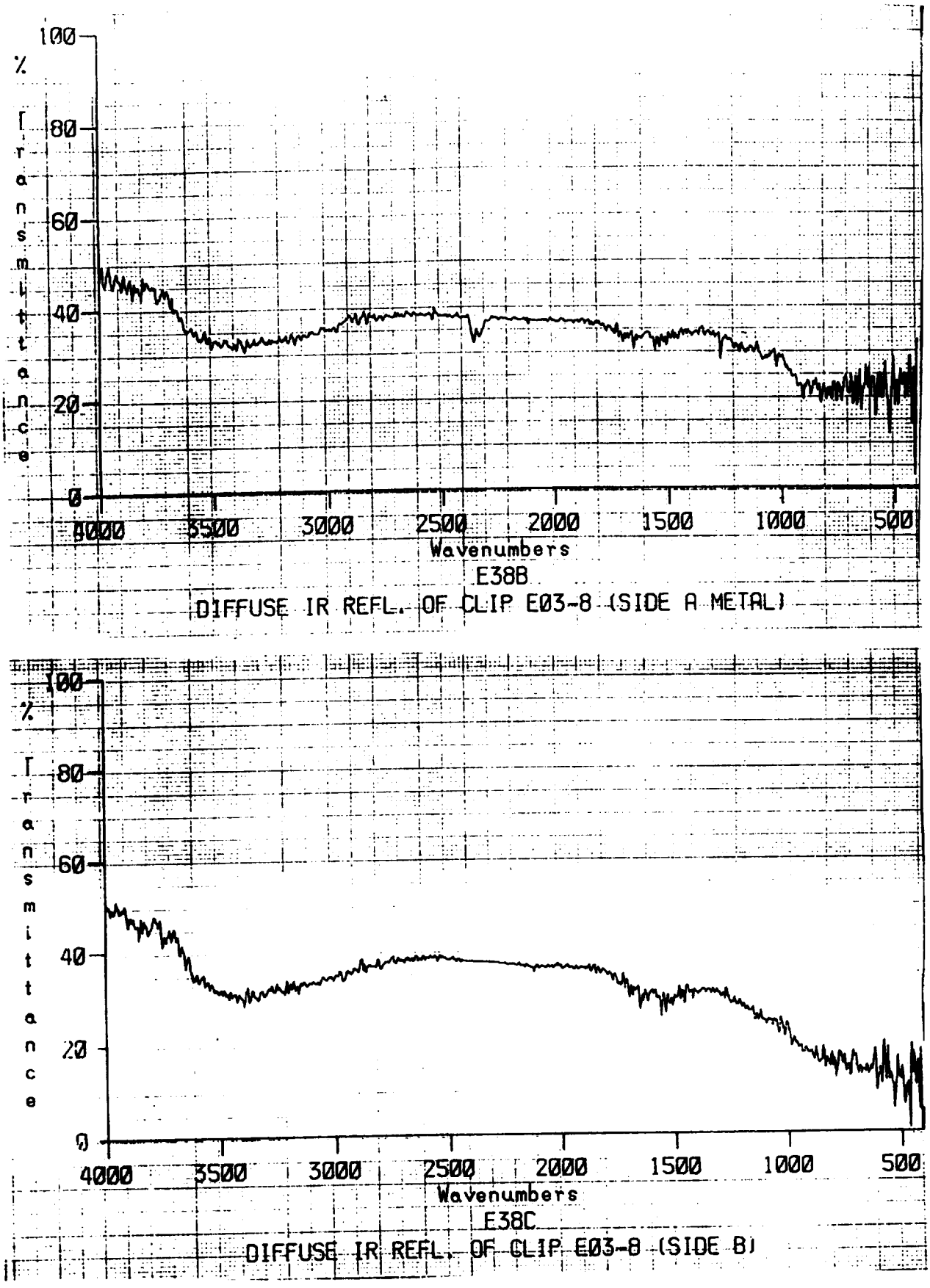

Figure A114: **Diffuse IR Reflectance of clip E03-8, (A) Front (B) Back.**

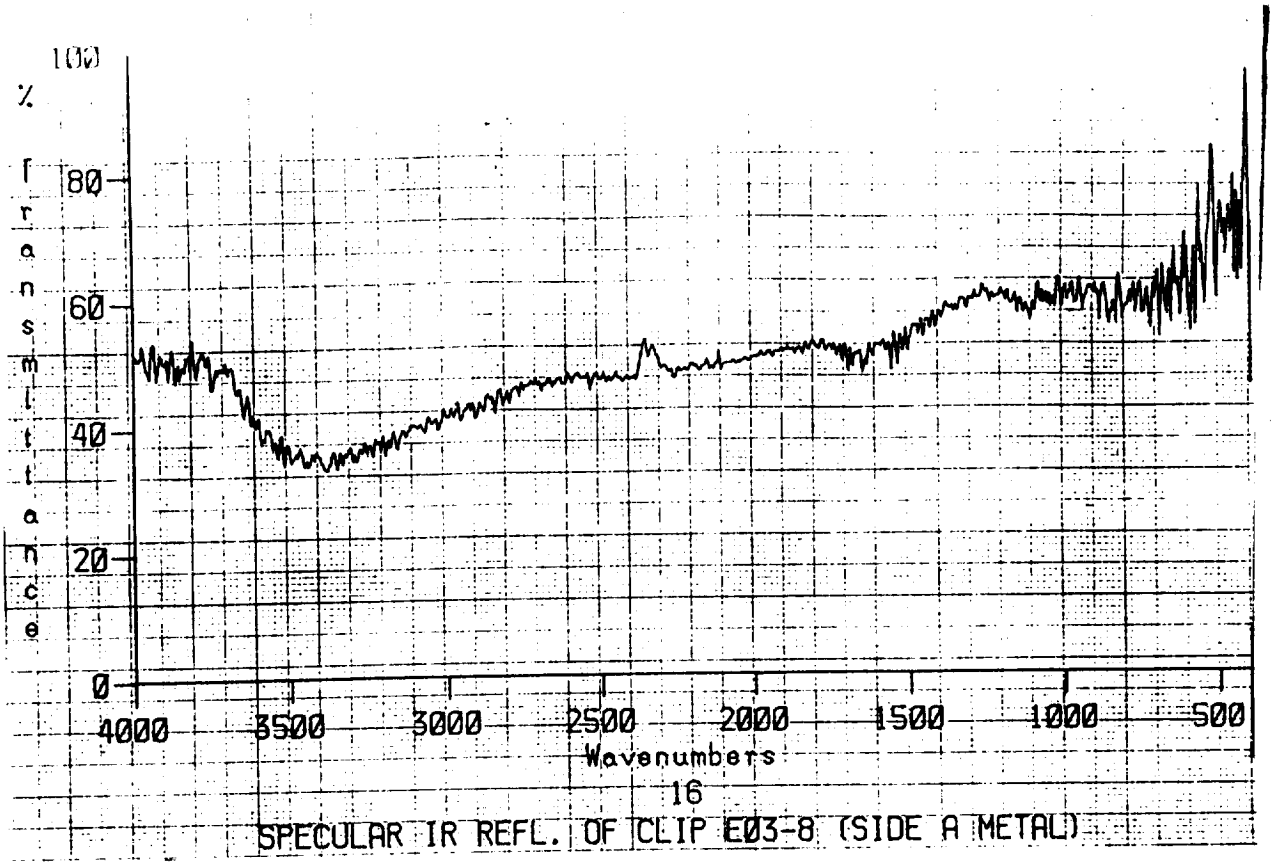

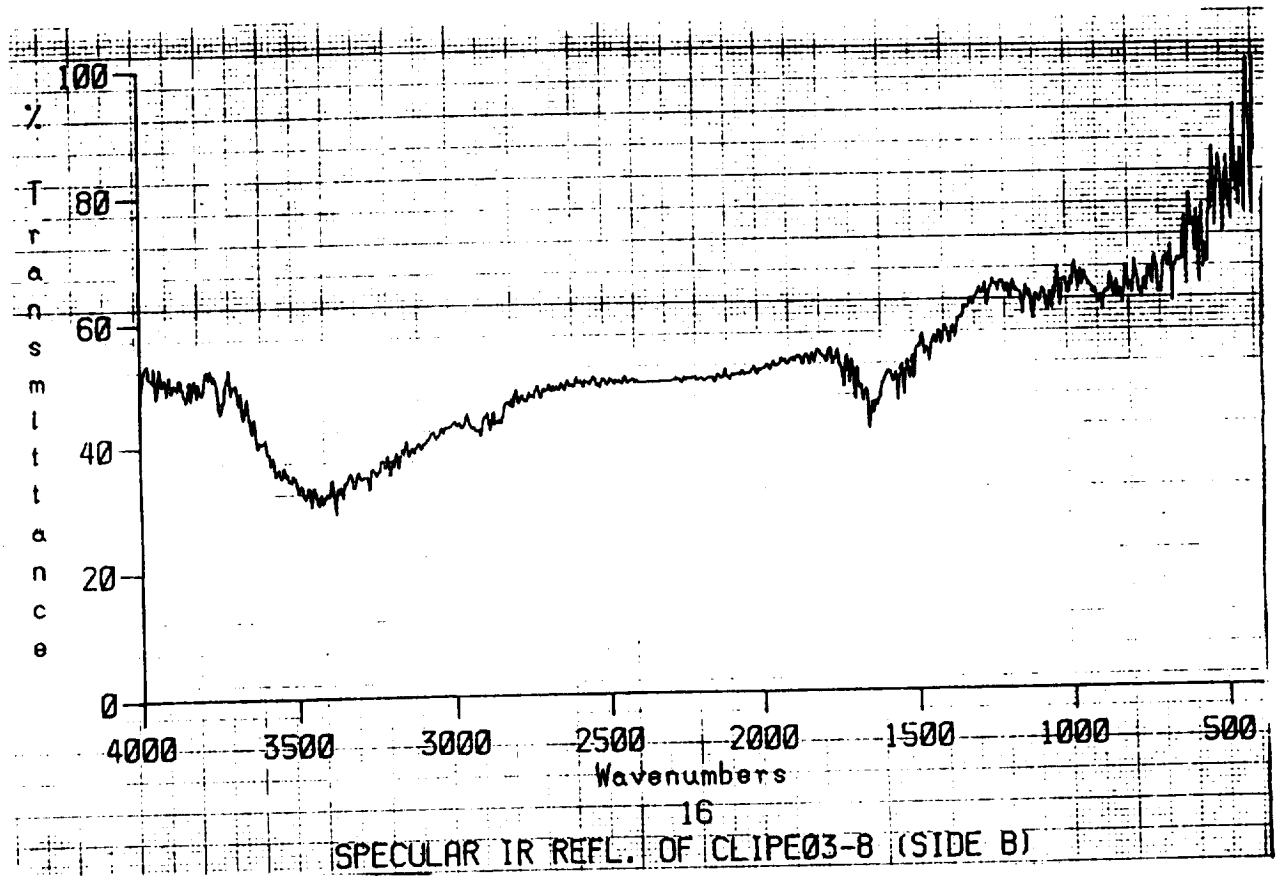

Figure A115: **Specular IR Reflectance of clip E03-8, (A) Front (B) Back.**

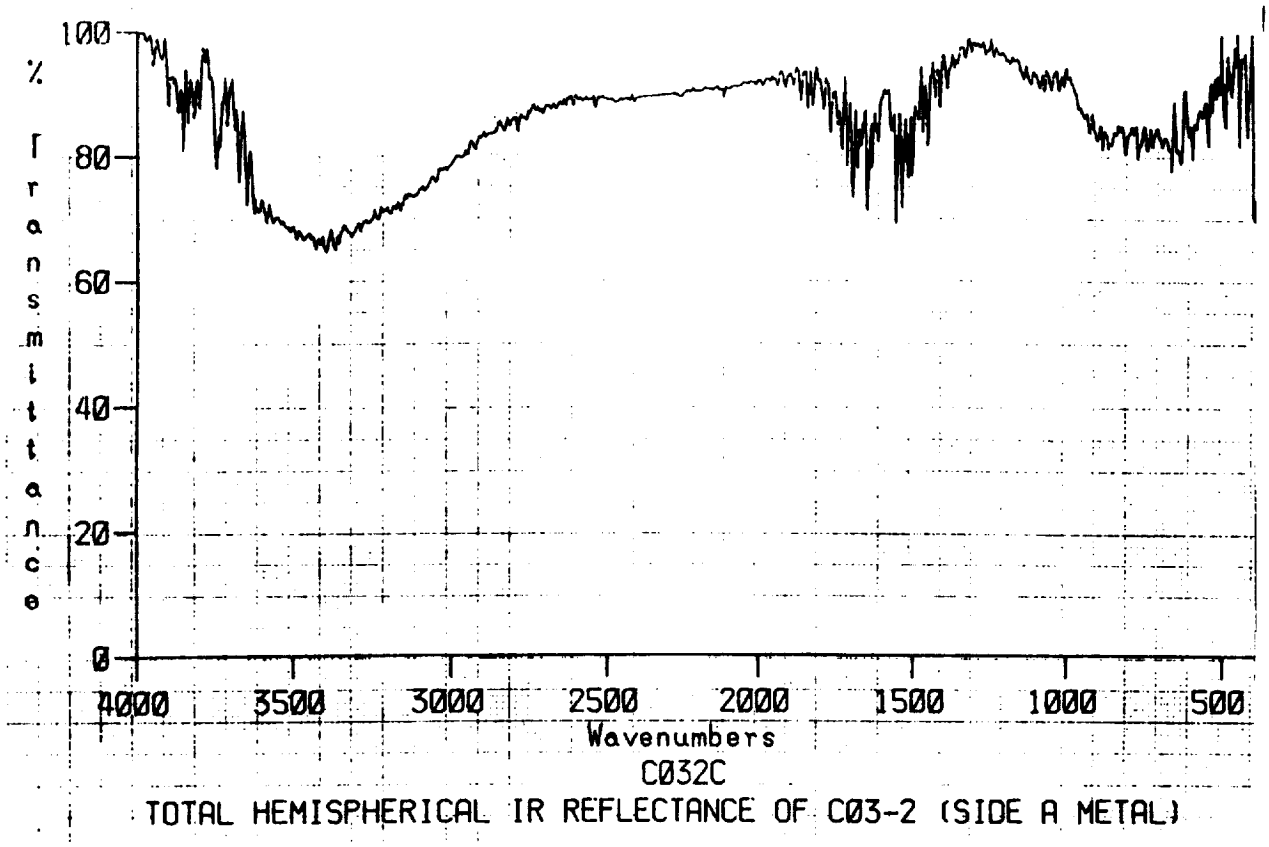

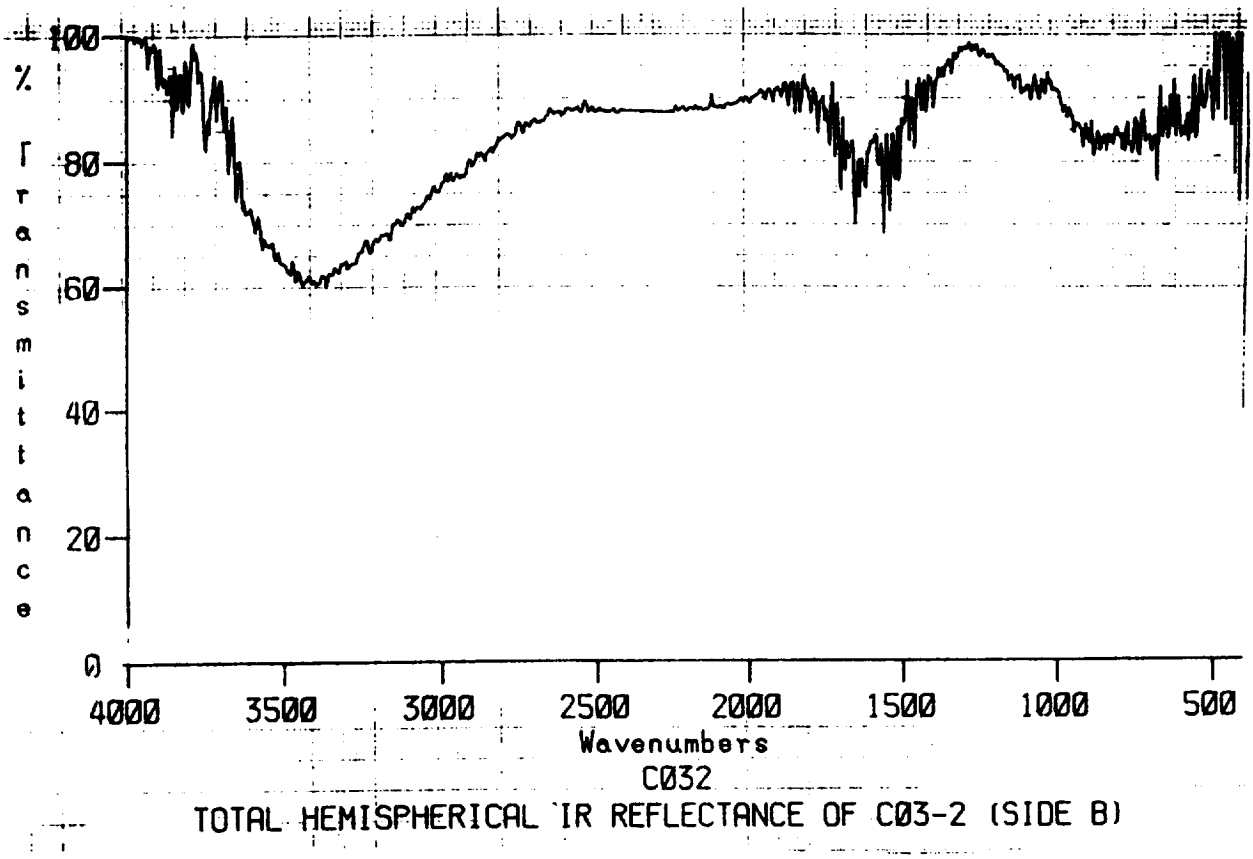

Figure A116: **Total Hemispherical IR Reflectance of C03-2, (A) Front (B) Back**

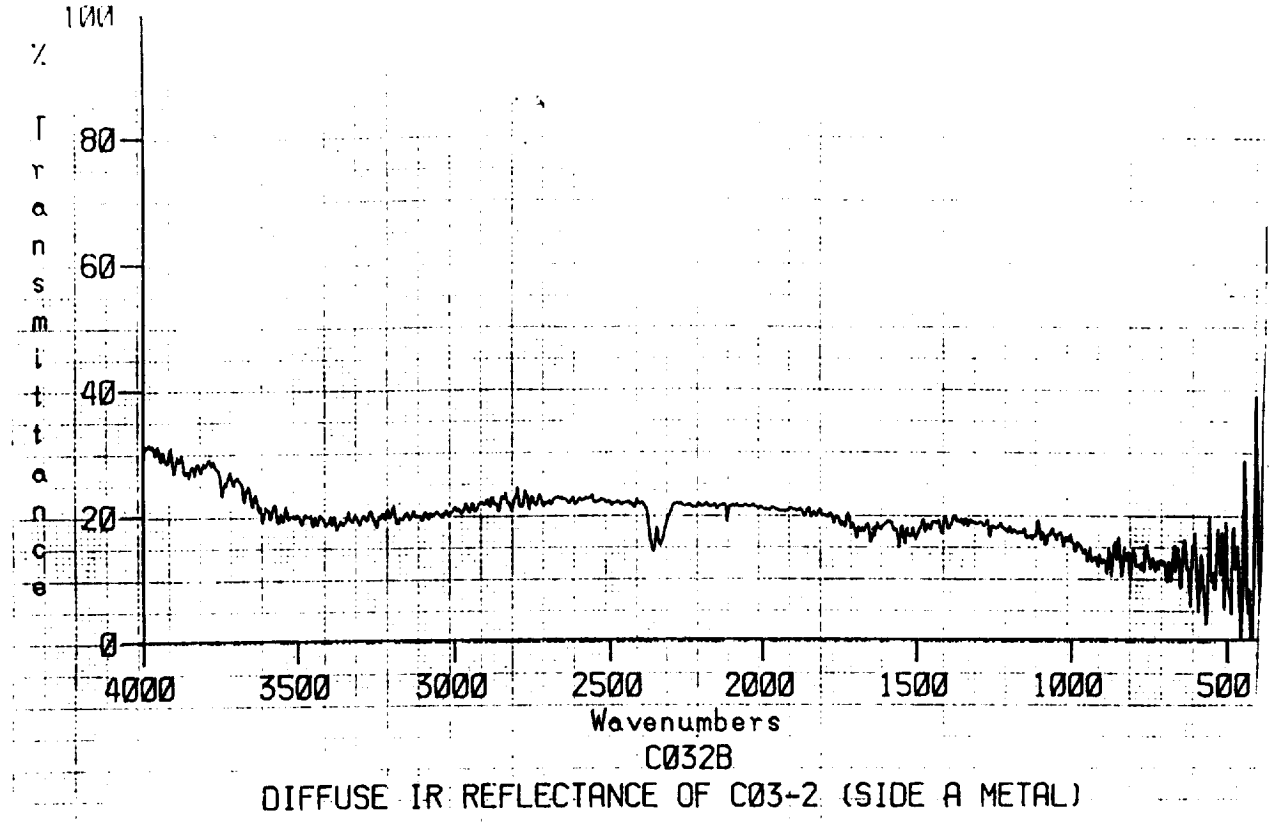

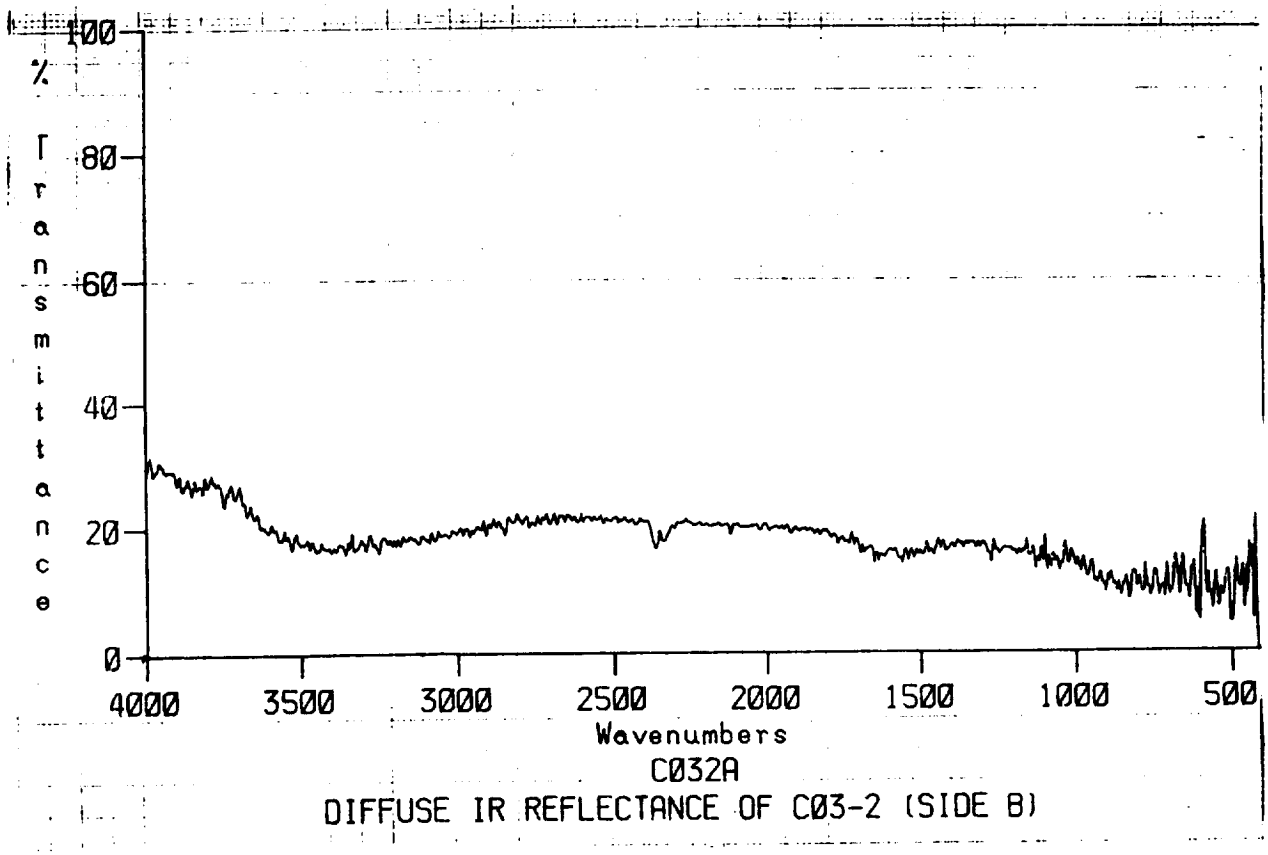

Figure A117: **Diffuse IR Reflectance of C03-2, (A) Front (B) Back.**

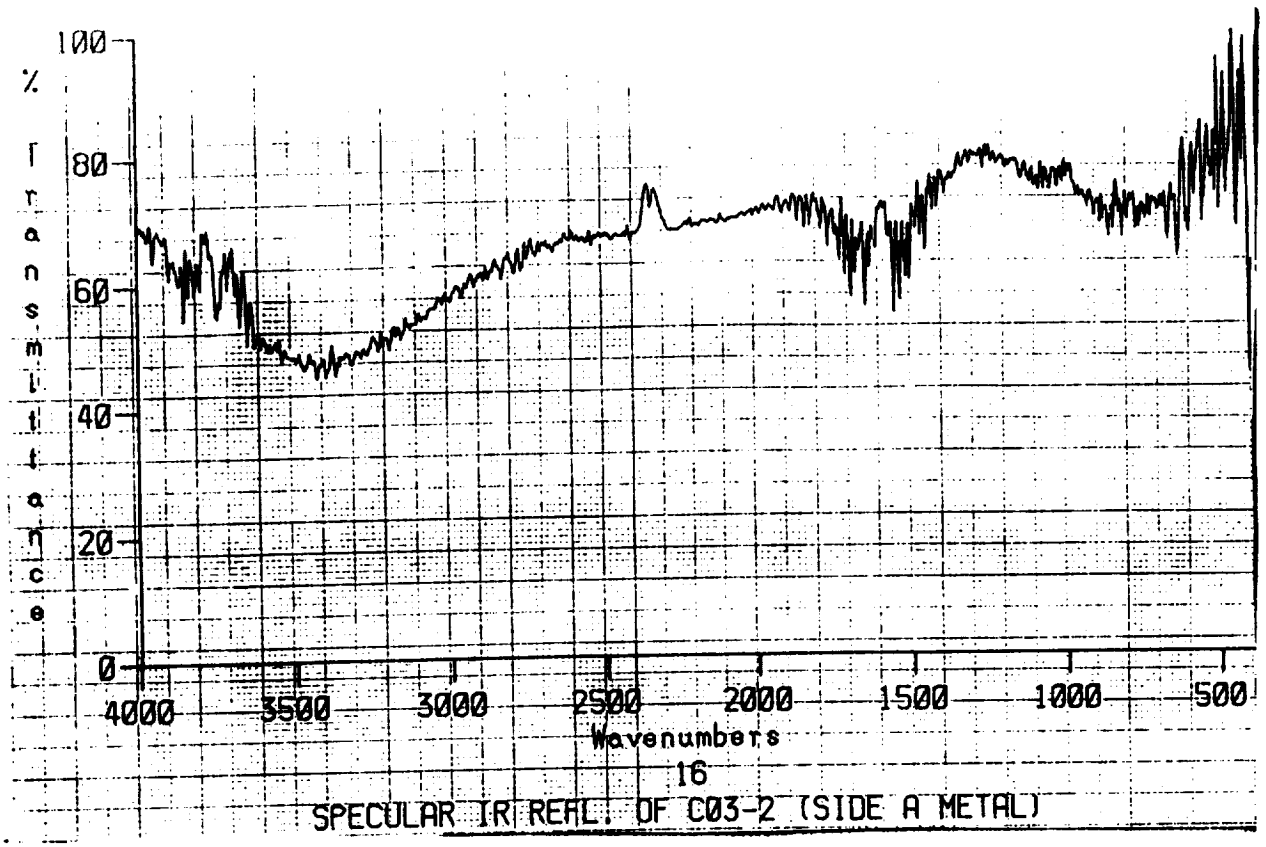

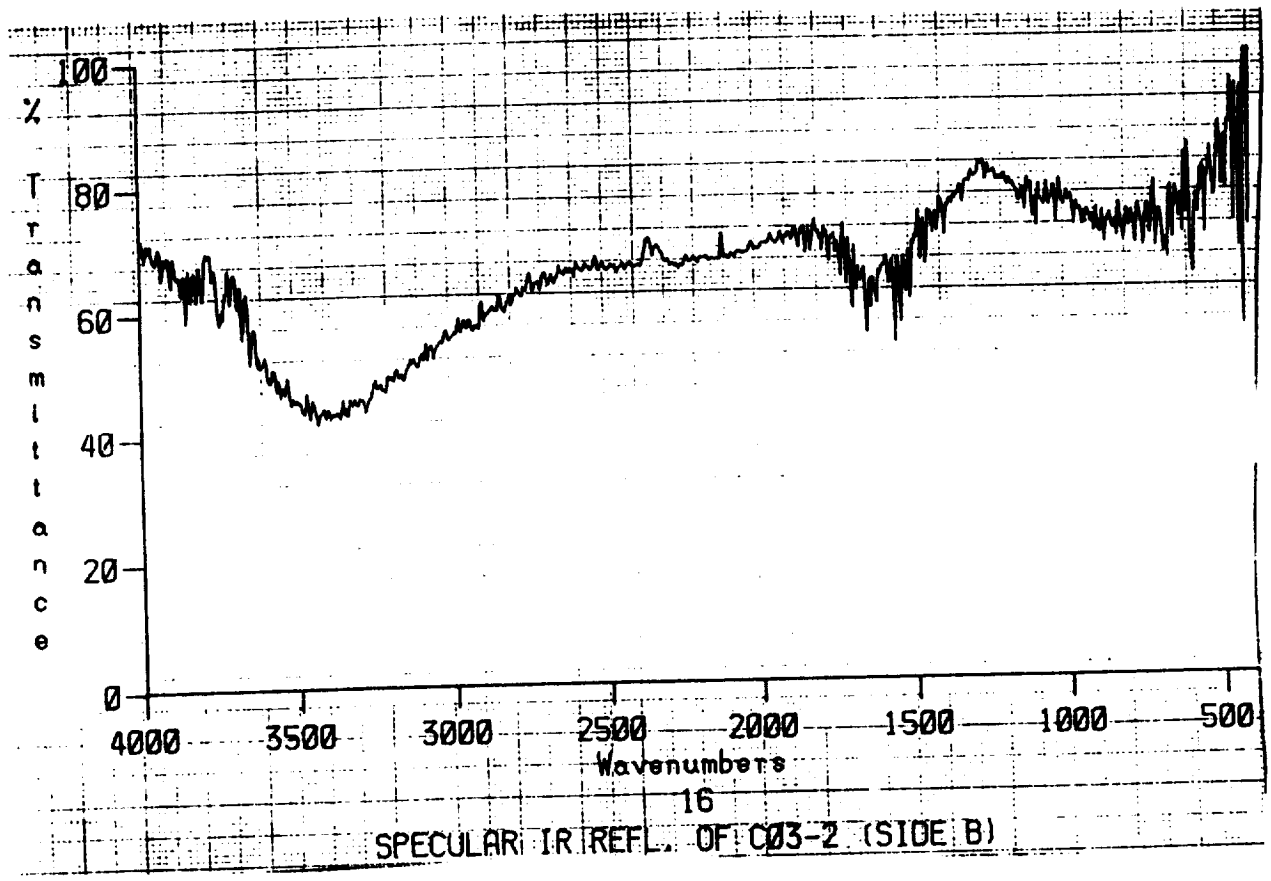

Figure A118: Specular IR Reflectance of C03-2, (A) Front (B) Back.

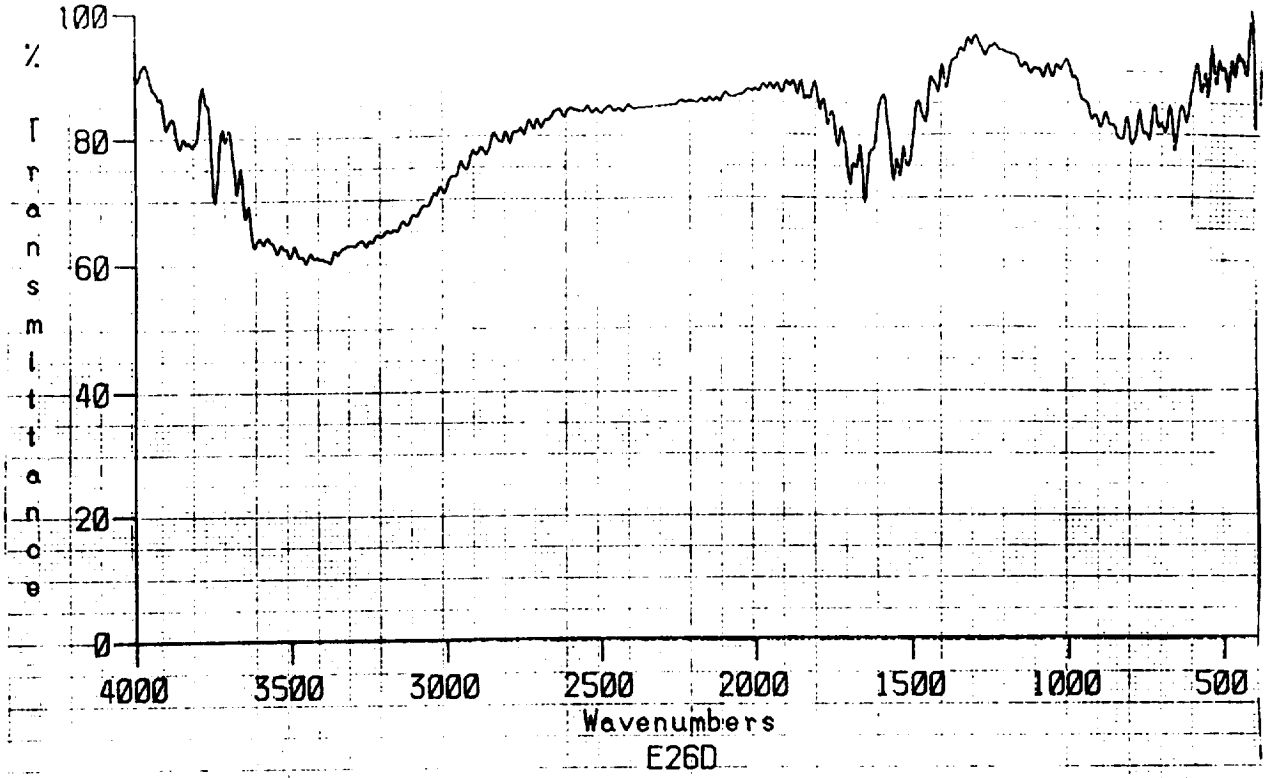

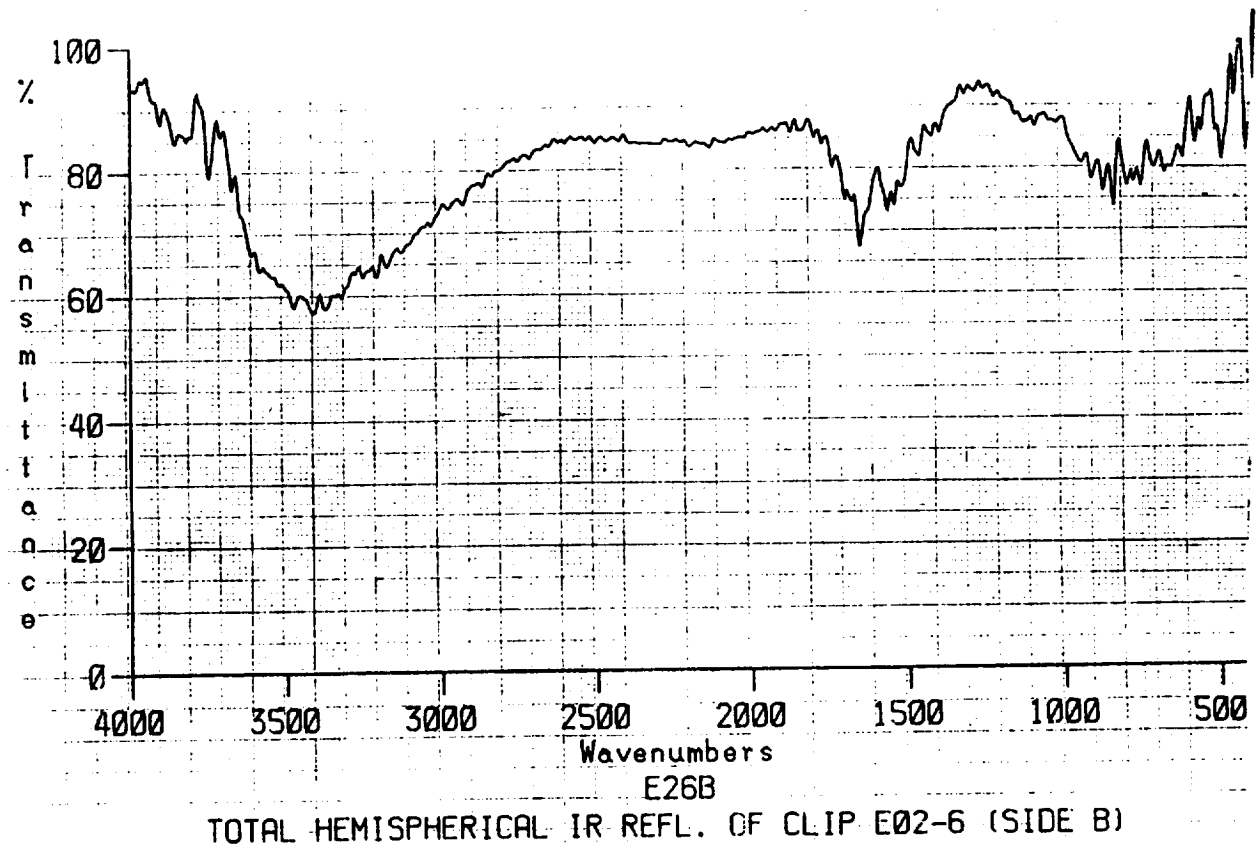

Figure A119: **Total Hemispherical IR Reflectance of clip E02-6, (A) Front (B) Back.**

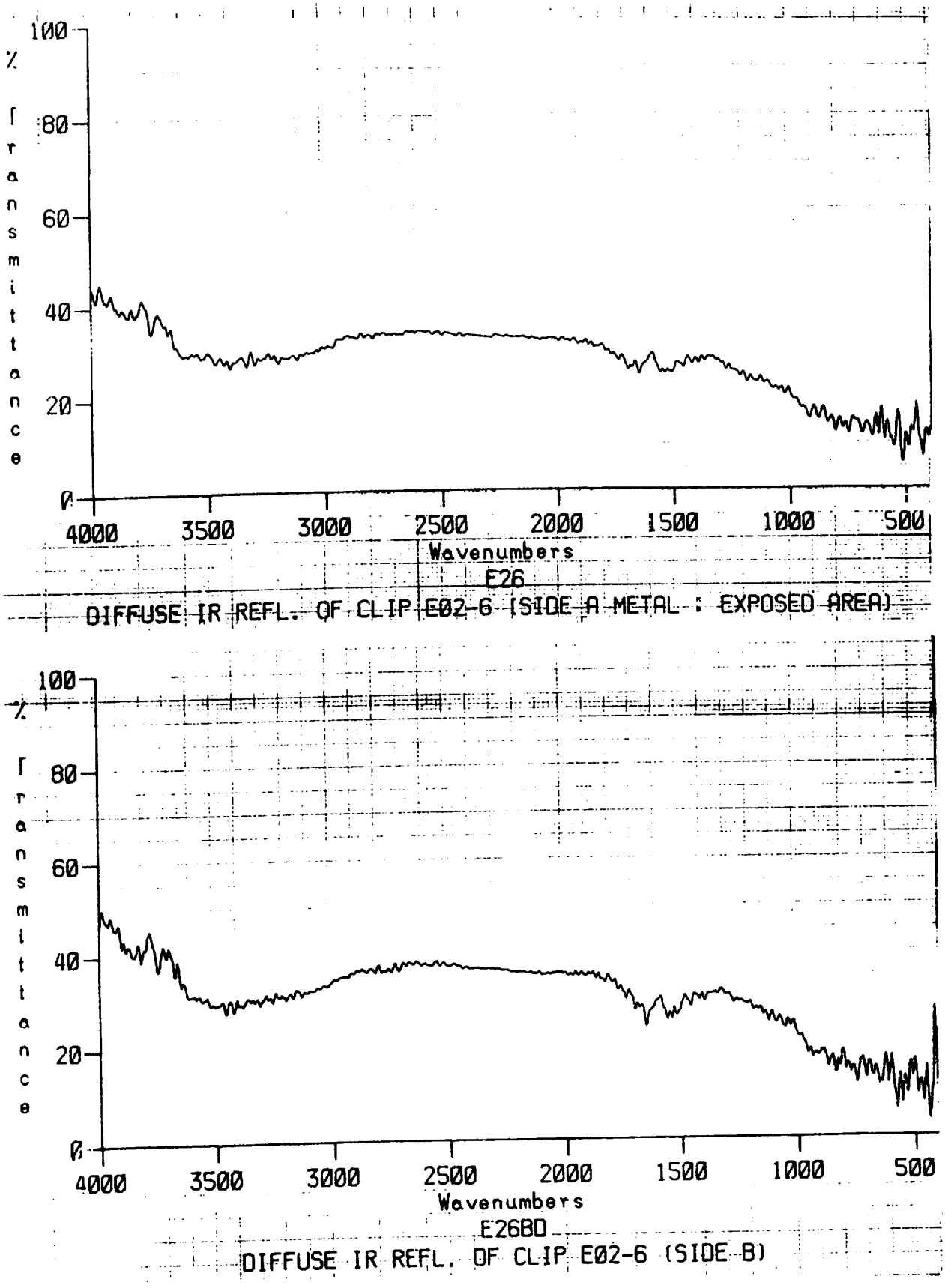

Figure A120: Diffuse IR Reflectance of clip E02-6, (A) Front (B) Back.

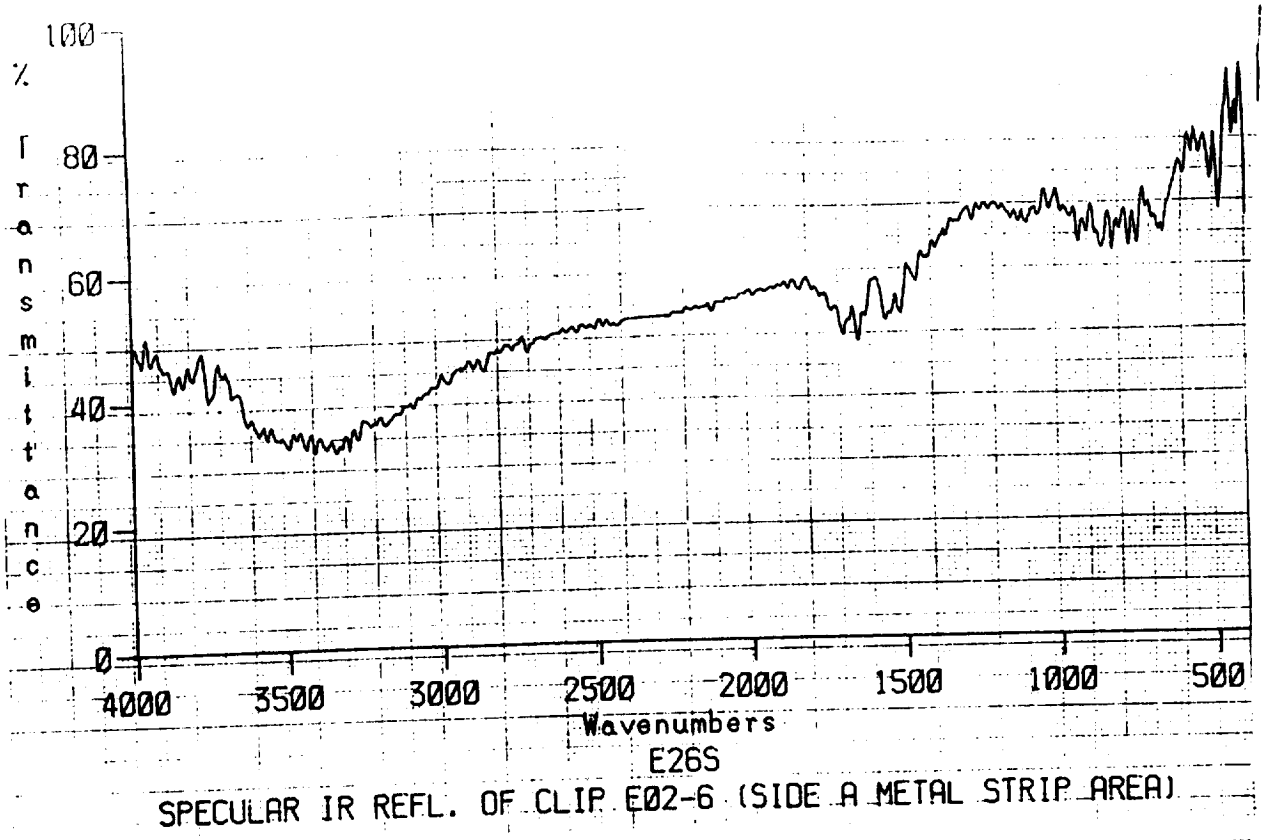

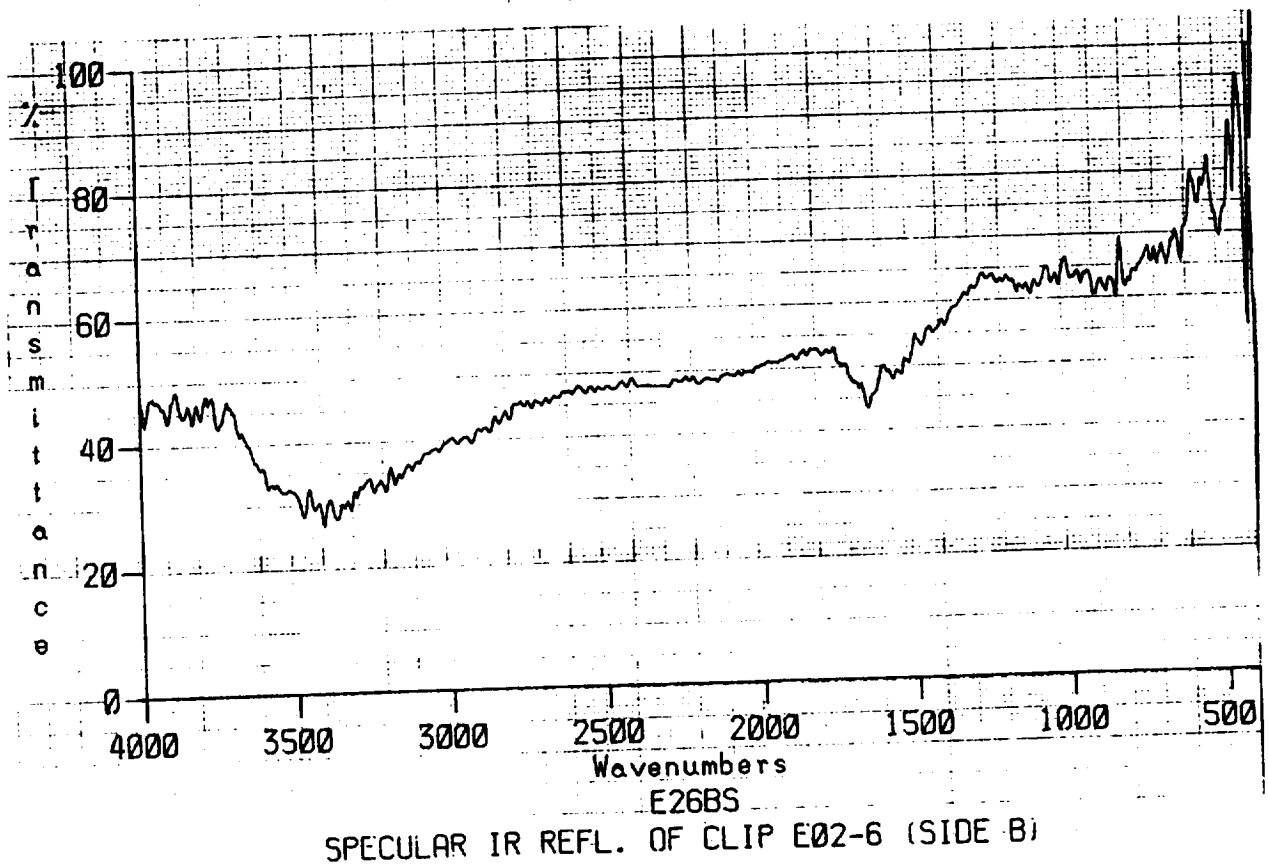

Figure A121: **Specular IR Reflectance of clip E02-6, (A) Front (B) Back.**

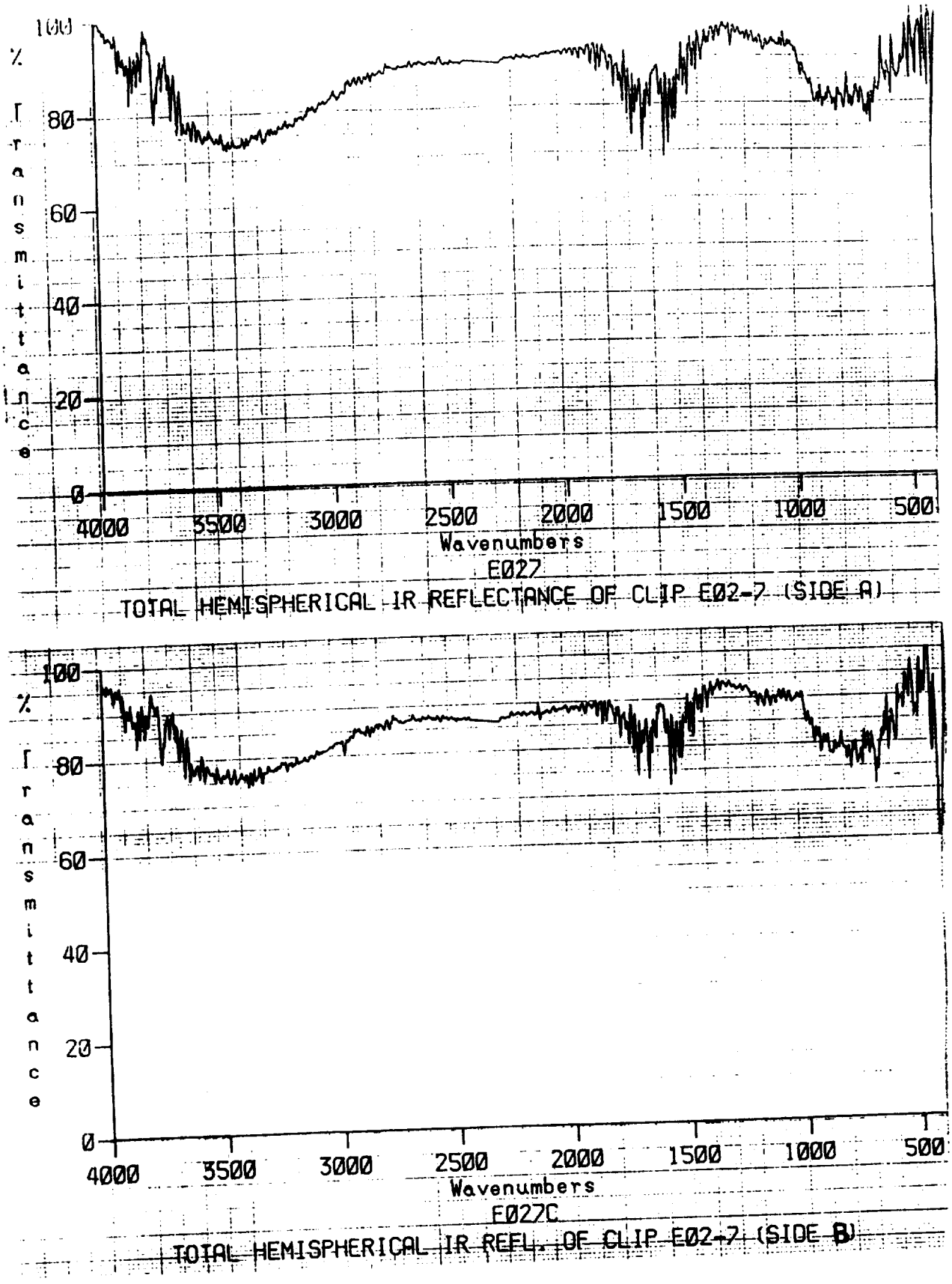

Figure A122: Total Hemispherical IR Reflectance of clip E02-7, (A) Front (B) Back.

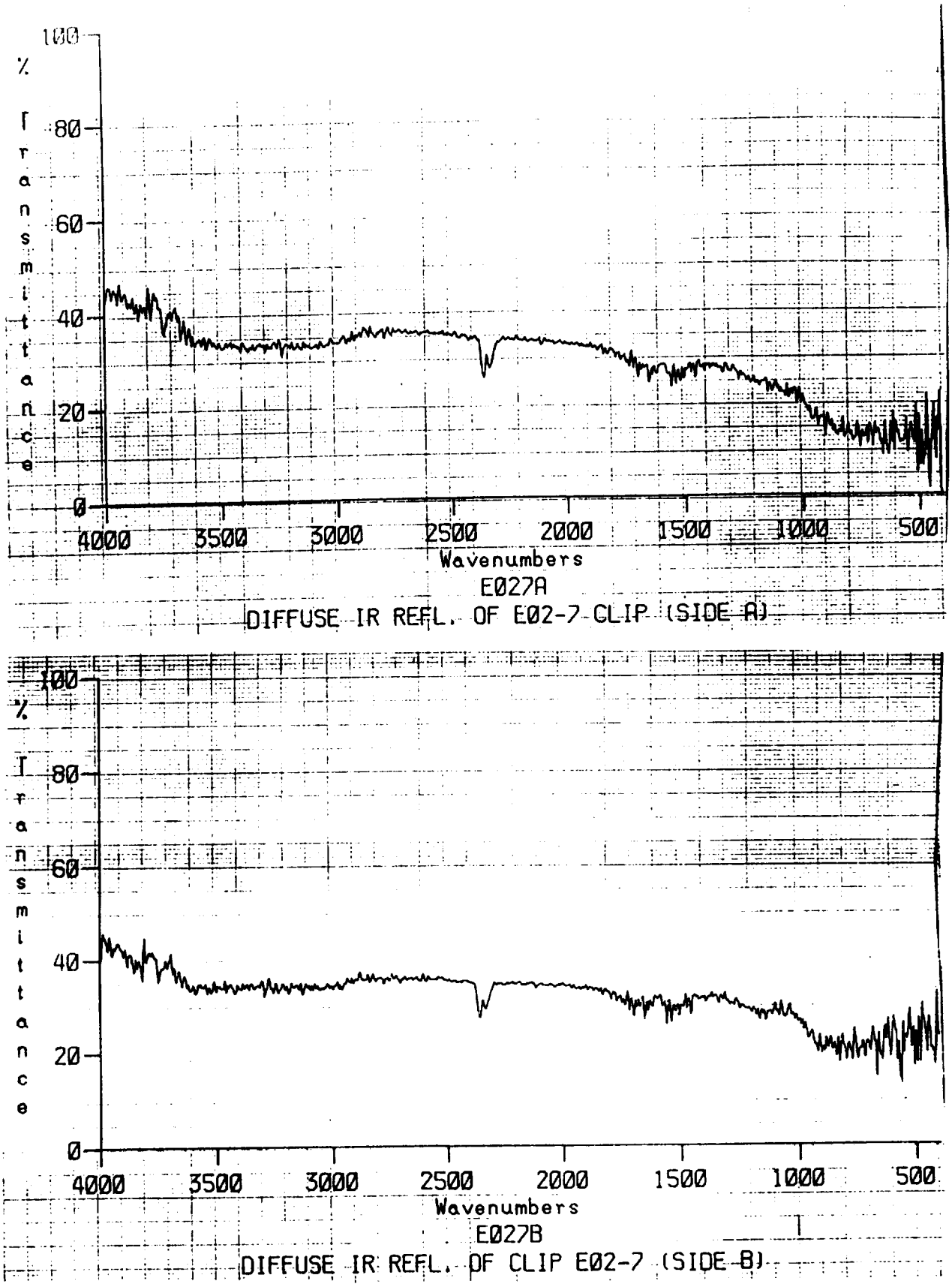

Figure A123: **Diffuse IR Reflectance of clip E02-7, (A) Front (B) Back.**

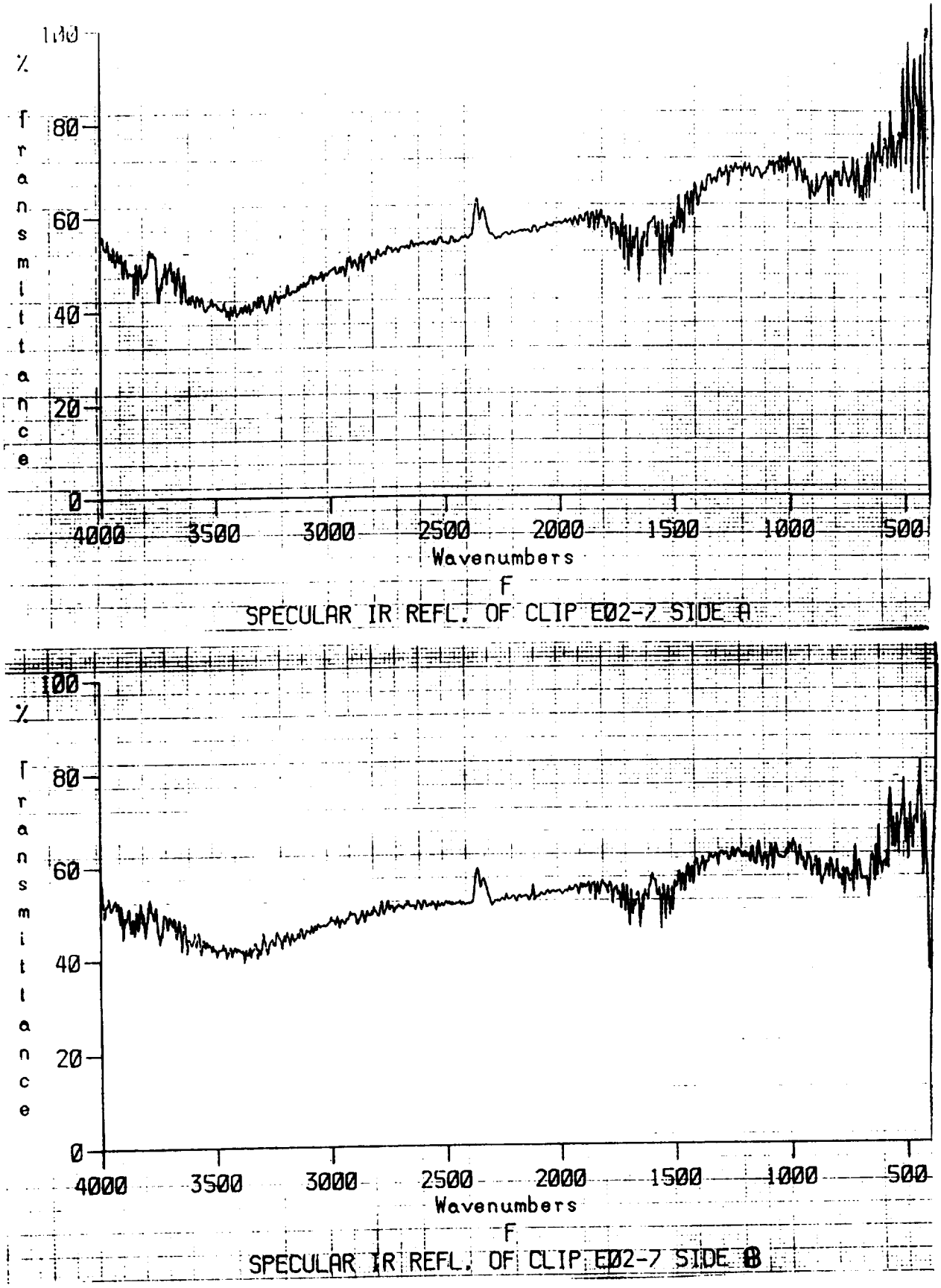

Figure A124: **Specular IR Reflectance of clip E02-7, (A) Front (B) Back.**

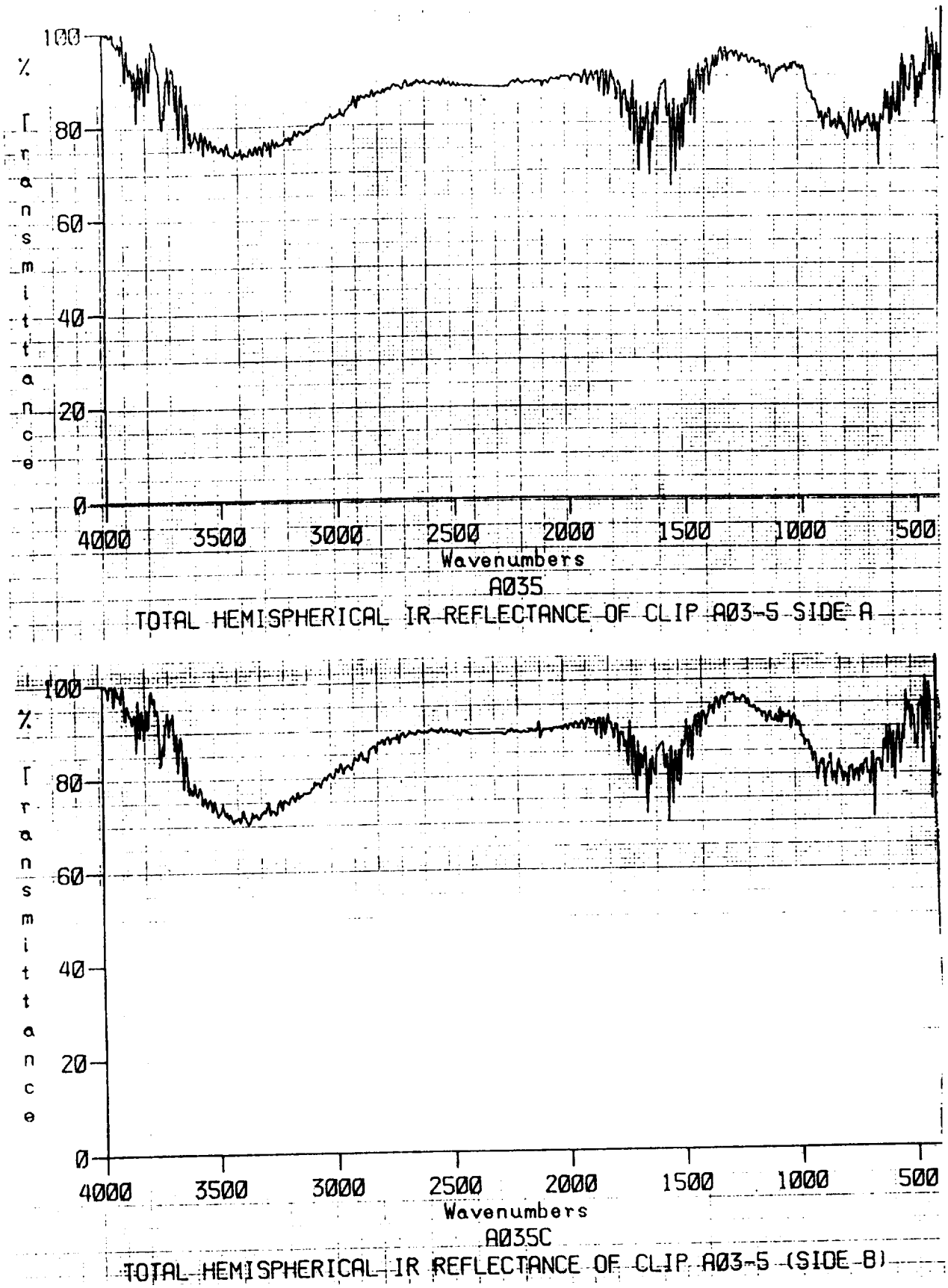

Figure A125: **Total Hemispherical IR Reflectance of clip A03-5, (A) Front (B) Back.**

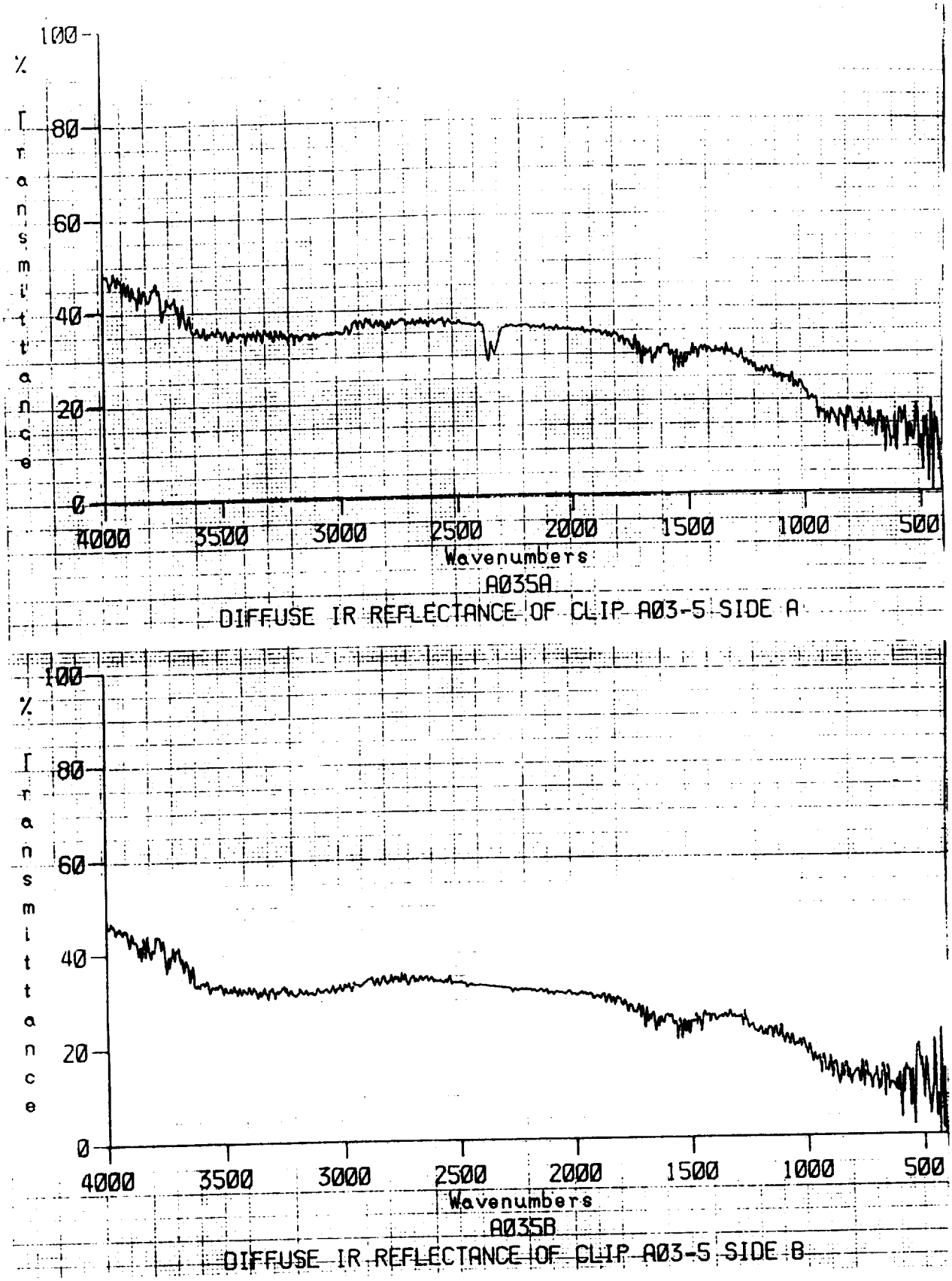

Figure A126: **Diffuse IR Reflectance of clip A03-5, (A) Front (B) Back.**

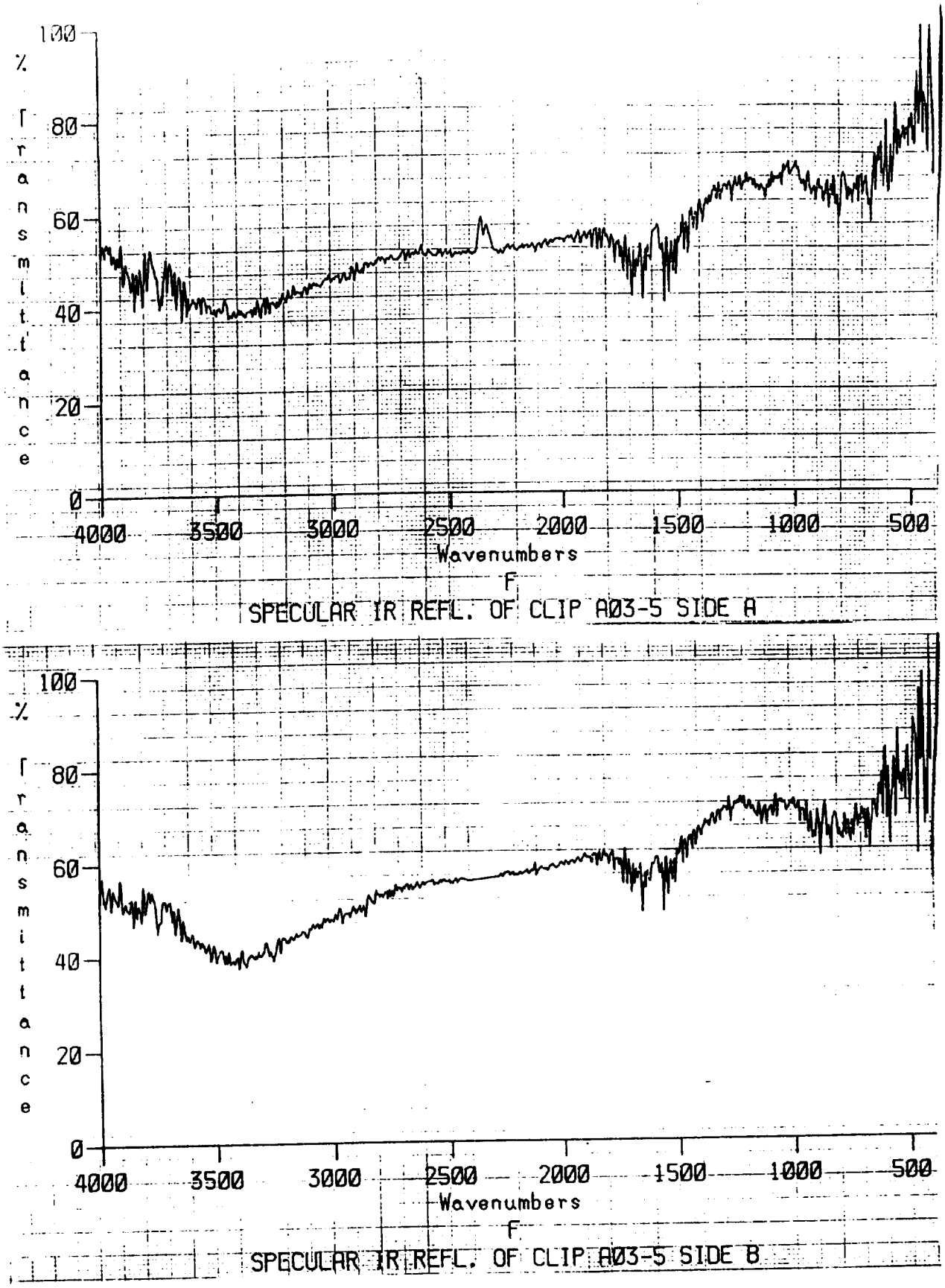

Figure A127: **Specular IR Reflectance of clip A03-5, (A) Front (B) Back.**

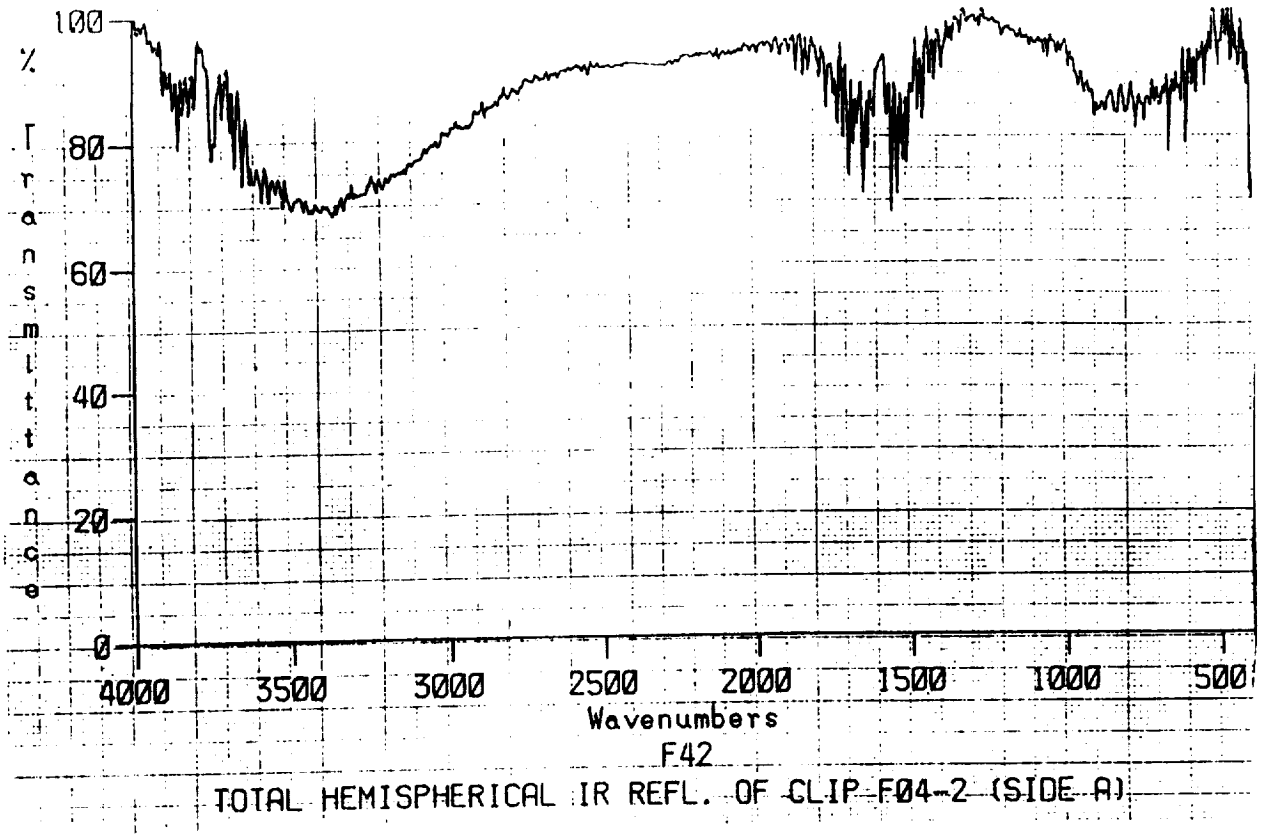

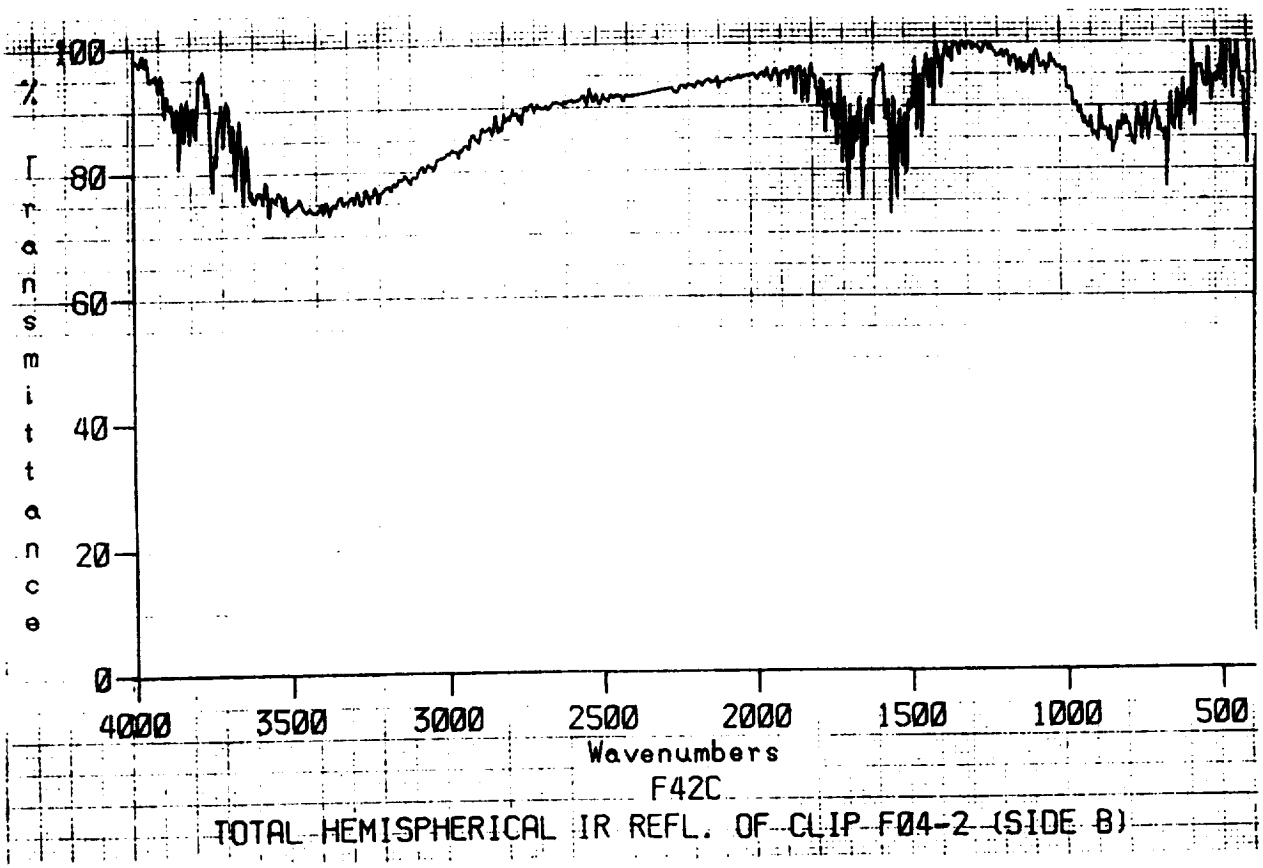

Figure A128: **Total Hemispherical IR Reflectance of clip F04-2, (A) Front (B) Back.**

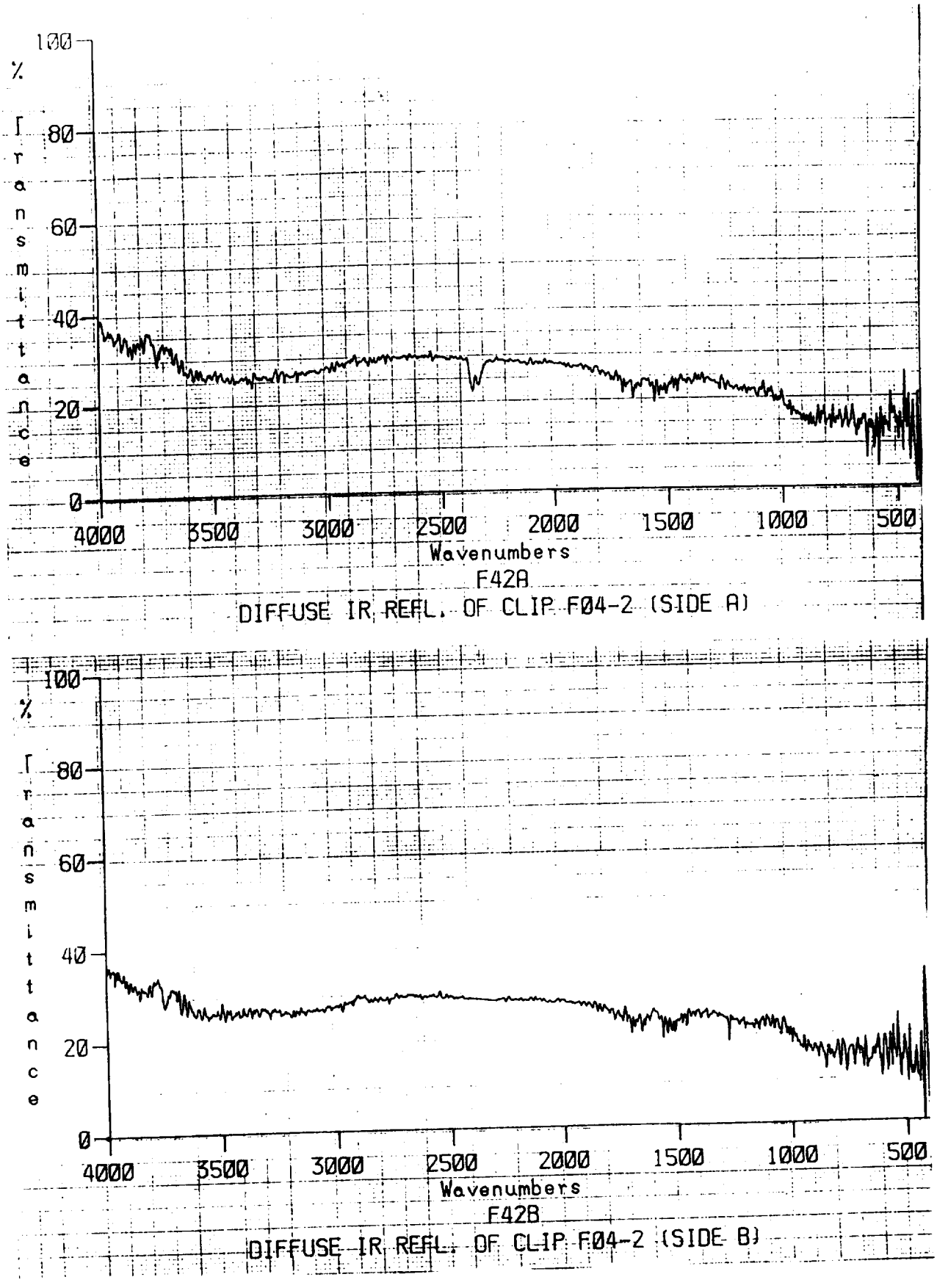

Figure A129: **Diffuse IR Reflectance of clip F04-2, (A) Front (B) Back.**

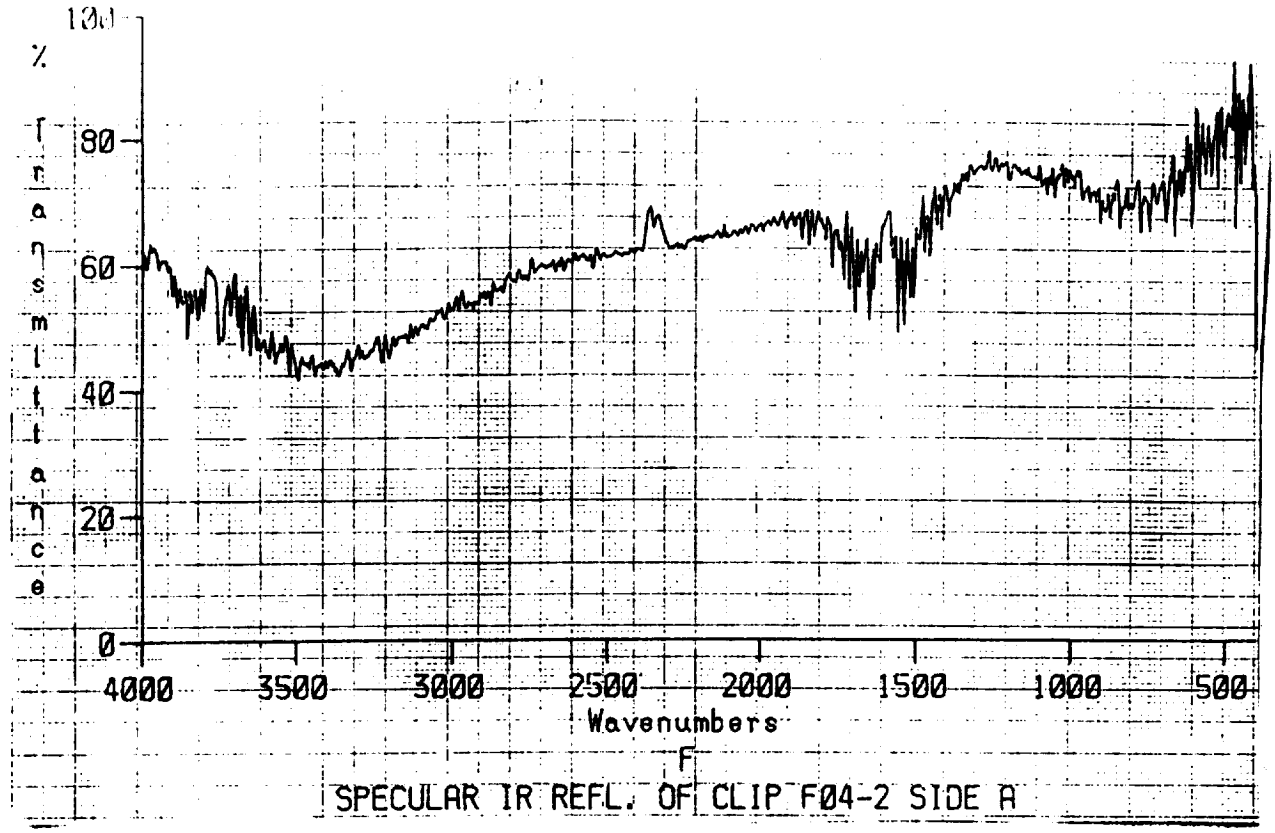

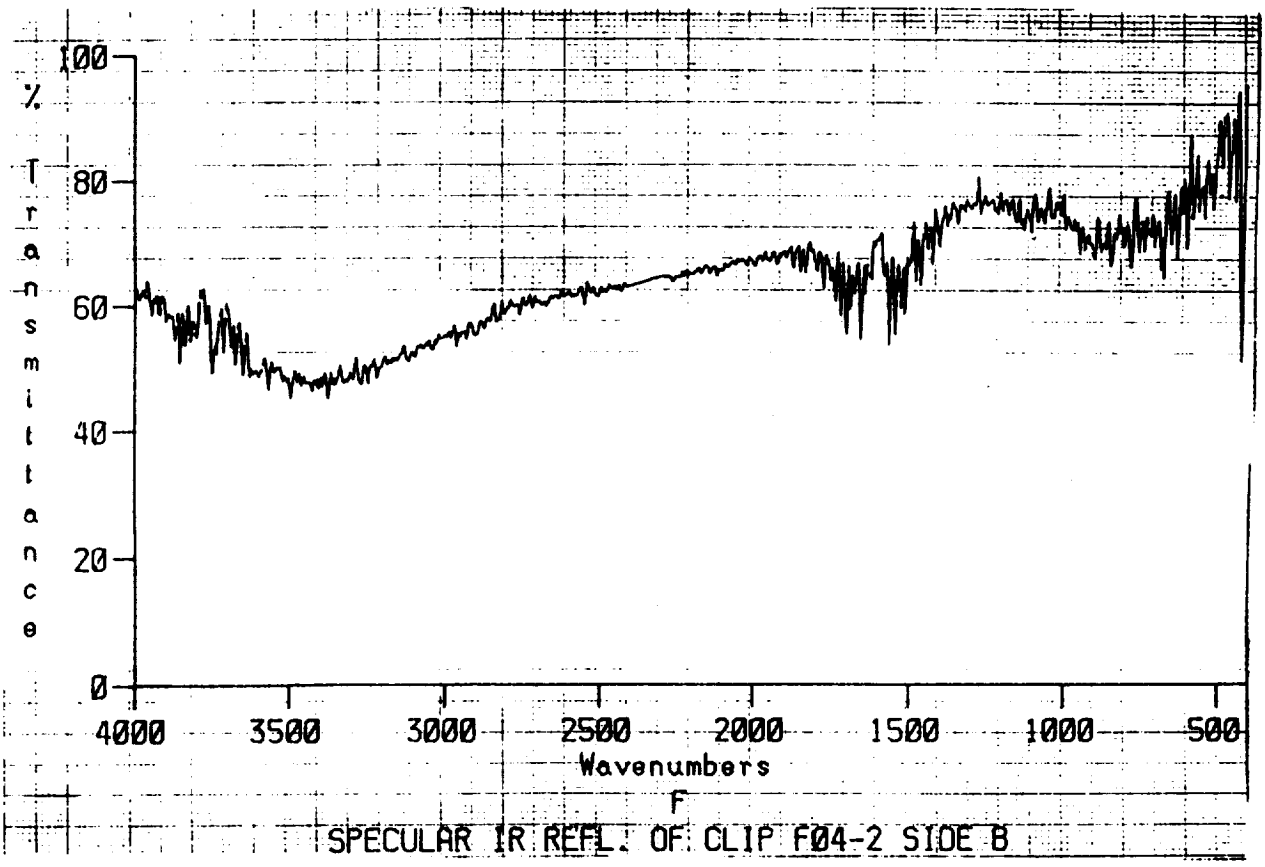

Figure A130: **Specular IR Reflectance of clip F04-2, (A) Front (B) Back.**

APPENDIX B

Photomicrographs of Coating Thickness

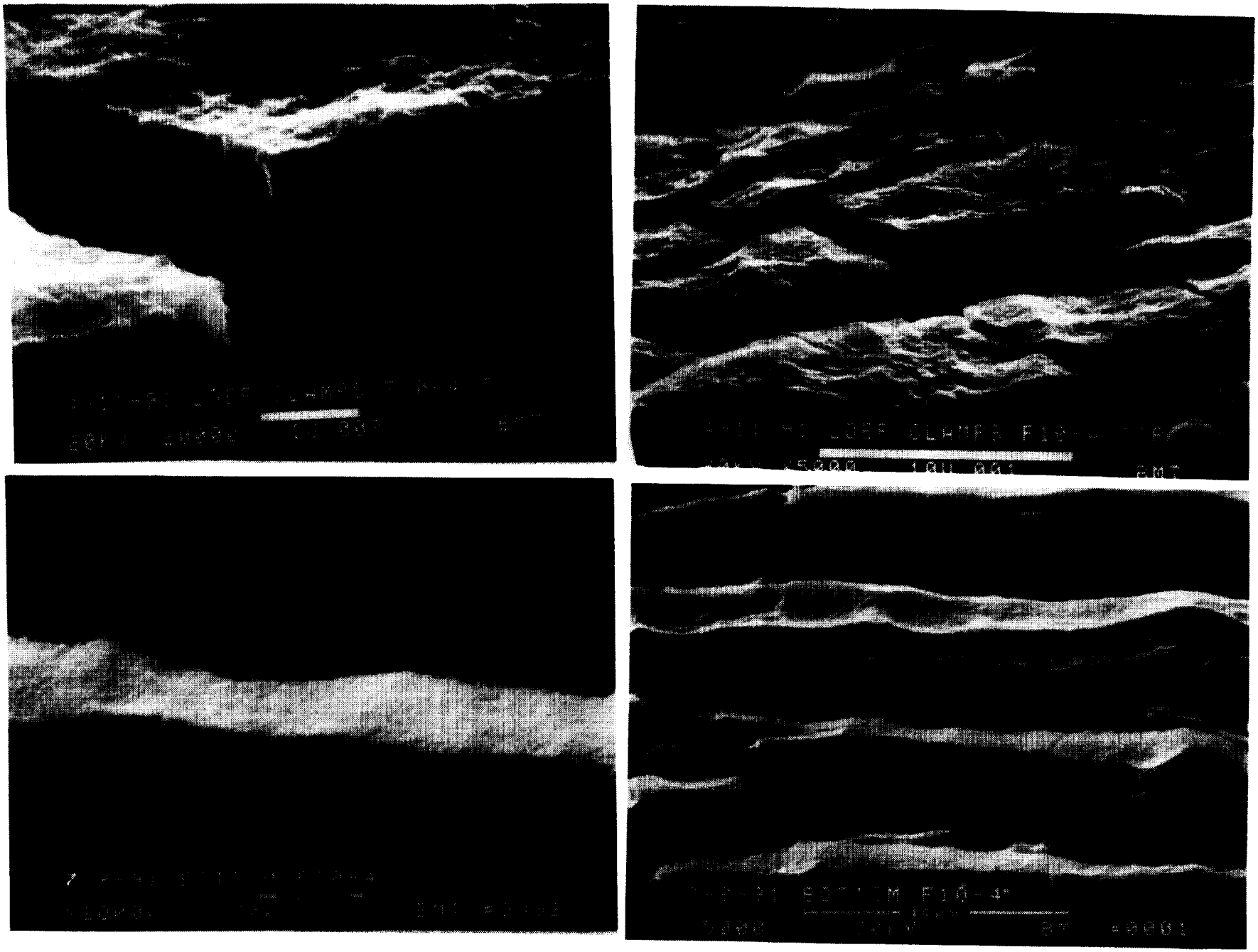

Figure B1: SEM Photomicrographs of coating thickness for tray clamp F10-4

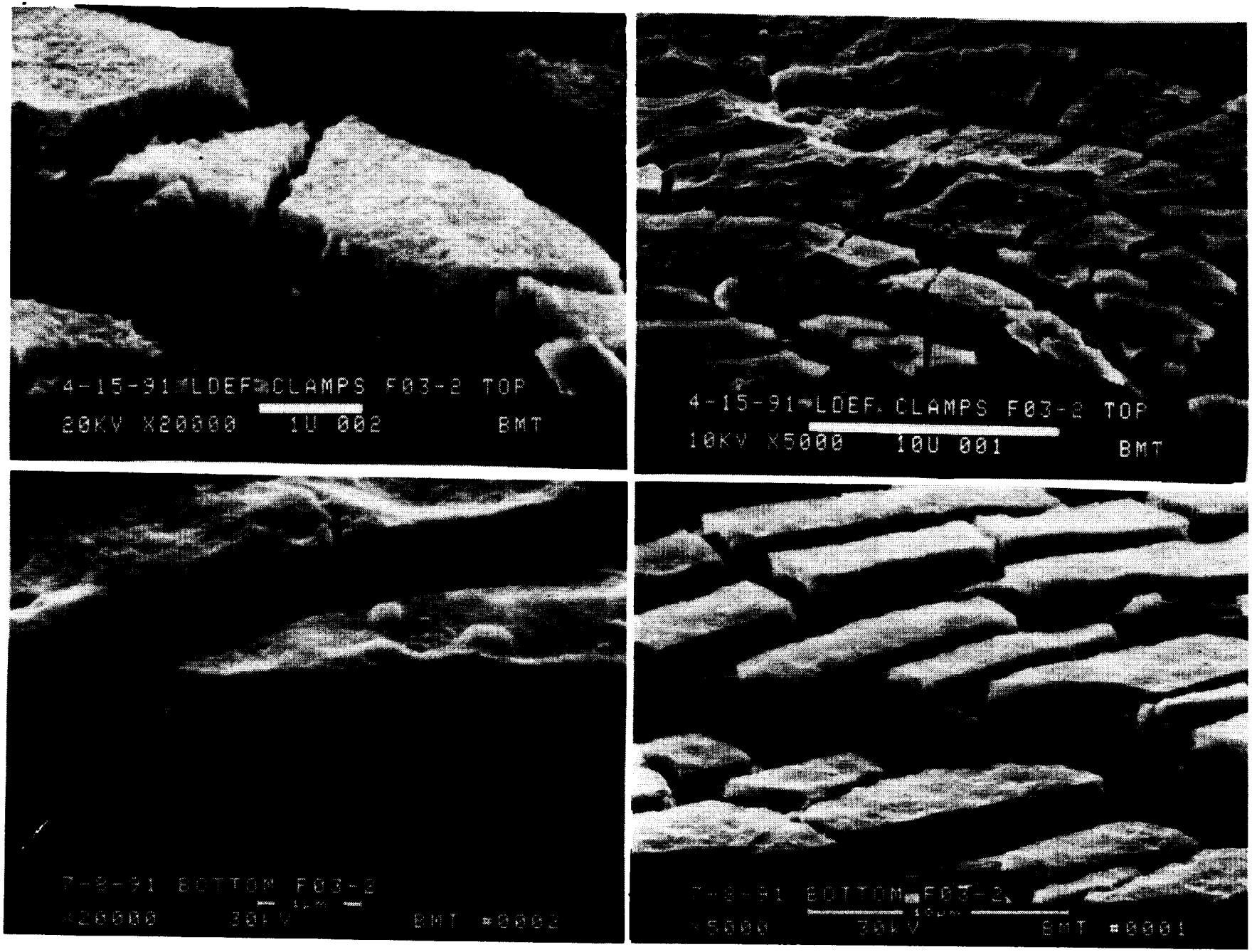

Figure B2: SEM photomicrographs of coating thickness for tray clamp F03-2

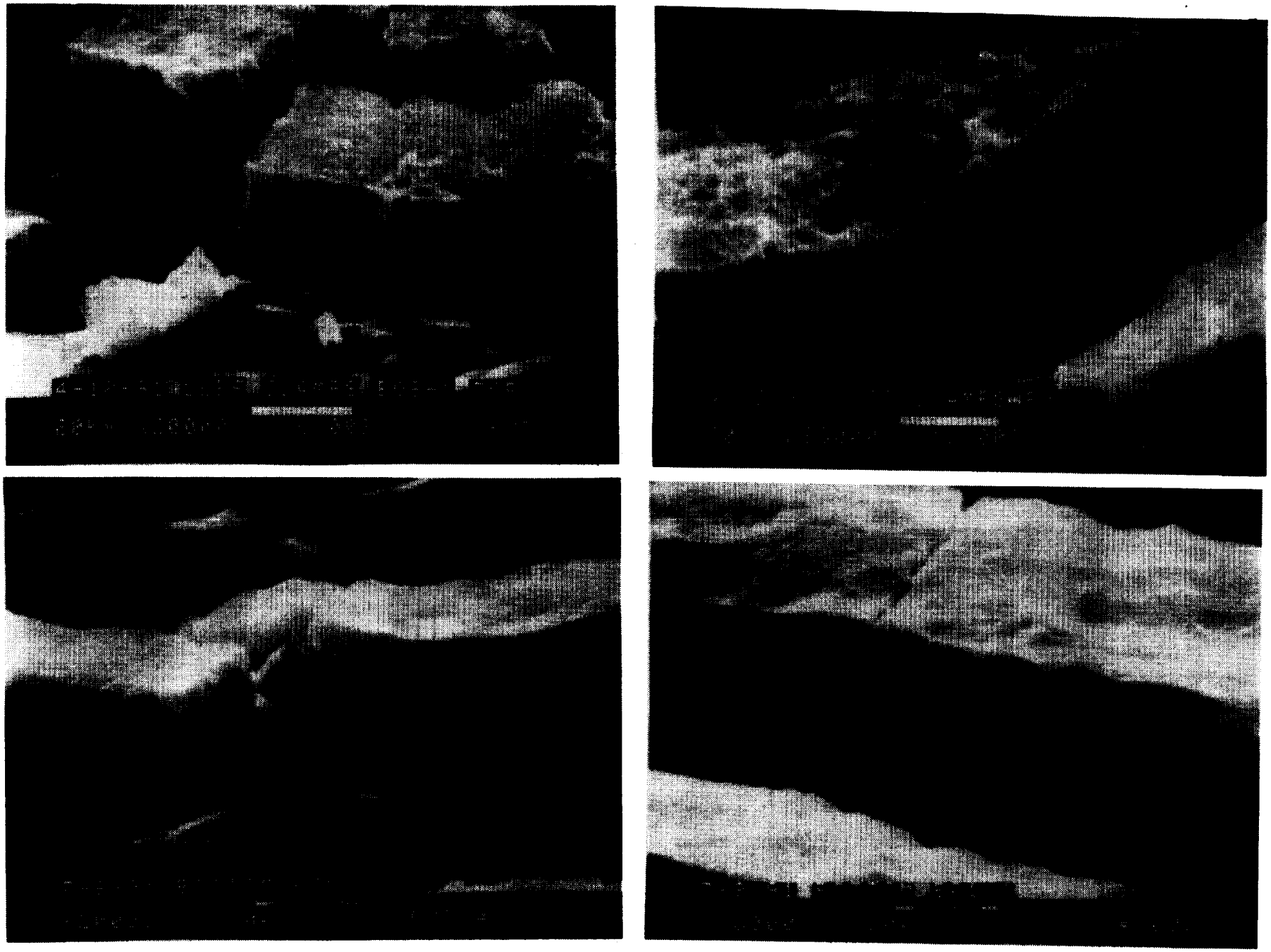

Figure B3: SEM photomicrograph of coating thickness for tray clamps Bo8-1 and Bo1-1

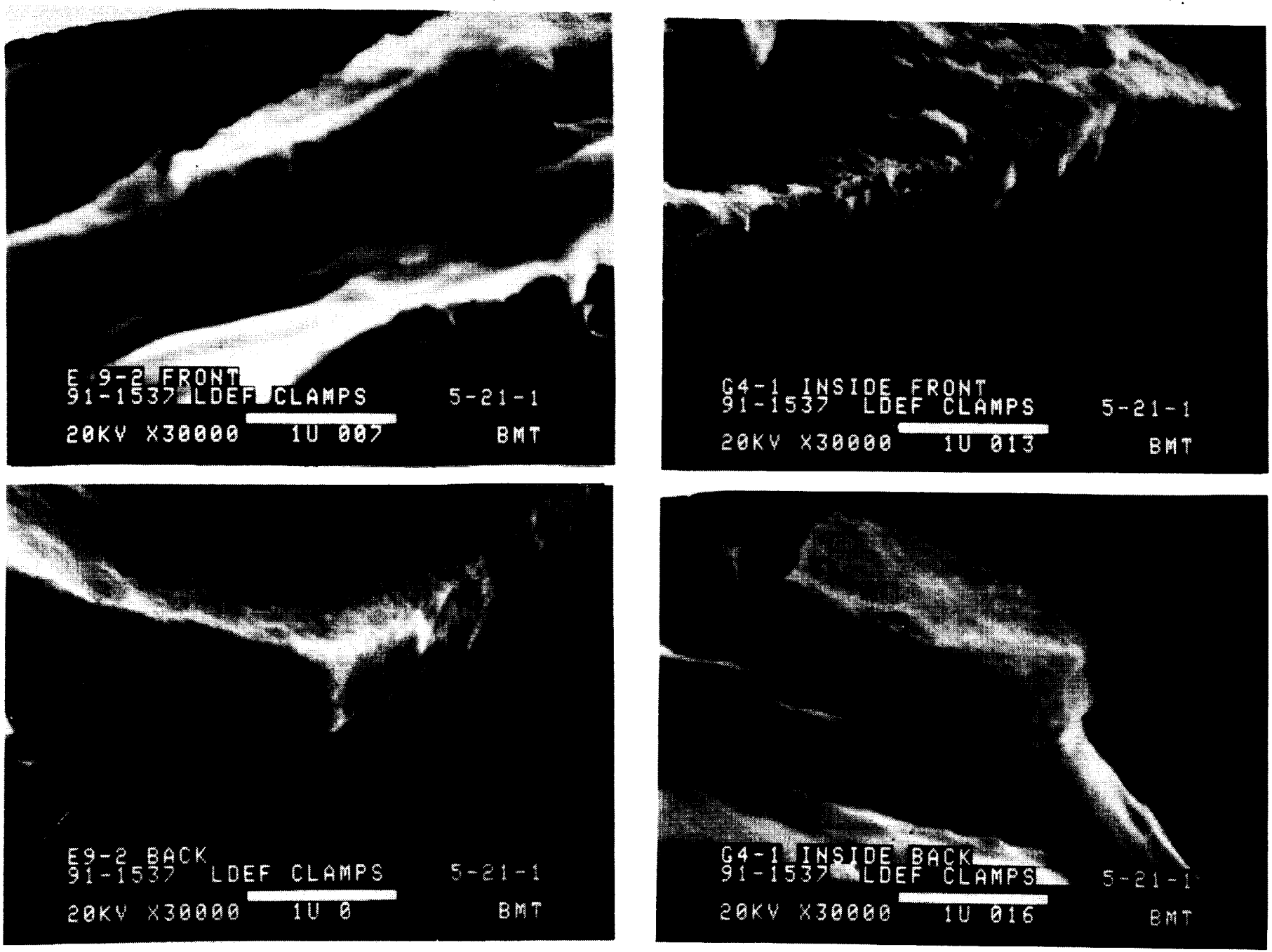

Figure B4: SEM photomicrographs of coating thickness for tray clamps E09-2 and G04-1

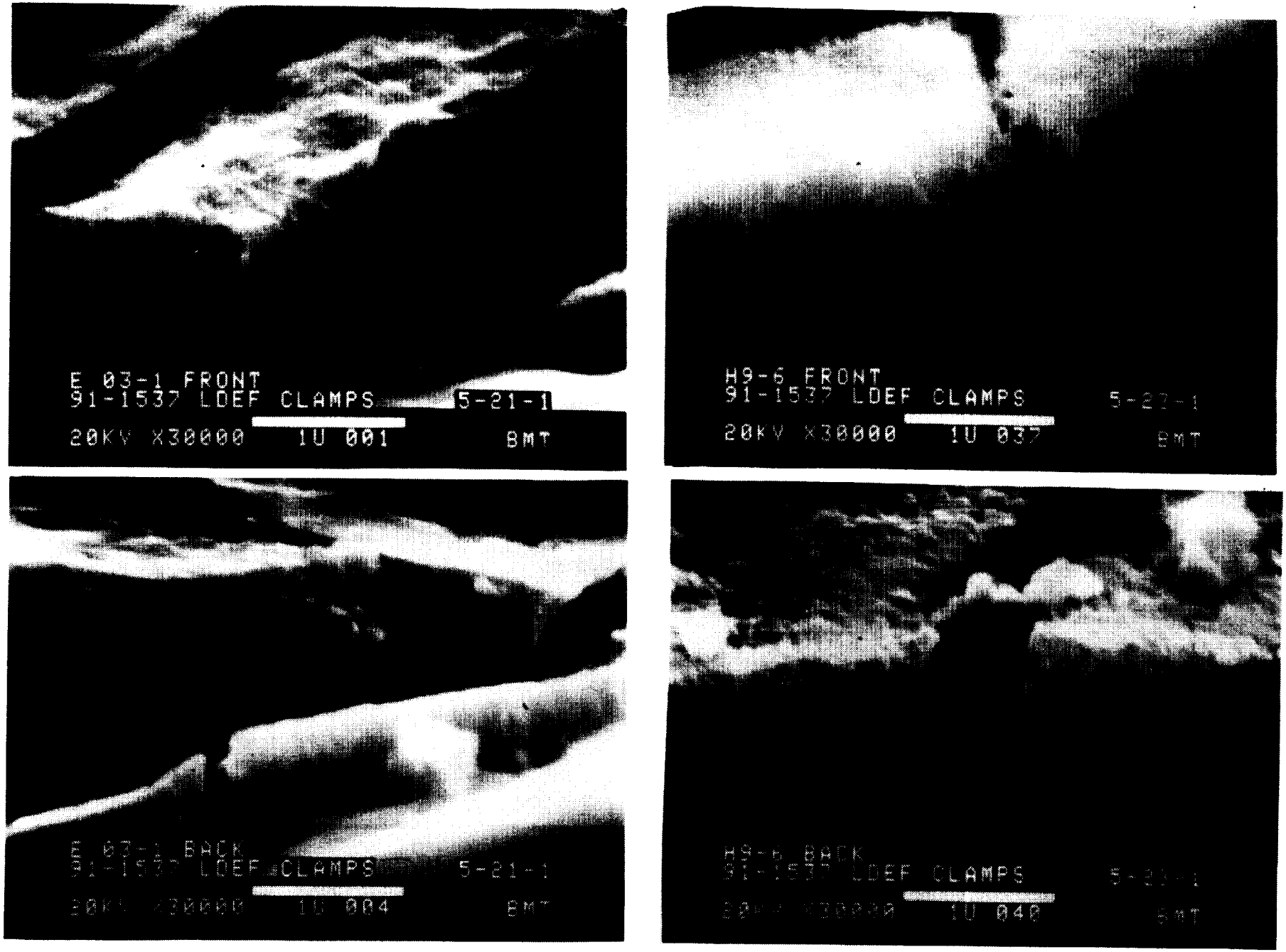

Figure B5: SEM photomicrographs of coating thickness for tray clamps E03-1 and H09-6

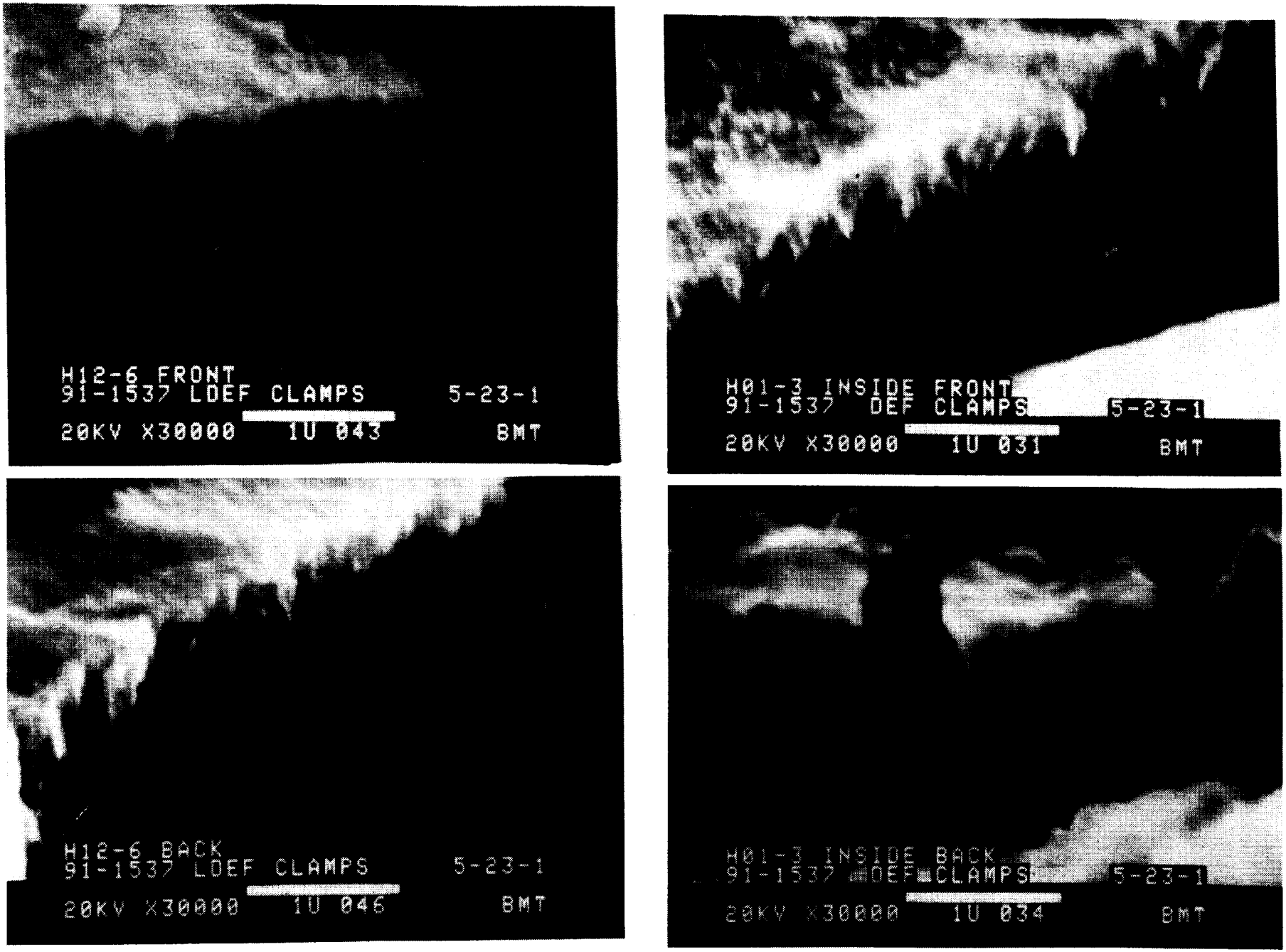

Figure B6: SEM photomicrographs of coating thickness for tray clamps H12-6 and H01-3

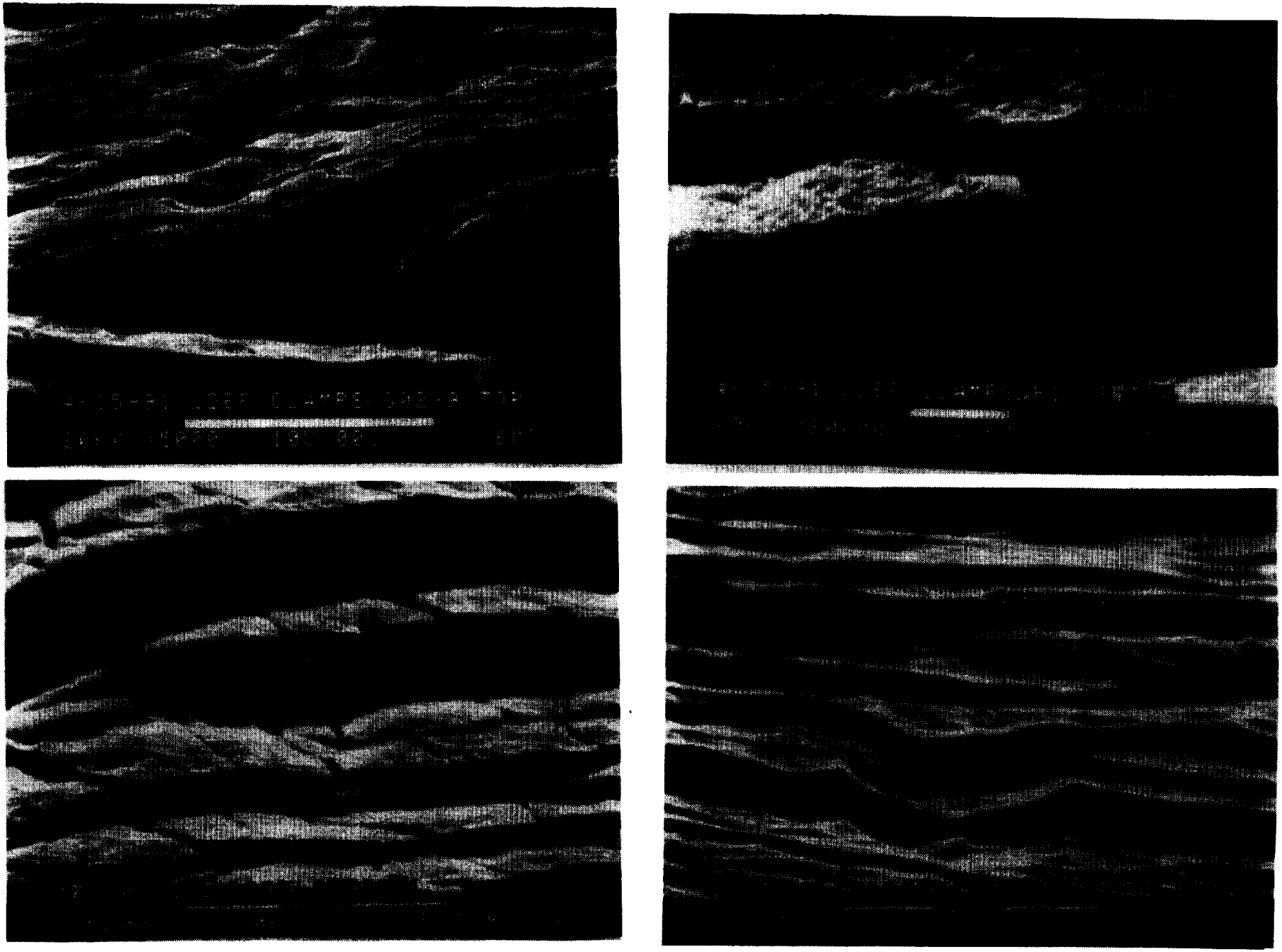

Figure B7: SEM photomicrographs of coating thickness for tray clamps G02-9 and H12-8

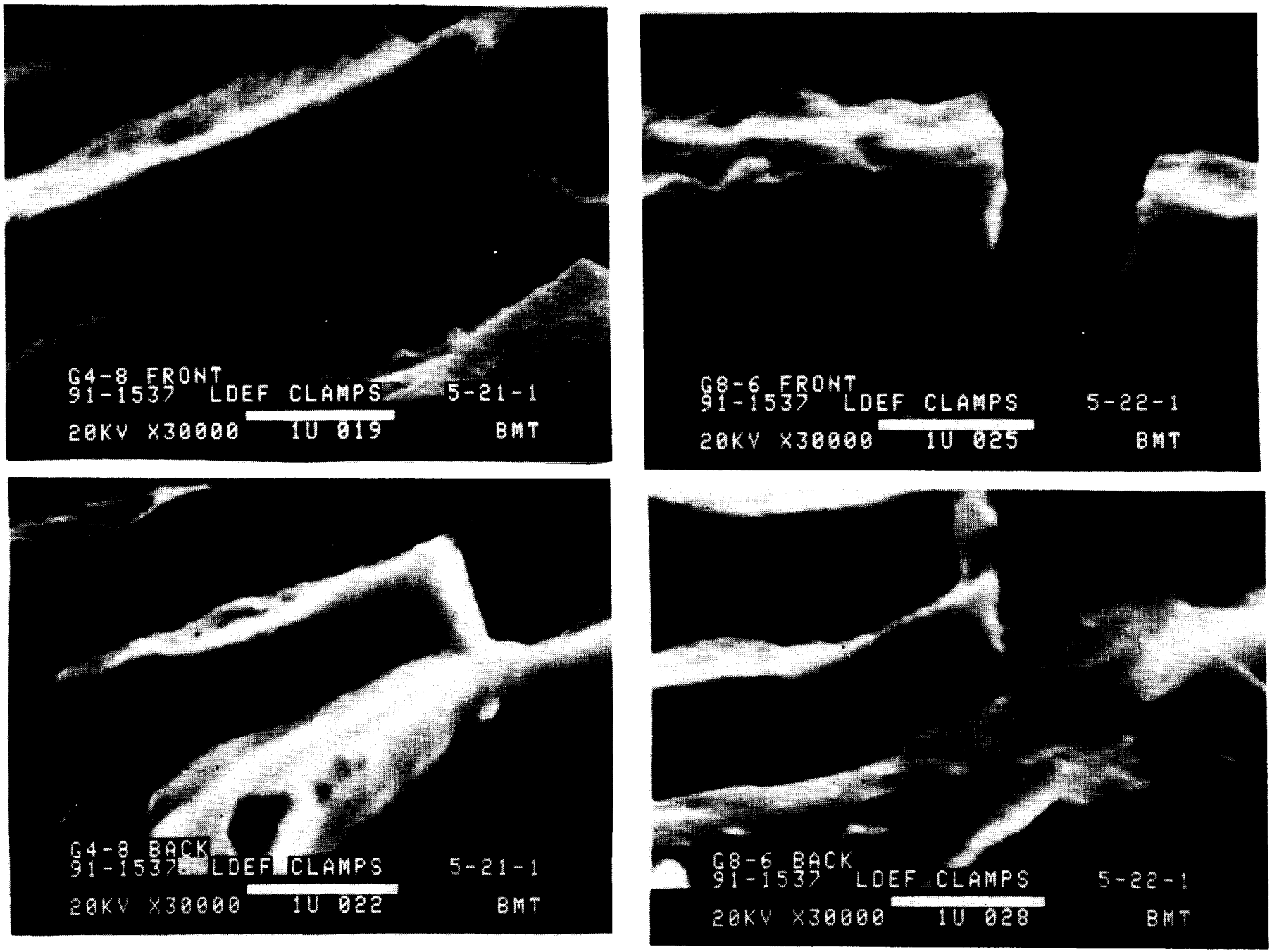

Figure B8: SEM photomicrographs of coating thickness for tray clamps G04-8 and G08-6

APPENDIX C

Photomicrographs of Coating Porosity

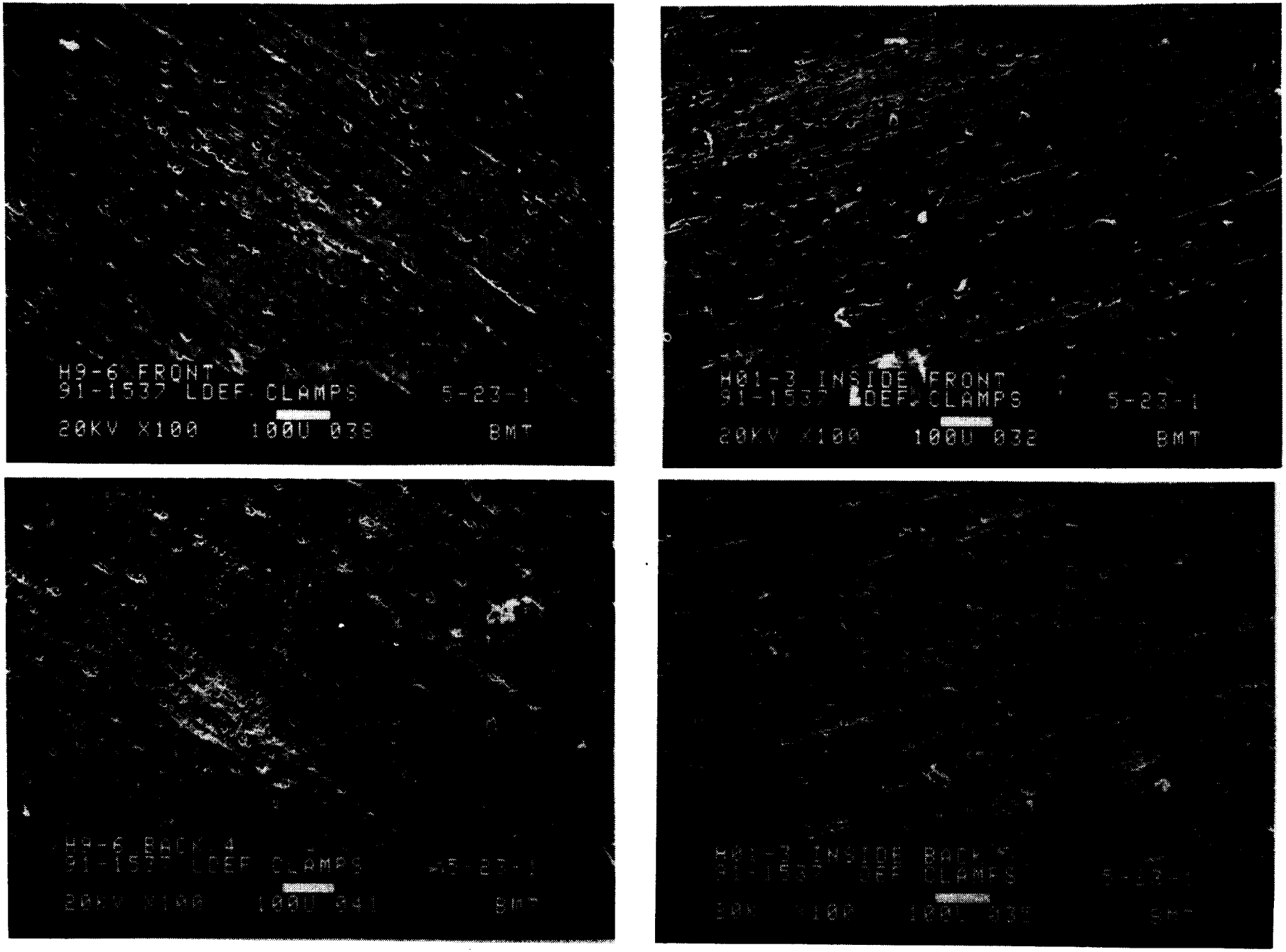

Figure C1: SEM photomicrographs of coating porosity for tray clamps Ho9-6 and H01-3

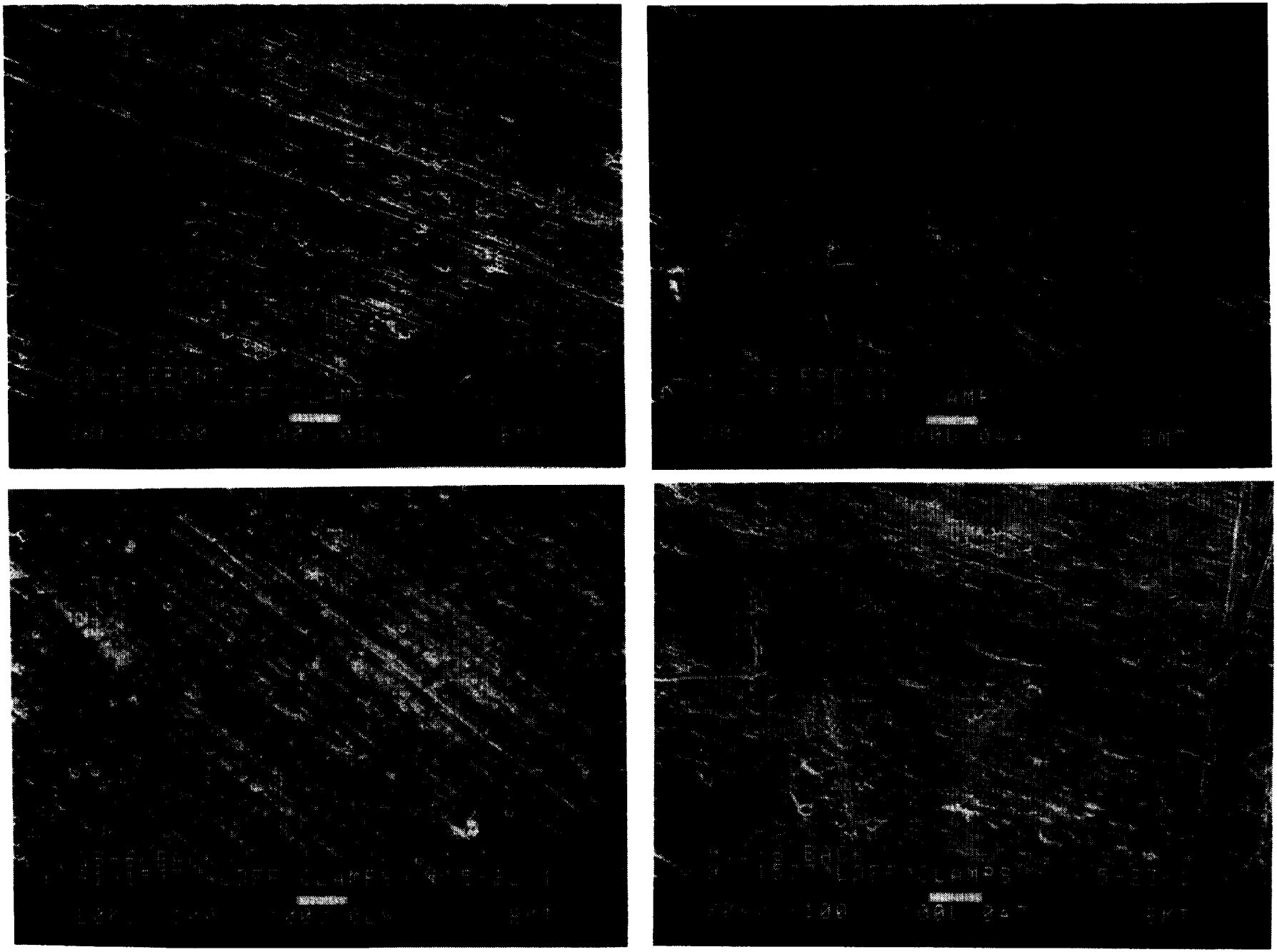

Figure C2: SEM photomicrographs of coating porosity for tray clamps G08-6 and H12-6

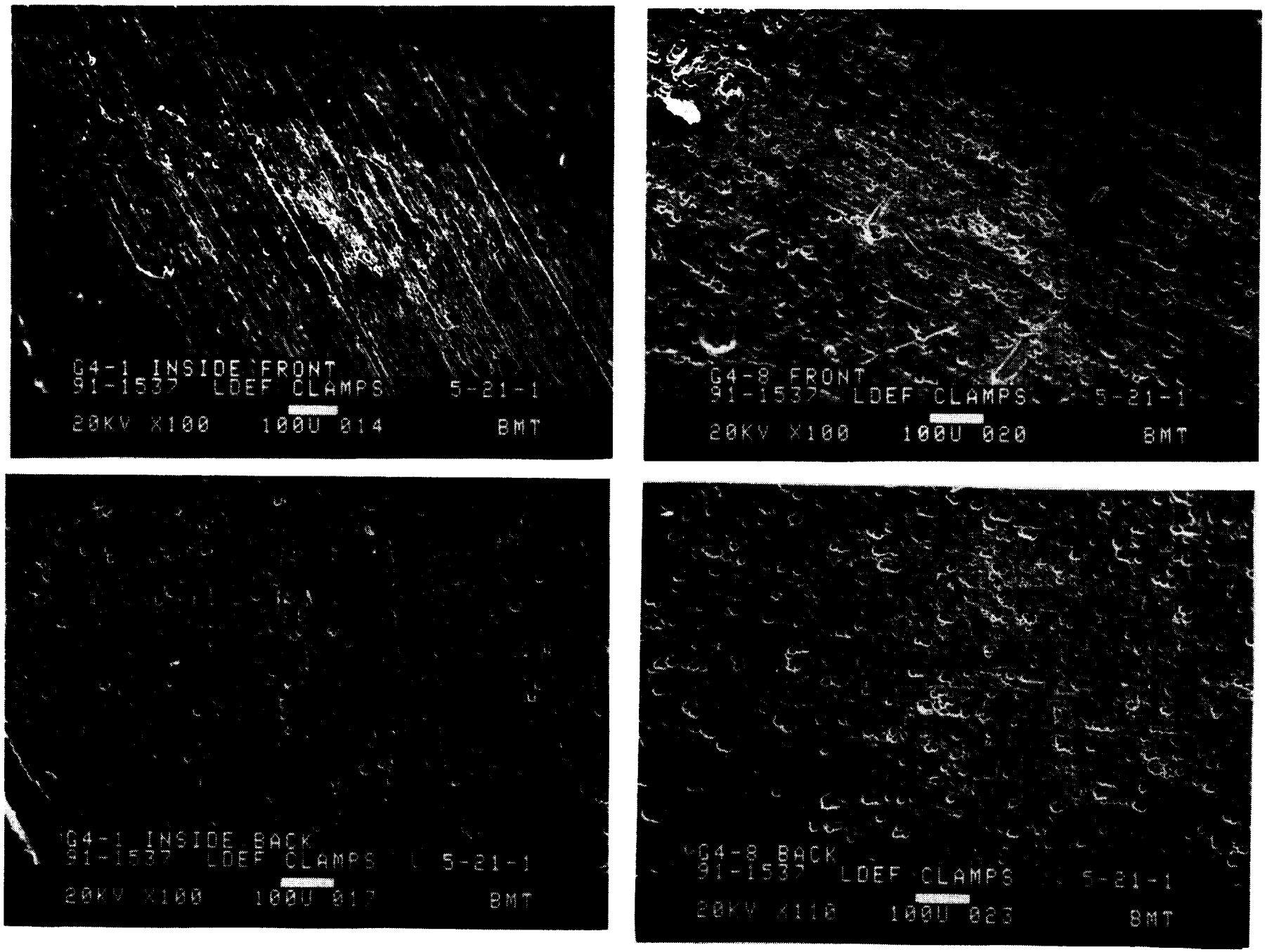

Figure C3: SEM photomicrographs of coating porosity for tray clamps G04-1 and G04-8

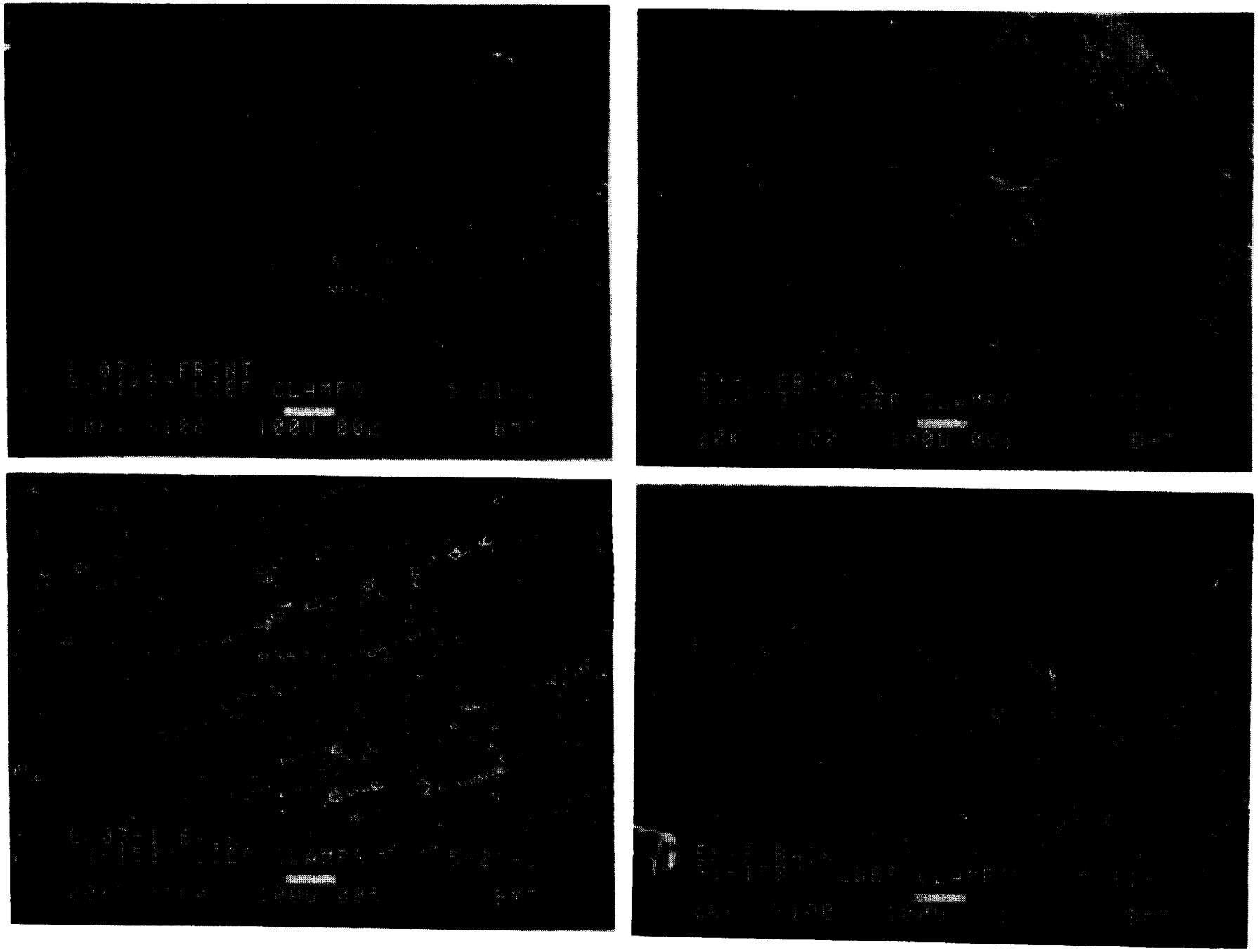

Figure C4: SEM photomicrographs of coating porosity for tray clamps E03-1 and E09-2

REPORT DOCUMENTATION PAGE

Form Approved
OMB No. 0704-0188

1. AGENCY USE ONLY *(Leave blank)*	2. REPORT DATE	3. REPORT TYPE AND DATES COVERED
	May 1993	Contractor Report Oct. 1989-Feb. 1992

4. TITLE AND SUBTITLE
Space Environmental Effects on the Integrity of Chromic Acid Anodized Coatings

5. FUNDING NUMBERS
NAS1-18224
and
NAS1-19247

506-43-61-02

6. AUTHOR(S)
W. L. Plagemann

7. PERFORMING ORGANIZATION NAME(S) AND ADDRESS(ES)
Boeing Defense & Space Group
P.O. Box 3999
Seattle, WA 98124-2499

8. PERFORMING ORGANIZATION REPORT NUMBER

9. SPONSORING/MONITORING AGENCY NAME(S) AND ADDRESS(ES)
National Aeronautics and Space Administration
Langley Research Center
Hampton, VA 23681-0001

10. SPONSORING/MONITORING AGENCY REPORT NUMBER
NASA CR-191468

11. SUPPLEMENTARY NOTES
Langley Technical Monitor: Joan G. Funk
Special Report

12a. DISTRIBUTION/AVAILABILITY STATEMENT
Unclassified--Unlimited
Subject Category 23

12b. DISTRIBUTION CODE

13. ABSTRACT *(Maximum 200 words)*

This report describes the condition of chromic acid anodized aluminum subsequent to a 69-month exposure to low Earth orbit (LEO) on the Long Duration Exposure Facility. Optical properties and the condition of anodized coating are reported. This material was exposed to each environmental parameter present in LEO. Only slight changes in the material were observed.

14. SUBJECT TERMS
Low Earth Orbit, Chromic Acid Anodized, and LDEF

15. NUMBER OF PAGES
188

16. PRICE CODE
A09

17. SECURITY CLASSIFICATION OF REPORT	18. SECURITY CLASSIFICATION OF THIS PAGE	19. SECURITY CLASSIFICATION OF ABSTRACT	20. LIMITATION OF ABSTRACT
Unclassified	Unclassified	Unclassified	UL